CATALYTIC HYDROGENATION OF AROMATIC KETONES IN MULTIPHASE REACTORS: CATALYSIS AND REACTION ENGINEERING STUDIES

A THESIS

SUBMITTED TO THE

UNIVERSITY OF PUNE

FOR THE DEGREE OF

DOCTOR OF PHILOSOPHY

IN

CHEMISTRY

BY

SUJU P. MATHEW

AT
HOMOGENEOUS CATALYSIS DIVISION
NATIONAL CHEMICAL LABORATORY
PUNE 411 008
INDIA

MAY 2001

Dedicated To Janja and Mummy

FORM 'A'

Certified that the work incorporated in the thesis entitled: "**CATALYTIC HYDROGENATION OF AROMATIC KETONES IN MULTIPHASE REACTORS: CATALYSIS AND REACTION ENGINEERING STUDIES**", submitted by **Mr. Suju P. Mathew** was carried under my supervision. Such material as has been obtained from other sources has been duly acknowledged in the thesis.

May, 2001 **Dr. R. V. Chaudhari**

Pune (Supervisor/Research Guide)

List Of Contents

List of Tables

List of Figures

Summary and Conclusions

Hydrogenation of organic compounds has wide ranging applications in the manufacture of fine chemicals and pharmaceuticals. Since most of the products in this category are non-volatile complex molecules, the hydrogenation reactions are usually carried out in liquid phase using soluble or supported metal catalysts. These reactions are generally carried out in multiphase reactors in which the catalyst is either suspended in liquid phase as fine particles (slurry reactors) or supported as a fixed bed with cocurrent down flow (trickle bed reactor) or up flow of gas and the liquid phases. The catalytic hydrogenation processes are gaining particular attention as they provide cleaner synthetic routes for fine chemicals and pharmaceuticals as against the multi step organic synthetic routes based on stoichiometric reagents, which generate large quantities of inorganic salts and byproducts posing environmental problems. Therefore, research on multiphase catalytic reactions/reactors is extremely important in developing cleaner and economically improved processes for a wide variety of industrial products. The overall performance of such processes depends not only on the catalytic chemistry but also on the suitable choice of the reactor. A systematic study of the fundamental principles in catalysis and reaction engineering is necessary to develop optimum processes. The subject of multiphase catalysis and reaction engineering is also of generic importance to several other reactions like alkylation, oxidation, carbonylation, hydroformylation, petroleum refining etc. The aim of this thesis was to investigate catalysis and reaction engineering aspects of hydrogenation of aromatic ketones in multiphase slurry and fixed bed reactors. The reaction systems chosen itself are industrially relevant as the products of hydrogenation of acetophenone, 1-phenylethanol is an intermediate for the production of styrene and is also used in pharmaceutical industry and another product 1-cyclohexylethanol is extensively used in the manufacture of polyvinyl cyclohexane, a high temperature resistant polymer. The product of hydrogenation of p-isobutyl acetophenone, p-isobutyl phenylethanol, is an important intermediate in the synthesis of ibuprofen, a non-steroidal, anti-inflammatory drug.[1] Also, the reactions provide interesting examples of multistep catalytic reactions allowing us to investigate important issues such as catalyst activity, selectivity, reaction kinetics and reactor performance.

The following specific problems were chosen for the present work

- Kinetics and modelling of semi-batch slurry and basket reactors under isothermal and non-isothermal conditions for hydrogenation of acetophenone using supported Ru catalysts.
- Reaction kinetics and modelling of a semi batch slurry reactor for hydrogenation of p-isobutyl acetophenone using a Ru/Al_2O_3 catalyst.
- Experimental and theoretical investigations on performance of a trickle bed reactor for the hydrogenation of acetophenone using supported Ru catalysts
- Experimental and theoretical investigations on performance of a fixed bed three phase reactor with co-current up-flow of gas and liquid phase for the hydrogenation of acetophenone and its comparison with trickle bed reactor performance.
- Activity and selectivity studies using various supported metal catalysts for hydrogenation of acetophenone.

The thesis will be presented in five chapters, the synopsis of which is presented here.

In chapter 1, literature review on catalytic hydrogenation of aromatic ketones and particularly acetophenone and p-isobutyl acetophenone has been presented. The type of catalysts used, their activity, selectivity, kinetic modeling and reaction engineering aspects has been discussed. Hydrogenations of aromatic ketones are known to give essential products as shown in the scheme below, (Figure 1) with acetophenone as an example.

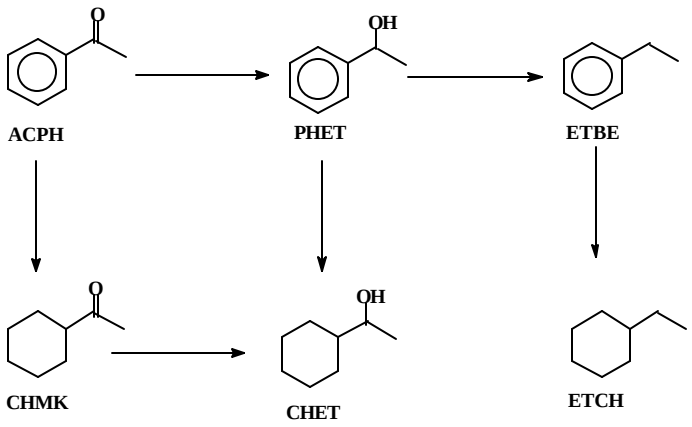

Figure 1. Reaction scheme for hydrogenation of acetophenone

However, the selectivity is dependant on the type of catalyst used. Catalysts consisting of supported Pt, Pd, Ru, Rh and Cu catalysts are known in the literature for the hydrogenation of acetophenone. The investigations on activity and selectivity of these catalysts and surface characterizations have been reviewed.[2,3] The kinetic modeling of hydrogenation of acetophenone and p-isobutyl acetophenone was studied by Isabelle et al.[4] and Rajasekharam et al.[3] respectively using supported Rh and Ni catalysts. Ru catalysts can provide an alternative to Pt and Rh based systems, particularly to achieve high selectivity to 1-cyclohexylethanol. No detailed reports of kinetics on these reactions have been published with Ru catalysts. The reaction engineering aspects, including analysis of external and intraparticle mass transfer effects, modelling of semi-batch slurry and fixed bed reactors and experimental verification for hydrogenation of aromatic ketones and for other important reaction systems have also been discussed and scope for the present thesis outlined.

In Chapter 2, a detailed study on the liquid phase hydrogenation of acetophenone in a semi-batch slurry and basket type of reactors using 2%Ru/Al_2O_3 is presented. The effect of agitation speed, catalyst loading, initial acetophenone concentration and H_2 partial pressure was studied experimentally over a temperature range of 373–423 K. For the purpose of kinetic parameter estimation a semi-batch slurry reactor model was developed, which was used in combination with an optimisation routine to evaluate different type of rate models. A Langmuir-Hinshelwood type rate model based on non-competitive adsorption of hydrogen and liquid phase components and different adsorption sites for the adsorption of different functional groups could explain well the intrinsic kinetics obtained from slurry reactor. In order to investigate the intraparticle diffusional effects, experiments were conducted in a basket type reactor. These data's were analysed using a dynamic model for semi-batch basket type reactor in which the intraparticle diffusion with reaction of various reactants and intermediates were considered. Further, the non-isothermal behaviour of the semi batch slurry reactor was studied, in which experimental concentration-time as well as temperature-time profiles were obtained. Mathematical model for a semi-batch slurry reactor was developed incorporating the non-isothermal effects, which was found to predict the observed experimental data satisfactorily.

Kinetics of hydrogenation of p-isobutyl acetophenone using a 2%Ru/Al_2O_3 catalyst in a semi-batch slurry reactor over a temperature range of 373-398 K is also presented in Chapter 2. The effect of catalyst loading, H_2 partial pressure and p-isobutyl acetophenone concentration on concentration-time and H_2 consumption profiles was studied. A rate equation has been proposed based on a Langmuir-Hinshelwood type mechanism in which reaction between non-dissociative adsorption of hydrogen and different liquid phase components are assumed to be rate determining. The kinetic parameters were evaluated by fitting the integral batch reactor data at different temperatures. The activation energies, heat of adsorption and the entropy of adsorption of hydrogen and various liquid phase components were evaluated.

In Chapter 3, hydrogenation of acetophenone using a supported ruthenium catalyst was studied in a trickle bed reactor. Increase in liquid velocity in the trickle bed reactor resulted in lower conversions of acetophenone considerably but had marginal effect on rate of hydrogenation. Of the main factors contributing to the reactor performance, the gas to solid mass transfer and gas to liquid mass transfer were found to be important. Increasing the inlet concentration of acetophenone resulted in marginal increase in rate of hydrogenation. The rate of hydrogenation varied almost linearly with the partial pressure of hydrogen proving the importance of gas phase reactant limitation. Increase in gas velocity was found to increase the conversion and rate of hydrogenation marginally. A plug flow model incorporating the mass transfer effects, partial wetting, non-isothermal effects and solvent evaporation effects was found to explain well the observed reactor performance. PHET was found to be the major product under the range of conditions studied. CHET formation increased with increase in residence of liquid phase and with increase in reactor pressure.

In Chapter 4, hydrogenation of acetophenone using 2%Ru/Al_2O_3 catalyst was investigated in a fixed bed reactor with cocurrent up-flow. It was observed that gas velocity, liquid velocity and inlet concentration of ACPH had only a mild influence on the reaction rates, while with respect to hydrogen partial pressure and temperature the rates increased significantly. In order to explain these results theoretical models for steady state conditions as well as dynamic analysis were developed. The model predictions agreed well for almost all the experimental data indicating that detailed

theoretical models can be reliably used for predicting the reactor performance. The literature correlations were found to be satisfactory. The temperature rise observed was not very large, but within the range of model predictions. Finally the experimental data from the up-flow reactor were compared with the corresponding results in a trickle bed reactor and observed that under conditions of low liquid velocity TBR outperformed up-flow reactor, where as at higher liquid velocities the rates were almost similar in both cases.

In Chapter 5, a detailed investigation on the hydrogenation of acetophenone using supported Ru catalysts has been reported. Supported ruthenium catalysts prepared by precipitation technique and impregnation technique showed the presence of some extent of ruthenium oxide even after activation at 573 K. With methanol as solvent, CHET formation took place mainly through PHET as the intermediate for supported ruthenium catalysts. With higher alcohols, CHET formation through CHMK and PHET as the intermediates in almost equal amounts was observed and with non-polar hydrocarbon solvents, reaction proceeded mainly through CHMK as the intermediate. With non-polar hydrocarbon solvents, 99% selectivity towards CHET was obtained where as with alcoholic solvents considerable amount of the side product, ethyl benzene, formation was observed. Studies with water as the immiscible phase with acetophenone was found to give high rates and high selectivity (> 98%) towards CHET. The catalysts were found to remain in the aqueous phase, which was recycled successfully four times, and in all the recycles the rates were found to be similar and the selectivity towards CHET was maintained. Ruthenium supported on NaY was found to give the maximum reaction rates owing to its high surface area. Catalysts prepared by impregnation technique were found to give a better activity than the catalysts prepared by precipitation technique and ethanol as the impregnation solvent was found to be better rates than water as the impregnation solvent. Addition of basic promoters like NaOH and triethylamine was found to suppress the formation of the side product, ethyl benzene, with ruthenium as catalyst and methanol as the solvent. Screening of other supported metal catalysts showed that Ni and Pd catalysts gave better selectivity towards PHET.

References

1. Sheldon R.A., Chem. Ind., 7 December, p. 903, 1992

2. Kluson P. and Cerveny L., Applied catalysis A: General, 128, 13, 1995

3. Rajashekharam M.V., Thesis submitted to the university of pune, India, 1997

4. Bergault I., Fouilloux P., Joly-Vuillemin C. and Delmas H., Kinetics and Intraparticle Diffusion Modelling of a complex Multistep Reaction: Hydrogenation of Acetophenone over a Rhodium Catalyst, J. Cata., 175, 328, 1998

Chapter 1

Introduction and Literature Survey

1.0 General Introduction

Catalysis forms an inseparable part of chemical industry in the modern world. Most industrial reactions and almost all biological reactions are catalytic in nature. The value of products made in United States in processes that involve catalysis is around a trillion dollar annually.[1] End products of catalytic processes include food, clothing, drugs, plastics, detergents and fuels. It also forms an integral part of environmental protection and emission control. Therefore, catalyst manufacture is a major industrial operation and catalysts worth 2-3 billion dollars are sold annually in US.[1] In most industrial catalytic reactions, the catalysts used may be supported metals/metal oxides or metal complexes along with one or more promoters/cocatalysts. Many important discoveries in catalysis have revolutionized technologies for the manufacture of pharmaceuticals and fine chemicals. Some examples are: synthesis of ibuprofen by catalytic hydrogenation/carbonylation, hydroxylation of phenol to hydroquinone and catechol using ZSM-5 catalyst, auto-oxidation of para-diisopropylbenzene to hydroquinone, oxidative carbonylation of methanol to dimethyl carbonate, catalytic asymmetric hydrogenation etc.[2] All these catalytic routes provide more economical and environmentally benign processes.

Most of the catalytic reactions involve gas, liquid and/or solid (catalyst) phases resulting in multiphase catalytic systems. The performance of the multiphase catalytic systems depends not only on the catalytic chemistry associated with the reactions occurring on the solid surface, but also on the reaction engineering aspects relating the kinetics of catalytic reactions coupled with interphase and intraparticle diffusional effects. Therefore, to achieve a complete understanding of the multiphase catalytic reactions, both catalysis and reaction engineering aspects have to be investigated. While in the literature, several examples have addressed these aspects in isolation, there are only limited reports on complex multiphase catalytic reactions. Multiphase reaction engineering aspects for fine chemicals and pharmaceuticals have been reviewed by Ramachandran and Chaudhari,[3] Doraiswamy and Sharma,[4] Mills et al.,[5] Mills and Chaudhari,[2] Mills and Chaudhari,[6] and Carpenter.[7] Extensive work on theoretical development of reaction rate/reactor performance models has been carried out but the experimental validation of models were limited to model reaction systems.

Hydrogenation of organic compounds has wide ranging applications in the manufacture of fine chemicals and pharmaceuticals. Since most of the products in this category are non-volatile complex molecules, the hydrogenation reactions are usually carried out in a liquid phase using soluble or supported metal catalysts. Even though hydrogenation reactions involving molecules with only one functional group is common, selective hydrogenation of one functional group in the presence of other functional groups still pose considerable challenge to researchers. Many of the industrially important reactions involve complex reaction networks and hence achieving selectivity to one particular product is still a difficult task. These reactions are generally carried out in multiphase reactors in which the catalyst is either suspended in liquid phase as fine particles (slurry reactors) or supported as a fixed bed with cocurrent down-flow (trickle bed reactor) or up-flow of gas and the liquid phases. The catalytic hydrogenation processes are gaining particular attention as they provide cleaner synthetic routes for fine chemicals and pharmaceuticals as against the multi step organic synthetic routes based on stoichiometric reagents, which generate large quantities of inorganic salts and byproducts posing environmental problems. Therefore, research on multiphase catalytic reactions/reactors is extremely important in developing cleaner and economically viable processes for a wide variety of industrial products. The subject of multiphase catalysis and reaction engineering is also of generic importance to several other reactions like alkylation, oxidation, carbonylation, hydroformylation, petroleum refining etc. The aim of this thesis was to investigate catalysis and reaction engineering aspects of hydrogenation of aromatic ketones in multiphase slurry and fixed bed reactors. The reaction systems chosen itself are industrially relevant as the products of hydrogenation of acetophenone, 1-phenylethanol is used in perfumery and in pharmaceutical industry and another product 1-cyclohexylethanol is extensively used in the manufacture of polyvinyl cyclohexane, a high temperature resistant polymer. Hydrogenation of another related aromatic ketone, p-isobutyl acetophenone, to p-isobutyl phenylethanol, is a key intermediate in the synthesis of ibuprofen, a non-steroidal, anti-inflammatory drug.[8] These reactions provide interesting examples of multistep catalytic reactions allowing us to investigate important issues such as catalyst activity, selectivity, reaction kinetics and reactor performance.

In the present chapter, a literature review on the catalysis and reaction engineering aspects of hydrogenation of aromatic ketones has been presented. In addition a detailed literature review on the analysis and design of multiphase catalytic reactors with special emphasis on batch slurry and down-flow and up-flow fixed bed reactors is presented.

1.1 Hydrogenation of Aromatic Ketones

Hydrogenation of aromatic ketones constitutes an important class of hydrogenation reactions. Majority of the products formed find applications in fine chemical and pharmaceutical industry. Aromatic ketones can undergo hydrogenation in two paths. One is the hydrogenation of only the ketonic functional group resulting in the formation of corresponding alcohol and other involves hydrogenation of the aromatic ring, giving rise to saturated alcohol or ketone. In general the reaction scheme involved can be represented as (Figure 1.1):

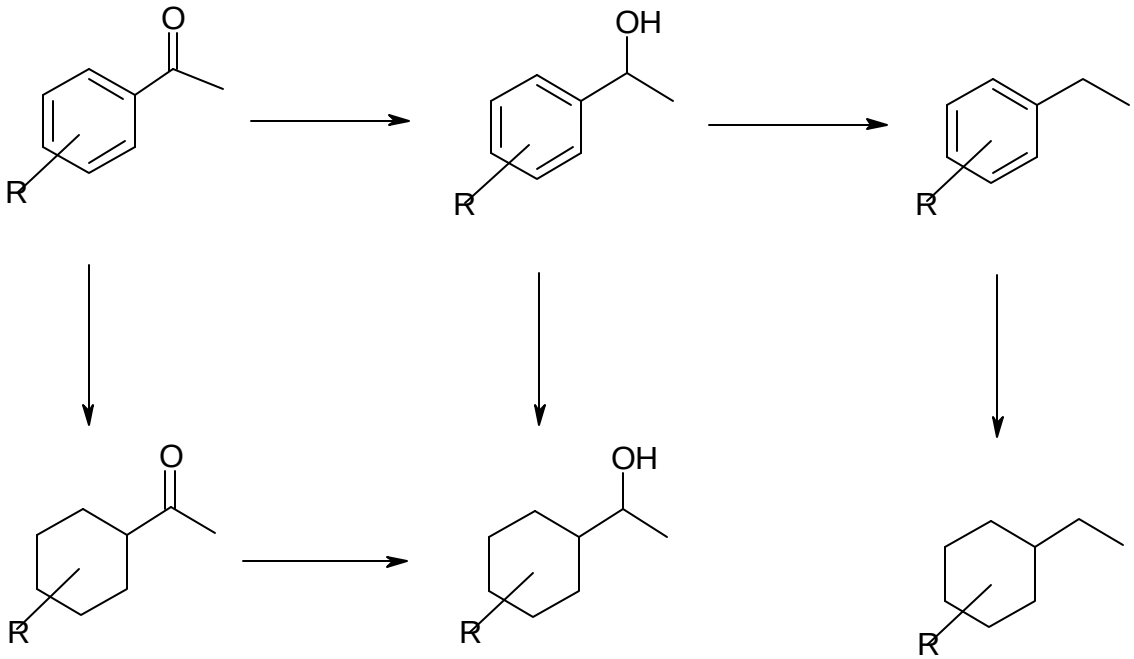

Figure 1.1: Reaction Scheme for Aromatic Ketone Hydrogenation

Examples of aromatic ketone hydrogenations and corresponding products formed are given in Table 1.1, with diverse industrial applications.

Table 1.1: Examples of Aromatic Ketone Hydrogenations Reported in the Literature

S. No.	Substrate	Product/Application	Catalyst System/ Reference
(1)	(2)	(3)	(4)
1	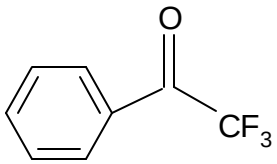	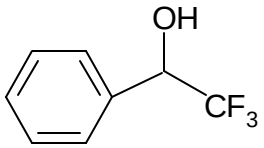 Agriculture and Pharmaceutical Industry	Pt/Alumina[9]
2	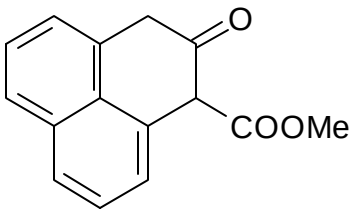	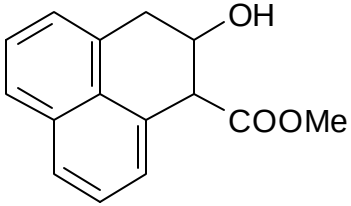 Fine chemical	Ru/Zeolite[10]
3	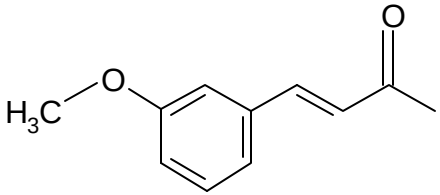	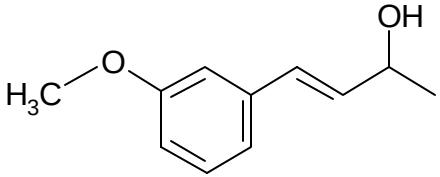	5%Pd/C[11]

(1)	(2)	(3)	(4)
4	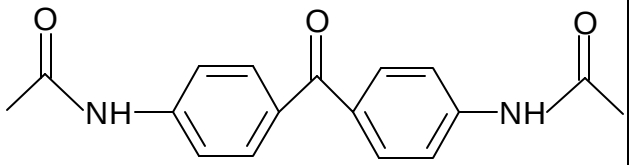	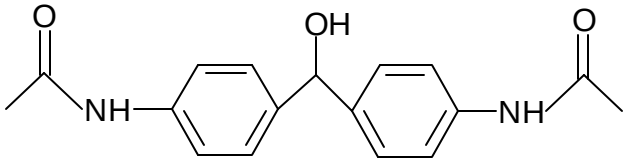 Pharmaceutical	5%Pd/C[12]
5	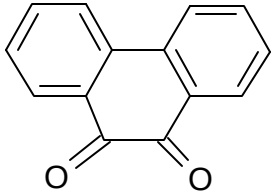	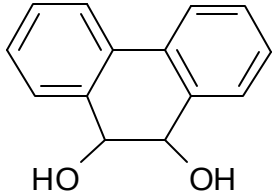	Platinum oxide, acetic acid[13]
6	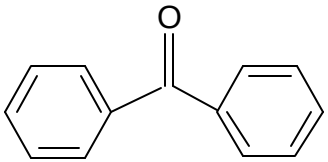	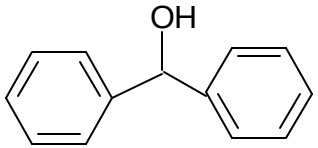 Pharmaceuticals	Ni/SiO_2[14]
7	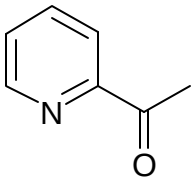	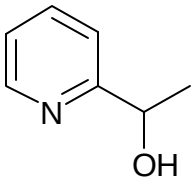	5%Pd/C[15]

(1)	(2)	(3)	(4)
8	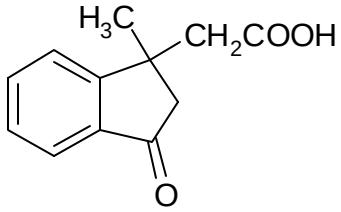	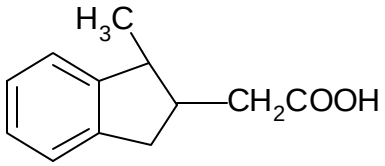	10%Pd/C, ethanol, H_2SO_4[16]
9	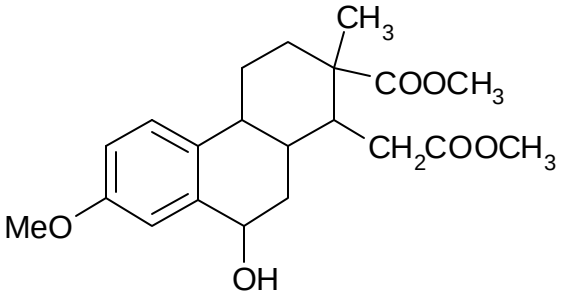	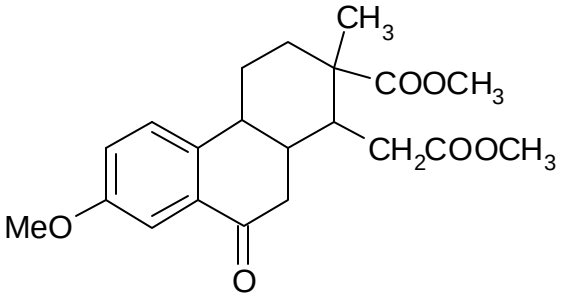	30% Pd/Stroncium carbonate, ethyl acetate[17]
10	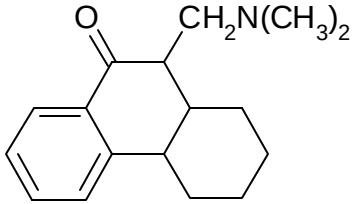	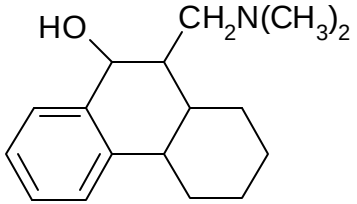	Platinum oxide, acidic buffer of ammonium acetate and acetic acid[18]
11	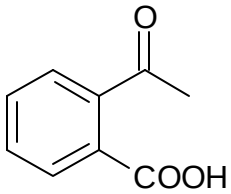	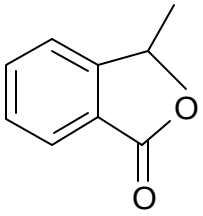	Raney Ni[19]

For the present investigation, acetophenone (ACPH) was chosen as the model system as it represents an interesting case of a complex multistep reaction with challenges in selectivity and reactor design. Another system studied is the hydrogenation of p-isobutyl acetophenone (p-IBAP), which a key intermediate in the manufacture of ibuprofen and this new catalytic route[20] is considered as a major innovation in ibuprofen technology both from environmental as well as economic point of view, as it eliminates the conventional stoichiometric synthetic routes, which produce a large amount of salts as by-products.

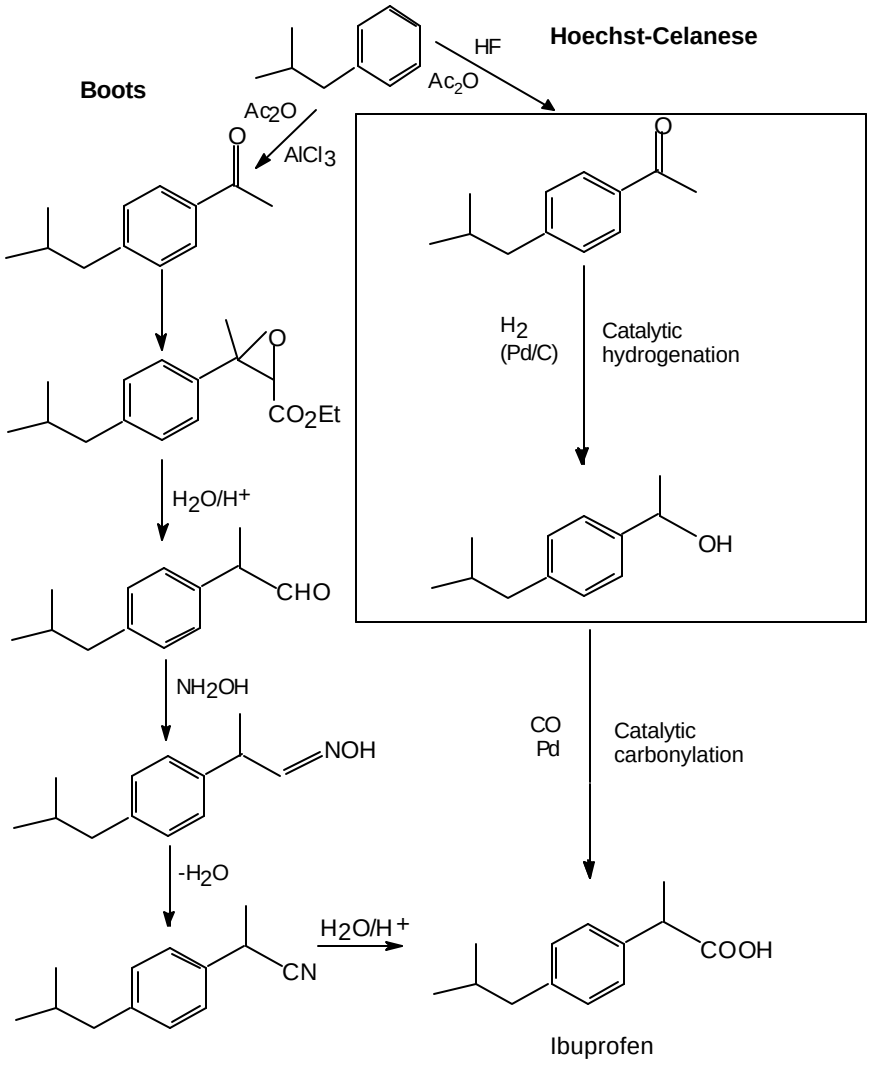

Figure 1.2: Conventional Boots Route and the Catalytic Hoechst-Celanese Route

1.1.1 Hydrogenation of Acetophenone and p-Isobutyl Acetophenone

Hydrogenation of acetophenone represents a complex reaction network with considerable exothermicity and the product distribution of hydrogenation depend on the catalyst type used. The catalysts used can be classified into two different categories: (a) One, which hydrogenate only the ketonic group and (b) the other, hydrogenating both ketonic group as well as the aromatic ring. The reaction mainly proceeds through two intermediates, (i) 1-phenylethanol (PHET) and (ii) cyclohexylmethylketone (CHMK). 1-cyclohexylethanol (CHET) is the end product in both these cases and ethylbenzene (ETBE) and ethylcyclohexane (ETCH) are obtained as undesired side products. The main emphasis of the earlier studies was to get selective formation of 1- phenyl ethanol or 1-cyclohexyl ethanol. Reports on hydrogenation of acetophenone using various metal catalysts are summarized in Table 1.2.

Table 1.2: Literature Reports on Hydrogenation of Acetophenone and p-Isobutyl Acetophenone Using Supported Metal Catalysts

S. No.	Substrate / Catalyst	Reaction Conditions	Conversion %	Product / Selectivity %	Reference
(1)	(2)	(3)	(4)	(5)	(6)
1	ACPH / Flourinated Pt (5-10%) supported on alumina	155-190^{0}C/ 20-30 atm	-	CHET	Serebryakov et al.[21]
2	ACPH / 1%Ru/TiO_2 (Activated at 773 K)	30^{0}C, 1 atm, Solvent: Cyclohexane	50%	PHET/ 50	Wismeijer et al.[22]

(1)	(2)	(3)	(4)	(5)	(6)
3	ACPH / 0.1-1% Ru/Support	80-160^{0}C, 200-350 atm, Fixed bed	-	CHET/ 96.4	Otte and Nehring [23]
4	ACPH / Pd/C and LiOH	150^{0}C, 20 atm, 2hrs	99%	PHET/ 96	Too et al.[24]
5	ACPH / 5:5 Rh-Sn/Al_2O_3	Solvent: H_2O		PHET/ 82.3	Zakumbaeva et al.[25]
6	ACPH / Raney Ni	80^{0}C, 9 atm, Solvent: cyclohexane, Time: 1.83hrs	100	PHET/ 70 CHET/ 10	Masson et al.[26]
7	ACPH / $NiCr_{1.5}$	80^{0}C, 9 atm, Solvent: cyclohexane, Time: 1.83hrs	99.3	PHET/ 89 CHET/ 4.9	Masson et al.[27]
8	ACPH / 2.5%Ru/TiO_2	30^{0}C, 1atm, Solvent: isopropanol	-	PHET/73	Kluson et al. [28]
9	ACPH / 2%Ru/Al_2O_3	30^{0}C, 1atm, Solvent: isopropanol	52	PHET/78	Kluson et al. [28]
10	ACPH / Ir/Al_2O_3	Room temp., 1 atm, Solvent: water, Time: 24hrs	100	PHET/ 68 CHET/ 32	Rocchini et al.[29]
11	ACPH / Rh/Al_2O_3	Room temp., 1 atm, Solvent: water, Time: 24hrs	100	PHET/ 100	Rocchini et al.[29]

(1)	(2)	(3)	(4)	(5)	(6)
12	ACPH / Pt/C	Room temp., 1 atm, Solvent: water, Time: 24hrs	100	PHET/ 59 CHET/ 41	Rocchini et al.[29]
13	ACPH / Silica supporting $CuO.CuCr_2O_4$ (CuO 3.6%, Cr_2O_3 3.4%)	130^0C, 2 atm, Time: 2hrs	75.4	PHET/ 99.1	Masaya et al.[30]
14	ACPH / Silica supporting $CuO.CuCr_2O_4$ (CuO: 15.3%, Cr_2O_3:14.7%)	130^0C, 2 atm, Time: 2hrs	72.9	PHET/ 96.9	Masaya et al.[30]
15	ACPH / CuO-Silica pellet	130^0C, 2atm, Fixed bed		PHET/ 99.5	Masaya et al.[31]
16	ACPH / Cu-ZnO with alk. earth carbonates and alkali metal salts	180^0C, 2 atm, Time: 46 min	75.0	PHET/ 97.6	Masaya et al.[32]
17	ACPH / Rh/C Solvent: cyclohexane	80^0C, 25 atm	100	CHET/ 100	Bergault et al.[33]
18	ACPH / acid modified Ru/C, solvent: isopropanol,	80^0C / 60 atm Time: 6hrs	100	CHET/ 95	Itoi [34]

(1)	(2)	(3)	(4)	(5)	(6)
19	p-IBAP / Ru/C	120^0C, 4 atm, Time: 5hrs	97	p-IBPE	Tadashi et al.[35]
20	p-IBAP / Raney Ni	140^0C, 68.03 atm, Time: 4hs	87	p-IBPE	Yoshiyaki[36]
21	p-IBAP / Pd/C	30^0C, 6.8 atm, Time: 1hr	99	p-IBPE / 97	Elango[37]
22	p-IBAP / Activated Ni sponge	60^0C, 17 atm, Time: 1.5hrs	99	p-IBPE	Ryan [38]
23	p-IBAP / Pd/$CaCO_3$	60^0C, 8.6 atm, Time: 18hrs	85	p-IBPE / 100	Saeki and Takashi[39]
24	p-IBAP / Pd/C	60^0C, 8.6atm, Time: 1hr	97	p-IBPE / 100	Saeki and Shima[40]
25	p-IBAP / 10%Ni/HY	100^0C, 30 atm, Time: 2hrs	75	p-IBPE / 75	Rajashekharam and Chaudhari[41]

Most of the studies on the selective synthesis of 1-phenylethanol and 1-cyclohexylethanol are patented. Earlier work for the selective synthesis of PHET was based on Raney Ni, Pd, Ru and Pt catalysts. The earlier work on hydrogenation of acetophenone using supported metal catalysts is summarized here. Wismeijer et al.[42] that found Ru/TiO_2 gives higher selectivity to PHET compared to Ru supported on SiO_2 and C. These catalysts were activated at 773 K before using for the hydrogenation of ACPH. The high selectivity was attributed to the metal support interaction between Ru and TiO_2 at 773 K while with other supports the metal support interaction doesn't occur at that temperature. With Ru/TiO_2 catalyst activated at a lower temperature (473 K) the selectivity obtained for PHET was found to be lower. At lower catalyst activation

temperatures, the metal support interaction is not expected and hence the lower selectivity. In metal support interaction, metal particles of the catalysts are decorated with titania sub-oxides generating new stable active sites for selective carbonyl group hydrogenation which is a possible explanation for the higher selectivity.[43] Masson et al.[26] investigated the influence of temperature, pressure and the nature of the solvent on the activity and selectivity of Raney Ni catalysts for hydrogenation of ACPH to PHET. In cyclohexane as the solvent, low temperature and high pressures were found to give 85% selectivity towards the formation of PHET. Lower alcohols as solvents gave higher selectivity to PHET (> 92%), which is explained as a result of inhibition of ring hydrogenation by polar molecules and has a correlation with dielectric constant of the solvent. Masson et al[27] investigated kinetics of acetophenone hydrogenation using Cr promoted Raney Ni catalysts in cyclohexane as the solvent. In the presence of Cr, the hydrogenation of the C=O bond is favored with respect to two side reactions: the hydrogenation of aromatic ring and the hydrogenolysis of the C-OH bond. Kluson et al.[28] have investigated the effect of supports and method of preparation and conditions of catalyst activation on hydrogenation of acetophenone using Ru supported catalysts. It was concluded that the catalyst prepared by impregnation technique with ethanol as the impregnating solvent gave better rates and selectivity for PHET. Ethanol has weaker complexing ability than water and accordingly the activity of the ruthenium catalysts prepared in ethanol medium was higher due to the inclusion of the impregnating solvent in the catalyst after activation. Rocchini et al.[29] showed that, in the hydrogenation of acetophenone molecules inserted in cyclodextrins with Ir, Rh and Pt supported catalysts ring hydrogenation was minimum. Organic compounds are known to form 1:1 adducts with cyclodextrins, if they possess a suitable hydrophobic group that can fit in its cavity. By the incorporation of acetophenone molecules in cyclodextrins, the phenyl ring of the acetophenone is inserted in the cyclodextrin cavity thus inhibiting its reduction. The adduct will approach the metallic surface from the side of the carbonyl group, thereby giving aromatic alcohol as the product.

Recent investigations on hydrogenation of acetophenone reveal that cheaper catalysts like copper based catalysts can be used for the selective synthesis of PHET. Ito Masaya et al.[30,31,32] have patented Cu based catalysts for the selective formation of PHET

from ACPH as mentioned in Table 1.2. Rajasekharam[44] investigated in detail the hydrogenation of ACPH using Ni/HY catalysts. FT-IR investigation of the acetophenone adsorbed catalysts showed that C=O bond is activated due to its interaction with the zeolite protons resulting in the weakening of C=O bond. He also observed that the acidic sites present on the support facilitated the formation of ether, 1-phenylethylmethyl ether, by the reaction between 1-phenyl ethanol and the solvent methanol. Rajasekharam et al.[45] studied the kinetics of hydrogenation of acetophenone using 10%Ni/HY catalyst with methanol as the solvent over a temperature range of 353-393 K. The effect of hydrogen partial pressure, initial concentration of acetophenone and temperature on the concentration-time profiles in a semi-batch slurry reactor was investigated. It was found that, water, a side product formed during the reaction had a strong inhibitory effect on hydrogenation activity. Liquid phase hydrogenation of acetophenone using Rh/C catalyst was studied by Bergault et al.[46] in trickle bed reactor and slurry airlift reactor and the performance of these two reactors were compared in terms of productivity and yield. Bergault et al.[33] investigated the kinetics of hydrogenation of acetophenone using 3%Rh/C catalyst with cyclohexane as the solvent. Various possible Langmuir-Hinshelwood type of rate models were considered and a rate model based on non-dissociative adsorption of hydrogen and non-competitive adsorption of the liquid phase components and the gaseous hydrogen was found to fit well the experimentally observed concentration-time profiles.

Most of the earlier literature on hydrogenation of p-isobutyl acetophenone (p-IBAP) is patented and there are only a few reports, dealing with the catalytic reaction mechanism, kinetic modeling and reaction engineering aspects. The previous work on hydrogenation of p-IBAP is also summarized in Table 1.2. The reaction scheme follows a path similar as shown in Figure 1.1. Detailed investigation on the hydrogenation of p-IBAP has been very limited in the literature. Rajashekharam and Chaudhari[41] investigated the kinetics of hydrogenation of p-IBAP using 10%Ni/HY catalyst in a semi-batch slurry reactor for a temperature range of 373-413 K. The effect of hydrogen partial pressure, initial concentration of p-IBAP, catalyst loading and catalyst pellet size on the concentration-time profiles was investigated. A Langmuir-Hinshelwood type of rate model based on non-dissociatively adsorbed hydrogen reacting directly with the organic

species present in the liquid phase was found to explain well the experimentally observed results. The kinetic parameters and activation energies were estimated.

1.2 Multiphase Reactors for Hydrogenation

Hydrogenation of organic compounds often involves multiphase catalytic reactions in which contacting of a gas (H_2), liquid (organic substrate) and solid (catalyst) phases are involved. The most common hydrogenations fall into the category of three phase (gas-liquid-solid) reactions. These processes are carried out in slurry or fixed bed reactors in a batch or continuous operation. The overall performance of these reactors depends on the inter phase mass transfer, intrinsic kinetics of reaction, physicochemical properties and mixing of the fluid phases. A theoretical analysis of the kinetic model, overall rate of reaction incorporating contribution of external as well as intraparticle mass transfer as well as reactor models has been extensively studied and the details are available in monographs by Ramachandran and Chaudhari[3] and Shah[47] and in reviews by Chaudhari and Ramachandran,[48] Doraiswamy and Sharma,[4] Chaudhari et al.[49], Mills et al.[5] and Mills and Chaudhari.[2] In this part, a brief review of the principal multiphase reactor types and current state of development on modeling of multiphase slurry and fixed bed reactors has been presented including experimental validation of reactor performance models.

1.2.1 Agitated Slurry Reactors

The agitated slurry reactors are most commonly used in industrial scales in liquid phase hydrogenation processes. In agitated reactors, the catalyst particles are used in a powder form and kept in suspension by means of mechanical agitation (Figure 1.3). Due to smaller catalyst particle size, intraparticle diffusional effects are negligible in these reactors. Also the overall mass and heat transfer efficiency is better than fixed bed reactors and these reactor are preferred for mass transfer limited reactions and those with high level of exothermicity.

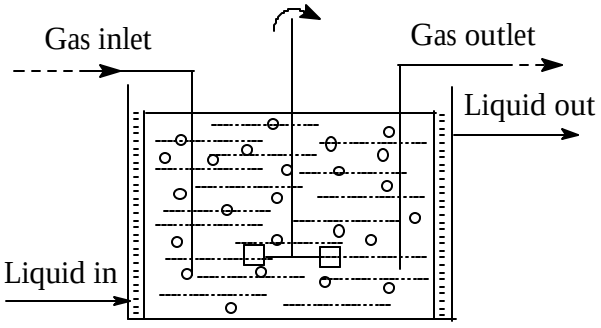

Figure 1.3: Mechanically Agitated Slurry Reactor

Many variation of these agitated slurry reactors are used in industry such as stirred reactors with multiple impellers and multiple gas injection points as shown in Figure 1.4. This is to ensure good mixing of reactants with minimum gas voidage.

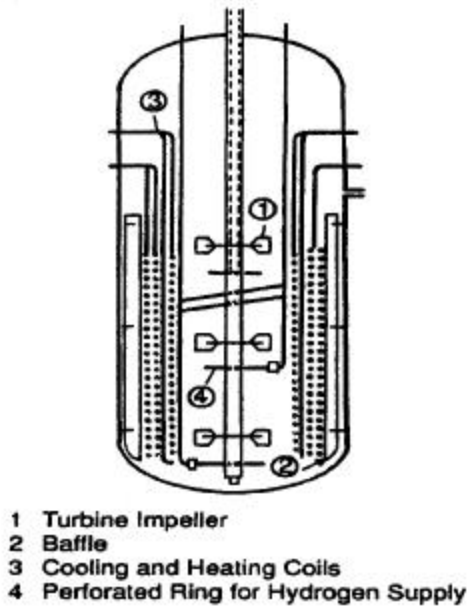

Figure 1.4: Stirred Reactor with Multiple Impellers and Gas Injection Points

The processes for small volume specialty chemicals are often operated in a batch mode. A dead-end operation with no discharge of hydrogen is very common for safety reasons and convenience. The agitated slurry reactors can also be operated in a semi-batch or continuous mode depending on the process requirement. The important design

parameters for agitated slurry reactors are selection of an agitator type, size, point of gas injection and the mode of heat removal which have a direct influence on gas-liquid and liquid-solid mass transfer and overall heat transfer efficiencies. It is also important to ensure that the catalyst particles are kept in complete and uniform suspension. Several correlations have been proposed for the estimation of mass transfer and heat transfer parameters, the details of which have been reviewed by Chaudhari and Ramachandran [48] and Ramachandran and Chaudhari.[3]

1.2.1.1 Models for Semi-batch Slurry Reactor

In a semi-batch operation of a three-phase reactor, the gas phase flow continuously through the system, while there is no net inflow or outflow of the liquid phase. These reactors find application in the manufacture of fine chemicals and pharmaceuticals where, small volume batch processes are involved. Also, these reactors are widely used for evaluating the catalyst performance of a three phase catalytic reaction and to obtain reliable data on the kinetics of a particular reaction. The design problem in a semi-batch slurry reactor is to predict the conversion of the liquid phase reactant as a function of time, so that the batch time of operation of such reactors can be fixed. Theoretical analysis of semi-batch slurry reactors was earlier presented by Chaudhari and Ramachandran,[48] Ramachandran and Chaudhari[3] for (1,0), (1,1) order kinetics and also in general for m-nth order kinetics. The equations for (1,1) order are:

$$t_B = \frac{B_{l_i} X_B}{\nu A^*}\left[\frac{1}{k_l a_B} + \frac{1}{k_s a_p}\right] + \frac{B_{li} R^2 \rho_p I}{3 A^* w D_e} \qquad (1.1)$$

Where,

$$I = \frac{2}{\phi_{oi}^2} \ln\left[\frac{\phi_{oi}\cosh\phi_{oi} - \sinh\phi_{oi}}{\phi_{oi}\sqrt{1-X_B}\cosh\phi_{oi}\sqrt{1-X_B} - \sinh\phi_{oi}\sqrt{1-X_B}}\right] \qquad (1.2)$$

with ϕ_{oi}, the Thiele modulus based on the initial concentration of B is given as,

$$\phi_{oi} = R\left[\frac{\rho_p k_{11} B_{l_i}}{D_e}\right]^{1/2} \qquad (1.3)$$

Some semi-batch reactor modeling and reaction engineering studies of complex hydrogenation reactions are summarized in Table 1.3.

Table 1.3: Summary of Reactor Modeling and Reaction Engineering Studies in Semi-batch Slurry Reactor

S. No.	**Hydrogenation system**	**Catalyst**	**Remarks**	**Reference**
1	Crotonaldehyde	Pd/Al_2O_3	Catalyst effectiveness factor determined	Kenney and Sedriks[50]
2	Chlorobenzene	Pt/C	Gas-liquid mass transfer important	Kawakami and Kusunoki[51]
3	Phenylacetylene	$0.5\%Pt/Al_2O_3$	Reactor modeling with intraparticle diffusional effects	Kawakami and Kusunoki[52]
4	Dimethylnitrobenzene	Pd/C	Kinetics and reactor modeling	Kut et al.[53]
5	Butenediol	$Pd\text{-}Zn\text{-}CaCO_3$	Kinetics and batch reactor modeling	Chaudhari et al.[54]
6	Phenylacetylene	Pd/C	Kinetics and reactor modeling	Chaudhari et al.[55]
7	Buytnediol	Pd/C	Kinetics and reactor modeling	Chaudhari et al.[56]
8	2-ethyl- 5,6,7,8 tetrahy -droanthraquinone	Pd/Al_2O_3	Reactor model incorporating both internal and external mass transfer resistance	Santacesaria et al.[57]
9	Furan amines	Rh/Al_2O_3	Kinetics and reactor design	Holm et al.[58]
10	Benzene	Ni	Kinetics, reactor modeling with intraparticle diffusion	Toppinen et al.[59]
11	1,5,9-cyclododecatriene	Pd/Al_2O_3	Kinetic modeling taking into consideration various isomers of the products	Benaissa et al.[60]
12	Acetophenone	3%Rh/C	Reactor modeling with intraparticle diffusional effects	Bergault et al.[33]
13	2,4-dinitrotoluene	10%Ni/HY	Intrinsic kinetics and reactor modeling	Rajashekharam and Chaudhari[61]

1.2.1.1.1 Non-Isothermal Effects in Slurry Reactors

Many industrially important hydrogenation reactions are exothermic in nature and hence understanding the non-isothermal behavior of slurry reactors is important for carrying out these reactions. In most of the reactions, the intraparticle temperature gradients and the temperature gradients between the catalyst and the gas-liquid phases may not be significant. However, the bulk liquid temperature is expected to change with residence time, thus affecting the rate of reaction due to changes in the kinetic parameters, solubility of the gas and other physical properties of the system. For a semi-batch reactor with reaction between a gas phase reactant A and liquid phase reactant B, and assuming that intraparticle diffusion effects are negligible, the following equation can be used to represent the material and heat balances.[3]

$$-\frac{d B_l}{d t} = \nu R_A = \nu A^*(T) \left[\frac{1}{k_l a_B} + \frac{1}{k_s a_p} + \frac{1}{W k_2(T) B_l}\right]^{-1} \quad (1.4)$$

and

$$(\varepsilon_g V_R \rho_g C_{Pg} + V_R(1-\varepsilon_g - \frac{w}{\rho_p})\rho_l C_{Pl} + V_R w C_{ps})\frac{dT}{dt} =$$

$$(-\Delta H) V_R A^*(T)\left[\frac{1}{k_l a_B} + \frac{1}{k_s a_p} + \frac{1}{W k_2(T) B_l}\right]^{-1} - U_W A_W (T - T_W) - Q_g \rho_g C_{pg} (T - T_g) \quad (1.5)$$

The initial conditions are, at t = 0, $B_l = B_{li}$ and $T = T_i$. The above equations can be solved numerically for B_l and T as a function of time. If the temperature change is large, the variation of k_L and k_S with temperature must also be considered. Non-isothermal modeling of semi-batch slurry reactors for exothermic reactions is rare in literature. Non-isothermal effects in slurry reactors have been reviewed by Ramachandran and Chaudhari.[3] Hydrogenation of m-nitrochlorobenzene to m-chloroaniline using sulphided platinum on carbon catalyst was studied by Rode and Chaudhari[62] in a semi-batch slurry reactor. It was observed that the rate of reaction was first order with respect to hydrogen partial pressure and was independent of the substrate concentration. At higher temperatures, gas-liquid mass transfer was found to be significant and the rate equations were solved incorporating the mass transfer effects. Experiments were carried out under non-isothermal conditions and hydrogen consumption-time profiles were found to match with a non-isothermal semi-batch reactor model developed. Another study under non-

isothermal conditions was for the hydrogenation of 2,4-dinitrotoluene using Pd/Al_2O_3 by Rajasekharam et al.[63] Apart from a detailed kinetic study, a non-isothermal slurry reactor model was developed to predict the H_2 consumption-time and temperature profile and compared with the experimental observations.

Jaganathan et al.[64] studied the hydrogenation of p-nitrocumene to p-cumidine over supported palladium catalyst in a laboratory-scale slurry reactor with the objective to demonstrate the methodology for development of a slurry reactor model that could predict either isothermal or non-isothermal performance using intrinsic kinetic and transport parameters that were determined from independent data and engineering correlations. The initial rate data showed that both the kinetic and mass-transfer resistances were important for higher temperatures, while the kinetic regime was controlling at lower temperatures. A Langmuir-Hinshelwood (L-H) model was proposed based on the rate data in the kinetic regime. The rate model was suitably modified to account for combined transport-kinetics resistances at higher temperatures. Using a basket reactor, intraparticle diffusion effects were also studied by transforming the catalyst powder used for the kinetic study into catalyst pellets. Equations for an overall catalyst effectiveness factor were derived for the L-H type rate model. The experimental data for different catalyst particles agreed well with the model predictions. To verify the applicability of the kinetic model over a wide range of conditions, a slurry reactor model was also developed for both isothermal and non-isothermal conditions.

1.2.2 Bubble Column Slurry Reactors

In the case of bubble column slurry reactors the particles are suspended by gas-induced agitation (Figure 1.5). The gas is dispersed through the liquid containing finely suspended catalyst particles. The reactor may be operated in a semi-batch manner for conversion of a liquid reactant or for continuous reaction between gaseous and liquid reactant. The advantages of these reactors include absence of moving parts, minimum maintenance, smaller floor space compared to agitated reactor and high liquid circulation rates leading to more efficient rates of heat transfer than in fixed beds. In addition, power consumption required is less than agitated reactors.

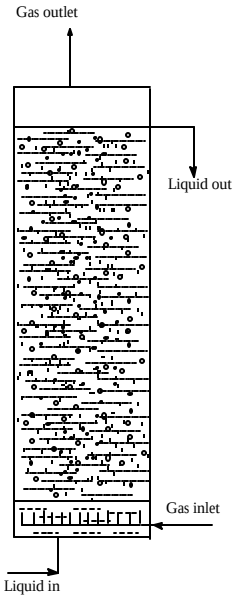

Figure 1.5: Bubble Column Reactor

As small particles sizes can be used, the intraparticle diffusional resistance is minimized and hence maximum utilization of the catalyst is possible. The disadvantages include the considerable back mixing of the liquid phase resulting in poorer reactor performance and when the gas is passed at atmospheric pressure, additional energy has to be spent to overcome the pressure drop in the column.[3] Ohorodnik et al.[65]designed a bubble column reactor for continuous operation with facilities for catalyst separation. Pruden and Weber[66] designed a bubble column reactor where catalyst and the liquid are recycled in the reactor by means of an external pump.

1.2.3 Loop Reactors

Loop reactors have been found to be attractive because of their high heat and mass transfer rates. These reactors find its application in hydrogenation of organic compounds and biochemical processes. Various types of loop reactors exist and its hydrodynamics and mass transfer have been reviewed by Blenke,[67] Chaudhari and Shah[68] and Chaudhari et al.[49] Loop reactors are mainly of two types (a) internal recirculation type and (b) external recirculation type[49] as shown in Figure 1.6.

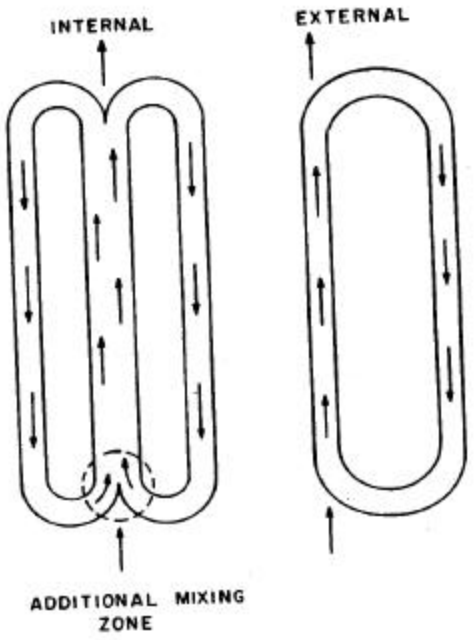

Figure 1.6: Jet Loop Reactors with Internal and External Recirculation

In internal recirculation type, the circulation flow can be created around a draft tube which is positioned concentrically in a slim tower reactor and which directs the coaxial circulation flow through the entire reactor volume. The circulation flow is created by a liquid jet injector, an airlift device or a propeller. External recirculation-type reactors are particularly useful for efficient heat removal. The most commonly used loop reactors are the jet loop reactors where in a liquid jet is injected with a very high velocity through at least one liquid nozzle either from the top or the bottom of the reactor. Blenke[67] proposed an internal recycle loop reactor where the liquid jet forces flow around the draft tube by momentum transfer and flows continuously out of the system as a super-imposed through flow. In batch operation it is completely recycled to the liquid nozzle by an external closed pump cycle. Gas can be introduced through a ring nozzle arranged concentric to liquid jet. The liquid jet causes not only the circulation drive but also very efficient primary dispersion of the gas and solid catalyst.[49] The most popular version of the jet loop reactor is developed by Buss Engineering Co.[69] Here the ejector nozzle is fixed at the top of the reactor and external circulation flow is normally selected. The nozzle acts as an eductor and the action of the slurry passing through creates intimate gas-liquid-solid mixing[49] (Figure 1.7).

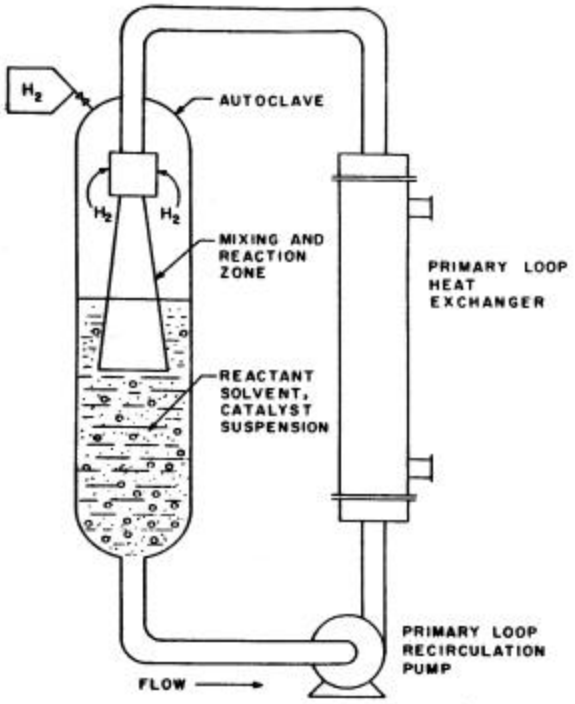

Figure 1.7: Buss Jet Loop Reactor

The chemical reaction take place mainly inside the nozzle and the autoclave acts mainly as a holding vessel. By means of a external heat exchanger, uniform temperature can be maintained, even for highly exothermic reactions.

1.2.4 Fixed Bed Reactors

In this type of reactors, the gas and the liquid phase flow over a fixed bed of catalysts. The fixed bed reactors can be classified into mainly three types (i) co-current down-flow of both gas and liquid phase (ii) downward flow of liquid with gas in the countercurrent upward direction and (iii) co-current up-flow of gas and liquid and these reactors are shown in Figure 1.8. Reactors with co-current down-flow of gas and liquid is called as trickle bed reactors (TBR) and the co-current up-flow reactors are also referred to as packed bubble column reactors.

Trickle bed reactors, wherein, the liquid reactant trickles down concurrently along with the gaseous reactant, over a fixed bed of catalyst pellets finds its application in wide variety of chemical, petrochemical and biochemical processes along with its application in waste water treatment. The examples of application of trickle bed reactors are given in

detail in several monographs.[70,71,72,73] This include oxidation, hydrogenation, isomerisation, hydrodesulfurisation, hydroprocessing, decomposition of hydrogen peroxide, deuterium exchange between hydrogen and water to produce heavy water, [74] adsorption of benzene from water on activated carbon particles,[75] hydration, catalytic dewaxing of lube stock [76] etc.

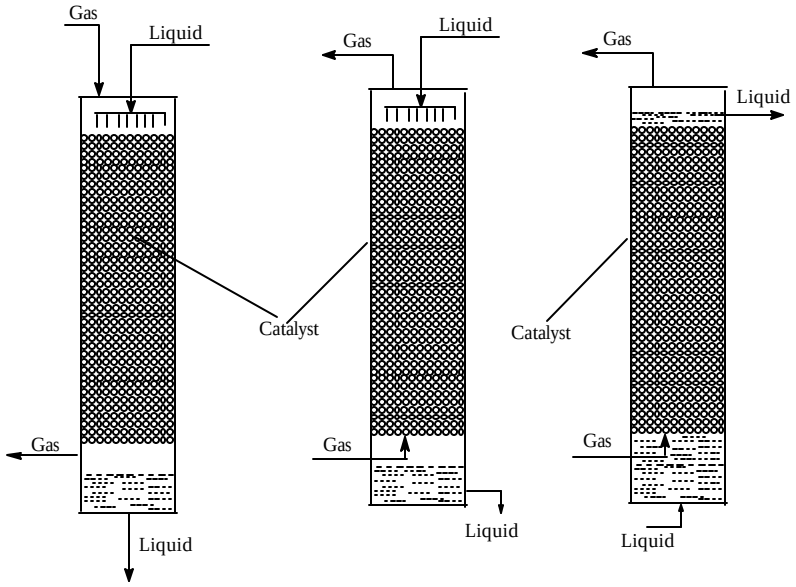

Figure 1.8: Fixed Bed Reactors (a) Trickle Bed Reactor (b) Countercurrent Reactor and (c) Up-flow or Packed Bubble Column Reactor

Fixed bed up-flow reactors, wherein, gaseous and liquid reactants co-currently flow upwards over a fixed bed of solid catalysts finds its application in wide variety of industrial processes. This include hydrodesulfurization of petroleum fractions, liquid phase hydrocracking, hydrogenation of nitro compounds, amination of alcohols, ethynylation of formaldehyde in butynediol synthesis, waste water treatment etc.[3,77] This type of reactor is mainly used when comparatively small amount of gas has to be processed with large amount of liquid and when a higher residence time for the liquid phase is required. The fixed bed up-flow reactor has the advantage of completely wetted catalysts due to its high liquid holdup. This can provide a better mass transfer and heat transfer between the liquid phase and the solid catalyst though it has the disadvantage of enhanced external mass transfer resistance. Various parameters affecting the reactor

performance of trickle bed reactors and fixed bed up-flow reactors and the details of reactor design will be discussed in later sections.

1.2.4.1 Trickle Bed Reactors

Of the various hydrodynamic, mass and heat transfer parameters that influence the trickle bed reactor performance, the flow regimes existing and the partial wetting of the catalysts inside the reactor constitute the special characteristic of the reactor.

1.2.4.1.1 Flow Regimes

The flow pattern in a trickle bed reactor can be identified as four regimes: (i) trickling flow, (ii) pulsing flow, (iii) spray flow and (iv) bubble flow and has been diagrammatically represented by Ng and Chu[78] as shown in Figure-1.9.

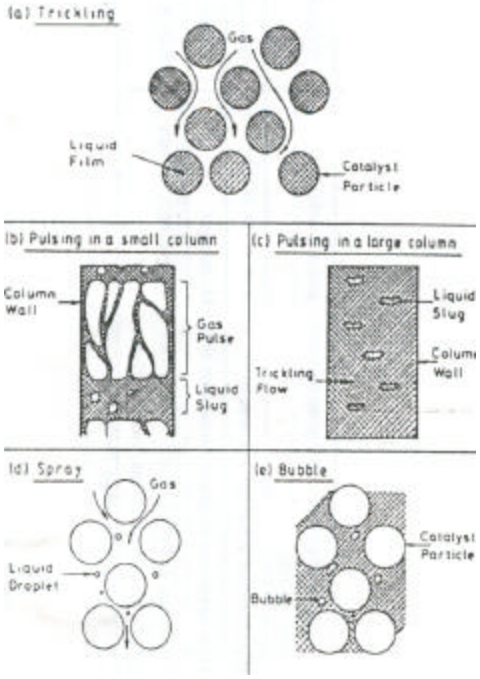

Figure 1.9: The Flow Regimes in a Trickle Bed Reactor

The trickling flow regime is observed at low gas (0.02 to 0.45 m/s) and liquid velocities (10^{-4} to 3 x10^{-3} m/s), where the liquid flow down the bed over the catalyst particles in the form of rivulets and films and the gas phase occupies the remaining space (Figure 1.9. (a)). Pulsing flow regime occurs at relatively high gas and liquid velocities and is

represented by formation of liquid slugs that have higher liquid content than the remainder of the bed. In columns of small diameter, the liquid slug and gas pulses pass down the column (Figure 1.9. (b)). The liquid slugs contain gas bubbles and the gas pulses contain some amount of liquid in it. There exists an exchange of mass between the liquid slug and gas pulse. In the case of large columns, multiple slugs are observed (Figure 1.9. (c)). Spray flow regime is observed at high gas velocities and low liquid velocities. The liquid phase in this regime is carried down the bed in the form of droplets by the continuous gas phase (Figure 1.9. (d)). At high liquid velocities and low gas velocities, the bed is filled with liquid and the gas phase passes down in the form of elongated bubbles and is called as bubble flow regime (Figure 1.9. (e)).

1.2.4.1.2 Catalyst Wetting Efficiency

Catalyst wetting efficiency is one of the most important parameters in the designing of trickle bed reactors, since it represents the extent of utilization of the catalyst particles. Wetting efficiency of catalyst particles can be of two types; (i) internal wetting efficiency and (ii) external wetting efficiency

1.2.4.1.2.1 Internal Wetting Efficiency

This is the measure of the amount of internal area of the catalyst available for the liquid reactants. Colombo et al.[79] measured the internally wetted area of the catalyst particles and concluded that even at lower liquid velocities like 5.0×10^{-4} m/s, the catalyst are internally wetted by the capillary forces. But this won't be the case for reactors with poor liquid distributor, where channeling and liquid maldistribution can lead to lower internal wetting.

1.2.4.1.2.2 External Wetting Efficiency

This is the area of the catalysts wetted externally by the liquid. The reaction rates under conditions of partially wetted catalysts can be higher or lower than under conditions of full catalyst wetting depending on whether the gas phase or the liquid phase components are rate limiting. Under conditions of gaseous phase limitations, the partial wetting of the catalysts results in enhancement in reaction rates, by the direct mass transfer from the gaseous phase to the solid catalyst, thereby eliminating the external

mass transfer resistances. If the reaction is limited by liquid phase and the liquid phase is non-volatile, then decrease in liquid-solid contacting will reduce the surface area for liquid-solid mass transfer and thus reduce the reaction rates. But, if the liquid reactants are volatile and significant heat effects are also present, then a gas phase reaction can occur in the dry catalyst part triggering up the reaction rates. Many correlations exist in literature for the determination of wetting efficiency of the catalyst and have been reviewed by Satterfield,[70] Shah Y.T.,[71] Herskowitz and Smith,[80] Ramachandran and Chaudhari,[3] Gianetto and Specchia,[81] Saroha and Nigam[73] and Al-Dahhan et al.[72] Recent studies are focused on incorporating the effect of pressure on the catalyst wetting efficiency. Al-Dahhan and Dudukovic[82] investigated the effect of pressure on the wetting characteristics and developed a semi-empirical model, incorporating the effect of reactor pressure and gas velocity and can be given as:

$$f_w = 1.104(\mathrm{Re}'_L)^{\frac{1}{3}}\left[\frac{1+(\Delta P/Z)/\rho_L g)}{Ga'_L}\right]^{\frac{1}{9}} \qquad (1.6)$$

It was found that for a constant liquid velocity, higher pressure and higher gas flow rates improves the wetting efficiency. This is due to the improved spreading of the liquid hold up over the external packing area as a result of the increase in the shear stress on the gas-liquid interface by means of higher pressure or gas velocity.

Other important parameters which influence the reactor performance include, pressure drop, liquid holdup, gas-liquid mass transfer coefficient, liquid-solid mass transfer coefficient and the heat transfer parameters such as effective thermal conductivity and bed to wall heat transfer coefficient. Various correlations exist in the literature for calculating all these parameters and have been reviewed from time to time in various monographs like Satterfield,[70] Hofman,[119] Shah Y.T.,[71] Herskowitz and Smith,[80] Ramachandran and Chaudhari,[3] Gianetto and Specchia,[81] Saroha and Nigam[73] and Al-Dahhan et al.[72] Recently, Lamine et al.[83] have published a detailed investigation on the heat transfer properties of both up-flow and down-flow mode of operations.

1.2.4.1.3 Modelling of Fixed Bed Reactors

For the purpose of modelling of continuous reactors, in addition to chemical reaction and transport effects, the variation of the reactant / product concentration along

the length of the reactor and the degree of mixing of the two phases have to be considered. Also, additional complexities can exist in trickle beds due to incomplete wetting of catalyst particles. In this section, modelling of continuous reactors has been presented assuming complete wetting of catalyst particles and uniform distribution of the catalyst.

For a psuedo-first order reaction, when one of the reactant concentrations is in excess and while the rate is first order with respect to the limiting reactant (A) and for constant gas phase concentration, the following equation represents the mass balance for A.[3]

$$\frac{1}{P_e}\left(\frac{d^2 a_l}{dz^2}\right) - \frac{da_l}{dz} + \alpha_{gl}(1 - a_l) = \alpha_{gs}(a_l - a_s) = \alpha_r \eta_c a_s \qquad (1.7)$$

The characteristic dimensionless parameters are given in Table 1.4.

Table 1.4: Dimensionless Parameters Used in Continuous Reactor Models

Parameter	Notation	Definition
Gas to liquid mass transfer coefficient	α_{gl}	$k_l a_B L / u_l$
Liquid to solid mass transfer coefficient	α_{ls}	$k_s a_p L / u_l$
Reaction rate constant for an m-nth order reaction following power law	α_r	$w k_{mn} (A^*)^{m-1} (B_{li})^n L / u_l$
Dimensionless concentration	a_l	A_l / A^*
Back mixing of the phase	Pe	$U_l L / De_l$

As Pe tends to infinity, the model reduces to a case of plug flow of liquid phase. The above equation then reduces to,

$$\frac{da_l}{dz} + (\alpha_{gl} + \beta_{ls}) a_l = \alpha_{gl} \qquad (1.8)$$

with the boundary conditions given as,

at, $z = 0$ $\quad a_l = a_{li}$

The solution of equation for the plug flow model can be given as,

$$a_l = \frac{\alpha_{gl}}{(\alpha_{gl} + \beta_{ls})} + \exp[-(\alpha_{gl} + \beta_{ls})z]\ (a_{li} - \frac{\alpha_{gl}}{\alpha_{gl} + \beta_{ls}}) \quad (1.9)$$

Where $\beta_{ls} = \frac{h_c \alpha_r \alpha_{ls}}{\alpha_{ls} + h_c \alpha_r}$ (1.10)

The case when Pe tends to zero represents the situation where the liquid phase is completely back mixed. Here, the liquid concentration is uniform throughout the reactor and may be assumed to be constant and equal to the outlet concentration, A_{lf}. The mass balance for species A for the liquid phase can now be written as,

$$Q_l(A_{li} - A_{lf}) + V_R k_l a_B (A^* - A_{lf}) = V_R k_s a_p (A_{lf} - A_s) = V_R W h_c k_1 A_s \quad (1.11)$$

Eliminating A_s from the above equation and solving the resultant equation for A_{lf} and non-dimensionlising, we obtain the back mixed model.

Theoretical analysis for the constant gas phase concentration with the limiting reactant in the liquid phase and varying gas phase concentration with limiting reactant in gas phase as well as for the liquid phase have been addressed in detail by Ramachandran and Chaudhari.[3] These authors have developed equations for the calculation of the reactor efficiency for plug flow as well as back mixed case for co-current as well as counter current operation in continuous reactors. A review of previous work on trickle bed reactor modeling is presented in Chapter 3, Section 3.0.

1.2.4.1.3.1 Reactor Performance and Model Evaluation Studies in TBR

Many of the industrially important reactions involve complex reaction network and may also be highly exothermic. Hence, detailed investigation of such complex multi step reactions and other reactor parameters which influence reactor performance for such reactions are looked forward. Most of the trickle bed reactor performance studies reported in literature are under isothermal conditions and involve simple reaction schemes. Investigation of TBR performance along with model validation for important complex multi step reactions is scarce in literature.[84,85,86,87] Recent investigations into performance studies and model validation are presented in the Table 1.5. Most of the studies were carried out under isothermal conditions and have considered pseudo-homogeneous model or heterogeneous models with plug flow of both gas and liquid phases. In most of the trickle bed reactor studies carried out at low liquid velocities,

partial wetting of the catalyst was observed resulting in enhanced rates by the direct transfer of gaseous limiting reactant from the gas phase to the internally wet catalyst particles.[86,88] It was observed generally that under conditions of gas phase reactant limitation, the rates decreased with increase in liquid velocity due to higher catalyst wetting at higher liquid velocities and hence reduced direct gas-solid mass transfer. Under conditions of liquid phase reactant limitation, the rates were found to decrease with lower wetting due to decrease in effective liquid-solid contacting. Al-Dahhan and Dudukovic[107] achieved an improvement in the performance of trickle bed reactor operating under conditions where limiting reactant is in the liquid phase by the use of fines. The addition of fines improved the liquid-solid contacting efficiency and a corresponding increase in the rate was observed. Rajasekharam et al.[89] investigated the importance of static liquid holdup in determining the reactor performance and found that the effect is not predominant. Other reactor models used for predicting the reactor performance include mixing cell model [90,91] and cross-flow model.[3]

Some recent studies and observations in trickle bed reactors where performance studies and model evaluation have been carried out are summarized in the sections below.

Hydrogenation of benzaldehyde to benzyl alcohol was studied in a slurry reactor using nickel catalysts by Herskowitz[92] and the Langmuir – Hinshelwood type of kinetic model developed was used to predict the performance of a trickle bed reactor for the above mentioned reaction. A completely wetted catalyst model was developed and all the mass transfer resistances were considered in the model assuming that hydrogen is the rate limiting reactant. The study was carried out for a varying range of gas velocity, temperature and pressure. The effectiveness factor was found to be very low indicating the presence of strong intraparticle mass transfer resistance. The gas-liquid mass transfer was found to be important, whereas the liquid-solid mass transfer was found to be negligible. It was concluded that slurry reactor was a better choice than a trickle bed reactor for such high rate reactions.

Table 1.5: Investigations of TBR and Fixed Bed Up-Flow Reactor (UFR) Performance Along with Model Validation

S. No.	Reaction / Reactor	Rate Analysis	Model Assumptions	Reference
1	H_2O_2 decomposition / TBR	Linear kinetics	Isothermal, partial wetting, 2-region cell model	Sims et al.[93]
2	Hydrogenation of C_4 olefins /UFR	L-H kinetics	Isothermal, plug flow	Vergel et al.[94]
3	Hydrogenation of 3-hydroxypropanal /TBR	L-H kinetics	Isothermal, plug flow, partial wetting, heat balance	Valerius et al.[95]
4	Hydrotreating of vacuum gas oil /TBR	L-H kinetics	Isothermal, plug flow, partial wetting	Korsten and Hoffmann[96]
6	Hydrogenation of α-methyl styrene /TBR	L-H kinetics	Isothermal, plug flow, partial wetting, high pressure	Khadilkar et al.[88]
7	Selective hydrogenation of 1,5,9-cyclododecatriene / UFR	Linear kinetics	Isothermal, axial dispersion, high pressure/temperature	Stuber et al.[97]
8	SO_2 oxidation /TBR	L-H kinetics	Isothermal, full wetting	Ravindra et al.[98]
9	SO_2 oxidation/ TBR/ UFR	L-H kinetics	Isothermal, partial wetting, axial dispersion, static-dynamic	Iliuta and Iliuta[99]

10	Phenol oxidation /TBR	L-H kinetics	Isothermal, full wetting, plug flow, high pressure/ temp.	Pintar et al.[100]
13	Hydrogenation of α-methyl styrene /TBR	Linear kinetics	Isothermal, plug flow, partial wetting	Castellari et al.[101]
14	Hydrogenation of acetophenone /TBR	L-H kinetics	Non-isothermal, plug flow, full wetting, high pressure/temp.	Bergault et al.[46]
15	Hydrogenation of unsaturated ketones in supercritical CO_2 /TBR	Power law kinetics	Non-isothermal, plug flow, full wetting	Devetta et al.[102]
16	Hydrogenation of 3-hydroxy propanal	L-H kinetics	Non-isothermal, deactivation, partial wetting, plug flow	Zhu and Hofmann[103]
17	Hydrogenation of 2,4-dinitrotoluene /TBR	L-H kinetics	Non-isothermal, plug flow, partial wetting, stagnant liquid	Rajasekharam et al.[89]
18	Hydrogenation of α-nitromethyl-2-furanmethanol /TBR	L-H kinetics	Isothermal, plug flow, partial wetting	Jiang et al.[104]
19	Oxidation of substituted phenols /TBR	Linear kinetics	Isothermal, plug flow	Tukac and Hanika[105]
21	Hydrogenation of maleic anhydride / UFR	L-H kinetics	Isothermal, axial dispersion, full wetting	Herrmann and Emig[106]

The impact of partial external wetting and liquid-vapor phase equilibrium on the catalyst performance was investigated for the hydrogenation of naphthalene over Pt/Al_2O_3 catalyst in a trickle bed reactor by Huang and Kang[86] using solvents of varying volatility. When the gas-liquid flow ratio was increased, the wetting efficiency of the catalyst particles decreased thus enhancing the reaction rates through direct gas-solid mass transfer. In order to understand the effect of solvent volatility on the reactor performance, naphthalene was dissolved in various solvents like n-hexadecane, n-dodecane and n-octane and the effect of gas velocity on the reactor performance under varying gas velocities were studied and observed that the rate of hydrogenation increased with increasing hydrogen flow rate. It was proved experimentally as well as theoretically that the lighter the solvent feed, more the extent of solvent evaporation with increasing gas flow rate. However it was found that the concentration of hydrogen in the liquid phase is nearly independent of the gas flow rate.

In an effort to represent the performance of a trickle bed reactor for the hydrogenation of 3-hydroxypropanal to 1,3-propanediol, Valerius et al.[95] considered two different approximations of the overall catalyst effectiveness factor. (1) the effectiveness factors of dry, half wetted and totally wetted slabs were weighted as proposed by Beaudry et al.[107] and (2) a new cylinder shell model was used, leading to one-dimensional mass balance equations inside the porous catalyst particle for all possible values of the external wetting efficiency on the particle scale. The aim of the investigation was to study the role of mass transfer and degree of wetting on the trickle bed reactor performance. It was found that, both the above mentioned parameters affect the reaction rates. For both the two models, parametric values of $f_w = 0.6 - 1.0$ lead to a higher pressure dependence and on increasing the liquid velocity a maximum in the reaction rate was observed. A three-phase reactor model for hydrotreating reactions in a pilot trickle bed reactor was developed by Korsten and Hoffmann.[96] The model based on the two-film theory, was tested with regard to the hydrodesulfurization of vacuum gas oil in a high pressure pilot plant reactor under isothermal conditions. The axial dispersion in both phases were found to be negligible and various mass transfer coefficients, gas solubility and other properties of the gas as well as the liquid phases were determined using various correlations. The kinetics of the reaction was represented by a Langmuir-Hinshelwood model and the

intraparticle mass transfer within the catalyst pellets were represented by catalyst effectiveness factor. The sulfur content of the product oil was found to depend strongly on the gas/oil flow ratio within the reactor. The poor conversion observed was explained with regard to the incomplete catalyst wetting properties. The simulation showed good agreement with the experimental values for a wide range of temperature, pressure, space velocity and gas/oil ratio.

Castellari et al.[101] studied the hydrogenation of α-methyl styrene to cumene over Pd/Al_2O_3 in a laboratory trickle bed reactor operated at low liquid velocities. Under these conditions, the catalyst pellets were incompletely wetted and also vaporization of liquid phase reactants was observed. The presence of gas-solid catalysis enhanced the reaction rate significantly. To improve the mass transfer between the phases, the length of inert post packing section was increased and the inert phase acted as an absorber of cumene produced in gas-phase. Experimental global rates determined from the liquid cumene concentrations varied with the post packing length. A one dimensional model taking into consideration three different zones, first pre-packing inert zone where H_2 getting saturated with α-methyl styrene, catalytic bed and post packing inert section acting as an absorber of the gas phase cumene produced, was found to agree well with the observed experimental results.

Liquid phase hydrogenation of acetophenone using Rh/C catalyst was studied by Bergault et al.[46] in trickle bed reactor and slurry airlift reactor and the performance of these two reactors were compared in terms of productivities and yields. For modeling trickle bed reactor performance, a non-isothermal plug flow reactor model incorporating the external and intraparticle mass transfer effects was developed. It was assumed that the catalyst was fully wetted and the mass and heat transfer correlations were estimated using various correlations available in the literature. It was concluded that the available correlations for gas-liquid mass transfer are not satisfactory and catalyst wetting is an important process that cannot be neglected in the modeling and intraparticle diffusional effects played an important role in determining the reactor efficiency.

Rajasekharam et al.[89] reported the experimental verification for a non-isothermal trickle bed reactor model for the hydrogenation of 2,4-dinitrotoluene using $5\%Pd/Al_2O_3$ catalyst, incorporating the partial wetting of the catalyst as well as the stagnant liquid

hold up. It was assumed that the catalyst can be divided into three zones, where the catalyst is exposed to dynamic liquid flow, static liquid pockets and exposed to gas phase. The external mass transfer effects and intraparticle diffusional effects of the gaseous reactant hydrogen was taken into consideration in the model and a Langmuir-Hinshelwood type of rate model was used to describe the intrinsic kinetics of the reaction. The effect of various parameters like liquid velocity, gas velocity, temperature and catalyst particle size on rate of hydrogenation, conversion and temperature rise inside the reactor was investigated. It was found that on increasing the liquid velocity, even though the conversion became low, the global rate of hydrogenation increased. The effect of gas velocity on the reactor performance was found to be negligible. The sensitivity of the model to gas-solid mass transfer, gas-liquid mass transfer, liquid-solid mass transfer and the role of stagnant liquid pockets were also investigated. It was found that the importance of parameters in the descending order was gas-solid > gas-liquid > liquid-solid and also concluded that the contribution by stagnant liquid pockets was negligible.

Another detailed study of a complex hydrogenation in a trickle bed reactor is the manufacture of a herbicide intermediate α-aminomethyl-2-furanmethanol from α-nitromethyl-2-furanmethanol using Raney nickel catalysts presented in two parts by Jiang et al.[104] and Khadilkar et al.[85] The first part deals with the experimental investigation of the effect of operating parameters on yields and productivity in a trickle bed reactor. It was found that liquid trickle flow pattern was preferable in getting the desired product, due to its high ratio of catalyst to liquid volume. For the given catalyst and under a particular operating pressure, the yield of the desired product improved by decreasing the feed concentration of substrate and by decreasing the liquid flow rate. Lower temperatures also lead to improvement in desired product selectivity and diluting the bed with solid fine particles resulted in a better utilization of the catalyst. In the second part, a kinetic scheme for the complicated reaction was developed and based on a trickle bed reactor model and parameter optimization programs, kinetic constants were obtained using the experimental data obtained.

Enhancing the reactor performance by using various techniques have been of great research interest in recent years. The periodic operation of liquid in trickle bed reactor has shown to enhance the reaction rate in the case of a gas limited reaction.[108] The

liquid flow on switching off, results in draining of the catalyst bed and thus reducing the mass transfer resistance offered by the liquid phase and facilitates the direct mass transfer from the gas phase to solid phase. The effect of such a periodic flow reversal for the oxidation of SO_2 under conditions of gas limitations were studied by Haure et al[109] and found an increase in reaction rate in the range of 30-40%. If the reaction is exothermic, such a break in liquid flow results in poor heat dissipation resulting in a temperature rise in bed thus further enhancing the reaction rate.[110] By exploiting the exothermicity of the reaction, Castellari and Haure[111] were able to get a drastic increase of about 400% in rate for hydrogenation for alpha methyl styrene (AMS) over palladium catalyst. Formation of controlled hotspots and evaporation of liquid phase leading to partial gas phase reaction were responsible for such a rate enhancement. Al-Dahhan and Dudukovic[112] achieved an improvement in the performance of trickle bed reactor operating under conditions where limiting reactant is in the liquid phase by the use of fines. The addition of fines improved the liquid-solid contacting efficiency and a corresponding increase in the rate was observed.

1.2.4.2 Fixed Bed Reactor with Co-Current Up-Flow

In fixed bed reactors with co-current up-flow of gas and liquid, the existence of different flow regimes was first indicated by Eisenklam and Ford.[113] They distinguished between two main flow regimes (i) single-phase pore flow at low gas flow rates and (ii) two-phase pore flow at higher gas flow rates. Turpin and Huntington[114] showed the existence of three distinct flow regimes (i) spray flow (ii) bubble flow and (iii) slug flow. The spray flow regime occurs at low liquid to gas flow rates and represents the condition where gas is the continuous phase and liquid is the dispersed phase. The bubble flow is characterized by the continuous flow of gas bubbles through the liquid and slug flow is characterized by alternate portions of more dense and less dense phases passing through the column which occurs generally for gas velocities higher than 7-10 $x10^{-2}$ m/s. Specchia et al.[115] also identified these flow regimes. Fukushima and Kusaka[116] suggested more flow regimes for packed bed with co-current up-flow. The main difference between this and the flow regimes suggested by Turpin and Huntington[114] was that the transition regimes were also identified. Iliuta and Thyrion[117] studied the flow regime transition for

up-flow reactors and suggested that the transition between the bubble and pulse flow regimes is unclear. The flow regime transition they observed and that superimposed on the flow regime diagram suggested by Turpin and Huntington[114] is shown in Figure 1.12.

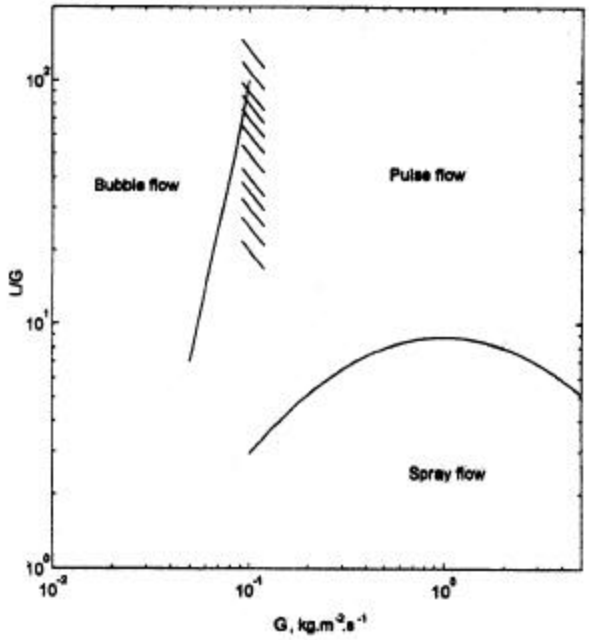

Figure 1.12: Flow Regimes in Fixed Bed Up-Flow Reactor (Iliuta and Thyrion[117])

The wetting efficiency of the catalysts in an up-flow reactor is assumed to be one. There are also reports where wetting efficiency of the catalyst was assumed less than one.[118] In such cases it was assumed that some part of the gas, which passes through the reactor, comes into direct contact with the catalyst particles and direct transfer of mass from the gas phase to the catalyst particle takes place. Various correlations exist in the literature for calculating other important parameters which influences the reactor performance and they include, pressure drop, liquid holdup, gas-liquid mass transfer coefficient, liquid-solid mass transfer coefficient and the heat transfer parameters which had been reviewed by Hofmann,[119] Shah Y.T.[71] and Ramachandran and Chaudhari.[3] Unlike trickle bed reactors detailed review on fixed bed up-flow reactors, covering the hydrodynamic, mass and heat transfer parameters is missing in the recent literature.

1.2.4.2.1 Up-Flow Reactor Studies and Model Evaluation

Reactor performance studies in fixed bed up-flow reactors are less compared to that of trickle bed reactor studies. Some of the studies carried out are enlisted in Table

1.6. The fixed bed up-flow reactor has the advantage of completely wetted catalysts due to its high liquid holdup. But it has the disadvantage of enhanced external mass transfer resistance. Al-Dahhan and Dudukovic[112] and Wu et al.[133] has shown that under conditions of liquid phase reactant limitation up-flow reactor outperform trickle bed reactor due to it's efficient liquid-solid contact. This higher liquid holdup and liquid-solid effective contact also results in a better heat dissipation in case of exothermic reactions and can be advantageous in reactions where temperature dependence of selectivity is sensitive.

For better catalyst life and cycle efficiency, up-flow reactor can be used in view of effective temperature control due to it's better heat transfer properties as shown by Ragaini and Tine[120] for the hydrogenation of diolefin compounds in pyrolysis gasoline. Mochizuki and Matsui[121] studied the selective hydrogenation of phenyl acetylene and styrene in an up-flow reactor using supported palladium catalyst and also investigated the various parametric effects like substrate concentration, temperature and pressure on the reactor performance. It was found that hydrogen was rate controlling in most cases and diffusional effects of phenyl acetylene was also important at it's lower concentrations. Herrmann and Emig[106] investigated the liquid phase hydrogenation of maleic anhydride using various copper based catalysts and a three-phase reactor model was developed to explain the influence of temperature, pressure, liquid feed rate, size of catalyst pellets and inlet feed concentrations on the reactor performance. Stuber et al[97] studied the partial hydrogenation of 1,5,9-cyclododecatriene in a fixed bed up-flow reactor and found that by increasing the gas flow rate, increased g-l mass transfer and also efficient heat transfer was possible. Higher reactor length was simulated by splitting up the process in two steps resulting in the significant improvement in selectivity. Van Gelder et al.[122,123] described a reactor model for the hydrogenation of 2,4,6- trinitrotoluene in an up-flow reactor in the presence of an evaporating solvent to absorb the heat of reaction. It was shown that a model incorporating dispersion of gas phase represents the experimental data better compared to a plug flow model.

Design aspects of co-current up-flow reactors were reviewed by Hofmann,[119] Ramachandran and Chaudhari[3] and Shah.[47] The generally used reactor model for fixed bed up-flow reactor is steady state, isothermal, heterogeneous, one dimensional model taking into consideration the back mixing of the phases involved. Dynamic models,

which can predict the startup and sudden changes in the reaction parameters on the performance of the reactors, applied for industrially important reactions are rare. Julcour et al.[124] have investigated the dynamic aspects for the hydrogenation of 1,5,9-cyclododecatriene using a Pd/Al_2O_3 catalyst incorporating resistance to heat and mass transfer at the gas-liquid and liquid-solid interfaces and the model predictions were compared with the experimental observations under varying gas and liquid velocities. Visser et al.[125] had investigated the influence of forced periodic oscillations of the gas phase component for the hydrogenation of phenyl acetylene based on a heterogeneous model considering both the transient mass balance over the reactor length as well as accumulation inside the catalyst pellets.

1.2.4.3 Comparison of Down-flow and Up-flow Mode of Operation

There are only few comparison studies on performances of up-flow and down-flow mode of operations applied to industrially important reactions. Goto et al.[126,118] studied successively the oxidation of ethanol and the hydration of an olefin at atmospheric pressure in the down-flow and up-flow modes. They concluded that the trickle-bed is more efficient at low gas and liquid velocities, because of the partial catalyst wetting leading to an enhanced transfer of the gaseous reactant. de Wind et al.[127] have evaluated the performance of hydrotreating catalysts in up-flow and down-flow fixed bed reactors. They found that the catalyst utilization was poor in bench sale reactors compared to commercial reactors, due to the lower mass velocities of liquid in the test reactors (bench scale). They also found that up-flow operation resulted in a better utilization of the catalyst, comparable to those in commercial reactors. Larachi et al.[128] have measured the liquid saturation in fixed bed reactors operated under higher pressures in concurrent up-flow and down-flow fixed bed reactors. They found that for up-flow, the saturation was greater than for the down-flow regardless of the operating pressure. However, in the pulsing flow regime an asymptotic value was observed for both flows. For a given mass flow rate, the liquid saturation increased with pressure but decreased when the liquid viscosity was decreased independently of the direction of flow or operating pressure. Yang et al.[129] have compared the hydrodynamics of up-flow and down-flow packed bed reactors and concluded that the hydrodynamic characteristics such

as pressure drop, and liquid hold up are similar for both up-flow and down-flow reactors in the high interaction regime. Vergel[130] investigated the selective hydrogenation of butadiene in a C_4 olefinic cut in trickle-bed and up-flow reactors of 5.5 cm diameter. The author noticed that the selectivity remains stable in the flooded-bed in a wide range of fluid velocities, but decreases in the trickle-bed at low liquid velocities. This low selectivity was explained by segregation phenomena inside the down-flow reactor.

Mills et al.[131] examined the productivity of packed beds with down-flow, up-flow and countercurrent flow of gas and liquid for a gas-limited reaction (the hydrogenation of α-methylstyrene in hexane). They obtained similar conversions for cocurrent down-flow and countercurrent modes in the low interaction regime, while the cocurrent up-flow generally yielded lower values. For the same reaction system, Khadilkar et al.[88] compared both reactors over a wide range of operating pressures (from 30 to 200 psig). They related the observed performance to the type of reaction system used (gas-limited or liquid-limited). When the reaction is gas-limited at low pressure and high liquid feed concentration, trickle-bed reactor outperforms the up-flow reactor due to ready access of the gas to the incompletely externally wetted catalyst. At high pressure and low liquid feed concentration, the reaction becomes liquid-limited and up-flow reactor performs better. In a recent report, Julcour et al.[132] investigated the hydrogenation of 1,5,9–cyclododecatriene and observed that the rate of hydrogenation was higher for the up-flow mode compared to down-flow in contrast to earlier reports. This can be due to the bigger dimension of the reactor used, where in the down-flow mode of operation, the catalyst may not be completely wetted internally.

In many of the studies in trickle bed reactor it was found that the partial wetting of the catalyst particle has a decisive role in determining the reactor efficiency. Catalyst bed dilution using fine particles was suggested by Al-Dahhan and Dudukovic[112] to improve the catalyst wetting efficiency in trickle bed reactor. The effect of fines on the catalyst wetting efficiency as well as on pressure drop and liquid holdup was investigated using tracer technique. The catalyst bed dilution using fines was found to give reliable and reproducible results. Wu et al.[133] investigated the performance of up-flow and down-flow reactors with and with out fines. Hydrogenation of α-methyl styrene to cumene with 2.5%Pd/Al_2O_3 as the catalyst and n-hexane as the solvent was chosen for this study. It

was shown that trickle bed reactor outperform up-flow reactors under conditions of catalyst partial wetting and gas phase reactant limitation, due to elimination of external mass transfer resistances at the no-wetted catalyst portions. Under conditions of liquid phase reactant limitation, it was found that up-flow reactor gave a better performance than the trickle bed reactor due to efficient catalyst wetting and hence availability of limiting reactant is enhanced. Performance of both the reactors at different pressures, liquid phase reactant feed concentrations and gas flow rates are compared and explained on the basis of shifting from the gas to liquid limitation. Experiments on dilution of bed with solid fines in both mode of operation gave identical reactor performances and showed that hydrodynamics and kinetics can be decoupled by the use of fines.

1.3 Scope and Objectives

It is evident from the literature review presented here that even though extensive work on theoretical development of reaction rate/reactor performance models has been carried out, the experimental validation of models were limited to model reaction systems. Particularly, the focus to analyze multistep, complex multiphase reactions has been inadequate. Considering the increasing importance of catalysis in complex catalytic reactions for fine chemicals, pharmaceuticals and specialty products, there is a need to investigate case studies on catalysis and reaction engineering aspects. Such information would be immensely valuable for process optimization as well as for designing of multiphase catalytic reactors. Hydrogenation of aromatic ketones constitutes an important class of hydrogenation reactions since majority of the products formed find applications in fine chemical and pharmaceutical industry. These reactions provide interesting examples of multistep catalytic reactions allowing us to investigate important issues such as catalyst activity, selectivity, reaction kinetics and reactor performance. Considering the importance of catalysis and reaction engineering studies in hydrogenation reactions with complex reaction pathway, the following specific problems were chosen for the present work

- Kinetics and modelling of semi-batch slurry and basket reactors under isothermal and non-isothermal conditions for hydrogenation of acetophenone using supported Ru catalysts.
- Reaction kinetics and modelling of a semi batch slurry reactor for hydrogenation of p-isobutyl acetophenone using a Ru/Al_2O_3catalyst.
- Experimental and theoretical investigations on performance of a trickle bed reactor for the hydrogenation of acetophenone using supported Ru catalysts
- Experimental and theoretical investigations on performance of a fixed bed three-phase reactor with co-current up-flow of gas and liquid phases for the hydrogenation of acetophenone and its comparison with trickle bed reactor performance.
- Activity and selectivity studies using supported ruthenium catalysts for hydrogenation of acetophenone.

Notations

A^* saturation solubility of gas A, $kmol/m^3$

B_{li} concentration of component B at t=0, $kmol/m^3$

C_{pg} specific heat capacity of gas, kJ/kg.K

C_p specific heat capacity of catalyst pellet, kJ/kg.K

C_{pl} specific heat capacity of liquid, kJ/kg.K

g gravitational acceleration, kg/m^2

Ga'_L dimensionless liquid Galileo number, $\frac{d_P^3 \rho_L^2 g \varepsilon_B^3}{\mu_L^2 (1-\varepsilon_B)^3}$

ΔH heat of reaction, kJ/kmol

$k_L a_b$ gas-liquid mass transfer coefficient, s^{-1}

$k_s a_p$ liquid-solid mass transfer coefficient, s^{-1}

k_i reaction rate constants $(m^3/kg)(m^3/kmol.s)$

$\Delta P/Z$ Pressure drop, Pa, m^{-1}

Re'_L Dimensionless liquid Reynolds number, $\frac{U_L \rho_L d_P}{\mu_L (1-\varepsilon_B)}$

T temperature, K

T_g temperature of incoming gas, K

T_w temperature of the wall, K

U_W overall wall heat transfer coefficient, $kJ/m^2.Sec.K$

V_L liquid volume, m^3

V_R reactor volume, m^3

w catalyst weight, kg/m^3

ρ_l density of liquid, kg/m^3

ρ_g density of gas, kg/m^3

ρ_p catalyst pellet density, kg/m^3

η_c effectiveness factor of the catalyst

References

1. Kirk Othmer encyclopedia, Section: Catalysis, P. 320, 1993

2. Mills P. L. and Chaudhari R. V., Multiphase catalytic reactor engineering and design for pharmaceuticals and fine chemicals, Catalysis Today, 37, 367, 1997

3. Ramachandran P. A. and Chaudhari R. V., Three phase catalytic reactors, Gorden breach science publishers, New York, 1983

4. Doraiswamy L. K. and Sharma M. M., Heterogeneous reactions, vol.2 Wiley, New York, 1984

5. Mills P. L., Ramachandran P. A. and Chaudhari R. V., Rev. Chem. Eng., 8, 1, 1992

6. Mills P. L., Chaudhari R. V., Reaction engineering of emerging oxidation processes, Catalysis Today, 48, 17, 1999

7. Carpenter K. J., Chemical reaction engineering aspects of fine chemicals manufacture, Chemical Engineering Science, 56, 305, 2001

8. Sheldon R. A., Chem. Ind., 7 December, p. 903, 1992

9. Bodmer M., Mallat T. and Backer A., Enantioselective hydrogenation of trifluroacetophenone over Pt/Al_2O_3, Catalysis of organic reactions, edited by Herkes F.E, Marcel Dekker Inc., New York, p.75, 1988

10. Caman S., Bendic C., Hillebrand M., Angelescu E., Parvulescu V. I., Petricle A. and Banciu M., Diastereoselective hydrogenation of cyclic β-ketoesters over modified Ru/zeolite catalysts, Marcel Dekker Inc., New York, p.169, 1988

11. Maryanoff C. A., Mills M. E., Stanzione R. C. and Hortenstine Jr. J. T., Catalysis from the perspective of an organic chemist; commom problems and possible solution, Catalysis of organic reactions, edited by Rylander P.N., Greenfield H. and Augustine R.L., Marcel Dekker Inc., New York, p.359, 1988

12. Hiskey R. G. and Northrop R. C., J. Am. Chem. Soc., 83, 4798, 1961

13. Linstead R. R. and Levine P., The stereochemistry of catalytic hydrogenation VII, The complete hydrogenation of Phenanthraquinone, J. Am. Chem. Soc., 64, 2022, 1942

14. Kumbar P. S. and Rajadhyaksha R. A., Liquid phase catalytic hydrogenation of benzophenone: Role of metal support interaction, bimetallic catalysts, solvents and additives, Stud. Surf. Sci. Cat., 78, 251, 1993

15. Freifelder M., Hydrogenation in the pyridine series I. Catalytic hydrogenation of the isomeric acetylpyridines, J. Org. Chem., 295, 2895, 1964

16. Wilt J. W. and Schneider C. A., Ring size effects in the neophyl rearrangement II the decarbonylation of (1-methylindanyl) acetaldehyde, J. Org. Chem., 26, 4196, 1961

17. Linstead R. P. and Thomas S. L. S, Dehydrogenation part II. The elimination and migration of methyl groups from a quarternary carbon atoms during catalytic dehydrogenation, J. Chem. Soc., p.1127, 1940

18. Murphy J. G., Synthesis of aminohydrophenanthrene analogs of morphine, J. Org. Chem., 26, 3104, 1961

19. Huisgen R. and Rauenbusch E., Ann. Chem., 51, 641, 1961

20. Elango V., Method for producing ibuprofen, Eur Pat., 400,892, (Cl.C07c57/30), CA :114: 206780, to Hoest Celanese and boots 1990

21. Serebryakov B. R., Smirnova N. A., Edigarova E. I. and Adamyan V. L., U.S.S.R. SU 1011625 A1 15 Apr 1983

22. Wismeijer A. A., Kieboom A. P. G. and van Bekkum H., Improved selectivity in carbon-oxygen double bond hydrogenation with Ru/TiO_2, React. Kinet. Catal. Lett., 29(2), 311, 1985

23. Otte W. and Nehring R., Preparation of cyclohexyl compounds, DE 3537228 A1 23 Apr 1987

24. Yasuhiko T. and Seiji I., JP 01272540, 1989

25. Zakumbaeva G. D., Beketaeva L. A., Aitmagambetova S. Z., and Vozdvizhenskii V. F., Zh. Prikl. Khim., 62(8), 1809, 1989

26. Masson J., Cividino P., Bonnier J.M. and Fouilloux P., Selective hydrogenation of acetophenone on unpromoted Raney Ni: Influence of reaction conditions, Heterogeneous Catalysis and Fine Chemicals II, Stud. Surf. Sci. Catal., 245, 1991

27. Masson J., Vidal S., Cividino P., Fouilloux P. and Court J., Selective hydrogenation of acetophenone on chromium promoted Raney nickel catalysts. II. Catalytic properties in the hydrogenation of acetophenone, determination of the reactivity ratios as selectivity criteria, Appl. Cata. A: General, 99, 147, 1993

28. Kluson P., Cerveny L. and Had J., Preparation and properties of ruthenium supported catalysts, Cat. Lett., 23, 299, 1994

29. Rocchini E., Spogliarich R. and Graziani M., Catalytic hydrogenation of aromatic ketones in the presence of cyclodextrines, J. Mol. Cat., 91, L313 -L318, 1994

30. Masaya I., Masaru I. and Takao H., JP 08198788, 1996

31. Masaya I., Takao H. and Noriaki O. and Masaru I., JP 09249599, 1996

32. Masaya I. and Takao H., JP 09077711, 1997

33. Bergault I., Fouilloux P., Joly-Vuillemin C. and Delmas H., Kinetics and Intraparticle Diffusion Modelling of a complex Multistep Reaction: Hydrogenation of Acetophenone over a Rhodium Catalyst J. Cat., 175, 328, 1998

34. Itoi Y., Hydrogenation of aromatic carbonyl compounds and catalysts for it, JP 2000103753 A2 11 Apr 2000

35. Tadashi Y., Yukituro Y. and Sangi Y., A process for preparation of 1-(1-hydroxy ethyl) alkyl cyclohexanes by catalytic hydrogenation of alkyl acetophenones, Jpn. Kokai Tokkyo Koho JP 62,185,032, 108: 167018, to Takiho Pharmaceutical company, 1987

36. Yoshiyaki H., Hydrogenation of aromatic ketones with Raney Ni- amine catalyst, Jpn. Jpn.Kokai Tokkyo Koho JP. 63630432,(Cl.C07C33/20), CA : 110 : 7852 , to Daicel Chemical Ind. Ltd., 1988

37. Elango V., Method for producing ibuprofen, Eur Pat., 400,892, (Cl.C07c57/30), CA :114: 206780, to Hoest Celanese and boots, 1990

38. Ryan D. A., Method for producing 1-(4-isobutyl phenyl) ethanol, Eur. Pat. 358,420, (Cl.c07c33/20), CA : 113 : 77897, to Hoest Celanese and Boots, 1990

39. Saeki K. and Takashi U., preparation of aromatic carbinols Jpn.Kokai Tokkyo Koho JP. 02,73,027, CA: 113: 58673, to Daicel Chemical Ind. Ltd., 1990.

40. Saeki K. and Shima K., preparation of aromatic carbinols from aromatic ketones,, Jpn.Kokai Tokkyo Koho JP. 02,62,837,(Cl.C07C33/20), CA : 113 : 58672, to Daicel Chemical Ind.Ltd., 1990

41. Rajasekharam M. V. and Chaudhari R. V., Kinetics of hydrogenation of p-isobutyl acetophenone using a supported Ni catalyst a slurry reactor, Chem. Eng. Sci., 51(10), 1663, 1996

42. Wismeijer A. A., Kieboom A. P. G and van Bekkum H., Improved selectivity in carbon-oxygen double bond hydrogenation with Ru/TiO_2, React. Kinet. Catal. Lett., 29(2), 311, 1985

43. Kluson P. and Cerveny L., Selective hydrogenation over ruthenium catalysts, Applied catalysis A: general 128, 13-31, 1995

44. Rajashekharam M. V., Thesis submitted to the university of Pune, India (1997)

45. Rajasekharam M. V., Bergault I., Fouilloux P., Schweich D., Delmas H. and Chaudhari R. V., Hydrogenation of acetophenone using 10%Ni supported on zeolites Y catalyst: Kinetics and reaction mechanism, Catalysis Today, 48, 83, 1999

46. Bergault I., Rajashekharam M. V., Chaudhari R. V., Schweich D. and Delmas H., Modelling of comparison of acetophenone hydrogenation in trickle-bed and slurry airlift reactors, Chem. Eng. Sci., 52 (21/22), 4033, 1997

47. Shah Y. T., Gas-Liquid-Solid reactor design, McGraw-Hill, New York, 1979

48. Chaudhari R. V. and Ramachandran P. A., Three phase slurry reactors, AIChE J., 26 (2), 177, 1980

49. Chaudhari R. V., Shah Y. T. and Foster N.R., Novel gas-liquid-solid reactors, Catal. Rev. - Sci. Eng., 28(4), 431, 1986

50. Kenney C. N. and Sedriks W., Effectiveness factors in a three-phase slurry reactor: the reduction of crotonaldehyde over a palladium catalyst, Chem. Eng. Sci., 27, 2029, 1972

51. Kawakami K. and Kusunoki K., Selectivity in consecutive hydrogenation of chlorobenzene in liquid phase, Kagaku Kogaku Ronbunshu, 1, 559, 1975

52. Kawakami K. and Kusunoki K., The effects of Intraparticle diffusion on the yield of the liquid phase hydrogenation of phenylacetylene in a stirred basket reactor, J. Chem. Eng. Japan, 9 (6), 469, 1976

53. Kut O. M., Gut G., Buehlmann T. and Lussy A., Mass transfer with chemical reaction in multiphase systems, Ed. Alper E., (NATO series), Martinus Nijhoff Publishers, The Hauge, 2, 228, 1983.

54. Chaudhari R. V., Parande M. G., Ramachandran P. A., Brahme P. H., Vadgaonkar H. G. and Jaganathan R., Hydrogenation of butynediol to cis-butenediol catalyzed by Pd-Zn-$CaCO_3$, Reaction kinetics and modeling of a batch slurry reactor, AIChE J., 31, 1891, 1985

55. Chaudhari R. V., Jaganathan R., Kohle D. S., Emig G. and Hofmann H., Kinetic modeling of a complex consecutive reaction in a slurry reactor: Hydrogenation of phenyl acetylene, Chem. Eng. Sci., 41, 3073, 1986

56. Chaudhari R. V., Jaganathan R., Kohle D. S., Emig G. and Hofmann H., Kinetic modeling of hydrogenation of butynediol using a 0.2%Pd/C catalyst in a slurry reactor, Appl. Catal., 29, 141, 1987

57. Santacesaria E., Di Serio M., Velotti R. and Leone U., Kinetics, mass transfer and palladium catalyst deactivation in the hydrogenation step of the hydrogen peroxide synthesis via anthraquinone, Ind. Eng. Chem. Res., 33, 2349, 1995

58. Holm D. R., Hill Jr. C. G. and Connor A. H., Kinetics of liquid phase hydrogenations of furan amines, Ind. Eng. Chem. Res., 34, 2349, 1995

59. Toppinen S., Rantakyla T. K., Salmi T. and Aittamaa J., Kinetics of the liquid phase hydrogenation of benzene and some mono substituted alkylbenzenes over a nickel catalyst, Ind. Eng. Chem. Res., 35, 1824, 1996

60. Benaissa M., Le Roux G. C., Joulia X., Chaudhari R. V. and Delmas H., Kinetic modeling of the hydrogenation of the hydrogenation of 1,5,9-Cyclododecatriene on Pd/Al_2O_3 catalyst including isomerization, Ind. Eng. Chem. Res., 35, 2091, 1996

61. Rajasekharam M.V. and Chaudhari R.V., Hydrogenation of 2,4-dinitrotoloune using a supported Ni catalyst: Reaction kinetics and semibatch slurry reactor modeling, Ind. Eng. Chem. Res., 38, 906, 1999

62. Rode C. V. and Chaudhari R. V., Hydrogenation of m-nitrochlorobenzene to m-chloroaniline: reaction kinetics and modelling of a non-isothermal slurry reactor, Ind. Eng. Chem. Res. 33,1645, 1994

63. Rajashekharam M. V., Nikhalje D. D., Jaganathan R. and Chaudhari R. V., Hydrogenation of 2,4-Dinitrotoluene using a Pd/Al_2O_3 catalyst in a slurry reactor: A molecular level approach to kinetic modelling and nonisothermal effects, Ind. Eng. Chem. Res., 35, 1824, 1996

64. Jaganathan R., Ghugikar V. G., Gholap R. V., Chaudhari R. V and Mills P. L., Catalytic hydrogenation of p-nitrocumene in a slurry reactor, Ind. Eng. Chem. Res., 38, 4634, 1999

65. Ohorodnik A., Sennewald K., Hindeck J. and Statzke P., Apparatus for the continuous carrying out heterogeneous catalytic reaction in liquid phase, U.S. Patent 3,901,660, 1975

66. Pruden B. B. and Weber M. E., Evaluation of three-phase catalytic reactor, Can. J. Chem. Eng., 48, 162, 1970

67. Blenke H., Adv. Biochem. Eng., 13, 122, 1979

68. Chaudhari R. V. and Shah Y. T., International Reactor Design Conference, Santa Fe, Argentine, August 1983.

69. Leuteritz G. M., Process Eng., 54, 62, 1973

70. Satterfield C. N., Trickle-bed reactors, AIChE J., 21(2), 209, 1975

71. Shah Y. T., Gas-Liquid-Solid reactor design, McGraw-Hill, New York, 1979

72. Al-Dahhan M. H., Larachi F., Dudukovic M. P. and Laurent A., High-pressure trickle-bed reactors: A review, Ind. Eng. Chem. Res., 36, 3292, 1997

73. Saroha A. K. and Nigam K. D. P., Trickle bed reactors, Rev. Chem. Eng., 12(3-4), 1996

74. Enright J. T. and Chuang T. T., Deuterium exchange between hydrogen and water in a trickle bed reactor, Canad. J. Chem. Eng., 56, 246, 1978

75. Seirafi H. A. and Smith J. M., Mass transfer and adsorption in liquid full and trickle beds, AIChE. J., 26, 711, 1980

76. Meyers R. A., Handbook of petroleum refining processes, 2nd ed., McGraw-Hill, New York, 1996

77. Hofmann H. P., Multiphase catalytic packed bed reactors, Catal. Rev. Sci. Eng., 17(1), 71, 1978

78. Ng K. M. and Chu C. F., Trickle-bed reactors, Chem. Eng. Prog. 55, Nov., 1987

79. Colombo A. J., Baldi G. and Sicardi S., Solid-liquid contacting effectiveness in trickle bed reactors, Chem. Eng. Sci., 31, 1101, 1976

80. Herskowitz M. and Smith J. M., Trickle bed reactors: A review, AIChE J.,29, 1, 1983

81. Gianetto A. and Specchia V., Trickle-bed reactors: State of art and perspectives, Chem. Eng. Sci., 47, 3197, 1992

82. Al-Dahhan M. H., and Dudukovic M. P., Catalyst wetting Efficiency In trickle-bed Reactors at high pressure, Chem. Eng. Sci., 50 (15), 2377, 1995

83. Lamine A. S., Gerth L., Le Gall H. and Wild G., Heat transfer in a packed bed reactor with cocurrent downflow of a gas and a liquid, Chem. Eng. Sci., 51(15), 3813, 1996

84. Rajashekharam M. V., Jaganathan R. and Chaudhari R. V., A trickle-bed reactor model for hydrogenation of 2,4 dinitrotoluene: experimental verification., Chem. Eng. Sci., 53(4), 787, 1998

85. Khadilkar M. R., Jiang Y., Al-Dahhan M., Dudukovic M. P., Chou S. K., Ahmed G. and Kahney R., Investigations of a complex reaction network: I Experiments in a high-pressure trickle bed reactor, AIChE J., 44 **(**4), 912, 1998

86. Huang T. and Kang B., Naphthalene hydrogenation over Pt/Al_2O_3 catalyst in a trickle bed reactor, Ind. Eng. Chem. Res., 34, 2349, 1995

87. Bergault I., Rajashekharam M. V., Chaudhari R. V., Schweich D. and Delmas H., Modelling of comparison of acetophenone hydrogenation in trickle-bed and slurry airlift reactors, Chem. Eng. Sci., 52 (21/22), 4033, 1997

88. Khadilkar, M. R., Wu Y. X., Al-Dahhan M. H. and Dudukovic M. P., Comparison of trickle bed and upflow reactor performance at high pressure: Model prediction and experimental observations, Chem. Eng. Sci., 51 (10), 2139, 1996

89. Rajashekharam M. V., Jaganathan R. and Chaudhari R. V., A trickle-bed reactor model for hydrogenation of 2,4 dinitrotoluene: experimental verification. Chem. Eng. Sci., 53(4), 787, 1998

90. Jaganathan R., Gholap R. V., Brahme P. H. and Chaudhari R.V, Performance of a continuous bubble column slurry reactor for hydrogenation of butynediol.Proceedings of ICREC 2, NCL, India II 141, 1987

91. Barhme P. H., Chaudhari R. V. and Ramachandran P. A., Modelling of hydrogenation of glucose in a continuous slurry reactor, Ind. Eng. Chem. Proc. Des. Dev., 23, 57, 1984

92. Herskowitz M, Hydrogenation of benzaldehyde to benzyl alcohol in a slurry and fixed-bed reactor, Stud. Surf. Sci. Catal., 59 (Heterog. Catal. Fine Chem. 2), 105, 1991

93. Sims B. W., Gaskey S. W. and Luss D., Effect of flow regime and liquid velocity on conversion in a trickle bed reactor, Ind. Eng. Chem. Res., 30, 2530, 1994

94. Vergel C., Euzen J. P., Trambouze P. and Wauquier J. P., Two-phase flow catalytic reactors, influence of hydrodynamics on selectivity, Chem. Eng. Sci., 50, 3303, 1995

95. Valerius G., Zhu X., Hofmann H., Arntz D. and Haas T., Modelling of a trickle-bed reactor II. The hydrogenation of 3-hydroxypropanal to 1,3-propanediol, Chem. Eng. Proc., 35, 11, 1996

96. Korsten H. and Hoffmann U., Three phase reactor model for hydrotreating in pilot plant trickle-bed reactors, AIChE J., 42(5), 1350, 1996

97. Stuber F., Benaissa M. and Delmas H., Partial hydrogenation of 1,5,9-cyclododecatriene in three phase catalytic reactors, Catalysis Today, 24, 95, 1995

98. Ravindra P. V., Rao D. P. and Rao M. S., A model for the oxidation of sulfur dioxide in a trickle bed reactor, Ind. Eng. Chem. Res., 36, 5125, 1997

99. Iliuta I. and Iliuta M. C., Comparison of two-phase upflow and downflow fixed bed reactors performance: Catalytic SO_2 oxidation, Chem. Eng. Technol., 20, 455, 1997

100. Pintar A., Bercic G. and Levec J., Catalytic liquid-phase oxidation of aqueous phenol solutions in a trickle bed reactor, Chem. Eng. Sci., 52, 4143, 1997

101. Castellari A. T., Cechini J. O., Gabarian L. J., and Haure P. M., Gas-phase reaction in a trickle-bed reactor operated al low liquid flow rates, AIChE J., 43(7), 1813, 1997

102. Devetta L., Canu P., Bertucco A., and Steiner K., Modeling of a trickle-bed reactor for a catalytic hydrogenation in supercritical CO_2, Chem. Eng. Sci., 52(21/22), 4163, 1997

103. Zhu X. D. and Hofman H, Hydrogenation of 3-hydroxy-propanal in trickle beds- experimental and modeling, Chem. Eng. Technol., 20, 131, 1997

104. Jiang Y., Khadilkar M. R., Al-Dahhan M. H., Dudukovic M. P., Chou S. K., Ahmed G. and Kahney R., Investigations of a complex reaction network: II Kinetics, mechanism and parameter estimation, AIChE J., 44(4), 921, 1998

105. Tukac V. and Hanika J., Catalytic wet oxidation of substituted phenols in the trickle bed reactor, Chem. Eng. Technol., 21, 262, 1998

106. Herrmann U. and Emig G., Liquid phase hydrogenation of maleic anhydride to 1-4, butanediol in a packed bubble column reactor, Ind. Eng. Chem. Res., 37, 759, 1998

107. Beaudry E. G., Dudukovic M. P. and Mills P. L., Trickle-bed reactors: liquid diffusional effects in a gas-limited reaction, AIChE J., 33, 1435, 1987

108. Silveston P., Hudgins R. R. and Renken A., Periodic operation of catalytic reactors – introduction and overview, Catalysis Today, 25, 91, 1995

109. Haure P. M., Hudgins R. R., Silveston P., Periodic operation of a trickle bed reactor, AIChE J., 35(9), 1437, 1989

110. Gabarain L., Cechini J. and Haure P., Effect of variables on the Periodic Operation of a Trickle Bed Reactor, Dynamics of Surfaces and Reaction Kinetics in Heterogeneous Catalysis, Edited by Froment G.F. and Waugh K.C., Elsevier Science, 1997

111. Castellari A. T., and Haure P. M., Experimental study of the periodic operation of a trickle bed reactor, AIChE J., 41(6), 1995

112. Al-Dahhan M. H. and Dudukovic M. P., Catalyst Bed Dilution for improving catalyst wetting in laboratory trickle bed reactors, AIChE J., 42(9), 2595, 1996

113. Eisenklam P. and Ford L. H., Flow regimes in fixed bed reactors with cocurrent upflow, Proceedings of symposium on the interaction of fluids and solids, Instn. Chem. Engrs., 333, 1962

114. Turpin J. L., and Huntington, R. L. Prediction of pressure drop for two phase, two component cocurrent flow in packed beds, AIChE J. 13, 1196, 1967

115. Specchia V., Sicardi S. and Gianetto A., Absorption in packed towers with cocurrent flow, AIChE J., 20, 646, 1974

116. Fukushima S. and Kusaka K., Gas-liquid mass transfer and hydrodynamic flow region in packed columns with cocurrent upward flow, J. Chem. Eng. Japan, 12(4), 296, 1979

117. Iliuta I. and Thyrion F. C., Flow regimes, liquid holdups and two-phase pressure drop for two-phase cocurrent downflow and upflow through packed beds: air/Newtonian and non-Newtonian liquid systems, Chem. Eng. Sci., 52 (21/22), 4045, 1997

118. Goto S., Chatani T. and Matouq M. H., Hydration of 2-methyl-2-butene in gas-liquid cocurrent upflow and downflow reactors, Can. J. Chem. Eng., 71, 821, 1993

119. Hofmann H. P., Multiphase catalytic packed bed reactors, Catal. Rev. Sci. Eng., 17(1), 71, 1978

120. Ragaini V. and Tine C., Upflow reactor for the selective hydrogenation of pyrolysis gasoline: Comparative study with respect to down flow, Appl. Catal., 10, 43, 1984

121. Mochizuki S. and Matsui T., Selective hydrogenation and mass transfer in a fixed bed catalytic reactor with gas-liquid concurrent upflow, AIChE J., 22(.5), 904, 1976

122. Van Gelder, K. B., Damhof J. K., Krouenga P. J. and Westertrep K. R., Three phase packed bed reactor with an evaporating solvent I: Experimental: The hydrogenation of 2,4,6 - trinitrotoluene in methanol, Chem. Eng. Sci., 45, 3159, 1990

123. Van Gelder, K. B., Borman P. C., Weenink R. E., and Westertrep K. R., Three phase packed bed reactor with an evaporating solvent II: Modelling the reactor, Chem. Eng. Sci., 45, 3171, 1990

124. Julcour C., Stuber F., Le Lann J. M., Wilhelm A. M. and Delmas H., Dynamics of a three-phase upflow fixed-bed catalytic reactor, Chem. Eng. Sci., 54, 2391, 1999

125. Visser J. B. M., Stankiewicz A., van Dierendonck L. L., Manna L., Sicardi S. and Baldi G., Dynamic operation of a three-phase upflow reactor for the hydrogenation of phenyl acetylene, Catalysis Today 20, 485, 1994

126. Goto S. and Mabuchi K., Oxidation of ethanol in gas-liquid cocurrent upflow and downflow reactors, Can. J. Chem. Eng., 62, 865, 1984

127. de Wind et al. Upflow versus downflow testing of hydrotreating catalysts. Applied Catalysis. 43, 239, 1988

128. Larachi F., Laurent A., Wild G. and Midoux N., Some experimental liquid saturation results in fixed bed reactors operated under elevated pressure in cocurrent upflow and downflow of the gas and the liquid, Ind. Eng. Chem. Res., 30, 2404, 1991

129. Yang X. L., Wild G. and Euzen J. P., A comparison of hydrodynamics between packed-bed reactors with cocurrent upflow and downflow of gas and liquid, Chem. Eng. Sci., 47, 1323, 1992

130. Vergel H., Les reacteurs a lit fixe avec ecoulement de gaz et de liquide. Comparaison sur le plan theorique et experimental de la performance du reacteur dans differents sens d'ecoulement. These de Doctorat de l'INP Lorraine, 1993

131. Mills, P. L., Beaudry, E. G. and Dudukovic, M. P., Comparison and prediction of reactor performance for packed beds with two-phase flow : downflow, upflow and countercurrent flow. I. Chem. E. Symp. Ser., 87, 527, 1984

132. Julcour C., Jaganathan R., Chaudhari R. V., Wilhelm A. M. and Delmas H., Selective Hydrogenation of 1,5,9-cyclododecatrien in up flow and down flow fixed bed reactors, experimental observations and modeling, Chem. Eng. Sci., 56, 557, 2001

133. Wu Y., Khadilkar M. R., Al-Dahhan M. H. and Dudukovic M. P., Comparison of upflow and downflow two-phase flow packed bed reactors with and without fines: Experimental observations, Ind. Eng. Chem. Res. 35, 397, 1996

Chapter 2

Part – A

Hydrogenation of Acetophenone Using Supported Ruthenium Catalyst: Kinetics, Intraparticle Diffusion and Non-Isothermal Effects

2 (A). 0 Introduction

Multiphase reactions when carried out in a slurry reactor have many advantages over the fixed bed reactors, due to its high efficiency for mass and heat transfer. Three-phase catalytic hydrogenation of organic compounds is widely used in several industrial processes and hydrogenation of acetophenone (ACPH) using supported metal catalysts is an example of such a reaction, since one of the products, 1-phenylethanol (PHET) is important in perfumery and pharmaceutical industry and another product 1-cyclohexylethanol (CHET) is used in the manufacture of polyvinylcyclohexane, a high temperature resistant polymer. Two types of catalysts are known for hydrogenation of acetophenone. (a) Catalysts for selective hydrogenation of the carbonyl group to PHET and (b) catalysts, which hydrogenate the ring as well as the carbonyl group to give CHET. The catalysts commonly used for the hydrogenation of ACPH to PHET are Raney Ni,[1] Raney Ni-Co catalysts,[2] Raney Ni-Cr catalysts,[3] supported Pd catalysts,[4,5] Co based catalysts, bimetallic Cu-Cr catalysts[6,7] and tri-metallic Cu-Cr-Ba catalysts.[8,9] The other type of catalysts used for the production of CHET include, supported Ru, Rh and Pt.[10,11,5] The details of earlier studies on hydrogenation of acetophenone have been given in Chapter 1. Even though many reports are published on the selective synthesis of 1-phenylethanol, literature on selective formation of 1-cyclohexylethanol is limited. The literature on selective synthesis of 1-cyclohexylethanol reveals that the catalysts used are mainly rhodium-based catalysts. Ruthenium is also known for such reactions, but needs further investigation as it has a potential in developing a more economical process due to its lower cost.

When catalyst particles of very small size are used, under conditions of negligible external mass transfer, the multiphase reactions are kinetically controlled and complete utilisation of catalyst is possible. The intrinsic kinetics thus obtained can be useful in explaining the apparent kinetics observed when catalyst particles of bigger size are used, as in the case of a basket type reactor. Modelling of intraparticle diffusional effects for multi-component system is a difficult task due to complexities in solving the model equations for simultaneous diffusion with reactions. Usually under conditions of higher liquid phase substrate concentration, the diffusional effects of the liquid substrate can be neglected with only the dissolved gas as a limiting reactant. But when the concentration

of liquid phase components is lower and comparable with the gas phase component solubility, the diffusional effects of liquid phase substrate and intermediates in the catalyst pellet becomes important and need to be considered to account for intraparticle diffusional effects. The problem is even more complex if the reaction involves considerable exothermicity and carried out under non-isothermal conditions. The temperature rise can alter the solubility, the effective diffusivity of different components and also the rate parameters. In most cases, for the analysis of non-isothermal catalytic liquid phase reactions, it is assumed that no temperature gradient exists within the catalyst pellets. Even though this is true in the case of reactions with mild exothermicity, for reactions with high exothermicity, analysis of intraparticle temperature gradient should be accounted for. Analysis of intraparticle diffusion effects for complex reactions are rare in literature. Kawakami and Kusunoki[12] studied the hydrogenation of phenylacetylene using 0.5%Pt/Al_2O_3 catalyst and found that with catalyst pellets of larger size, the reaction rates and yield were significantly influenced by diffusional effects. The liquid-phase hydrogenation kinetics of benzene and three mono substituted alkylbenzenes, toluene, ethylbenzene, and cumene, was studied by Toppinen et al.[13] in a semi-batch slurry reactor and the analysis of the data with a reaction-diffusion model revealed that the kinetics was influenced by pore diffusion. Bergault et al.[14] studied the effect of intraparticle diffusion for hydrogenation of acetophenone using 3%Rh/C catalyst with cyclohexane as the solvent. Julcour et al.[15] investigated dynamic and pseudo-steady state diffusion-reaction models for the three-phase consecutive hydrogenation of 1,5,9-cyclododecatriene using Pd/Al_2O_3 catalyst in order to examine the time evolution of concentration profiles inside the catalyst pellet. It was concluded that the diffusion of organic species could control the reaction rate only for lower concentrations of organic species and higher pressures of hydrogen.

Even though the kinetics of hydrogenation of acetophenone have been studied using Raney Ni-Cr catalyst and supported Ni and Rh catalysts, detailed analysis of mechanistic models and reaction engineering aspects of hydrogenation of acetophenone using supported ruthenium catalyst have not been reported. In this chapter, a detailed study on intrinsic kinetics of hydrogenation of acetophenone using 2%Ru on alumina catalyst with methanol as a solvent has been presented. A semi-batch slurry reactor model

was developed to predict the experimentally observed concentration - time profiles. The activation energies and heat of adsorption were evaluated from the temperature dependencies of rate parameters. A basket type reactor model was derived for the above system incorporating diffusional effects of gaseous as well as liquid phase components and the resulting set of non-linear partial differential equations were solved by orthogonal collocation method. A theoretical analysis is also extended to study the dynamic behaviour of the concentration profiles inside the pellet. The concentration-time profiles of bulk liquid phase components were simulated and compared with the experimentally observed values. Non-isothermal effects were studied for slurry and basket type reactors with n-decane as the solvent and the temperature-time profile in the bulk was compared with the experimental values.

2 (A). 1 Experimental

2 (A). 1.1 Reactor Set-up

All the hydrogenation experiments were carried out in a 3 x 10^{-4} m^3 capacity stirred autoclave reactor made of SS 316 and supplied by Parr Instrument Co., USA, with provision for operation up to 523 K and 10 MPa pressure (Figure 2.1).

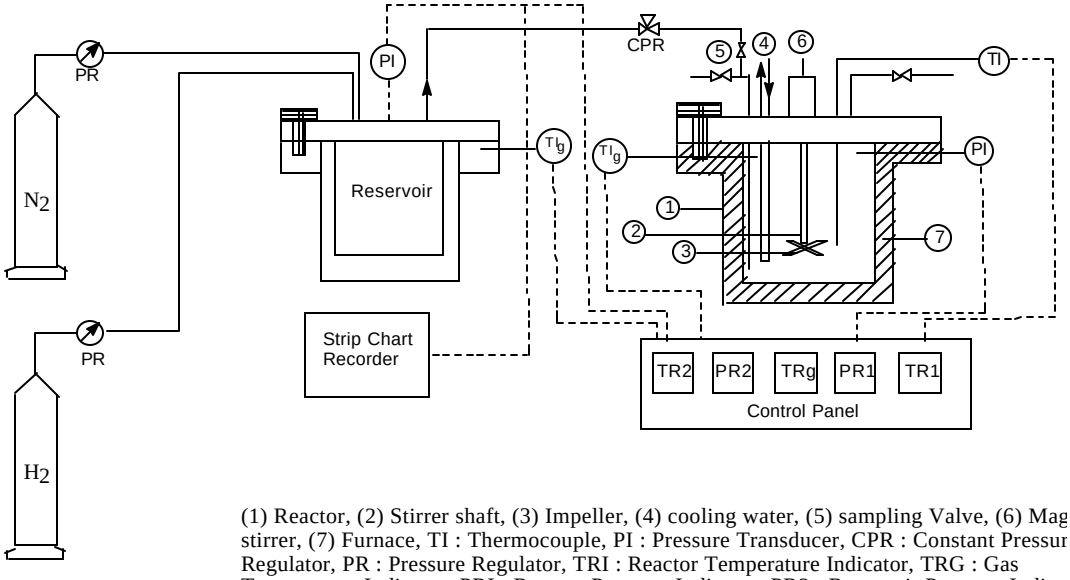

(1) Reactor, (2) Stirrer shaft, (3) Impeller, (4) cooling water, (5) sampling Valve, (6) Mag stirrer, (7) Furnace, TI : Thermocouple, PI : Pressure Transducer, CPR : Constant Pressur Regulator, PR : Pressure Regulator, TRI : Reactor Temperature Indicator, TRG : Gas Temperature Indicator, PRI : Reactor Pressure Indicator, PR2 : Resorvoir Pressure Indica TR2 : Reservoir Temperature Indicator

Figure 2.1: Schematic of the Reactor Setup

It was equipped with facilities such as automatic temperature control, gas inlet/outlet, sampling of the liquid contents, variable agitation speed, safety rupture disc and pressure transducer. A storage reservoir for H_2 gas was used along with a constant pressure regulator to determine H_2 consumption as a function of time, while maintaining the reactor at a constant desired pressure.

2 (A). 1.2 Catalyst Preparation

The catalyst, 2%Ru/Al_2O_3 was prepared in our own laboratory by precipitation technique. Required amount of support (alumina) was charged in water and the slurry was stirred for 2 hrs in a round bottom flask fitted with half moon stirrer, condenser and an addition funnel on a water bath (temperature ~368 K). Required amount of ruthenium trichloride dissolved in distilled water was added to the stirred suspension. After stirring for three hours, aqueous ammonia solution was added drop wise until the solution became strongly alkaline. The solution was then allowed to stir for 3-4 hrs. The contents were then filtered, washed using hot distilled water and dried in an oven at 393 K for 8 hrs and then activated in a furnace at 573 K for 7 hrs under hydrogen flow. After activation, the catalyst was brought to room temperature, flushed with nitrogen and used for reaction. Catalyst particles of larger size were made by pelletising the powder catalyst and sieving through standard sieves to get particles in different size ranges.

2 (A). 1.3 Experimental Procedure for Carrying Out Reaction

In a typical experiment, desired amount of acetophenone (Aldrich, U.S.A) was charged into the reactor along with the catalyst and solvent methanol, to make up a total volume of 1 x 10^{-4} m^3. The reactor was flushed using nitrogen, 2-3 times, at room temperature and the contents were heated to a desired temperature and then pressurised with hydrogen. The reaction was started by switching the stirrer on. The hydrogen consumption was monitored from the pressure drop in the hydrogen reservoir vessel as a function of time. Liquid samples were withdrawn at regular intervals of time and analysed by gas chromatographic technique using a HP-6890 Gas chromatograph fitted with a HP-FFAP capillary column (30 m x 0.53 μm x 0.1 mm film thickness on polyethylene glycol

stationary phase). The conditions of GC analysis were: FID temperature: 573 K, column temperature: 373-458 K (Programmed at 30 K/min), injection temperature: 523 K, carrier gas: He. A few samples were also analysed and confirmed by a Shimadzu GC-MS QP 2000A.The range of operating conditions for which the kinetic study was carried out is given in Table 2. 1.

Table 2.1: Range of Operating Conditions

Catalyst loading	:	10-40 kg/m^3
Agitation speed	:	7.5-15 Hz
H_2 pressure	:	14 - 62 atm
ACPH concentration	:	0.8-2.5 kmol/m^3
Temperature	:	398-423 K

2 (A). 1.4 Experimental Procedure for Solubility Measurement

For interpretation of kinetic data, knowledge of concentration of the gaseous reactants in the reaction medium (solubility) is essential. The solubility of H_2 in ACPH/methanol mixtures was determined experimentally at 373, 398 and 423 K, using a method described by Purwanto et al.[16] The solubility measurement was conducted in 6.0 x 10^{-4} m^3 capacity stirred autoclave supplied by Parr Instrument Company, USA designed for 250 atm pressure. The equipment was provided with automatic temperature control and a pressure recording system. The temperature of the liquid in the reactor was controlled within ±1 K. A pressure transducer having a precession of ± 0.01 atm was used to measure the autoclave pressure.

In a typical experiment for the measurement of solubility of H_2, a known volume (300 ml) of liquid mixture was introduced into the autoclave and the contents were heated to the desired temperature after flushing with nitrogen. After the thermal equilibrium was attained, the void space in the reactor was pressurised with H_2 to the level required. The contents were then stirred for about ten minutes to equilibrate the liquid phase with the solute gas. In general, it required, about 2-5 minutes to saturate the liquid phase. The change in the pressure in the autoclave was recorded on-line as a function of time till it remained constant, indicating the saturation of the liquid phase.

2 (A). 2 Results and Discussion

2 (A). 2.1 Product Identification and Distribution

The various products formed during the course of hydrogenation reaction include 1-phenylethanol (PHET) and ethylbenzene (ETBE) along with the ring hydrogenated products such as cyclohexylmethylketone (CHMK), 1-cyclohexylethanol (CHET) and ethyl cyclohexane (ETCH). Typical concentration-time profile obtained at 398 K is shown in Figure 2.2. Based on the products identified and characterised by GC and GC-MS, the reaction scheme shown in Figure 2.3 has been proposed for hydrogenation of acetophenone using 2% Ru/Al_2O_3 catalyst. Due to the acidic sites on the catalyst, PHET also undergoes dehydration to give styrene, which on further hydrogenation gives ethyl benzene (ETBE), and ethyl cyclohexane (ETCH). The observed concentration of styrene in the reactor mixture was negligible (< 1.0 %). On further continuation of the hydrogenation, formation of ETCH from CHET was not observed. Also, the rate of formation of CHET from CHMK was found to be very slow.

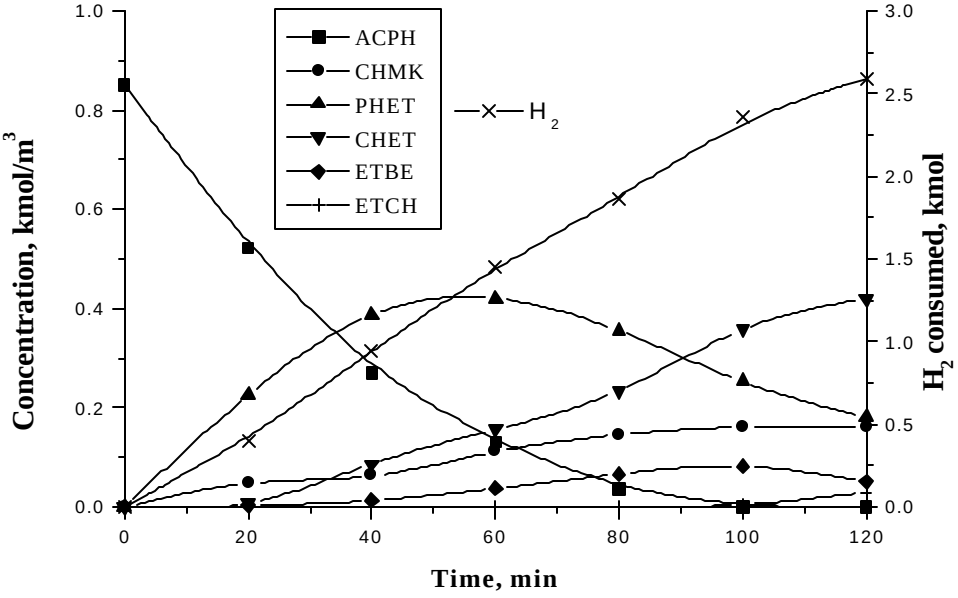

Figure 2.2: Concentration – Time Profile at 398 K

Reaction Conditions: Concentration of ACPH: 0.84 kmol/m^3, Catalyst Loading: 10 kg/m^3, P_{H2}: 47.6 atm, Solvent: Methanol, Agitation Speed: 15 Hz

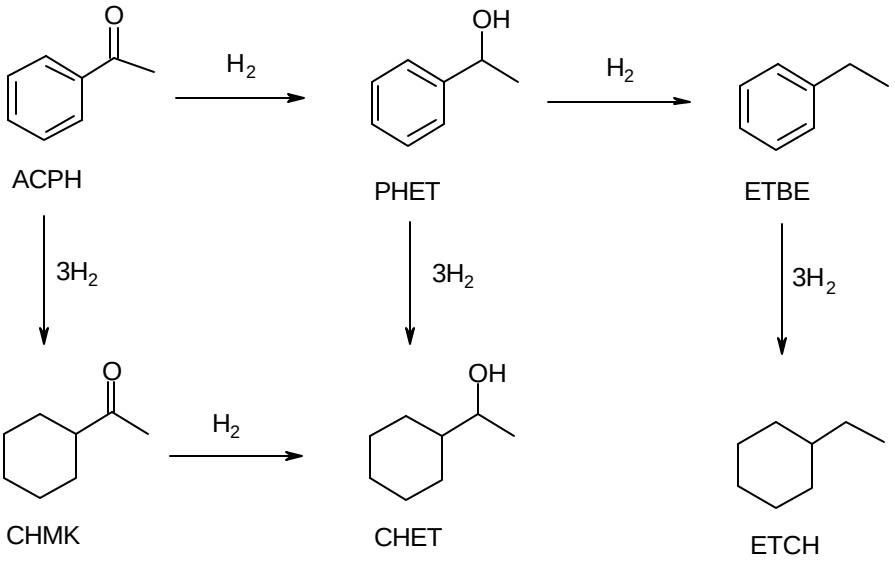

Figure 2.3: Reaction Scheme for Hydrogenation of Acetophenone Using 2%Ru/Al_2O_3

ACPH: Acetophenone, PHET: 1-Phenylethanol, ETBE: Ethyl Benzene, CHMK: Cyclohexyl Methylketone, CHET: 1-Cyclohexylethanol, ETCH: Ethyl Cyclohexane

2 (A). 2. 2 Catalyst Recycle

In order to check the deactivation of the catalyst, recycle study was done without exposing the catalyst to air (Figure 2.4).

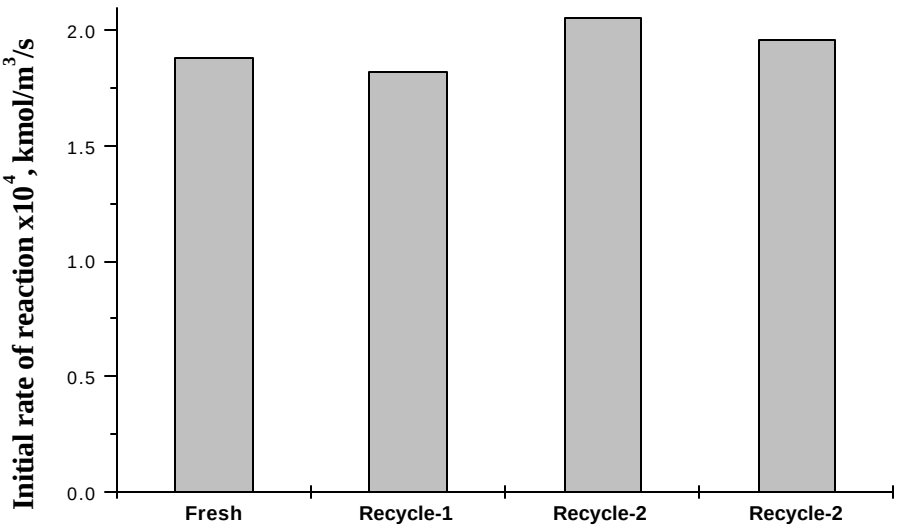

Figure 2.4: Initial Rates with Fresh and Recycled Catalysts

For this, first a reaction was carried out for 2 hours and then the reaction mixture was cooled to room temperature, H_2 released and known amount of acetophenone was added through the dip tube of the reactor and reaction was continued after pressurisation to original level used in the first reaction. The initial rate of reactions based on ACPH consumption, for fresh and the recycled reactions were found to be similar (Figure 2.4) confirming that the catalyst was not getting deactivated during the reaction.

2 (A). 2. 3 Effect of Water

In order to understand the effect of water (a side product formed during the reaction), reactions were carried out with known amount of water along with acetophenone, solvent and catalyst at the beginning of reaction. The concentration of water was varied from 0.1 - 0.25 kmol/m^3 and found that the initial rate does not vary with water concentration showing that water has no influence on the reaction rate, at least in the concentration range studied.

2 (A). 2. 4 Initial Rate Data and Analysis of Mass Transfer

It is important to investigate whether external and intraparticle mass transfer is rate limiting under conditions used for kinetic study and this was done based on overall hydrogen consumption rates. In most experiments, H_2 consumption vs. time was observed (See Figure 2.2) along with liquid phase reactant/product concentration profiles. The H_2 consumption vs. time data observed under different conditions were fitted by a second order polynomial as

$$Y = a + bt + ct^2 \qquad (2.1)$$

Where Y is the hydrogen consumed in kmol/m^3; t, the reaction time in sec; and a, b and c are constants. The rate of reaction at any time can be calculated as

$$R_{H2} = dY/dt = b + 2ct \qquad (2.2)$$

Then, initial rate of hydrogenation can be calculated at t = 0 from the above equation as

$$R_A = [\, dY/dt]_{t=0} = b \qquad (2.3)$$

The initial rate also can be calculated based on ACPH consumption in the similar way. For determining the effect of catalyst loading, partial pressure of hydrogen and initial ACPH concentration on the initial rate of reaction, the initial rates were calculated based on ACPH consumption. The effect of catalyst loading on the initial rate was found to be

linearly dependent (Figure 2.5) and the agitation speed also showed no influence on the initial rate, beyond a speed of 11 Hz suggesting that the external mass transfer (gas-liquid, liquid-solid) resistances can be neglected.

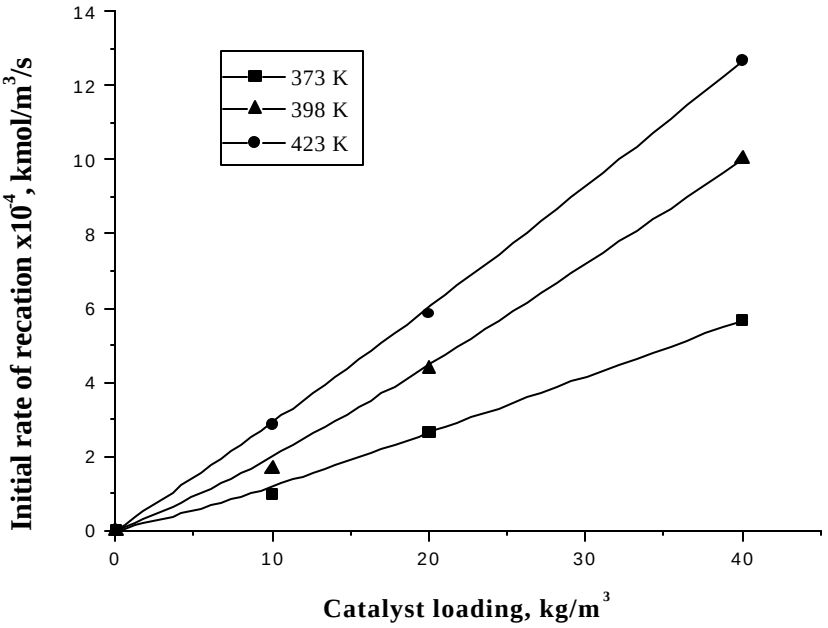

Figure 2.5: Effect of Catalyst Loading on Initial Rate of Reaction

Reaction Conditions: Concentration of ACPH: 0.84 kmol/m^3, P_{H2}: 47.6 atm, Solvent: Methanol, Agitation Speed: 15 Hz

However, a detailed analysis to check for the role of external and intraparticle mass transfer is necessary before proceeding to kinetic study. The criteria involves evaluation of factors α_1, α_2 and ϕ_{exp}[17] which are defined as the ratio of observed rate of hydrogenation to the maximum rates of gas-liquid mass transfer, liquid-solid mass transfer and intraparticle mass transfer respectively. The criteria for kinetic control as suggested by Ramachandran and Chaudhari[17] are:

(a) Gas-liquid mass transfer is unimportant, if

$$\alpha_1 = \frac{R_A}{k_l a_b C_H^*} < 0.1 \qquad (2.4)$$

(b) Liquid-Solid mass transfer resistance negligible, if

$$\alpha_2 = \frac{R_A}{k_s a_p \quad C_H^*} \quad < \quad 0.1 \qquad (2.5)$$

$$\text{Where} \quad a_p = \frac{6w}{\rho_p d_p} \qquad (2.6)$$

(3) Pore diffusion is negligible, if

$$\phi_{exp} = \frac{d_p}{6}\left[\frac{\rho_p R_A}{w \quad D_e \quad C_H^*}\right]^{0.5} < \quad 0.2 \qquad (2.7)$$

Where, D_e represents the effective diffusivity, which is given as

$$D_e = D_M \varepsilon / \tau \qquad (2.8)$$

The molecular diffusivity, D_M, was evaluated from the correlation proposed by Wilke and Chang.[18] In the present case, since the catalyst pellets were made by pelletising the powder catalyst, the pores were assumed to be much bigger in size. Hence the tortousity value (τ) chosen was 1.25 [19,20] and the porosity of the catalyst pellet (ε) was assumed to be 0.6.

The gas-liquid mass transfer coefficient, $k_L a_b$, was evaluated from the correlation proposed by Bern et al.[21] for a stirred tank reactor as:

$$k_l a_b = 1.099x10^{-2} \; N^{1.16} \; d_I^{1.797} \; u_g^{0.32} \; V_L^{-0.52} \qquad (2.9)$$

For the calculation of liquid-solid mass transfer coefficient, k_s, the correlation proposed by Sano et al. [22] was used.

$$\frac{k_s d_p}{DF_c} = 2 + 0.4\left[\frac{\varepsilon d_p^{\,4} \rho_L^{\,3}}{\mu_L^{\,3}}\right]^{0.25}\left[\frac{\mu_L}{\rho_L D_M}\right]^{0.333} \qquad (2.10)$$

Where F_c is the shape factor, assumed to be unity for spherical particles and e, the energy supplied to the liquid, was calculated by the procedure described by Calderbank.[23] Calculations done for the highest possible reaction rates showed that gas-liquid, liquid-solid and intraparticle mass transfer resistances were negligible, as evident from the values of α_1, α_2 and ϕ_{exp} given in Table 2.2

Table 2.2: Range of Values of a_1, a_2 and f_{exp} for Experiments at 423 K

Range of α_1	0.008 – 0.043
Range of α_2	1.8×10^{-5} - 5.3×10^{-5}
Range of ϕ_{exp}	0.006 – 0.015

From the above analysis it was concluded that the data obtained in the range of conditions shown in Table 2.1 were in the kinetic regime and can be used to determine the intrinsic kinetic parameters of the reaction.

The effect of acetophenone concentration on initial rate of reaction showed a first order tending to zero order dependence (Figure 2.6) whereas, the initial rate varied linearly with H_2 partial pressure (Figure 2. 7).

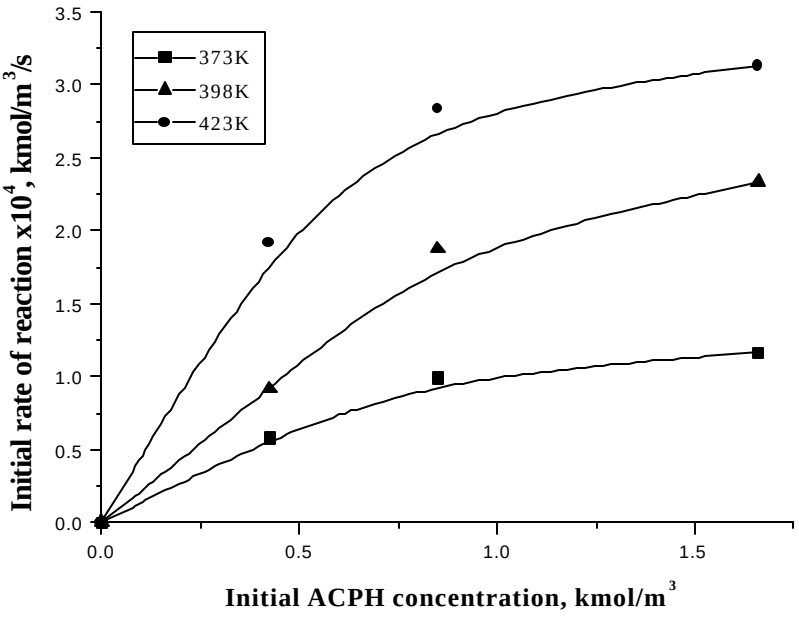

Figure 2.6: Effect of Acetophenone Concentration on Initial Rate of Reaction

Reaction Conditions: P_{H2}: 47.6 atm, Solvent: Methanol, Catalyst Loading: 10 kg/m^3, Agitation Speed: 15 Hz

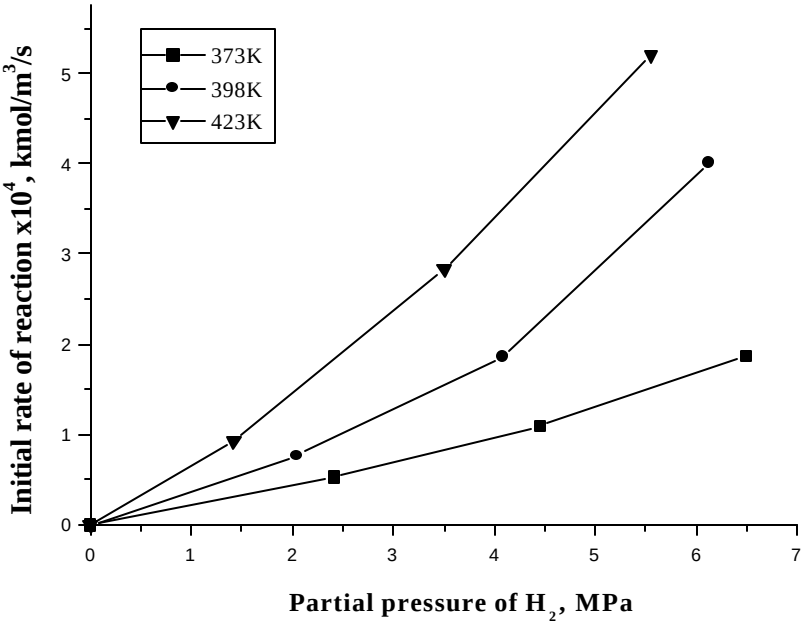

Figure 2.7: Effect of Hydrogen Partial Pressure on Initial Rate of Reaction

Reaction Conditions: Concentration of ACPH: 0.84 kmol/m^3, Solvent: Methanol, Catalyst Loading: 10kg/m^3, Agitation Speed: 15 Hz

2 (A). 2.5 Solubility of Hydrogen in Mixture of Methanol and Acetophenone

Solubility data for H_2 in liquid medium is most essential for interpretation of kinetics and mass transfer effects. The solubility of hydrogen in methanol (C_H^*) is expressed by Henry's relation as:

$$C_H^* = H_e P_{H2} \qquad (2.\ 11)$$

Where H_e is the Henry's constant, kmol/m^3.atm and P_{H2} is the partial pressure of hydrogen, atm. The value of Henry's constant at different temperatures and for various mixtures of acetophenone and methanol were determined experimentally (Section 2 (A). 1.4.) and given in Table 2.3.

The solvent vapour pressure at different temperatures was calculated using the relation

$$\log(P_v) = (-0.2185\ A / T) + B \qquad (2.\ 12)$$

Where A and B are constants and for methanol,[24] A=8978.8 and B=8.639821; T is the temperature in K.

Table 2.3: Values of Henry's Constant at Different Temperatures for Various Mixtures of ACPH and Methanol

S. No.	Temp., K	H_e Values for Mixtures of ACPH + MeOH (%V/V) $x10^3$, $kmol/m^3.atm$		
		5% ACPH	10% ACPH	20% ACPH
1	373	5.01	4.7	4.2
2	398	5.06	5.2	4.6
3	423	5.5	5.65	5.015

2 (A). 2. 6 Kinetic Study

For kinetic study, several experiments were carried out in which concentration-time profiles were observed over a range of conditions given in Table 2.1. The mass transfer analysis showed that the data were obtained in kinetic regime. Therefore the experimental data can be used for kinetic analysis and evaluation of intrinsic kinetic parameters.

2 (A). 2.6.1 Assumptions and Simplification of Reaction Scheme

- The formation of ETCH was found to be negligible in most of the experiments, and hence not taken into account for kinetic modelling.
- It was assumed that CHET is essentially formed from PHET hydrogenation and since the rate of formation of CHET by hydrogenation of CHMK was very low, CHET formation from CHMK was assumed to be negligible.
- The rate of surface reaction is rate limiting and rates of adsorption and desorption are high compared to the reaction rate. All species concentrations are in equilibrium with concentrations of adsorbed species.
- Only the reactive species are chemisorbed on active sites and solvent moieties do not occupy the active sites.
- The adsorption of saturated product, CHET was assumed to be negligible due to its weak adsorption characteristics.[25]

- The adsorption of ETBE was not taken into account, due to its lower concentration level.

The simplified reaction scheme is shown in Figure 2.8.

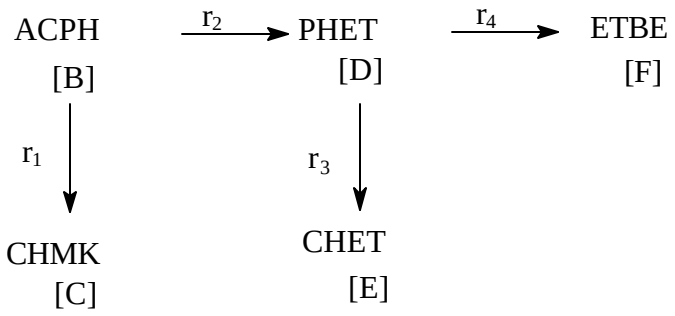

Figure 2.8: Simplified Reaction Scheme

2 (A). 2.6.2 Derivation of Rate Models

Different mechanisms were considered for the derivation of Langmuir-Hinshelwood type of rate models to explain the observed trends and the concentration - time profiles. Keeping in mind the simultaneous hydrogenation of both ketonic and aromatic ring, different type of active sites on the catalyst surface was considered (see Figure 2.9). Two types of sites were assumed, one where ketonic group and the alcoholic group getting attached to the catalyst surface through site S_X and the other type of site where, aromatic ring getting attached through the site S_Y. A similar type of model was considered earlier by Neri et al.[25]

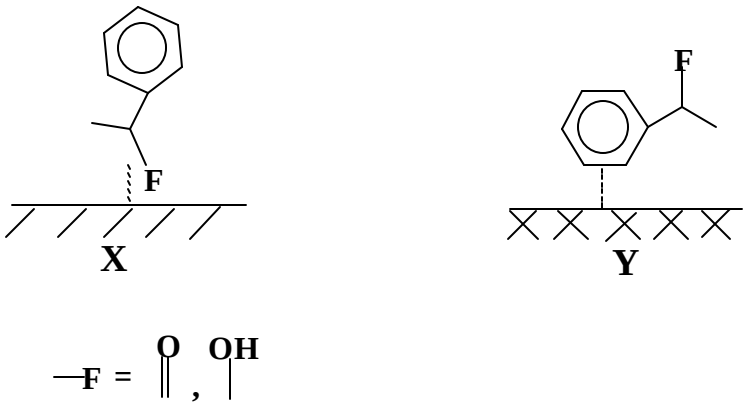

Figure 2.9: Adsorption of Functional Groups on Different Sites

H_2 was assumed to get activated on different sites represented here as S_H and it does not compete with organic species for adsorption. The reaction mechanism involved can now be represented as:

$$S_H + H_2 \Leftrightarrow S_H H_2 \quad (2.13)$$

$$A + S_X \Leftrightarrow A S_X \quad (2.14)$$

$$A + S_Y \Leftrightarrow A S_Y \quad (2.15)$$

$$A S_X + S_H H_2 \rightarrow P S_X + S_H \quad (2.16)$$

$$A S_Y + S_H H_2 \rightarrow P S_Y + S_H \quad (2.17)$$

$$P S_X \Leftrightarrow P + S_X \quad (2.18)$$

$$P S_Y \Leftrightarrow P + S_Y \quad (2.19)$$

Where P corresponds to the products formed and PS_X and PS_Y are the sites where product moieties are adsorbed. Notation A corresponds to any liquid phase reacting component. The rate corresponding to any reaction step can be given as:

$$r_i = k_i \Theta_i \Theta_H \quad (2.20)$$

Where, k_i is the corresponding reaction rate constant for the i^{th} reaction step and Θ_i and Θ_H are the surface fractional coverages with i^{th} component and hydrogen respectively. The surface coverage of components adsorbed on X or Y type of sites can be given as

$$\Theta_{i\,X\,or\,Y} = \frac{K_{i\,X\,or\,Y}\, C_i}{(1+\sum_{i=1}^{n} K_{i\,X\,or\,Y}\, C_i)} \quad (2.21)$$

Where, n is the number of reaction components that can get adsorbed on X or Y type of sites and K_i is the corresponding adsorption equilibrium constant. The fractional coverage of hydrogen can be represented as

$$\Theta_H = \frac{K_H C_H^*}{(1+K_H C_H^*)} \quad (2.22)$$

Where, K_H is the adsorption constant corresponding to hydrogen. From the initial rate analysis it was found that the partial pressure effect of hydrogen on the initial reaction

rate was linear and hence we assume that the adsorption term corresponding to hydrogen is negligible compared to unity (ie. $K_H C_H << 1$) and hence

$$\Theta_H = K_H C_H^* \quad (2.\ 23)$$

The reaction rate can now be expressed as

$$r_i = \frac{w k_i K_{i\,X\,or\,Y} C_i K_H C_H^*}{(1+\sum K_{i\,X\,or\,Y} C_i)} \quad (2.\ 24)$$

We represent $k_i K_H = k'_i$ and the final rate form can be given as

$$r_i = \frac{w k_i' K_{i\,X\,or\,Y} C_i C_H^*}{(1+\sum K_{i\,X\,or\,Y} C_i)} \quad (2.\ 25)$$

In general, the rate equations corresponding to reaction steps involving ring hydrogenation can be written as

$$r_i = \frac{w k_i' K_{iY} C_H^* C_i}{(1+\sum_i K_{iY} C_i)} \quad (2.\ 26)$$

and the rate equations for reaction step involving ketonic group can be written as

$$r_i = \frac{w k_i' K_{iX} C_H^* C_i}{(1+\sum_i K_{iX} C_i)} \quad (2.\ 27)$$

Since the hydrogenation of acetophenone involves multi step reactions, integral concentration-time data in a semi-batch slurry reactor have to be simulated. The change in concentration with time can be represented by the following equations:

$$-\frac{dC_B}{dt} = R_B = \frac{1}{3}\frac{w k_1' K_{BY} C_H^* C_B}{(1+K_{BY}C_B+K_{DY}C_D)} + \frac{w k_2' K_{BX} C_H^* C_B}{(1+K_{BX}C_B+K_{DX}C_D)} \quad (2.\ 28)$$

$$\frac{dC_C}{dt} = R_C = \frac{1}{3}\frac{w k_1' K_{BY} C_H^* C_B}{(1+K_{BY}C_B+K_{DY}C_D)} \quad (2.\ 29)$$

$$\frac{dC_D}{dt} = R_D = -\frac{1}{3}\frac{wk_3' K_{BY} C_H^* C_D}{(1+K_{BY}C_B+K_{DY}C_D)} + \frac{wC_H^*(k_2' K_{BX} C_B - k_4' K_{DX} C_D)}{(1+K_{BX}C_B+K_{DX}C_D)} \quad (2.30)$$

$$\frac{dC_E}{dt} = R_E = \frac{1}{3}\frac{wk_3' K_{BY} C_H^* C_D}{(1+K_{BY}C_B+K_{DY}C_D)} \quad (2.31)$$

$$\frac{dC_F}{dt} = R_F = \frac{wk_4' K_{DX} C_H^* C_D}{(1+K_{BX}C_B+K_{DX}C_D)} \quad (2.32)$$

The initial conditions are

$$\text{At } t = 0,\ C_B = C_{B0} \text{ and } C_C = C_D = C_D = C_E = 0 \quad (2.33)$$

The total rate of hydrogenation at any point is given by

$$R_{H_2} = r_1 + r_2 + r_3 + r_4 \quad (2.34)$$

A non-linear least square regression analysis was used to obtain the best-fit values of the parameters. For this purpose, an optimization program based on Marquarts method combined with a Runge-Kutta method was used to solve the above set of equations.

The model parameters were estimated by minimizing the following objective function:

$$f_{min} = \sum_{i=1}^{5} \sum_{i=1}^{n} (Y_{i_{exp}} - Y_{i_{mod}})^2 \quad (2.35)$$

Where $Y_{i_{exp}}$ is the measured concentration of component i, $Y_{i_{mod}}$ is the calculated concentration of component i and n is the number of samples. The rate parameters estimated are given in Table 2.4. The experimental and the predicted concentration - time data were found to agree well within 5-8% error as shown in Figures 2.10 and 2.11, for rate equations (2.28) to (2.32).

From the temperature dependence of rate parameters, the activation energies of various reaction steps were calculated. These values of activation energies for steps (1) to (4) in Figure 2.8 were found to be 49, 50, 63 and 57 kJ/mol respectively. The enthalpies

of adsorption corresponding to adsorption constants K_{BX}, K_{BY}, K_{DX} and K_{DY} were calculated as 24, 22, 15 and 30.6 kJ/mol respectively.

Table 2.4: Values of Rate and Adsorption Constants

Temp., K	Rate Constants x10^4				Adsorption Constants			
	k'_1	k'_2	k'_3	k'_4	K_{BX}	K_{BY}	K_{DX}	K_{DY}
373	2.25	1.94	4.20	0.38	5.50	3.19	1.63	0.28
398	3.81	3.22	9.70	0.82	3.37	2.38	1.03	0.23
423	5.69	5.51	14.17	1.88	2.20	1.35	0.51	0.16

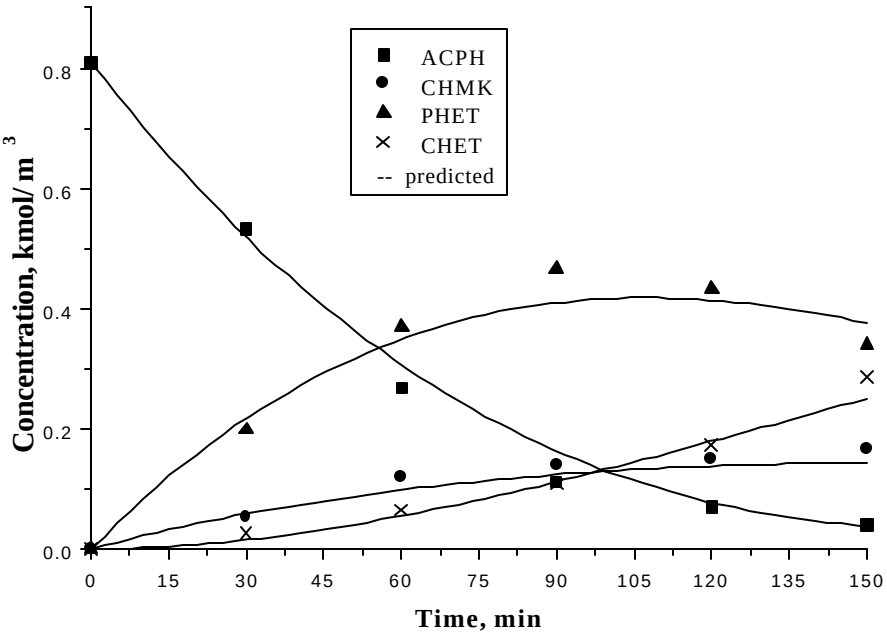

Figure 2.10: Concentration – Time Profile at 373 K

Reaction Conditions: Concentration of ACPH: 0.85 kmol/m^3, Catalyst Loading: 10 kg/m^3, P_{H2}: 47.6 atm, Solvent: Methanol, Agitation Speed: 15 Hz

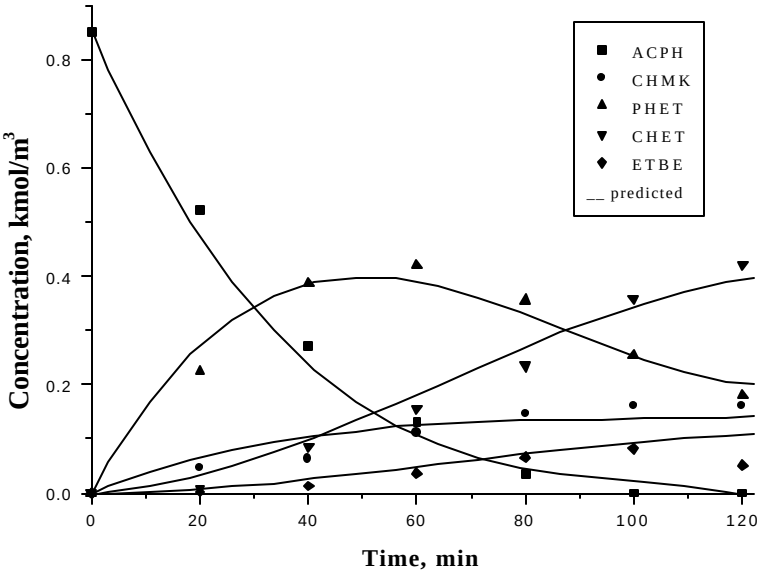

Figure 2.11: Concentration – Time Profile at 398 K

Reaction Conditions: Concentration of ACPH: 0.85 kmol/m^3, Catalyst Loading: 10 kg/m^3, P_{H2}: 47.6 atm, Solvent: Methanol, Agitation Speed: 15 Hz

2 (A). 2.7 Modeling of a Basket Type of Reactor

The reactions were carried out using catalyst particles of various diameters ranging from 1-4 mm. Known amount of catalyst was placed in the basket attached to the dip tube and precaution was taken to ensure that the catalyst particles are immersed well within the liquid mixture. In order to confirm that the intraparticle mass transfer resistance is the rate-limiting step it was necessary to analyse the role of external mass transfer effects on the reaction.

2 (A). 2.7.1 Analysis of External Mass Transfer

External mass transfer analysis was done to confirm that gas-liquid and liquid-solid mass transfer is not influencing the reaction rate as described in the earlier section.

2(A).2.7.2 Analysis of Intraparticle Diffusional Effects for Liquid Phase Components

To check whether the diffusional effects of liquid phase components were also important, the criteria proposed by Ramachandran and Chaudhari[17] was used. According

to this criteria, the intraparticle diffusional effects of the liquid phase components can be neglected only if the ratio of the product of effective diffusivity of liquid phase components and its concentration to that of product of effective diffusivity of hydrogen and its concentration in equilibrium with the liquid phase is greater than 10.

$$\frac{D_{ei}\, C_i}{\boldsymbol{n}\, D_{eA}\, C_A^{*}} \quad > \quad 10 \qquad (2.36)$$

It was found that at lower initial substrate concentrations (~ < 0.6 kmol/m^3), the diffusional effects of liquid phase components could be significant. In order to account for simultaneous diffusion of all the liquid phase reactants/intermediates along with dissolved H_2, a detailed theoretical model was developed as described here.

. 2 (A). 2.7.3 Modelling and Simulation

The mass balance for any component in a spherical particle can be written in the dimensionless form to represent simultaneous diffusion with reaction in catalyst pores.

$$\boldsymbol{e}\left(\frac{\partial c_i}{\partial t}\right) = \frac{D_{ei}}{R^2}\left[\frac{\partial}{\partial r}\left(r^2\,\frac{\partial c_i}{\partial r}\right) + \boldsymbol{f}^2 R_i\right] \qquad (2.37)$$

For hydrogen

$$R_i = \quad r_1^{'} + r_2^{'} + r_3^{'} + r_4^{'} \qquad (2.38)$$

$$r_i^{'} = \frac{k_{i1}\, c_H^{'}\, c_i^{'}}{\left(1 + \sum K_{iXorY}^{'}\, C_i^{'}\right)} \qquad (2.39)$$

where

$$k_{i1} = k_i^{''} \Big/ k_1^{''} \text{ and } k_i^{''} = k_i^{'}\, K_{iXorY}, K_{iXorY}^{'} = K_{iXorY}\, B_{li},\ C_i^{'} = C_i / B_{li},\ C_H^{'} = C_H / B_{li} \qquad (2.40)$$

$$\boldsymbol{f}^2 \quad = \quad \frac{\boldsymbol{r}\, k_1\, C_{Bli}\ R^2}{D_e} \qquad (2.41)$$

Boundary conditions are

At time t = 0 and r = 1, $C'_H = C_H^*/B_{li}$ (2.42)

$t \leq 0$ and $0 \leq$ r not defined at the end ≥ 1 $C'_B = 1$, $C'_c = C'_d = C'_e = C'_f = 0$ (2.43)

At t = 0 and r < 1, $C'_H = 0$ (2.44)

For t > 0

At r = 0, i.e. at the centre of the pellet,

$$\left[\frac{\partial C_i}{\partial r}\right]_{r=0} = 0 \tag{2.45}$$

At r = 1, i.e., at the surface of the catalyst, concentration of components will be same as that of the bulk concentration, since external mass transfer is assumed to be negligible.

$C'_H = C_H^*/B_{li}$ and $C'_i = C'_{il}$ (2.46)

Where C^*_H is the saturation solubility of hydrogen and C'_{il} is the concentration of i^{th} component in the liquid phase.

The variation of bulk liquid concentration can be related to the flux at the catalyst surface as

$$\frac{d c_i}{d t} = \frac{3 w D_{ei}}{\rho_p R^2}\left(\frac{\partial c_i}{\partial r}\right)_{r=1} \tag{2.47}$$

For a semi-batch reactor, due to continuous feed of hydrogen, the external hydrogen concentration at the particle surface remains same as that of solubility. Above equations were solved simultaneously to obtain the concentration distribution in the pellet as well as in the bulk liquid stream using orthogonal collocation method.

2 (A). 2.7.4 Prediction of Bulk Concentrations

Experimental results showed that the rate of reaction decreases with increasing particle size due to intraparticle diffusional effects. The simulated results were found to agree well with the observed experimental results (Figures 2.12 and 2.13). As the concentration in bulk varied with time, the boundary conditions change and hence the

concentration profile of various liquid phase components inside the particle also changed with time.

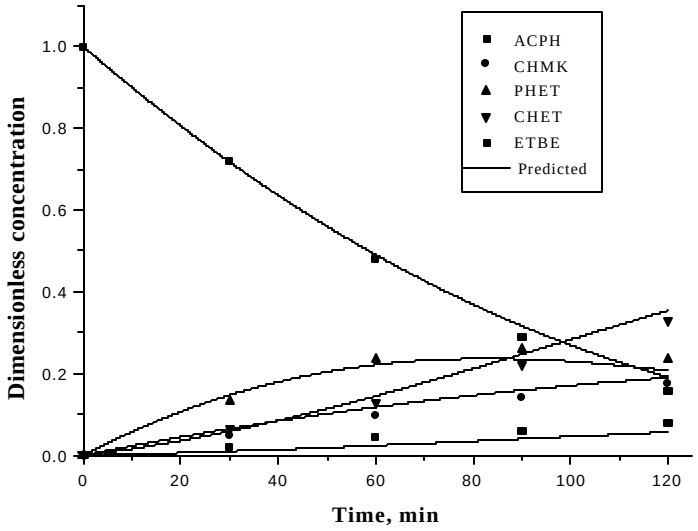

Figure 2.12: Predicted and Experimental Concentration - Time Profiles for the Bulk Liquid.

Reaction Conditions: Pellet Diameter: $2x10^{-3}$ m, Temperature: 398 K, Initial Substrate Concentration: 0.84 kmol/m^3, P_{H2}: 47.6 atm, Catalyst Loading: 10 kg/m^3

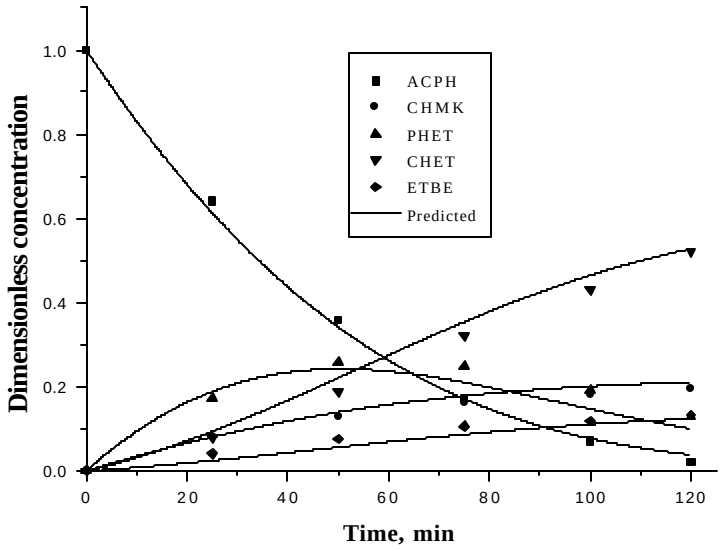

Figure 2.13: Predicted and Experimental Concentration - Time Profiles for the Bulk Liquid

Reaction Conditions: Pellet Diameter: $2x10^{-3}$ m, Temperature: 423 K, Initial Substrate Concentration: 0.8 kmol/m^3, P_{H2}: 47.6 atm, Catalyst Loading: 10 kg/m^3

2 (A). 2.7.5 Effectiveness Factor

Since, the reactions were carried out under conditions of negligible external mass transfer, catalyst effectiveness factor can be used instead of overall effectiveness factor to explain the performance of the reactor. Effectiveness factor is the average rate of reaction with diffusion effects inside the pellet divided by average rate of reaction evaluated based on surface concentrations. Effectiveness factor was calculated from the following equation for a spherical particle[26]

$$\eta = \frac{3 \left.\frac{\partial c}{\partial r}\right|_{r=1}}{\phi^2} \qquad (2.48)$$

The variation of effectiveness factor with time obtained for pellets of 2mm size at different temperatures is shown in Figure 2.14, which was found to decrease with increase in temperature.

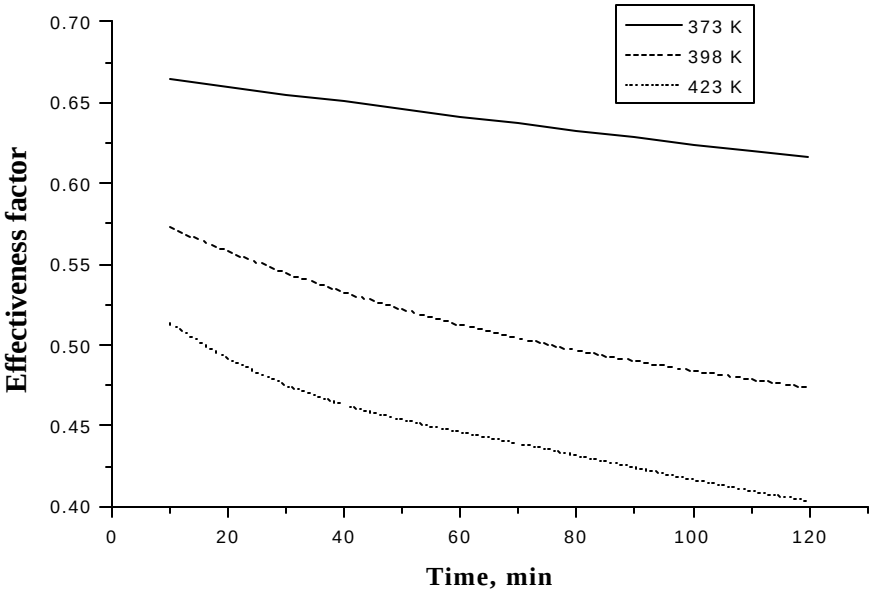

Figure 2.14: Variation of h_C with Time for a Pellet Size $2x10^{-3}$ m

Similarly, as the pellet size decreases, the effectiveness factor tends to unity showing that no intraparticle diffusional effects exist at very low particle radii (~10^{-5}m). The variation of effectiveness factor as a function of the square of Theile modulus is shown in Figure 2.15.

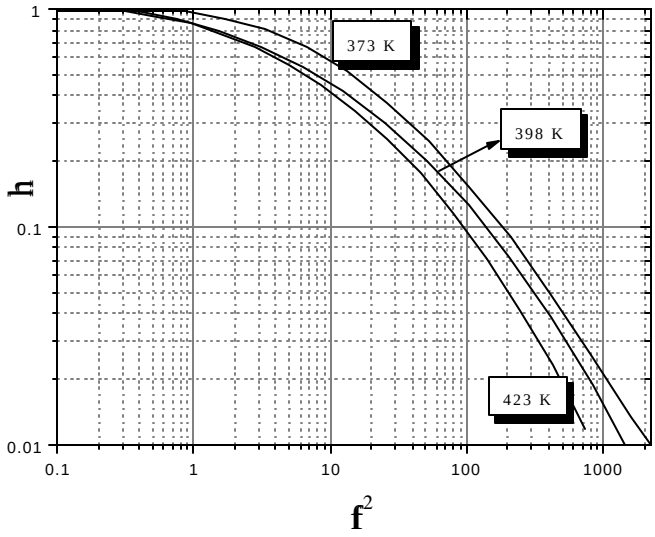

Figure 2.15: Variation of Effectiveness Factor with the Thiele Modulus

2 (A). 2.7.6 Pellet Dynamics

The dynamic behaviour of the concentration profiles inside the pellet was obtained by assuming the initial concentration of liquid phase components (except acetophenone) and hydrogen as zero inside the pellet. For acetophenone it was assumed that, at the starting of reaction the dimensionless concentration was one throughout the pellet radius. The concentration profile inside the pellet for hydrogen and acetophenone from the very beginning (t = 0) till steady state, are shown in Figures 2.16 and 2.17 respectively. The dynamics were obtained assuming that within such a short time period, the bulk concentration change is negligible compared to the total reaction time. Due to the higher diffusivity values of hydrogen, it was observed that the steady state for hydrogen reached within a comparatively shorter period (10-15 sec) than that of acetophenone (30-40s).

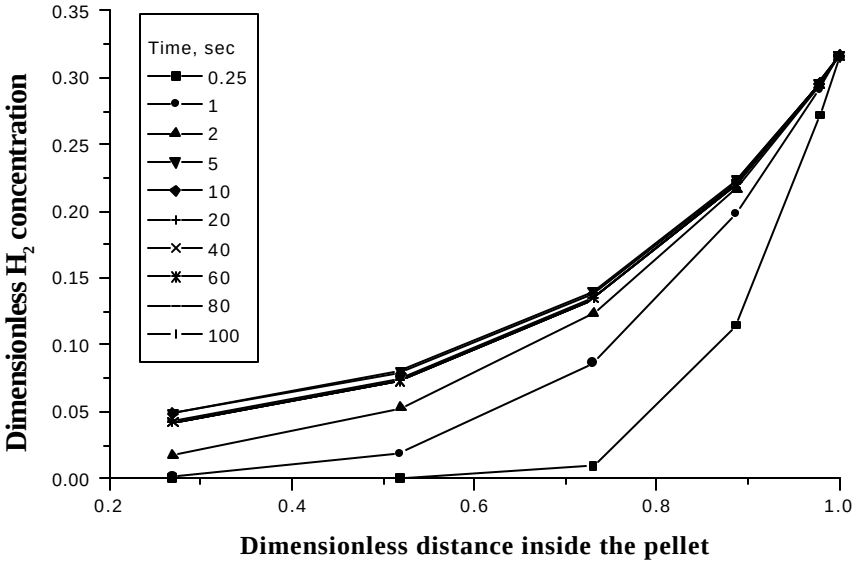

Figure 2.16: Concentration profile of Hydrogen Inside the Pellet During Initial Period

Reaction Conditions: Pellet Diameter: 2mm, Temperature: 398K, P_{H2}: 47.6 atm, Initial Substrate Concentration: 0.8 kmol/m^3, Solvent: Methanol

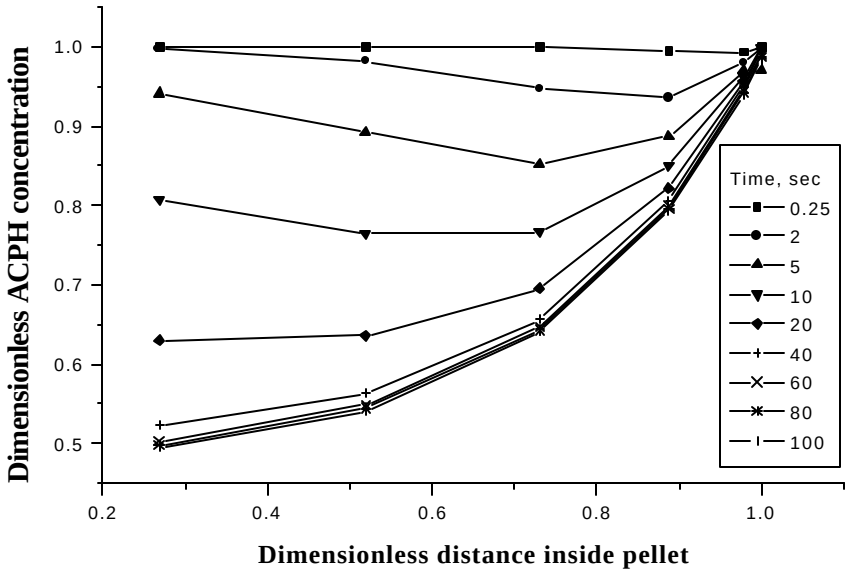

Figure 2.17: Concentration Profile of ACPH Inside the Pellet During Initial Period

Reaction Conditions: Pellet Diameter: 2mm, Temperature: 398K, P_{H2}: 47.6 atm, Initial Substrate Concentration: 0.8 kmol/m^3, Solvent: Methanol, Catalyst Loading: 10kg/m^3

It was observed that, in the initial course of reaction, when acetophenone and hydrogen are the only reacting species, the reaction inside the pellet was limited by hydrogen. As the reaction proceeds, 1-phenylethanol is produced, which further undergoes hydrogenation to give 1-cyclohexylethanol or ethyl benzene. In the initial stages, the concentration of 1-phenylethanol is very low and can be rate limiting since the hydrogen concentration is higher.

The concentration profile of PHET and hydrogen inside the particle and in the bulk liquid during the entire reaction time was simulated to check when PHET will be rate limiting and at what positions inside the pellet and is given in Figure 2.18.

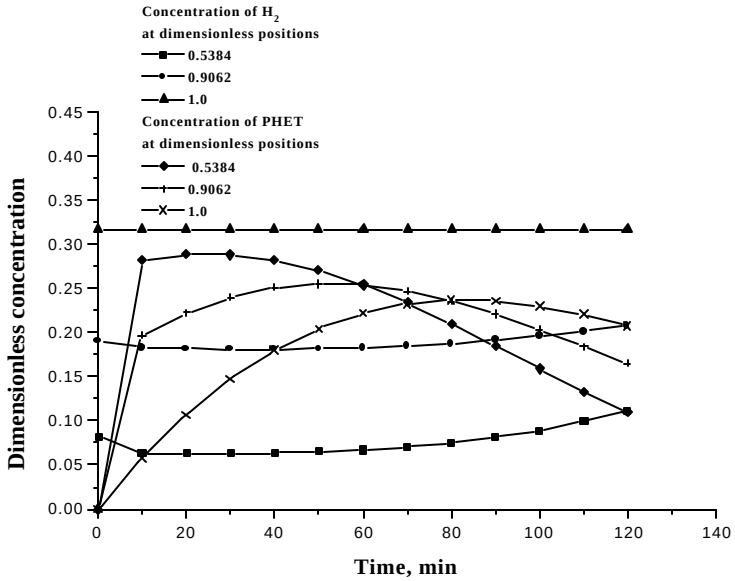

Figure 2.18: Distribution of Dimensionless Concentration of Phenyl Ethanol and Hydrogen at Various Positions Inside the Pellet During the Entire Course of Reaction

Reaction Conditions: Pellet Diameter: $2x10^{-3}$ m, Temperature: 398 K, Initial Substrate Concentration: 0.84 kmol/m^3, P_{H2}: 47.6 atm, Catalyst Weight: 10 kg/m^3, Solvent: Methanol

From Figure 2.18 it can be seen that at dimensionless position 0.9062, PHET is rate limiting in the initial period (till 6-7 minutes). Also it becomes limiting reactant towards the end of reaction time (100-120 minutes). When we consider an interior dimensionless pellet position (0.5384), hydrogen is the limiting reactant almost during the entire course of reaction. Similarly for acetophenone also, at times when its concentration is very low (i.e. towards the end of reaction) it was found to be limiting. To see how important is the

liquid diffusional effects of the intermediates, the concentration distribution of PHET inside the pellet as well as in bulk liquid was investigated, under two conditions (i) when liquid component diffusion is taken into consideration along with that of gaseous hydrogen and (ii) when only diffusion of hydrogen is considered (This was done by multiplying the diffusivity of liquid phase component by factor of 10). The simulated results are shown in Figure 2.19. It can be seen from the graph that when diffusion of liquid phase is not considered the external as well as the concentration at the internal points remain the same, where as there is a considerable difference between the external concentration of PHET and that inside the pellet in presence of liquid diffusional effects.

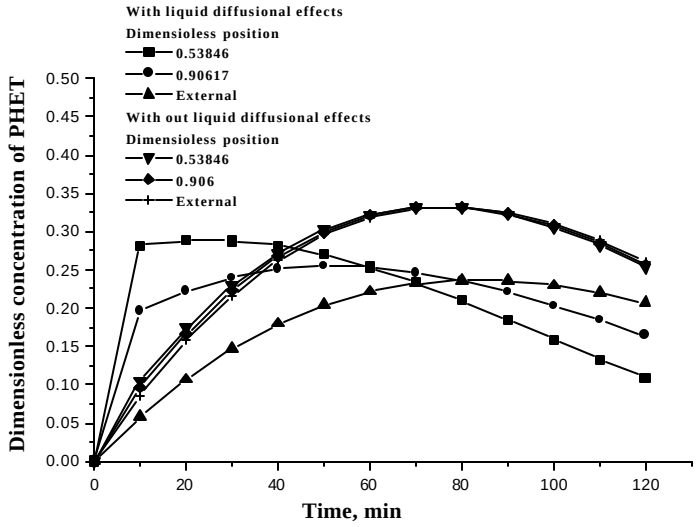

Figure 2.19: Comparison of Concentration - Time Profile Predicted in the Bulk Phase and within the Pellet With and Without Taking in to Consideration the Diffusional Effects of Liquid Phase Components

Reaction Conditions: Pellet Diameter: $2x10^{-3}$ m, Temperature: 398 K, Initial Substrate Concentration: 0.84 kmol/m^3, P_{H2}: 47.6 atm, Catalyst Loading: 10 kg/m^3

2 (A). 2.8 Non-Isothermal Effects in a Semi-batch Slurry Reactor

Even though the formation of PHET from ACPH is not a highly exothermic reaction (ΔH_r = -59.3 kJ/mol), the formation of ring hydrogenated products are comparatively exothermic (ΔH_r = -202.2 kJ/mol for ACPH $\rightarrow$ CHMK, and ΔH_r = -195.5 kJ/mol for PHET $\rightarrow$ CHET). The temperature rise in the reactor under non-isothermal conditions can lead to changes in rate parameters, solubility of gaseous reactant, molecular

diffusivity of reaction components etc. Non-isothermal modeling of semi-batch slurry reactor has been reported earlier for different reaction systems.[27,28] Here we present a detailed non-isothermal modelling of slurry reactor and a basket type reactor for the ACPH hydrogenation using 2%Ru/Al_2O_3 catalyst. Reaction conditions were chosen in such a way that the reaction was almost completed within 30min to get a reasonable temperature rise in the reactor.

The net heat balance can be written as

$$(e_g V_R r_g C_{Pg} + V_R (1-e_g) r_l C_{Pl}) \frac{dT}{dt} = (-\sum \Delta H_i r_i) V_R - U_W A_W (T-T_W) - Q_g r_g (T-T_g) \quad (2.49)$$

Where T_g is the inlet gas temperature, T_W is the temperature of the outer jacket, C_{Pg} and C_{Pl} are the specific heats of gas and liquid respectively, U_W is the overall heat transfer coefficient, A_W is the wall heat transfer area, e_g is the gas holdup, ΔH_i is the heat of reaction for i^{th} reaction step, V_R is the volume of gas-liquid dispersion. The value of the overall heat transfer parameter, U_W, is specific to reactor configuration and a value of 0.08 kJ/m^2.sec.K was reported for the same reactor by Rode and Chaudhari[28] and this value was used in this case also. The effect of temperature variation on various parameters affecting the reaction rate was taken into consideration. The variation of rate constants and adsorption constants with temperature can be given as

$$(k_i')_T = (k_i')_{T0} \exp\left[\frac{-E_1}{R}\left[\frac{1}{T} - \frac{1}{T_0}\right]\right] \quad (2.50)$$

$$(K'_{iX\ or\ Y})_T = (K'_{iX\ or\ Y})_{T0} \exp\left[\frac{-\Delta H_1}{R}\left[\frac{1}{T} - \frac{1}{T_0}\right]\right] \quad (2.51)$$

The variation in Henry's constant with temperature was determined by extrapolating the known values in the same range. The change in the vapour pressure of the solvent was calculated based on the equation 2.12 and the change in solubility of H_2 due to solvent evaporation could be accounted as:

$$C_H^* = [P - (P_{sol})_T](He)_T \quad (2.52)$$

The mass balance equations incorporating the various temperature dependencies are:

$$-\frac{dC_B}{dt} = \frac{1}{3}\frac{wk_1'(T) K_{BY}(T) C_H^*(T) C_B}{(1 + K_{BY}(T) C_B + K_{DY}(T) C_D)} + \frac{wk_2'(T) K_{BX}(T) C_H^*(T) C_B}{(1 + K_{BX}(T) C_B + K_{DX}(T) C_D)} \quad (2.53)$$

$$\frac{dC_C}{dt} = \frac{1}{3}\frac{wk_1^{'}(T)K_{BY}(T)\ C_H^*(T)C_B}{(1+K_{BY}(T)\ C_B+K_{DY}(T)\ C_D)} \quad (2.54)$$

$$\frac{dC_D}{dt} = -\frac{1}{3}\frac{wk_3^{'}(T)K_{BY}(T)\ C_H^*(T)\ C_D}{(1+K_{BY}(T)\ C_B+K_{DY}(T)C_D)} + \frac{wC_H^*(T)(k_2^{'}(T)K_{BX}(T)C_B - k_4^{'}(T)K_{DX}(T)C_D)}{(1+K_{BX}(T)\ C_B+K_{DX}(T)\ C_D)} \quad (2.55)$$

$$\frac{dC_E}{dt} = \frac{1}{3}\frac{wk_3^{'}(T)\ K_{BY}(T)C_H^*(T)C_D}{(1+K_{BY}(T)\ C_B+K_{DY}(T)\ C_D)} \quad (2.56)$$

$$\frac{dC_F}{dt} = R_F = \frac{wk_4^{'}(T)K_{DX}(T)\ C_H^*(T)C_D}{(1+K_{BX}(T)\ C_B+K_{DX}(T)C_D)} \quad (2.57)$$

The initial conditions are

At t =0, $C_B = C_{B0}$, $T=T_0$ and $C_C = C_D = C_D = C_E = 0$

The mass and heat balance equations were solved using a fourth order Runge-Kutta method.

The theoretically predicted results were compared with the experimentally observed values, when methanol was used as a solvent and is shown in Figure 2. 20.

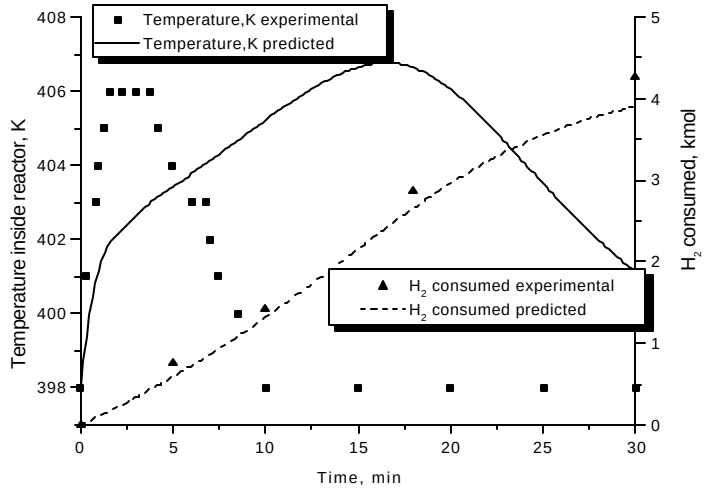

Figure 2.20: Temperature Profile and Hydrogen Consumption with Time Under Non-Isothermal Conditions when Methanol was Used as a Solvent in a Slurry Reactor

Reaction Conditions: Concentration of ACPH: 1.211 kmol/m^3, Catalyst Loading: 30 kg/m^3, P_{H2}: 47.6 atm, Solvent: Methanol, Initial Temperature: 398 K, Agitation Speed: 15 Hz

It was observed that the temperature rise in the reactor was not in accordance with the model prediction. This may be due to the heat removal by the low boiling solvent evaporation. The heat of evaporation of methanol is very high (32.5 kJ/mol), compared to other non-polar solvents and hence will significantly affect the temperature profile.

In order to understand the performance of the reactor under non-isothermal condition when considerable ring hydrogenation occurs and in the absence of solvent evaporation, a solvent with very high boiling point is necessary. Hence n-decane with a boiling range of 171-176^{o}C was chosen as the solvent. Since, it was found that the reaction path changes drastically, when n-decane was used as a solvent, the kinetic parameters for n-decane solvent was re-determined. When n-decane was used, mainly ring hydrogenation took place in the initial period leading to the formation of CHMK. Formation of PHET was much less compared to methanol as the solvent. Also, the formation of CHET from CHMK was found to be significant, which was negligible in the methanol system. The formation of ETBE from CHET was negligible, may be due to the non-polar nature of the solvent hydrocarbon. The new reaction scheme is shown below in Figure 2. 21.

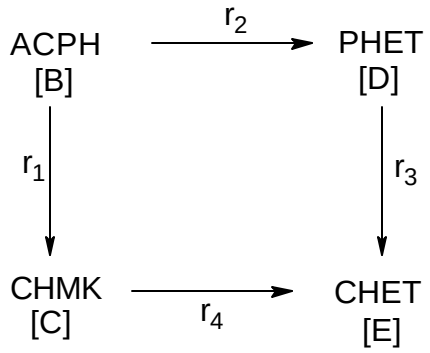

Figure 2.21: Reaction Scheme when n-Decane was Used as the Solvent

A few experiments were carried out with n-decane as a solvent to determine the intrinsic kinetics. The same model equations used with methanol as solvent were found to explain the observed trends and concentration time profiles as shown in Figure 2.22. The new addition to the reaction steps considered was the formation of CHET from CHMK. For this step, the rate constant k'_4 and a new adsorption constant K_{CX} corresponding to the

ketonic group adsorption of CHMK was included in the model in place of the formation of ETBE which was found to be negligible in this case. The mass balance of different components can be written as for a semi-batch slurry reactor.

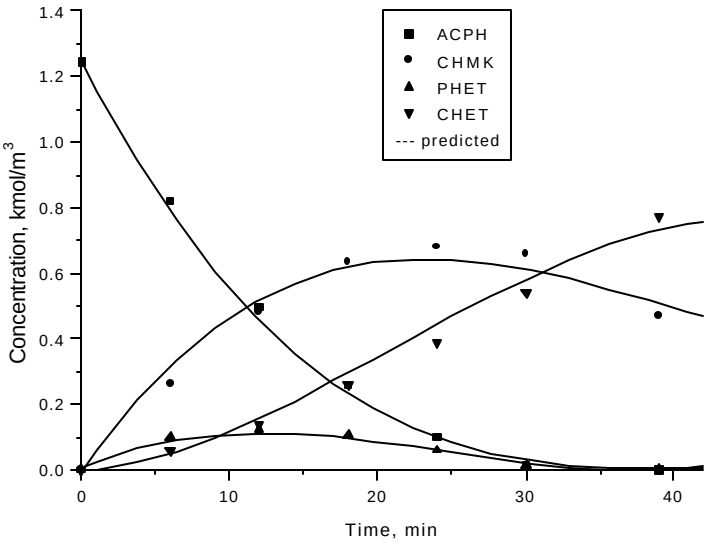

Figure 2.22: Concentration – Time Profile when n-Decane was Used as a Solvent

Reaction Conditions: Temperature: 413 K, Concentration of ACPH: 1.243 kmol/m^3, Catalyst Loading: 5 kg/m^3, P_{H2}: 47.6 atm, Solvent: n-Decane, Agitation Speed: 15 Hz

$$-\frac{dC_B}{dt} = R_B = \frac{1}{3}\frac{wk_1' K_{BY} C_H^* C_B}{(1+K_{BY}C_B+K_{DY}C_D)} + \frac{wk_2' K_{BX} C_H^* C_B}{(1+K_{BX}C_B+K_{CX}C_C)} \quad (2.58)$$

$$\frac{dC_C}{dt} = R_C = \frac{1}{3}\frac{wk_1' K_{BY} C_H^* C_B}{(1+K_{BY}C_B+K_{DY}C_D)} - \frac{wk_4' K_{CX} C_H^* C_B}{(1+K_{BX}C_B+K_{CX}C_C)} \quad (2.59)$$

$$\frac{dC_D}{dt} = R_D = -\frac{1}{3}\frac{wk_3' K_{BY} C_H^* C_D}{(1+K_{BY}C_B+K_{DY}C_D)} + \frac{wC_H^* k_2' K_{BX} C_B}{(1+K_{BX}C_B+K_{CX}C_C)} \quad (2.60)$$

$$\frac{dC_E}{dt} = R_E = \frac{1}{3}\frac{wk_3' K_{BY} C_H^* C_D}{(1+K_{BY}C_B+K_{DY}C_D)} + \frac{wC_H^* k_4' K_{CX} C_B}{(1+K_{BX}C_B+K_{CX}C_C)} \quad (2.61)$$

The initial conditions are

At t =0, $C_B = C_{B0}$ and $C_C = C_D = C_D = C_E = 0$ (2.62)

The total rate of hydrogenation is given by

$$R_{H_2} = 3r_1 + r_2 + 3r_3 + r_4 \quad (2.63)$$

The optimised rate parameters for three temperatures 373, 393 and 143 K were obtained for reaction in n-decane in the same manner as in the case of methanol system and the temperature dependencies of these rate parameters were determined and are given in Table 2. 5.

Table 2.5: Values of Rate and Adsorption Constants at 373 K and it's Temperature Dependencies

Combined Rate Constant	Value at 373 K x 10^3	ΔE, kJ/mol	Adsorption Constant	Value at 373 K	Heat of Adsorption, ΔH, kJ/mol
k'_1	2.29	40	K_{BY}	3.140	17.20
k'_2	4.69	47	K_{BX}	0.042	21.52
k'_3	6.81	55	K_{DY}	1.002	35.53
k'_4	5.32	50	K_{CX}	0.039	14.13

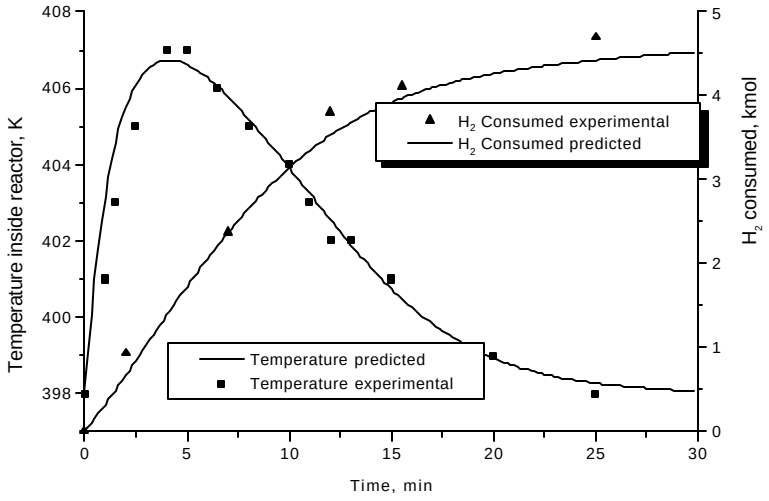

Figure 2.23: Temperature Profile and Hydrogen Consumption with Time Under Non-Isothermal Conditions when n-Decane was Used as a Solvent

Reaction Conditions: Concentration of ACPH: 1.25 kmol/m^3, Catalyst Loading: 10 kg/m^3, P_{H2}: 47.6 atm, Solvent: n-Decane, Initial Temperature: 398 K, Agitation Speed: 15 Hz

The reaction rate was found to be very high compared to the methanol system. The non-isothermal effects for the present system was predicted using the same heat balance equation explained above and was found to agree well with the experimentally observed values as shown in Figure 2. 23. It was also found that the hydrogen consumption as well as the temperature-time profiles predicted by the model was in good agreement with the experimental data.

2 (A). 2.9 Non-isothermal Model for a Basket Type Reactor

In this study we have tried to understand the intraparticle temperature gradient within individual catalyst pellet as well as the external bulk liquid temperature variation with time. It was assumed that the temperature at the surface of the catalyst was the same as that of the bulk liquid i.e. no solid-liquid heat transfer resistance exists. The dimensionless heat balance within a catalyst pellet can be given as:

$$\frac{\partial \Theta}{\partial t} = \frac{\lambda_e}{\rho_p C_p R^2}\frac{\partial^2 \Theta}{\partial r^2} + \frac{(-\sum \Delta H_i r_i)}{C_p T_0} \qquad (2.64)$$

Where $\Delta H_i r_i$ represents the heat generated for a particular reaction step i, Θ is the dimensionless temperature, ρ_p and C_p are the density and specific heat of catalyst pellet respectively, λ_e is the thermal conductivity and the value was taken as 0.15 W/m.K.[13] The boundary condition at the surface of the catalyst particle is:

$$T\big|_{r=1} = T_l \qquad (2.65)$$

Where T_l is the bulk liquid temperature. At the centre of the particle, we have

$$\left.\frac{\partial T}{\partial r}\right|_{r=0} = 0 \qquad (2.66)$$

The heat flux from the catalyst surface can be given in dimensionless form as

$$\left.\frac{3 w \lambda_e V_l T_0}{\rho_p R^2}\frac{d\Theta}{dr}\right|_{r=1} \qquad (2.67)$$

This will act as the heat source for the bulk phase and heat dissipation terms all remain the same as discussed earlier. So the final heat balance for the basket type reactor can be written in the dimensionless form as

$$V_R C_{pl} r_l T_0((1-e_g)+\frac{e_g r_g C_{pg}}{C_{pl} r_l T_0})\frac{d\Theta}{dt} = \frac{3 w l_e V_l T_0}{r_p R^2}\left.\frac{d\Theta}{dr}\right|_{r=1} - U_W A_W T_o(\Theta-1) - Q_g r_g T_0(\Theta-\frac{T_g}{T_0}) \quad (2.68)$$

The above equation along with the heat balance in the pellet and the equations representing temperature dependence of various parameters were solved using the same numerical treatment carried out for solving the isothermal basket type reactor model. Here, at time t=0, it was assumed that at all points inside the pellet as well as in the bulk liquid, the temperature was T_0. The temperature profile predicted for the bulk reaction mixture was compared with the experimental values and was found to agree well as shown in Figure 2.24. It should be noted that the catalyst loadings used for methanol and n-decane as solvents were different and hence the temperature rise almost same. The temperature profile inside the pellet when the temperature of the bulk liquid was maximum is shown in Figure 2.25. It was found that the maximum temperature gradient existing between the pellet centre and the substrate was about 0.05 K and is negligible.

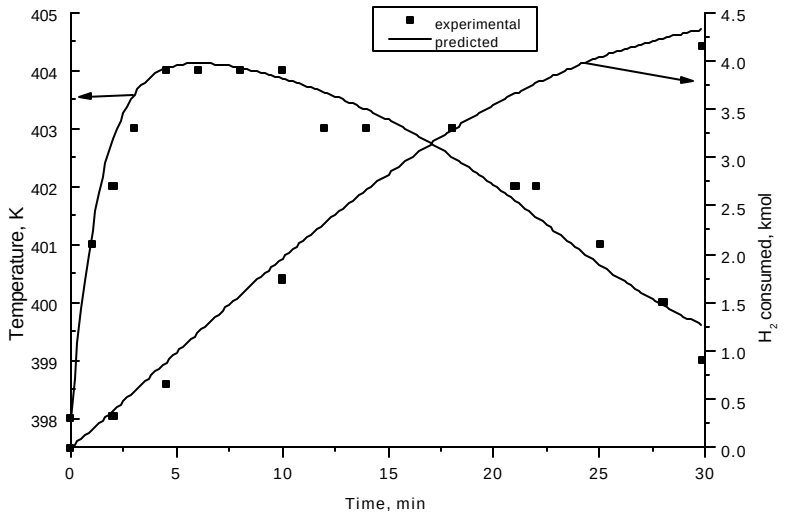

Figure 2.24: Temperature profile and Hydrogen Consumption with Time Under Non-Isothermal Conditions when n-Decane was Used as a Solvent in a Basket Type Reactor

Reaction Conditions: Catalyst Particle Size: 10^{-3}m, Concentration of ACPH: 1.25 kmol/m^3, Catalyst Loading: 22.02 kg/m^3, P_{H2}: 47.6 atm, Initial Temperature: 398 K, Agitation Speed: 15 Hz

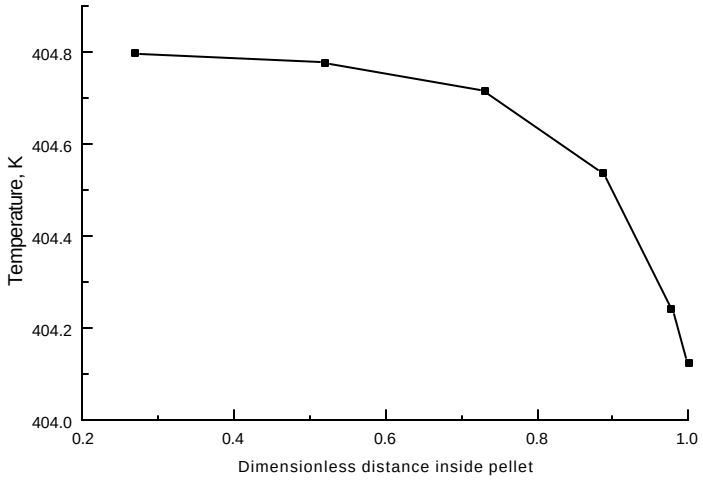

Figure 2.25: The Temperature Profile Inside the Pellet when the Temperature of the Bulk Liquid was Maximum

Reaction Conditions: Catalyst Particle Size: 10^{-3}m, Concentration of ACPH: 1.25 kmol/m^3, Catalyst Loading: 22.02 kg/m^3, P_{H2}: 47.6 atm, Solvent: n-Decane, Initial Temperature: 398 K, Agitation Speed: 15 Hz

2 (A). 3. Conclusion

Hydrogenation of acetophenone was studied in semi-batch slurry and basket type of reactors using 2%Ru/Al_2O_3. A Langmuir-Hinshelwood type rate model based on non-competitive adsorption of hydrogen and liquid phase components and different adsorption sites for the adsorption of different functional groups could explain well the intrinsic kinetics obtained from slurry reactor in kinetic regime. A basket reactor model was derived by incorporating diffusional effects of gaseous as well as liquid phase components, which was found to predict well the experimentally observed concentration - time profiles. The dynamic behaviour of the concentration profiles of all the components inside the pellet was also studied and found that due to the higher diffusivity values of hydrogen, the steady state for hydrogen reached within a comparatively shorter period than that of acetophenone. Investigations on non-isothermal behaviour of the semi-batch slurry reactor showed that the temperature-time profile were not found to agree with the observed trends due to the volatility of the solvent methanol at the reaction

conditions. However, the data in a non-volatile solvent n-decane agreed very well with model predictions. The temperature-time profiles observed in a basket type reactor were also found to agree well with the experimental data. Thus this investigation represents a systematic study of a complex multistep, multiphase catalytic reaction including intrinsic kinetics, intraparticle diffusion and non-isothermal effects.

Chapter 2

Part – B

Hydrogenation of p-Isobutyl Acetophenone Using a Ru/Al_2O_3 Catalyst: Reaction Kinetics and Modelling of a Semi Batch Slurry Reactor

2 (B). 0 Introduction

Hydrogenation of p-isobutyl acetophenone (p-IBAP) is an important step in a new catalytic route developed for Ibuprofen, a non-steroidal, anti-inflammatory drug. This new catalytic route[29] is considered as a major innovation in Ibuprofen technology both from environmental as well as economic point of view, as it eliminates the conventional stoichiometric synthetic routes, which produce a large amount of salts as by-products. Moreover, this reaction is an excellent example of a complex multistep catalytic hydrogenation leading to a variety of products. Most of the earlier literature on this reaction is patented and there are only a few reports, which deal with the catalytic reaction mechanism, kinetic modelling and reaction engineering aspects.

The reduction of a carbonyl group is known to be catalysed by a variety of supported metal catalysts such as Pd, Ni and Ru. During this reaction, along with the reduction of carbonyl group the reduction of benzene ring can also occur leading to a variety of products and hence, understanding of the selectivity behaviour is important. Most of the previous work has reported investigations on the activity and selectivity of the catalysts and some aspects of reaction mechanism using Ni and Pd catalysts. No detailed investigations have been published using Ru catalysed hydrogenation of p-IBAP. In this chapter, kinetic modelling of hydrogenation of p-IBAP using 2%Ru/Al_2O_3 as a catalyst has been reported. The effect of catalyst loading, partial pressure of hydrogen and initial substrate concentration on the hydrogen consumption as well as the concentration - time behaviour in a semi batch slurry reactor has been studied. Based on these data, rate equations have been proposed, based on a model discrimination procedure and rate parameter evaluated.

2 (B). 1 Experimental

The catalyst used was same, as that used in the study of hydrogenation of acetophenone and the experimental methods were also the same. The liquid samples in this case was analysed by gas chromatographic technique using a HP-6890 Gas chromatograph fitted with a HP-FFAP capillary column (30 m x 0.53 μm x 0.1 mm film thickness on polyethylene glycol stationary phase). The conditions of GC analysis were as follows: FID temperature: 573 K, column temperature: 438-463 K (Programmed at 25 K/min), injection

temperature: 523 K, carrier gas: N_2. A few samples were analysed by GC-MS (Shimadzu QP 2000A). The range of operating conditions used in this work is given in Table 2.6.

Table 2.6: Range of Parameters

Catalyst loading	2.5 - 10 kg/m^3
Agitation speed	7.5-15 Hz
H_2 partial pressure	34 - 62 atm
p-IBAP concentration	0.25 - 1.1 kmol/m^3
Temperature	373 - 398 K
Volume of liquid	10^{-4} m^3

2 (B). 2 Results and Discussion

2 (B). 2.1 Experimental Results

The main objective of this work was to study (a) intrinsic kinetics of hydrogenation of p-IBAP using a 2% Ru/Al_2O_3 catalyst in a slurry reactor and (b) performance of a semi-batch slurry reactor under isothermal conditions. For this purpose, a few experiments were first carried out to confirm the product distribution and define a reaction scheme. Catalyst recycle experiments were also carried out without exposing the catalyst to atmosphere, as done for the case of acetophenone, and it was found that the activity remains constant during the course of a batch experiment.

A typical concentration - time profile of various components involved in the hydrogenation of p-IBAP using 2%Ru/Al_2O_3 is shown in Figure 2.26. It was observed that in the initial stages, p-IBAP undergoes hydrogenation through two different path ways: (i) hydrogenation of a carbonyl group to give p-isobutyl phenyl 2-ethanol (p-IBPE) and (ii) ring hydrogenation of p-IBAP to 4-isobutyl cyclohexyl methylketone (4-IBCMK). The formation of p-IBPE was much higher compared to the ring hydrogenated product 4-IBCMK. During the course of reaction p-IBPE also undergoes ring hydrogenation to give 4-isobutyl cyclohexyl 2-ethanol (4-IBCHE) where as the formation of 4-IBCHE by ketonic hydrogenation of 4-IBCMK is comparatively very slow.

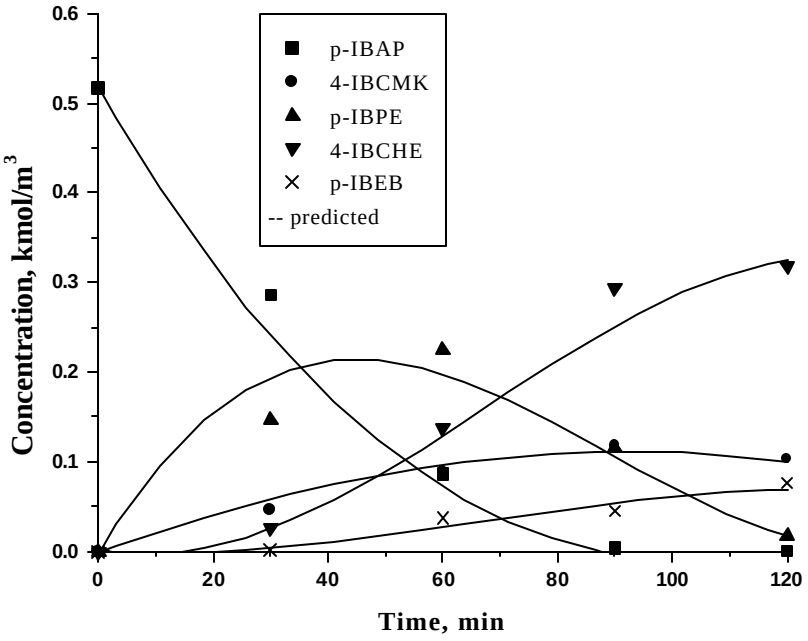

Figure 2.26: Concentration – Time Profile at 398 K

Reaction Conditions: Concentration of pIBAP: 0.53 kmol/m^3, Catalyst Loading: 5 kg/m^3, P_{H2}: 46.7 atm, Solvent: Methanol, Agitation Speed: 15 Hz

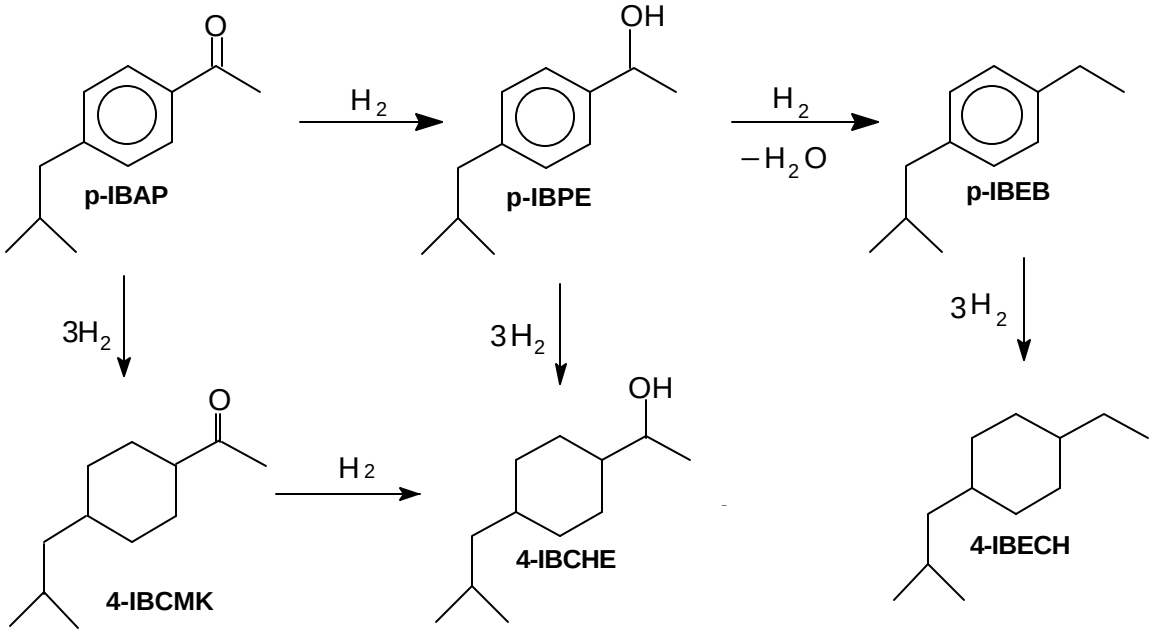

Figure 2.27: Reaction Scheme for Hydrogenation of p-IBAP Using 2%Ru/Al_2O_3 Catalyst

p-IBPE undergoes dehydration to form p-isobutyl styrene(p-IBSTY) which on further hydrogenation gives p-isobutyl ethyl benzene(p-IBEB). In the range of conditions studied, the formation of p-IBSTY was very negligible and hence is not included in the reaction scheme. Ring hydrogenated product of p-IBEB, 4-isobutyl ethyl cyclohexane (4-IBECH) was found to be less than 3%. Based on the products identified and characterised by GC and GC-MS, the reaction scheme is shown in Figure 2. 27.

2 (B). 2.2 Analysis of Initial Rate

The initial rate of reaction was calculated from substrate and hydrogen consumption data under different conditions. To ensure that the rate data obtained for kinetic analysis were obtained under conditions of chemical reaction control and mass transfer limitations are not significant, the values of α_1, α_2 and ϕ_{exp} were calculated as described earlier for all temperatures and found to be below 0.05, 0.0003 and 0.08 respectively showing that these mass transfer effects are negligible. For particle size $d_p > 5 \times 10^{-4}$ m, intraparticle diffusion effects were found to be significant. The initial rates were found to be independent of stirring speed beyond 600 rpm. Also, the initial rates at different catalyst loadings showed a linear dependence. This further supports our conclusion that the gas-liquid mass transfer resistance is not significant.

The general trends observed for the variation of initial rates with different parameters were: (i) the rate of reaction was linearly dependent on H_2 pressure in low-pressure range and tending towards zero order at higher pressures (Figure 2.28.) (ii) the rate vs p-IBAP concentration passed through a maxima indicating substrate inhibition beyond 0.7 kmol/m^3 concentration (Figure 2.29). These data, however, represent only the reactions in the initial stages and hence are not useful to develop kinetic models. For this purpose integral concentration - time profiles under different initial conditions should be considered.

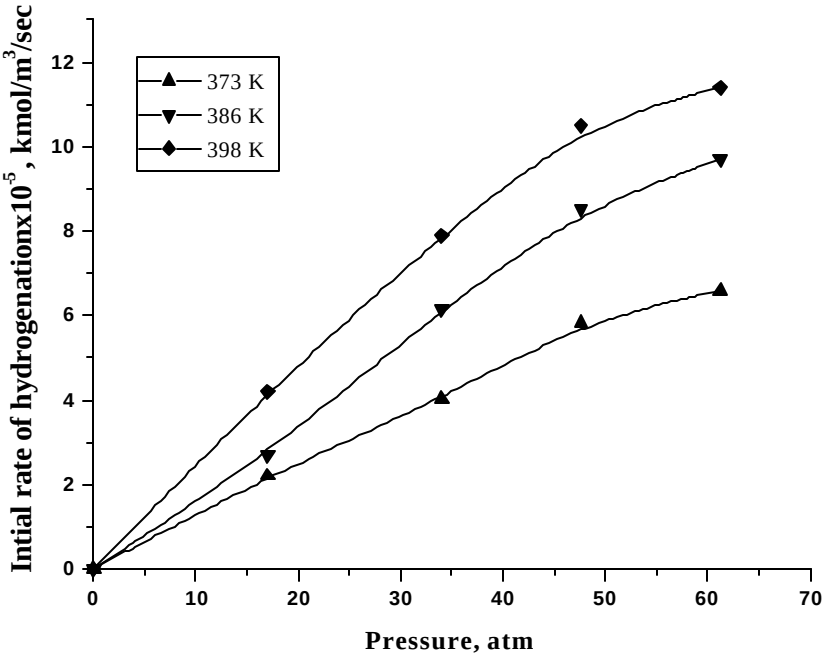

Figure 2.28: Effect of H_2 Partial Pressure on Initial Rate of Reaction

Reaction Conditions: Concentration of pIBAP: 0.53 kmol/m^3, Solvent: Methanol, Catalyst Loading: 5 kg/m^3, Agitation Speed: 15 Hz

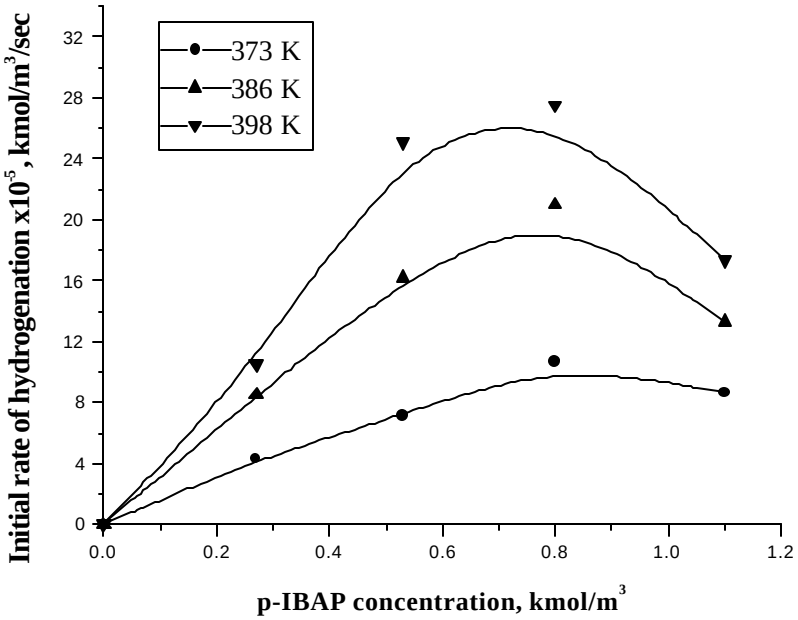

Figure 2.29: Effect of p-IBAP Concentration on Initial Rate of Reaction

Reaction Conditions: P_{H2}: 46.7 atm, Solvent: Methanol, Catalyst Loading: 5 kg/m^3, Agitation Speed: 15 Hz

2 (B). 2.3 Kinetic Modelling

The experimental concentration-time data in the kinetic regime were used to evaluate the different rate equations. Since, the formation of 4-IBECH was negligible in most of the experiments, the reaction scheme shown in Figure 2.28 was simplified as shown below (Figure 2.30).

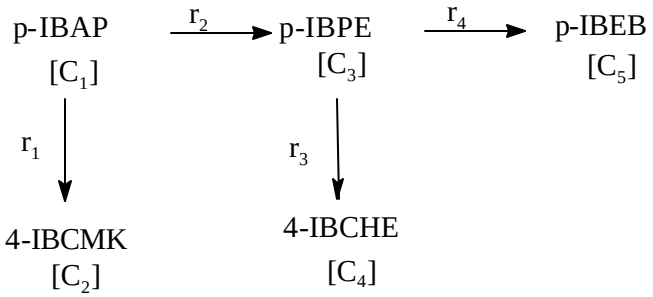

Figure 2.30: Simplified Reaction Scheme

In this scheme, it was assumed that 4-IBCHE is essentially formed from p-IBPE hydrogenation and the rate of hydrogenation of 4-IBCMK is negligible. This is consistent with our observation that after p-IBPE concentration depletes significantly no further increase in 4-IBCHE formation was observed even though the concentration of 4-IBCMK was significant. In order to develop the rate equations, several assumptions were made: (i) the rate of surface reaction is rate limiting and rate of adsorption and desorption is very high compared to the reaction rate (ii) only the reactive species are adsorbed on active sites and sites occupied by solvent are negligible (iii) the adsorption of saturated product, 4-IBCHE was assumed to be negligible due to weak adsorption characteristics.[25] The adsorption of p-IBEB was not taken into account, due to its lower concentration and also was observed only in the final stages of the reaction, but the adsorption of 4-IBCMK was taken into account.

The following reaction mechanisms were considered to derive rate equations:

(i) reaction between associatively adsorbed hydrogen and adsorbed liquid phase components on two different type of sites

(ii) reaction between adsorbed hydrogen (associatively) and adsorbed liquid phase components on the same site

(iii) reaction between dissociatively adsorbed hydrogen and adsorbed liquid phase components on the same site.

In order to test the applicability of these equations (see Table 2.7) a semi-batch reactor model was used under isothermal conditions. The material balances of different components are given below for model (ii) as an example:

$$\frac{dC_1}{dt} = -(r_1 + r_2) = -\frac{w\,K_H\,C_H^*\;\;K_1\,(k_1\,C_1 + k_2\,C_1)}{(1 + K_H\,C_H^* + \Sigma_{j=1,3}\,K_j\,C_j)^2} \qquad (2.69)$$

$$\frac{dC_2}{dt} = r_1 = \frac{w\,k_1\,K_H\,K_1\,C_H^*\,C_1}{(1 + K_H\,C_H^* + \Sigma_{j=1,3}\,K_j\,C_j)^2} \qquad (2.70)$$

$$\frac{dC_3}{dt} = r_2 - r_3 - r_4 = -\frac{wK_H\,C_H^*\,(k_2\,K_1\,C_1 - k_3\,K_3\,C_3 - k_4\,K_3\,C_3)}{(1+K_H\,C_H^* + \Sigma_{j=1,3}\,K_j\,C_j)^2} \qquad (2.71)$$

$$\frac{dC_4}{dt} = r_3 = \frac{w\,k_3\,K_H\,K_3\,C_H^*\,C_3}{(1 + K_H\,C_H^* + \Sigma_{j=1,3}\,K_j\,C_j)^2} \qquad (2.72)$$

$$\frac{dC_5}{dt} = r_4 = \frac{w\,k_4\,K_H\,C_H^*\,K_3\,C_3}{(1 + K_H\,C_H^* + \Sigma_{j=1,3}\,K_j\,C_j)^2} \qquad (2.73)$$

The initial conditions are

At t =0, $C_1 = C_{10}$ and $C_2 = C_3 = C_4 = C_5 = 0$, (2.74)

Here k_1, k_2, k_3, k_4 represent the rate constants of steps r_1,r_2,r_3 and r_4 respectively in the scheme shown in Fig. 3. K_H, K_1, K_2 and K_3 represent the adsorption constants of various components and C_H^*, C_1, C_2 and C_3 their concentrations respectively.

The total rate of hydrogenation is given by

$$R_{H_2} = 3r_1 + r_2 + 3r_3 + 2r_4 \qquad (2.75)$$

In order to select a suitable rate equation, a non-linear least square regression analysis was used for each rate equation to obtain the best fit values of the parameters. For this purpose, an optimisation program based on Marquarts method combined with a Runge Kutta method was used. The solubilities of hydrogen for different p-IBAP concentrations were determined experimentally at different temperatures and are presented in Table 2.8.

Table 2.8: Solubility of H_2 in p-IBAP and Methanol Mixtures

Temperature, K	Henry's constant x 10^3, kmol/m^3/atm		
	5%p-IBAP + 95%MeOH	10%p-IBAP + 90%MeOH	15% p-IBAP + 85% MeOH
373	4.388	4.748	5.324
386	5.084	6.035	6.073
398	6.631	7.578	7.219

The model parameters were estimated by minimizing the objective function:

$$f_{\min} = \sum_{i=1}^{5} \sum_{i=1}^{n} (Y_{i_{\exp}} - Y_{i_{\mathrm{mod}}})^2 \qquad (2.76)$$

Where $Y_{i_{exp}}$ is the measured concentration of component i, $Y_{i_{mod}}$ is the calculated concentration of component i and n is the number of samples. The rate parameters estimated and ϕ_{min} values are given in Table 2.7. Out of the three models considered, models (i) and (iii) gave negative values for some constants and therefore were rejected. Model (ii) was found to be the best to represent the kinetics of hydrogenation of p-IBAP using 2%Ru/Al_2O_3 catalyst. The experimental and the predicted concentration - time data were found to agree within 5-8% error as shown in Figures 2.31 and 2.32.

From the temperature dependence of rate parameters (Figure 2.33 and 2.34), the activation energies of various reaction steps were calculated. Thee values of activation energies for steps r_1, r_2, r_3 and r_4 were found to be 46.57, 42.24, 43.82 and 56.8 kJ/mol respectively. The enthalpy of adsorption and the entropy of adsorption of hydrogen and various liquid components were also calculated (see Table 2.9) as follows,[30]

$$K_i = K_{i0} \exp\left(-\frac{\Delta H_i}{RT}\right) \qquad (2.77)$$

$$K_{i0} = \exp\left(\frac{\Delta S_i}{R}\right) \qquad (2.78)$$

K_{i0} , ΔH and ΔS represent the pre-exponential factor, enthalpy and entropy of adsorption respectively. The observation of adsorption enthalpy $-\Delta H > 0$ and $-\Delta S > 0$, also indicate that the rate parameters obey the Arrhenius temperature dependence.

Table 2.7: Comparison of Various Models for Hydrogenation of p-Isobutyl Acetophenone

S. No.	Model	Temp., K	Rate Constants x 100				Adsorption constants				f_{min} x 10^4
			k1	k2	k3	k4	K_H	K_1	K_2	K_3	
1	$r_i=\frac{k_i K_H K_j C_j C_H^*}{(1+K_H C_H^*)(1+\sum_{j=1,3} K_j C_j)}$	373	0.0128	0.0342	0.1211	0.157	0.2739	8.7646	0.3311	2.9057	2.37
		386	0.0213	0.0231	0.0189	0.0361	1.9079	8.9866	-7.5938	2.0907	0.13
		398	0.0058	0.0166	0.0304	0.0784	0.6552	7.6712	-19.560	4.3798	0.21
2	$r_i=\frac{k_i K_H K_j C_j C_H^*}{(1+K_H C_H^*+\sum_{j=1,3} K_j C_j)^2}$	373	0.5000	0.8588	1.8224	0.141	0.0281	4.5312	0.2137	2.5493	0.11
		386	1.0470	1.3525	3.0736	0.203	0.0226	4.289	1.1720	2.3524	0.23
		398	1.5192	2.0219	4.4193	0.272	0.0201	4.1263	1.2600	2.1335	0.14
3	$r_i=\frac{k_i (K_H)^{1/2} K_j C_j (C_H^*)^{1/2}}{(1+(K_H C_H^*)^{1/2}+\sum_{j=1,3} K_j C_j)^2}$	373	0.0247	0.0397	0.2576	0.0331	0.242	9.0544	0.5033	1.2717	0.22
		386	1.2873	1.3399	2.1422	-0.5478	-0.011	6.1884	-2.5160	3.0693	2.37
		398	0.0123	0.0384	0.0576	0.0163	0.4260	5.4702	-5.9806	3.5582	0.13

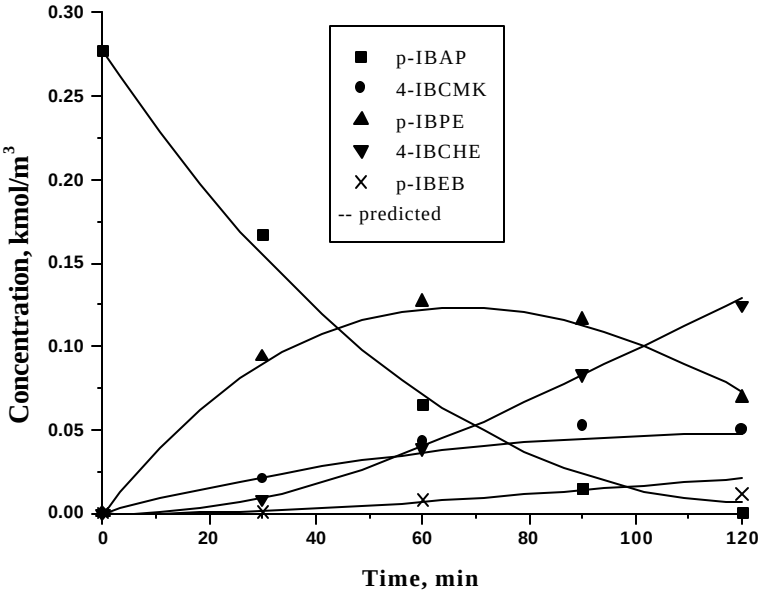

Figure 2.31: Concentration – Time Profile at 373 K

Reaction Conditions: Concentration of pIBAP: 0.27 kmol/m^3, Catalyst Loading: 5 kg/m^3, P_{H2}: 46.7 atm, Solvent: Methanol, Agitation Speed: 15 Hz

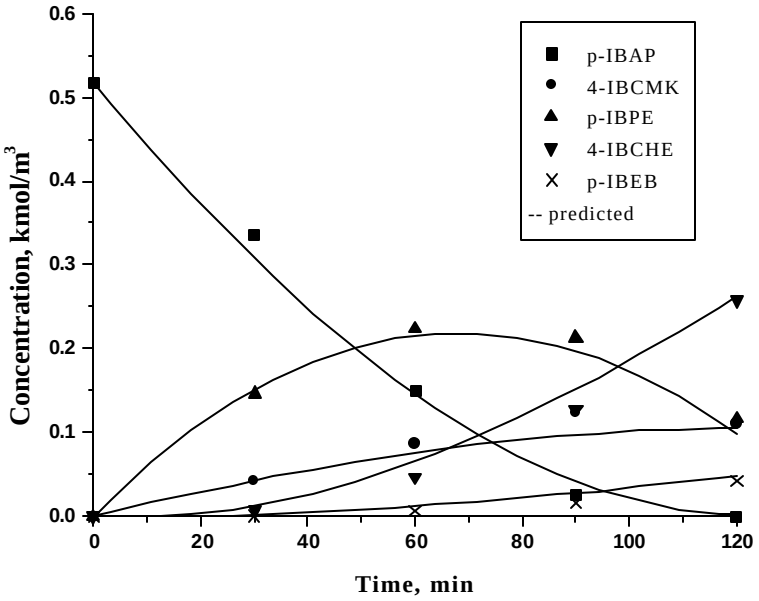

Figure 2. 32: Concentration – Time Profile at 386 K

Reaction Conditions: Concentration of pIBAP: 0.53 kmol/m^3, Catalyst Loading: 5 kg/m^3, P_{H2}: 46.7 atm, Solvent: Methanol, Agitation Speed: 15 Hz

Table 2.9: Values of DH and DS

Adsorbing species	-ΔH, kJ/mol	-ΔS, J/mol K
H_2	16.69	74.57
p-IBAP	4.63	4.97
4-IBCMK	25.9	82.9
p-IBPE	8.75	15.65

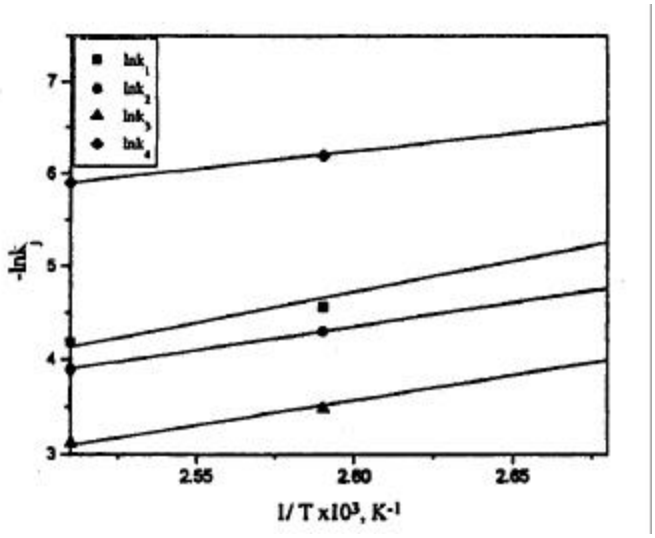

Figure 2.33: Temperature Dependence of Rate Constants

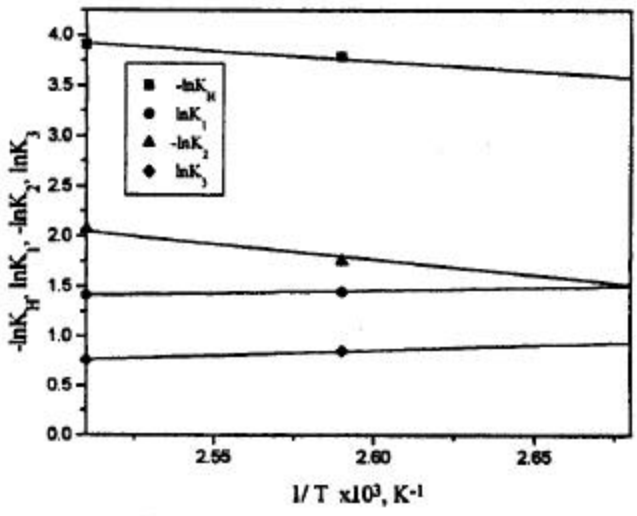

Figure 2. 34: Temperature Dependence of Adsorption Constants

2 (B). 3 Conclusion

Hydrogenation of p-IBAP using a 2%Ru/Al_2O_3 catalyst was studied in a slurry reactor for a temperature range of 373-398 K. The products p-Isobutyl phenyl 2-ethanol, 4-isobutyl cyclohexyl methyl ketone, 4-isobutyl cyclohexyl 2-ethanol, p-isobutyl ethyl benzene and 4-isobutyl ethyl cyclohexane were characterised by GC-MS. The effect of catalyst loading, p-isobutyl acetophenone concentration and H_2 pressure on concentration - time profile was studied and a detailed kinetic analysis has also been presented. The accuracy of rate model and discrimination of various rate models are discussed. A rate model based on competitive, non-dissociative adsorption of hydrogen and different liquid phase components followed by surface reaction was found to fit well the concentration - time profile at all temperatures. The rate parameters were determined and activation energies calculated corresponding to each rate constant. Similarly, from the temperature dependence of adsorption constants, heat of adsorption and entropy values were also evaluated.

Notations for part - A

A_W	wall heat transfer area, m^2
C_H^*	saturation solubility of H_2, kmol/m^3
B_{li}	concentration of acetophenone at t=0, kmol/m^3
C_i	concentration of component i, kmol/m^3
C_p	specific heat capacity of catalyst pellet, kJ/kg.K
C_{pl}	specific heat capacity of liquid, kJ/kg.K
C_{pg}	specific heat capacity of gas, kJ/kg.K
d_p	catalyst particle diameter, m
d_I	diameter of the impeller, m
e	energy supplied (by the agitator) to the liquid per unit mass, m^2/s^3
F_c	shape factor of the catalyst
D_M	molecular diffusivity, m^2/sec
D_e	effective diffusivity, m^2/sec
ΔE	activation energy, kJ/mol
ΔH_i	heat of reaction for step i, kJ/mol

H_e Henry's constant, kmol/m^3/atm

k'_1, k'_2, k'_3, k'_4 reaction rate constants (m^3/kg)(m^3/kmol.sec)

$K_{BX}, K_{BY}, K_{DX}, K_{DY}$ adsorption equilibrium constants, m^3/kmol

K_H adsorption equilibrium constant for hydrogen, m^3/kmol

$k_L a_b$ gas-liquid mass transfer coefficient, s^{-1}

$k_s a_p$ liquid-solid mass transfer coefficient, s^{-1}

N agitation speed, Hz

P_{H_2} partial pressure of hydrogen, atm

P_{sol} vapour pressure of solvent, atm

Q_g volumetric gas flow rate, m^3/s

r ratio of distance from the centre to the radius of the pellet

r_1 to r_4 reaction rates of respective steps in Figure 2.8, kmol/m^3/s

R catalyst pellet radius

R_{H2} total rate of hydrogenation, kmol/m^3/s

R_A initial rate of hydrogenation, kmol/m^3/s

S_i adsorption site for component i

T temperature, K

T_0 reference temperature (taken as the external wall temperature), K

T_{gi} temperature of incoming gas, K

T_w temperature of the wall, K

U_W overall wall heat transfer coefficient, kJ/m^2.sec.K

U_g gas velocity, m/s

V_L liquid volume,m^3

V_R reactor volume, m^3

w catalyst weight, kg/m^3

Greek

α_1 parameter defined in Equation 2.4

α_2 parameter defined in Equation 2.5

ϕ_{exp} parameter defined in Equation 2.6

ϕ_{min} parameter defined in Equation 2.35

μ_l viscosity of liquid, P

ε_p porosity of the catalyst particle

ε_g gas hold up

ρ_p catalyst pellet density, kg/m^3

ρ_l liquid density, kg/m^3

f defined in equation (2.41)

ρ_g density of gas, kg/m^3

ρ_L density of liquid, kg/m^3

λ_e thermal conductivity, kJ/sec.m.K

τ tortousity factor

η effectiveness factor as defined by equation (2.48)

Θ_{iXorY} surface coverage of component i on X or Y type of site

Θ_H surface coverage of hydrogen

Θ dimensionless temperature

Notations for part - B

C_{H2}^* saturation solubility of H_2, kmol/m^3

$C_{1,0}$ concentration of p-isobutyl acetophenone at t=0 ,kmol/m^3

C_1 concentration of p-isobutyl acetophenone, kmol/m^3

C_2 concentration of 4-isobutyl cyclohexyl methyl ketone, kmol/m^3

C_3 concentration of p-isobutyl phenyl ethanol, kmol/m^3

C_4 concentration of 4-isobutyl cyclohexyl ethanol, kmol/m^3

C_5 concentration of p-isobutyl ethyl benzene, kmol/m^3

k_1, k_2, k_3, k_4 reaction rate constants (m^3/kg)(m^3/kmol.sec)

K_1, K_2, K_3 adsorption equilibrium constants, m^3/kmol

K_H adsorption equilibrium constant for hydrogen, m^3/kmol

r_1 to r_4 reaction rates of respective steps in Figure (2.30), kmol/m^3/s

R_{H2} total rate of hydrogenation, kmol/m^3/s

ΔS entropy change, J/mol.K

References

1. Masson J., Cividino P., Bonnier J. M. and Fouilloux P., Selective hydrogenation of acetophenone on unpromoted Raney Ni: Influence of reaction conditions, Heterogeneous Catalysis and Fine Chemicals II, Stud. Surf. Sci. Catal., 245, 1991

2. Zakumbaeva G. D., Urumbaeva S. U. and Dautkulov A. B., Hydrogenation of acetophenone on cobalt catalysts, Zhurnal Prikladnoi Khimii, 65, 1349, 1992

3. Hamer-Thibault S., Masson J., Fouilloux P., and Court J., Selective hydrogenation of acetophenone on chromium promoted Raney nickel catalysts. I. Characterization of the catalysts, Appl. Catal. A : General, 99, 131, 1993

4. Barinov N. S., Lebedeva E. G. and Mushenko D. V., Comparative study of the catalytic properties of Pt, Pd, Rh and Ni in hydrogenation of acetophenone in solvents, Zhurnal Prikladnoi Khimii, 42, 2613, 1969

5. Mushenko D. V., Barinov N. S. and Lebedeva E. G., Kinetics of hydrogenation of acetophenone on Ni, Pt and Pd catalysts in solvent, Zhurnal Organicheskoi Khimii, 7, 314, 1971

6. Csomontanyi G., Netta M. and Balmez M., Hydrogenation Catalytique de 1'acetophenone, Revue roumaine de chimie, 18, 1367, 1973

7. Ziyatdinov A. S., Stepanenko V. V., Chernykh I. S., Leonova E. B., Pisarenko V. N. and Kafarov V. V., Kinetics of hydrogenation of acetophenone to methyl carbinol on KGA -43 copper-chromium catalyst, Zhurnal Prikladnoi Khimii, 61, 565, 1988

8. Garbuzov V. G., Serebyrakov B. R., Grishkan I. A. and Smirnova N. A., Kinetics of acetophenone hydrogenation on a copper-chromium-barium catalyst, Azerb.Khim. Zh., 3, 7, 1976

9. Del Amo, Kinetic model of the hydrogenation of acetophenone, Ingeneria Quimica (Madrid), 23, 115, 1991

10. Barinov N. S., Mushenko D. V. and Lebedeva E. G., Conversions of acetophenone during hydrogenation on Ru catalyst, Zhurnal Prikladnoi Khimii, 39, 2599, 1966

11. Barinov N. S. and Mushenko D. V., Kinetics of hydrogenation of acetophenone, Zhurnal Prikladnoi Khimii, 42, 2613, 1973

12. Kawakami K. and Kusunoki K., The effects of Intraparticle diffusion on the yield of the liquid phase hydrogenation of phenylacetylene in a stirred basket reactor, J. Chem. Eng. Japan, 9 (6), 469, 1976

13. Toppinen S., Rantakyla T. K., Salmi T. and Aittamaa J., Kinetics of the liquid phase hydrogenation of benzene and some monosubstituted alkylbenzenes over a nickel catalyst, Ind. Eng. Chem. Res., 35 1824, 1996

14. Bergault I., Fouilloux P., Joly-Vuillemin C. and Delmas H., Kinetics and Intraparticle Diffusion Modelling of a complex Multistep Reaction: Hydrogenation of Acetophenone over a Rhodium Catalyst, J. Cata., 175, 328, 1998

15. Julcour C., Le Lann J. M., Wilhelm A. M. and Delmas H., Dynamics of internal diffusion during the hydrogenation of 1,5,9-cyclododecatriene on Pd/Al2O3, Catalysis Today, 48(1-4), 147, 1999

16. Purvanto P., Deshpande R. M., Chaudhari R. V. and Delmas H., J. Chem. Eng. Data, 41, 1996, 1414

17. Ramachandran P. A. and Chaudhari R.V., 'Three phase catalytic reactors', Gorden breach science publishers, New York, 1983

18. Wilke C. R. and Chang P., Correlation of diffusion co-efficients in dilute solutions, AIChE J. 1, 264, 1955

19. Xu Z. P. and Chuang K. T, Effect of internal diffusion on heterogeneous catalytic esterification of acetic acid, Chem. Eng. Sci., 52(17), 3011, 1997

20. Satterfield C. N., Mass Transfer in Heterogeneous Catalysis, M.I.T press, London.

21. Bern L., Hell M. and Schoon N. H., Kinetics of hydrogenation of rapeseed oil: Rate equations of chemical reactions, J. Am. Oil. Chem. Soc., 52, 391, 1975

22. Sano Y., Yamaguchi N. and Adachi T., Mass transfer coefficients for suspended particles in agitated vessels and bubble columns, J. Chem. Eng. Japan., 1, 255, 1974

23. Calderbank P. H., physical rate processes in industrial fermentation Part I. The interfacial area in gas-liquid contacting with mechanical agitation, Trans. Inst. Chem. Eng., 36, 443, 1958.

24. Schlessinger G. G., Vapor pressure of organic compounds, Handbook of chemistry and Physics, Chemical Rubber Co., (CRC), D155, 1970

25. Neri G. and Bonaccorsi L., Kinetic Analysis of cinnamaldehyde hydrogenation over alumina-Supported ruthenium Catalysts, Ind. Eng. Chem. Res., 36, 3554, 1997

26. Finlayson B. A., Non-linear Analysis in Chemical Engineering, McGraw-Hill Chemical Engineering Series, US, 1980

27. Rajashekharam M. V., Nikhalje D. D., Jaganathan R. and Chaudhari R. V., Hydrogenation of 2,4-Dinitrotoluene using a Pd/Al_2O_3 catalyst in a slurry reactor: A molecular level approach to kinetic modelling and non-isothermal effects, Ind. Eng. Chem. Res., 35, 1824, 1996

28. Rode C. V. and Chaudhari R. V., Hydrogenation of m-nitrochlorobenzene to m-chloroaniline: reaction kinetics and modelling of a non-isothermal slurry reactor, Ind. Eng. Chem. Res., 33, 1645, 1994

29. Elango V., Method for producing ibuprofen, Eur Pat., 400,892, (Cl.C07c57/30), CA :114: 206780, to Hoest Celanese and boots 1990

30. Zhu X. D., Valerius G., Hofmann H., Haas T. and Arntz D., Intrinsic Kinetics of 3-Hydroxypropanal Hydrogenation over $Ni/SiO_2/Al_2O_3$ Catalyst, Ind. Eng. Chem. Res., 36, 2897, 1997

Chapter 3

Performance of a Trickle Bed Reactor for the Hydrogenation of Acetophenone Using Supported Ruthenium Catalysts

3.0 Introduction

Three phase fixed bed catalytic reactors such as trickle bed reactors (TBR) where liquid reactants as well as gaseous reactant flow downward co-currently over a fixed bed of catalyst particles finds applications in a wide range of industrial processes. This includes petroleum refining, oxidation processes, effluent treatment, hydrogenation processes etc.[1,2] Many of the industrially important reactions involve complex reaction network and may also be highly exothermic. Detailed investigation of such complex multi step reactions and other reactor design parameters, which influence the reactor performance, is necessary to understand reactor design and scale up. Most of the earlier studies on modeling of multiphase reactors were based on simple reaction systems[3,4] with only limited efforts on modeling and experimental verification of industrially important complex reactions with considerable exothermicity.[5,6,7,8] A review of previous work on trickle bed reactor modeling and related experimental studies has been presented in Chapter 1, Section 1.2.4.1.3.1.

The models proposed for the performance of trickle reactors range from simple psuedo homogeneous models to more detailed heterogeneous models incorporating partial wetting phenomena, external and intraparticle mass transfer limitations, axial mixing of both gas and liquid phases and non-isothermal effects. The models for TBR's were mainly focused on analysis of the partial wetting effect on reactor performance. The simplest models involve empirical description of the dependency of conversion on liquid hourly space velocity (LHSV), length of the reactor, particle size and catalyst effectiveness factor.[9,10] However, these models were applicable to specific systems and therefore more detailed models incorporating the various complexities of mass transfer, mixing and wetting characteristics were also developed. Ramachandran and Smith[11] analyzed the performance of a trickle bed reactor using a mixing cell approach in which the three-phase reactor was visualized as a number of mixing cells in series. A cross flow dispersion model was suggested by Hinduja et al.[12] which takes into account the axial and radial dispersion and can be solved using only initial conditions. In order to predict the overall effectiveness factor for a partially wetted catalysts, Ramachandran and Smith[13] represented the catalyst by an infinitely long rectangular slab with three sides

impermeable to the reactants and the fourth side covered by liquid up to some distance and some distance with gas and proposed approximate solution for the partially wetted catalyst. Dudukovic[14] proposed a similar method for calculation of the effectives factor for the partially wetted catalyst in which the limiting reactant is present in the liquid phase and solid-liquid mass transfer is not rate limiting. This model takes into consideration effects of both internal and external partial wetting. Mills and Dudukovic[15] obtained dual series solution to catalyst effectiveness factor in trickle bed reactors for isothermal, irreversible, first-order reactions with respect to the non-volatile liquid phase reactant for various geometries of catalyst particles (slab, cylinder and sphere). Mills and Dudukovic[16] later extended the study to all cases of interest such as gas or liquid limiting reactant, finite or negligible external surface resistance and volatile or non-volatile liquids. Herskowitz et al.[17] modelled the problem by assuming that the catalyst shape is a cube and one or more faces of this cube is covered by gas or liquid and the differential equations were solved analytically by superposition theory. Goto et al.[18] have studied the effect of partial wetting on the overall effectiveness factor for an n^{th} order reaction. Two cases of the limiting reactants being present either in a gas or in a liquid phase have been considered and approximate solutions for the effectiveness factor for the partially wetted catalyst was derived using Bischoff's approximation.[19] Tan and Smith[20] suggested that the overall effectiveness factor under conditions of partial wetting can be given as a sum of the weighted averages of the effectiveness factors in the wetted part and in the un-wetted part. Beaudry et al.[21] developed a model for predicting the performance of a partially wetted trickle bed reactor for a gas limiting reaction of order less than or equal to one and showed that under certain conditions the liquid reactant may affect the reaction rate due to its inability to rapidly diffuse to catalyst areas that are in direct contact with the gas. Hydrogenation of α-methylstyrene and maleic acid were used as the systems to predict the experimental results and a criteria to predict the importance of liquid phase reactant limitations was also suggested. Khadilkar et al.[22] proposed a rigorous model for the solution of the reactor and pellet scale flow-reaction-transport phenomena based on multicomponent diffusion theory in which Stefan-Maxwell formulations were used to model interphase and intra particle mass transport.

Considering wider applicability of trickle bed reactors in industrial hydrogenation processes, investigations of more case studies of practical relevance will further establish the confidence in the use of predictive models for understanding TBR performances. It is in this context, that this work was undertaken in which hydrogenation of acetophenone using ruthenium metal supported on alumina (an excellent example of complex multistep reaction with considerable exothermicity) was studied in a high-pressure trickle bed reactor. The intrinsic kinetics of the reaction was first studied in a semi-batch slurry reactor and a Langmuir-Hinshelwood type of rate model was developed. The studies in a trickle bed reactor were mainly focused on the effect of various parameters that affect the reactor performance such as liquid velocity, gas velocity, inlet concentration of substrate, reactor pressure and temperature. Under the range of conditions studied, partial wetting and mass transfer effects of gaseous hydrogen can play a decisive role in controlling the reaction rates. A plug flow model incorporating the non-isothermal effects and solvent evaporation effects was developed to explain the observed experimental data.

3.1 Experimental

3.1.1 Materials

Acetophenone (Aldrich, USA) and solvent, methanol (S.D. Fine. Chem., India) were used as received. Hydrogen and nitrogen gases were obtained from M/s Indian Oxygen Ltd., India and 2%Ru/Al_2O_3 catalyst was procured from Arrora Matthey, India, properties of which are given in Table 3.1.

Table 3.1: Catalyst Characteristics

Catalyst	2%Ru/Al_2O_3
Catalyst particle diameter	3.2×10^{-3} m
Density of catalyst	2020 kg/m^3
Tortousity of catalyst	6.0
Porosity of catalyst	0.40

3.1.2 Equipment

The experiments were carried out in a high-pressure trickle bed reactor supplied by "Vinci Technologies", France and the reactor characteristics are given in Table 3.2. The unit consists of four parts (Figure 3.1).

Table 3.2: Reactor Characteristics

Reactor length	53×10^{-2} m	Weight of catalyst	52.4×10^{-3} Kg
Catalyst packing length	23.85×10^{-2} m	Reactor inner diameter	1.9×10^{-2} m
Reactor area	2.33×10^{-4} m^2	Bed voidage	0.53
Thermo well inner diameter	8×10^{-3} m		

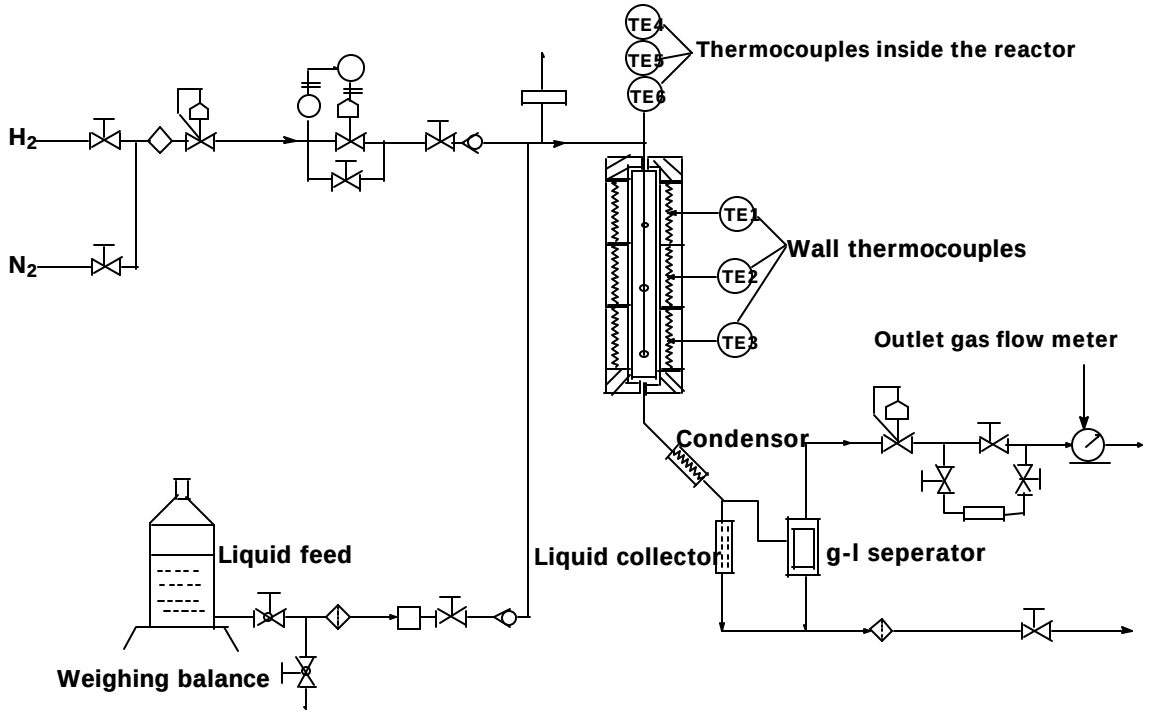

Figure 3.1: Schematic Diagram of the Trickle Bed Reactor Used

(i) The Reactor

The reactor used was 53 cm long and 1.9 cm diameter divided into three zones: (a) the first zone of 17.4 cm, filled with inert Si-C pellets, (b) the second section of 23.85 cm filled with catalyst and (c) the third section 11.6 cm again filled with inert Si-C.

Characteristics of the reactor are given in Table 3.2. The gas and liquid flows were mixed before entering the reactor. The reactor could be operated at a maximum pressure of 15 MPa and a temperature of 823 K. The heating of the three zones of the reactor was independent with its own temperature control. The reactor was provided with three thermocouples axially placed along the reactor length in a thermo well.

(ii) Liquid Feed

The liquid feed from a storage, consisting of a glass vessel (5 litre capacity) was introduced into the reactor using a high-pressure liquid feed pump with a maximum capacity of 2.5 lit/hour. The glass feed vessel was kept on a weighing balance with an accuracy of 0.5 gm, which allowed measurement of flow rate precisely.

(iii) Gas Feed

This section consists of a hydrogen inlet stop valve, a filter and a nitrogen inlet valve. The mass flow controller was adjusted to set inlet gas flow rate and the outgoing gas flow rate was measured by a wet gas flow meter. For quick pressurization of the unit, the mass flow controller was by-passed by a manual valve. Nitrogen was used to flush the reactor before each run. Tuning a new set point on the electronic rack can attain accurate control of hydrogen flow rate. A maximum gas flow rate of 1000 Nl/h could be attained by this set up.

(iv) Outlet

It consists of a condenser and a high-pressure gas-liquid separator and accumulator with one gas outlet line and a liquid outlet. The gas outlet line is equipped with a backpressure controller, which ensures a constant pressure in the unit by continuous pressure release. A wet gas flow meter measures the total gas outflow. The liquid outlet line is equipped with a filter, a manual stop valve and a drain valve to withdraw liquid continuously.

3.1.3 Experimental Procedure

The lines of the reactor were flushed with the liquid feed before the start of any experiment. In the beginning, the reactor was flushed with nitrogen and the wall temperatures of the different zones were set to the desired limits. The liquid flow was

started after adjusting the required flow rate. Once the temperature of the wall was attained and the temperature inside the reactor was stable, the reactor was pressurized with hydrogen after setting the gas flow rate. The temperatures were monitored at three positions inside the reactor. The catalyst was filled in such a way that the first thermocouple was at the inlet of the catalyst bed, second one at the middle of the catalyst bed and the third thermocouple at the exit of the catalyst bed. Following this procedure, experiments were carried out at different inlet conditions and steady state performance of the reactor was observed by analysis of reactants and products in the exit streams. The range of operating conditions for which the present study was carried out is given in Table 3.3. Liquid samples withdrawn at regular intervals of time were analyzed by gas chromatographic technique using a HP-6890 Gas chromatograph fitted with a HP-FFAP capillary column (30 m x 0.53 μm x 0.1 mm film thickness on polyethylene glycol stationary phase). The conditions of GC analysis were same as that mentioned in Chapter 2.

Table 3.3: Range of Operating Conditions

Inlet concentration of ACPH	0.84 - 2.5 kmol/m^3
Reactor pressure	20 – 70 atm
Liquid flow rate	0.54 – 2.4 x 10^{-3} m/s
Gas flow rate	30 – 600 Nl/h
Temperature	353 - 423 K

3.2 Reactor Model

3.2.1 Intrinsic Kinetics

The catalysts used for the intrinsic kinetic study in Chapter 2 were pelletized and on packing the bed, found to be not suitable for TBR studies due to poor strength. Hence, catalyst pellets with same metal loading were procured from Arrora Matthey, India for trickle bed experiments. Since the source and batch of catalysts used for trickle bed reactor performance were different, kinetic experiments were carried out again to correct the rate parameters using the same model equations as described in Chapter 2. The

kinetic trends observed was similar to that observed earlier and hence the same model was used. The rate equations corresponding to reaction steps involving ring hydrogenation can be written as

$$r_i = \frac{wk_i' K_{iY} A_l^* I_l}{(1+\sum_i K_{iY} I_l)} \tag{3.1}$$

and the rate equations for reaction step involving ketonic group can be written as

$$r_i = \frac{wk_i' K_{iX} A_l^* I_l}{(1+\sum_i K_{iX} I_l)} \tag{3.2}$$

Where, A_l^* is the hydrogen saturation solubility in kmol/m^3 and I_l is the concentration of ith component in the liquid phase in kmol/m^3. Since the hydrogenation of acetophenone involved multi step reactions, integral concentration-time data in a semi-batch slurry reactor had to be simulated. The change in concentration with time can be represented by the following equations:

$$-\frac{dB_l}{dt} = R_B = \frac{1}{3}\frac{wk_1' K_{BY} A_l^* B_l}{(1+K_{BY}B_l + K_{DY}D_l)} + \frac{wk_2' K_{BX} A_l^* B_l}{(1+K_{BX}B_l + K_{DX}D_l)} \tag{3.3}$$

$$\frac{dC_l}{dt} = R_C = \frac{1}{3}\frac{wk_1' K_{BY} A_l^* B_l}{(1+K_{BY}B_l + K_{DY}D_l)} \tag{3.4}$$

$$\frac{dD_l}{dt} = R_D = -\frac{1}{3}\frac{wk_3' K_{BY} A_l^* D_l}{(1+K_{BY}B_l + K_{DY}D_l)} + \frac{wA_l^*(k_2' K_{BX} B_l - k_4' K_{DX} D_l)}{(1+K_{BX}B_l + K_{DX}D_l)} \tag{3.5}$$

$$\frac{dE_l}{dt} = R_E = \frac{1}{3}\frac{wk_3' K_{BY} A_l^* D_l}{(1+K_{BY}B_l + K_{DY}D_l)} \tag{3.6}$$

$$\frac{dF_l}{dt} = R_F = \frac{wk_4' K_{DX} A_l^* D_l}{(1+K_{BX}B_l + K_{DX}D_l)} \tag{3.7}$$

The initial conditions are

$$\text{At } t = 0,\ B_l = B_{l,0} \text{ and } C_l = D_l = E_l = F_l = 0 \tag{3.8}$$

The total rate of hydrogenation at any point is given by

$$R_{H_2} = r_1 + r_2 + r_3 + r_4 \quad (3.9)$$

Where r_1, r_2, r_3 and r_4 represents the reaction rates corresponding to the reaction steps shown in Figure 2.8 (Chapter 2). The values of the rate parameters were determined by optimization of concentration-time data (Figure 3.2 and 3.3) for three temperatures (373 K, 398 K and 423 K) and the corresponding activation energies and heat of adsorptions are given below in Table 3.4.

Table 3.4: Rate Parameters and it's Temperature Dependency

Rate constants at 398K	Activation energy, kJ/mol	Adsorption constants at 398 K	Heat of adsorption, kJ/mol
$k'_1 = 2.42 \times 10^{-4}$	53	$K_{BX} = 1.12$	-10.4
$k'_2 = 1.05 \times 10^{-4}$	52	$K'_{BY} = 3.04$	-23.16
$k'_3 = 1.26 \times 10^{-4}$	57	$K_{DX} = 7.8$	-15.77
$k'_4 = 1.48 \times 10^{-4}$	55	$K'_{DY} = 0.40$	-11.43

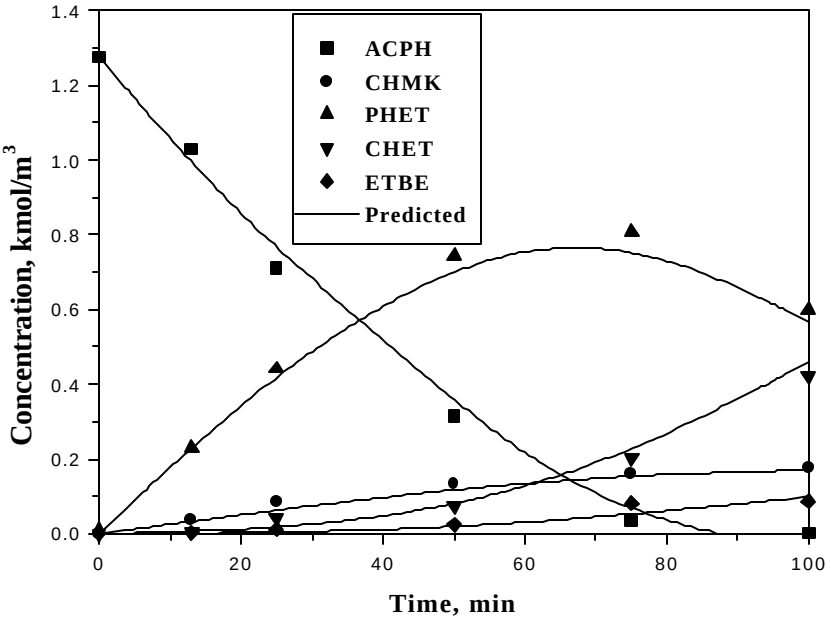

Figure 3.2: Concentration – Time Profile at 398 K

Reaction Conditions: Concentration of ACPH: 1.27 kmol/m^3, Catalyst Loading: 20 kg/m^3, P_{H2}: 47 atm, Solvent: Methanol, Agitation Speed: 15 Hz

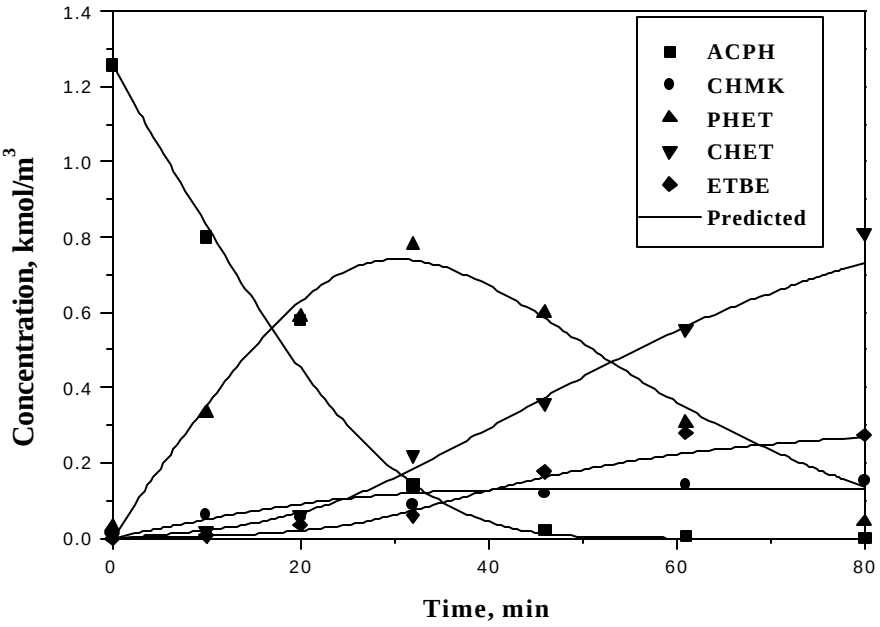

Figure 3.3: Concentration – Time Profile at 423 K

Reaction Conditions: Concentration of ACPH: 1.27 kmol/m^3, Catalyst Loading: 20 kg/m^3, P_{H2}: 45 atm, Solvent: Methanol, Agitation Speed: 15 Hz

3.2.2 Trickle Bed Reactor Model

The model described here is basically an extension of the approach used by Rajashekharam et al.[5] by incorporating the solvent evaporation effects for the hydrogenation of acetophenone with 2%Ru/Al_2O_3 as the catalyst and methanol as the solvent. The assumptions made in derivation of reactor model are: (1) gas and liquid are in plug flow, (2) external as well as intraparticle mass transfer effects of liquid phase components can be neglected, (3) the contribution by stagnant liquid pockets can be neglected, (4) no radial concentration and temperature gradients exist within the reactor, (5) there is no heat conduction in the axial direction, (6) the liquid phase reactants are non-volatile and (7) the gas phase behaves ideally.

The total amount of reaction for a partially wetted catalyst particle can be represented as sum of the contributions due to mass transfer of reactants to the liquid covered and gas covered outer surfaces. The contribution to the liquid covered surface can be assumed to be equal to the amount of reaction if the entire surface was covered by

liquid multiplied by the wetted fraction (f_w). The contribution from gas covered surface can also be calculated in a similar way. The overall effectiveness factor (η) can be given as[20]

$$\eta = f_w \eta_l + (1 - f_w)\eta_g \tag{3.10}$$

η_l is the overall effectiveness factor for the liquid covered surface and η_g that corresponding to the dry zone in direct contact with the gas phase.

Under the conditions of significant intraparticle gradients for the gas-phase reactant (H_2) and when the liquid-phase reactant was in excess, the overall rate of hydrogenation can be expressed as

$$R_A = \eta w \frac{A_g}{H_A}\left[\frac{(k_1 B_l + k_3 D_l)}{(1 + K_B B_l + K_D D_l)} + \frac{(k_2 B_l + k_4 D_l)}{(1 + K_C B_l + K_E D_l)}\right] \tag{3.11}$$

Where, η is given by eq. (3.10) and η_l and η_g can be given by the following expression for a spherical catalyst particle:

$$\eta_l = \eta_c \frac{a_l}{\left[1 + \frac{\eta_c f^2}{N_L}\right]} \text{ and } \eta_g = \eta_c \frac{a_g}{\left[1 + \frac{\eta_c f^2}{N_G}\right]}$$

Where, $a_l = \frac{A_l}{A_{gi}/H_A}$ and $a_g = \frac{A_g}{A_{gi}}$, A_l is the liquid phase hydrogen concentration at any point inside the reactor, A_{gi} is the gas phase hydrogen concentration at the inlet, A_g is the gas phase hydrogen concentration at any point inside the reactor and $H_A = \frac{A_g}{A_l}$ at equilibrium, N_L and N_G are the Nusselt numbers for the liquid covered and gas covered zones respectively and are defined in Table 3.5.

Table 3.5: Dimensionless Parameters Used in the Model

Mass transfer parameters	
Gas-liquid mass transfer	$\alpha_{gl} = k_l a_B L / U_l$
Liquid-solid mass transfer	$\alpha_{ls} = k_s a_p L / U_l$
Gas-solid mass transfer	$\alpha_{gs} = k_{gs} a_p L / U_l$
Nusselt number in dynamic zone	$N_L = Rk_{s_d} / 3D_e$
Nusselt number in dry zone	$N_G = Rk_{g_s} / 3D_e$
Heat transfer parameters	
Thermicity parameter	$\beta_1 = \dfrac{(-\Delta H) B_{l_i}}{T_o C_{p_l} \rho_l \left[1 + U'_g C'_{p_g} \rho'_g / U_l C_{p_l} \rho_l\right]}$
Bed-to-wall heat transfer	$\beta_2 = \dfrac{4U_w L}{d_T U_l C_{p_l} \rho_l \left[1 + U'_g C'_{p_g} \rho'_g / U_l C_{p_l} \rho_l\right]}$
Parameter for heat transfer by Solvent evaporation	$b_3 = \dfrac{\Delta H_{ev} L}{T_0 U_l C_{pl} \rho_l \left[1 + U'_g C'_{p_g} \rho'_g / U_l C_{p_l} \rho_l\right]}$

The catalytic effectiveness factor (η_c) applicable to hydrogenation of ACPH was developed following the well-known approaches of Bischoff[19] and Ramachandran and Chaudhari[23], and can be given as

$$\eta_c = \frac{1}{\phi}\left(\coth 3\phi - \frac{1}{3\phi}\right) \tag{3.12}$$

Where ϕ is the Thiele parameter and can be defined as:

$$\phi = \frac{R}{3}\left[\frac{\rho_P}{D_e}\left(\frac{(k_1 B_l + k_3 D_l)}{(1 + K_B B_l + K_D D_l)} + \frac{(k_2 B_l + k_4 D_l)}{(1 + K_C B_l + K_E D_l)}\right)\right]^{\frac{1}{2}} \tag{3.13}$$

or in dimensionless form as :

$$\Ö = f_0 \left[\frac{(b_l + k_{31} d_l)}{(1 + k_B b_l + k_D d_l)} + \frac{(k_{21} b_l + k_{41} d_l)}{(1 + k_C b_l + k_E d_l)} \right]^{\frac{1}{2}} \quad (3.14)$$

$$f_0 = \frac{R}{3} \left[\frac{r_p k_1 B_{l_i}}{D_e} \right]^{\frac{1}{2}} \quad (3.15)$$

3.2.2.1 Mass Balance for Gaseous and Liquid Phase Components

For hydrogen in liquid phase the dimensionless mass balance can be given as

$$-\frac{da_l}{dz} + a_{gl}(a_g - a_l) = f_w a_{ls}(a_l - a_{sl}) \quad (3.16)$$

and $$f_w a_{ls}(a_l - a_{sl}) = f_w h_c a_r k_{RA} \frac{f_w a_l}{[1 + \frac{h_c \Phi^2}{N_L}]} \quad (3.17)$$

Where $K_{RA} = [\frac{(b_l + k_{31} d_l)}{(1 + k_B b_l + k_D d_l)} + \frac{(k_{21} b_l + k_{41} d_l)}{(1 + k_C b_l + k_E d_l)}]$, $a_r = \frac{Lwk_1 B_{li}}{U_l}$, a_{gl} and a_{ls} are the dimensionless gas-liquid and liquid-solid mass transfer coefficients and are defined in Table 3.5. a_{sl} is the dimensionless hydrogen concentration at the catalyst surface covered by the flowing liquid.

For liquid phase components

$$-\frac{db_l}{dz} = \frac{h_c a_r b_l c_A}{q_B(1 + k_B b_l + k_D d_l)} + \frac{h_c a_r k_{21} b_l c_A}{q_B(1 + k_C b_l + k_E d_l)} \quad (3.18)$$

$$c_A = \frac{(1 - f_w) a_g}{[1 + \frac{h_c \Phi^2}{N_g}]} + \frac{f_d a_l}{[1 + \frac{h_c \Phi^2}{N_L}]} \quad \text{and } q_B = B_{li} / (A_g/H_A) \quad (3.19)$$

$$\frac{dc_l}{dz} = \frac{h_c a_r b_l c_A}{q_B(1+k_B b_l + k_D d_l)} \tag{3.20}$$

$$\frac{dd_l}{dz} = \frac{h_c a_r (k_{21} b_l - k_{41} d_l) c_A}{q_B(1+k_C b_l + k_E d_l)} + \frac{h_c a_r k_{31} d_l c_A}{q_B(1+k_B b_l + k_D d_l)} \tag{3.21}$$

$$\frac{de_l}{dz} = \frac{h_c a_r k_{31} d_l c_A}{q_B(1+k_B b_l + k_D d_l)} \tag{3.22}$$

$$\frac{df_l}{dz} = \frac{h_c a_r k_{41} d_l c_A}{q_B(1+k_C b_l + k_E d_l)} \tag{3.23}$$

The variation of hydrogen concentration in the gas phase can be given as:

$$\frac{da_g}{dz} = -\frac{f_w a'_{gl}}{H_A}(a_g - a_l) - \frac{(1-f_w) a'_{gs}}{H_A}(a_g - a_{sg}) \tag{3.24}$$

Where, a_{sg} is the dimensionless hydrogen concentration at the catalyst surface exposed to direct gas phase and can be given as $a_{sg} = \frac{A_{sg}}{A_{gi}/H_A}$, $a'_{gl} = \frac{k_L a_B L}{U_g}$, $a'_{gs} = \frac{k_g a_p L}{U_g}$.

The dimensionless gas phase solvent concentration (sol_g) can be given as

$$\frac{d\,sol_g}{dz} = -\frac{L}{\rho U_g} Sol_{Trans,g} \tag{3.25}$$

Where $Sol_{Trans,g}$ is the moles of solvent getting transferred to the gas phase per unit volume of the reactor per unit time and is given by $Sol_{Trans,g} = \frac{sol_g}{a_g} f_{tot}$.

f_{tot} is the net molar flow rate of the gas phase in kmol/m^3/sec, and sol_g is the dimensionless gas phase concentration of the solvent which also varies along the bed length.

The variation in liquid velocity in the dimensionless form can be given as:

$$\frac{dU'_l}{dz} = -\frac{32.0\,L}{\rho_{MeOH}\,U_{li}}\,Sol_{Trans,g} \qquad (3.26)$$

Where U'_l is the dimensionless liquid velocity given as $U'_l = \frac{U_l}{U_{li}}$, in which, U_l is the liquid velocity at any point inside the reactor and U_{li} is the velocity at the inlet of the catalyst bed.

The variation of gas velocity along the bed length is

$$\frac{dU'_g}{dz} = -\frac{2.0\,f_w a'_{gl}}{\rho_{H2}\,H_A}\left(a_g - a_l\right) + \frac{32.0L}{\rho_{MeOH,Gas}U_g}\,Sol_{Trans,g} - \frac{2.0\,(1-f_w)\,a'_{gs}}{\rho_{H2}\,H_A}\left(a_g - a_{sg}\right) \qquad (3.27)$$

The total molar flow rate of gas at any point inside the reactor can be given in kmol/m^3/sec as:

$$f_{tot} = \frac{U_g\,A_g}{L} + \frac{U_g\,Sol_g}{L} \qquad (3.28)$$

Where U_g is the gas velocity in m/s, A_g is the hydrogen concentration in gas phase in kmol/m^3 and Sol_g is the gas phase solvent concentration in kmol/m^3.

The heat balance can be given as

$$(U_l C_{pl}\rho_l + U'_g\,C'_{pg}\,\rho'_g)\frac{dT_b}{dX} = \frac{-\Delta H_i \eta_c w k_1 k_{RA}}{q_B}\left[\frac{(1-f_w)}{\left[1+\frac{\eta_c\Phi^2}{N_g}\right]} + \frac{f_w a_l}{\left[1+\frac{\eta_c\Phi^2}{N_d}\right]}\right] - \frac{4U_w(T_b - T_w)}{d_T} - \Delta H_{ev}\,Sol_{Trans,g} \qquad (3.29)$$

Where $U'_g\,C'_{pg}\,\rho'_g = U_{g,H}\,C_{pH}\,\rho_{g,H} + U_{g,sol}\,C_{pg,sol}\,\rho_{g,sol}$ (3.30)

The dimensionless heat balance can be given as:

$$\frac{d\Theta_b}{dz} = \frac{3b_1 h_c a_r k_{RA}}{q_B}\left[\frac{(1-f_w)}{\left[1+\frac{h_c\Phi^2}{N_g}\right]} + \frac{f_w a_{ld}}{\left[1+\frac{h_c\Phi^2}{N_d}\right]}\right] - b_2(\Theta_b - \Theta_w) - b_3 Sol_{Trans,g} \quad (3.31)$$

Θ_b is the dimensionless catalyst bed temperature given as $\Theta_b = T_b / T_I$, where T_b is the bed temperature and T_I is the catalyst bed inlet temperature. b_1, b_2 and b_3 are the dimensionless heat parameters as defined in Table 3.5.

Differential equations 3.16, 3.18, 3.20 – 3.27 and 3.31 were solved numerically using a fourth order Runge-Kutta method by applying the following initial conditions to obtain the axial concentration distribution of each component as well as the temperature distribution.

At z =0, $b_l = a_l = 1$, $c_l = d_l = e_l = f_l = 0$, $U'_g = U'_l = a_g = sol_g = \theta = 1$ (3.32)

Since the liquid velocity changes along the bed length, the new inlet substrate concentration correspondingly will be:

$$B_{li} = \frac{B_{li,inlet}\, U_{l,inlet}}{U_l} \quad (3.33)$$

This new B_{li} was used for dimensionlising various parameters discussed earlier. In calculating the term for solvent removal by solvent evaporation, $Sol_{Trans,g}$, the solvent vaporized for the differential element was directly used.

3.2.3 Effect of Reaction Conditions on the Properties of Gas and Liquids

The variation of vapor pressure of the solvent, methanol, with temperature can be correlated by

$\log (P_v) = (-0.2185\ A / T) + B$ (3.34)

where A and B are constants for methanol[24] (A=8978.8 and B=8.639821); T is the temperature in K.

The viscosity of methanol at different temperatures were taken from literature[25] and fitted using the polynomial to obtain the relation

$$m = -0.0025 + 1.69153 x10^{-5} xT - 2.535855 x10^{-8} xT^2 \quad (3.35)$$

The molecular diffusivity, D_M, was evaluated based on the correlation proposed by Wilke and Chang.[26]

The temperature dependency of Henry's constant was taken into account by extrapolating the values given in Chapter 2, Section 2 (A). 2. 5 (Table 2.3). The temperature dependency of rate constants can be given as

$$k_i(T) = k_i(T_0) \exp\left[\frac{E_i}{R T_0}\left(1-\frac{1}{\theta}\right)\right] \quad (3.36)$$

The temperature dependency adsorption constants was calculated as

$$K_i(T) = K_i(T_0) \exp\left[\frac{\Delta H_i}{R T_0}\left(1-\frac{1}{\theta}\right)\right] \quad (3.37)$$

The hydrodynamic, mass and heat transfer parameters needed for the prediction of reactor performance was calculated using various correlations in the literature and those correlations were chosen which gave a better prediction of the experimental observations. The values of bed to wall heat transfer coefficient calculated using the correlation suggested by Specchia and Baldi[30] was found to be high and multiplying it by a factor of 0.25 was found to predict the experimental values observed for the whole range of operating condition. The list of various correlations used in this study is given in Table 3.6.

Table 3.6: List of Correlations Used for Predicting TBR Performance

Parameter	Correlation	Reference
Gas-liquid mass transfer coefficient	$\frac{K_L a_B d_p}{D(1-\varepsilon_L/\varepsilon_B)} = 2\left(\frac{S_p}{d_p^{\,2}}\right)^{0.2} \mathrm{Re}_L^{\,0.73}\,\mathrm{Re}_G^{\,0.2}\left(\frac{m_L}{\rho_L D}\right)^{0.5}\left(\frac{d_p}{d_T}\right)^{0.2}$	Fukushima and Kusaka [27]
Liquid-Solid mass transfer coefficient	$\frac{K_s d_p}{D}\frac{a_W}{a_p} = 0.815\,\mathrm{Re}_L^{\,0.822}\left(\frac{m_L}{\rho_L D}\right)^{0.333}$	Satterfield et al. [28]
Total liquid holdup	$\log(1-\varepsilon_l) = -\frac{1.22\,We_L^{0;15}}{\mathrm{Re}_L^{0.20}\,X_G^{0.15}}$	Larachi et al. [29]
Bed to wall heat transfer coefficient	$\frac{U_W d_p}{\lambda_L} = 0.057\left(\frac{\mathrm{Re}_L}{\varepsilon_L}\right)^{0.09}\mathrm{Pr}_L^{\,1/3}$	Specchia and Baldi [30]
Pressure drop	$\frac{\Delta P}{Z} = \frac{2\rho_g U_g^2}{d_K\left(X_G(\mathrm{Re}_L We_L)^{\frac{1}{4}}\right)^{\frac{3}{2}}}\left[31.3+\frac{17.3}{\sqrt{X_G(\mathrm{Re}_L We_L)^{\frac{1}{4}}}}\right]$	Larachi et al. [29]
Wetting efficiency	$f_w = 1.104\,\mathrm{Re}_L^{\,1/3}\left[\frac{1+[(\Delta P/Z)/\rho_L g]}{Ga_L}\right]^{1/9}$	Al-Dahhan and Dudukovic [31]

3.3 Results and Discussion

3.3.1 Flow Regime Analysis

It is important to analyze the flow regimes in a trickle bed reactor since the mass transfer, wetting efficiency and heat transfer parameters are strongly dependent on the flow regime. To check the flow regime existing at different gas and liquid velocities studied, the correlation proposed by Charpentier and Favier[32] was used (Figure 3.4). The results in Figure 3.4 showing a plot of liquid mass flow rate (L, kg/m^2/sec) vs. gas mass flow rate (G, kg/m^2/sec) indicate the ranges for trickle flow and pulse flow regimes. It is evident that below a liquid mass flow rate of 1.75 kg/m^2/sec (~2.4 x10^{-3} m/s) trickle flow regime (low interaction regime) prevails under the conditions used in this work. Hence, the liquid velocity range used was kept to a limit of 2.4 x10^{-3} m/s so that all the experiments carried out were in trickle flow regime and for calculation of various parameters, the correlations corresponding to this regime was used.

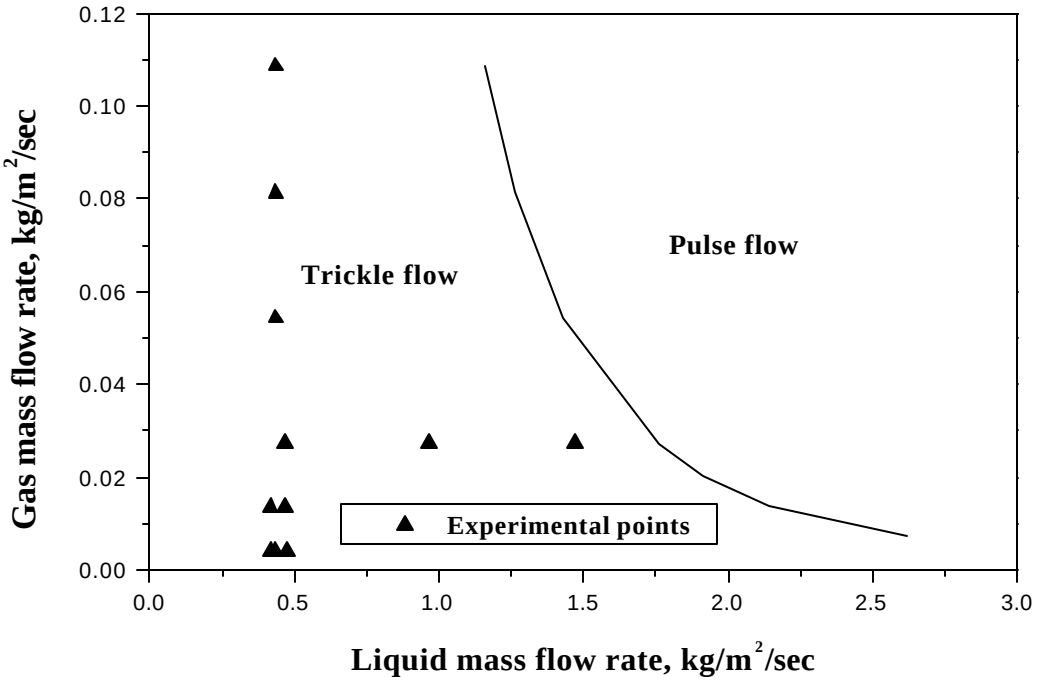

Figure 3.4: Flow Regime in a Trickle Bed Reactor Used for this Study (Predicted from Charpentier and Favier[32])

Experiments were carried out over wide ranging conditions (Table 3.3) and the results are discussed in terms of rate of hydrogenation, conversion of acetophenone, product distribution at the exit of the reactor and temperature rise at steady state conditions. The rate of total hydrogenation was calculated as:

$$R_A = \frac{U_l}{L}\left(3C_l + D_l + 4E_l + 2F_l\right) \quad (3.38)$$

Where, U_l is the liquid velocity in m/s, L is the length of the catalyst bed in m, $C_l, D_l, E_l \text{ and } F_l$ are the concentrations of CHMK, PHET, CHET and ETBE respectively in the liquid phase at the exit of the reactor in kmol/m^3.

The conversion of acetophenone was calculated as:

$$X_{ACPH} = (1 - b_l)\, x\, 100 \quad (3.39)$$

Where b_l is the dimensionless concentration of acetophenone at the reactor outlet. The selectivity towards a particular product was defined as:

$$\%\ Selectivity = \frac{No.\ of\ moles\ of\ product\ formed}{No.\ of\ moles\ of\ substrate\ converted} \times 100 \quad (3.40)$$

The temperature rise (ΔT) across the catalyst bed was calculated as

$$\Delta T = T_{exit} - T_{inlet} \quad (3.41)$$

3.3.2 Effect of Inlet Liquid Velocity

The Effect of liquid velocity on rate of hydrogenation is shown in Figure 3.5 for 373, 398 and 423 K. The rate of hydrogenation was found to decrease marginally with increase in liquid velocity. With increase in liquid velocity, one expects increase in the wetted fraction of the catalyst as well as increase in the gas-liquid and liquid-solid mass transfer coefficients. The variation of gas-liquid mass transfer and wetting efficiency for the liquid velocity range considered was estimated using the correlations suggested by Fukushima and Kusaka[27] and Al-Dahhan and Dudukovic[31] respectively and is shown in Figure 3.6. At lower liquid velocities, catalyst particles are partially wetted (f_w = 0.47 for a liquid velocity of 5.4 x10^{-4} m/s) and under these conditions, the rate increases due to direct transfer of gas phase reactant to the catalyst surface (already wetted internally due to capillary forces). Hence, with increase in liquid velocity, increase in wetted fraction is

expected to retard the rate of reaction, while increase in external mass transfer coefficients will enhance the rate, resulting in opposing effects.

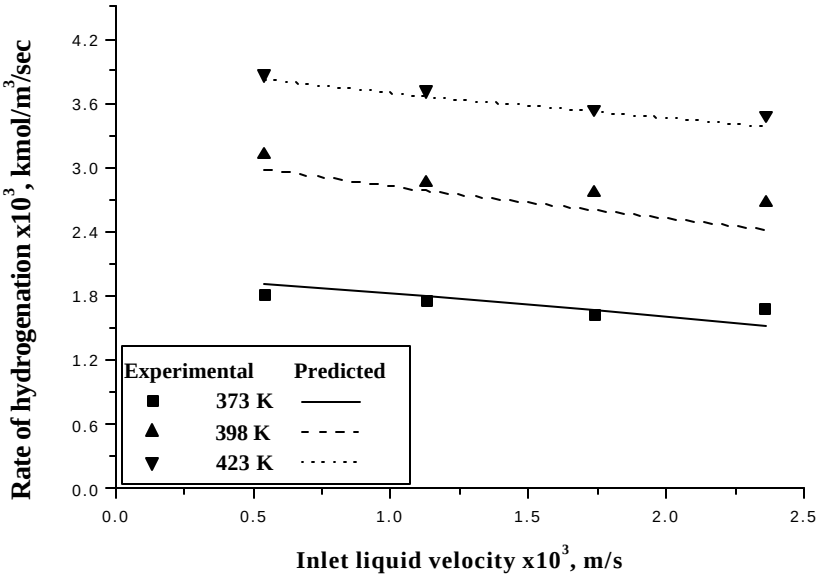

Figure 3.5: Effect of Liquid Velocity on Rate of Hydrogenation

Reaction Conditions: Reactor Pressure: 52 atm, Temperature: 398 K, Inlet ACPH Concentration: 1.27 kmol/m^3, Gas Flow Rate: 30 Nl/h

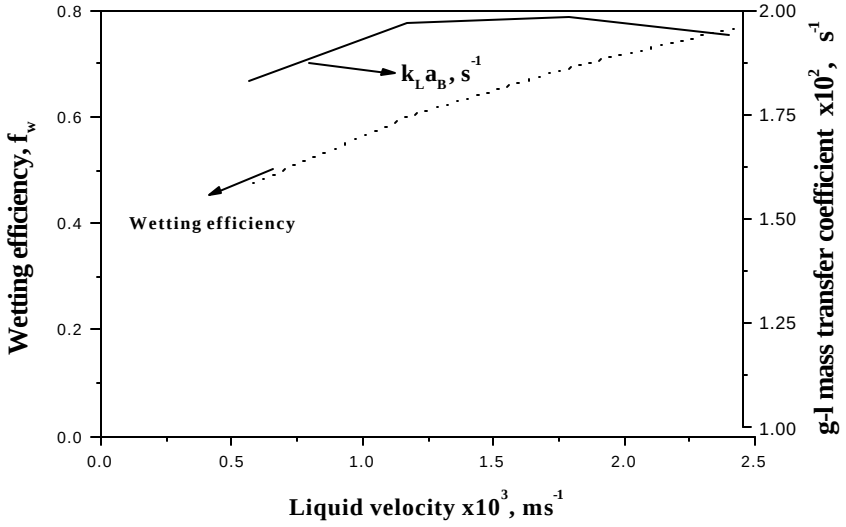

Figure 3.6: Effect of Liquid Velocity on f_w (Al-Dahhan and Dudukovic[31]) and k_La_B (Fukushima and Kusaka[27])

Reaction Conditions: Reactor Pressure: 52 atm, Temperature: 398 K, Inlet ACPH Concentration: 1.27 kmol/m^3, Gas Flow Rate: 30 Nl/h

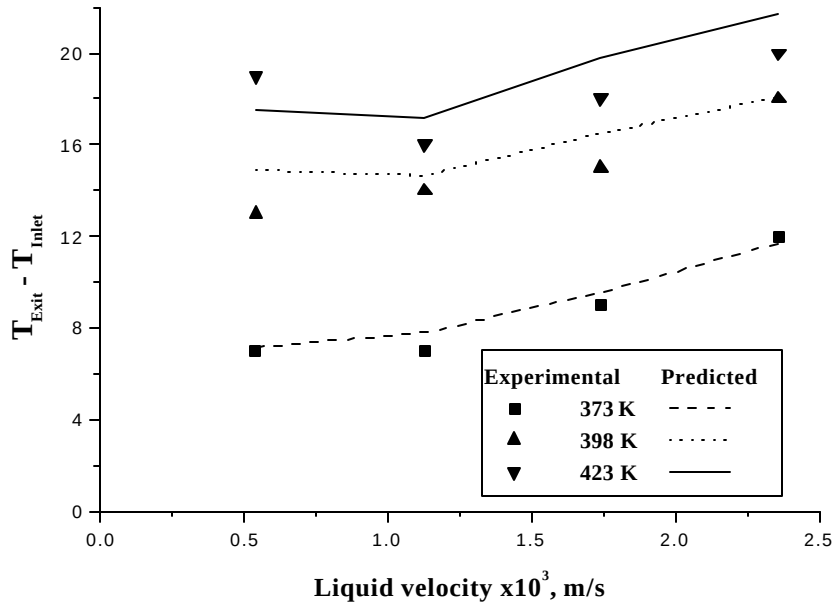

Figure 3.7: Effect of Liquid Velocity on Temperature Rise Across the Catalyst Bed

Reaction Conditions: Reactor Pressure: 52 atm, Inlet ACPH Concentration: 1.27 kmol/m^3, Gas Flow Rate: 30 Nl/h

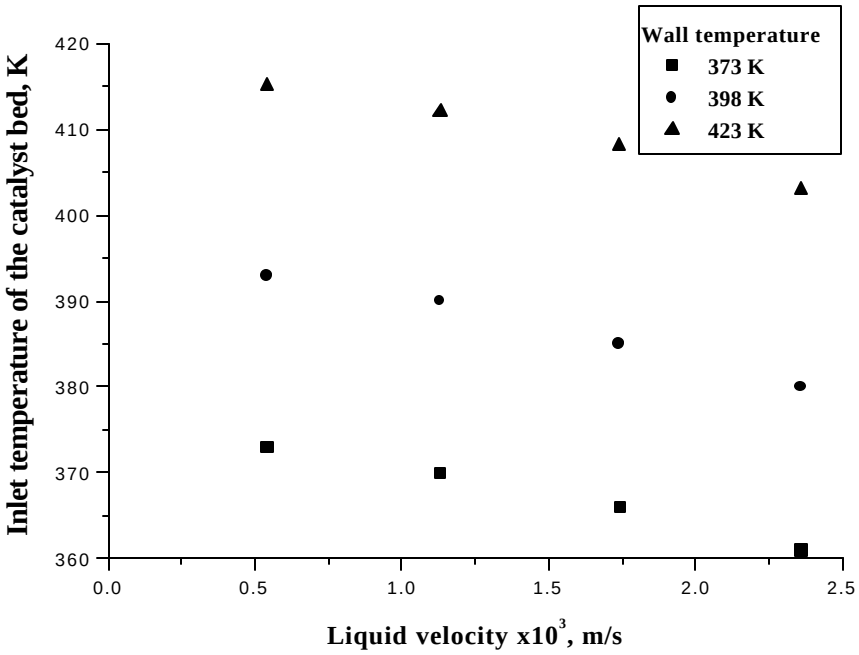

Figure 3.8: Inlet Temperature of the Catalyst Bed for Different Liquid Velocities

Reaction Conditions: Reactor Pressure: 52 atm, Inlet ACPH Concentration: 1.27 kmol/m^3, Gas Flow Rate: 30 Nl/h

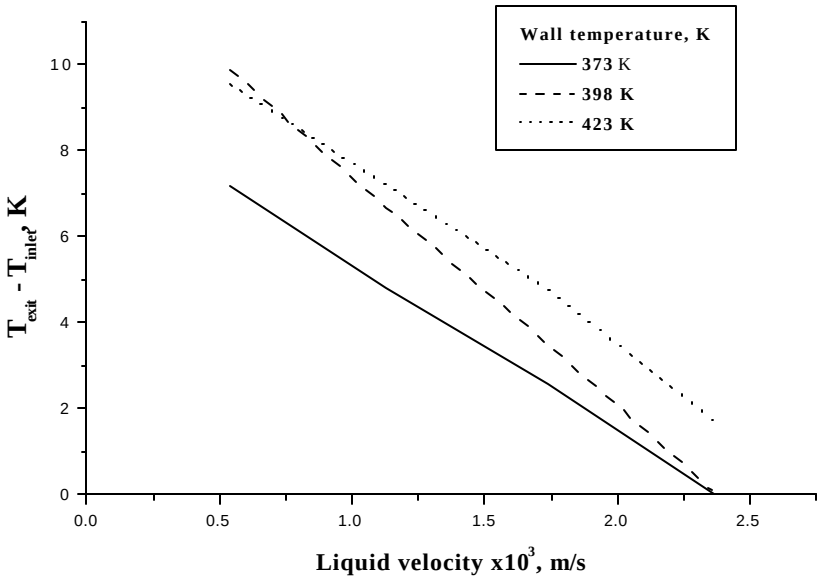

Figure 3.9: Model Prediction of the Temperature Rise with Liquid Velocity at Constant Inlet Catalyst Bed Temperature

Reaction Conditions: Reactor Pressure: 52 atm, Inlet ACPH Concentration: 1.27 kmol/m^3, Gas Flow Rate: 30 Nl/h

In order to assess the relative importance of gas-liquid and liquid-solid mass transfer contribution the total rate of hydrogenation was compared with maximum rates of gas-liquid and liquid-solid mass transfer (given as $k_l a_b A_{gi}/H_A$ and $k_s a_p A_{gi}/H_A$ respectively based on inlet conditions). These ratios were found to be 0.76 and 0.06 respectively, which indicated that the gas-liquid mass transfer was rate limiting while liquid-solid mass transfer was not significant. The temperature rise observed across the catalyst bed with increase in liquid velocity shows an increase in ΔT with liquid velocity as shown in Figure 3.7. While considering the non-isothermal effects, one important point to be mentioned is that at higher liquid velocities, the temperature at the inlet of the catalyst bed was found to be lower than that for lower the liquid velocities (Figure 3.8). For the experimental setup used, at higher liquid velocities, the temperature of liquid feed at catalyst bed inlet does not attain equilibrium with the set wall temperature and hence the results in Figure 3.7 represent data at a fixed wall temperature but a variable inlet catalyst bed temperature (observed experimentally). The temperature gradient, ΔT vs. liquid velocity shown in Figure 3.7 is a result of this limitation accompanied with

hydrogenation reaction. It is important to note that the model predictions agreed well for these data also with appropriate initial conditions. Some theoretical results were also predicted assuming that the inlet catalyst bed temperature was constant (same as the wall temperature) for all liquid velocities and the model predictions showed that the temperature rise in the reactor drops sharply with increase in liquid flow rate (Figure 3.9). The lowering of temperature rise with increase in liquid velocity is a result of higher rate of heat dissipation at higher liquid velocities compared to heat generated due to reaction.

3.3.3 Effect of Inlet Substrate Concentration and Pressure

On increasing the inlet concentration of ACPH from 0.84 – 2.34 kmol/m^3, the global rate of hydrogenation increased marginally (Figure 3.10) and was in accordance with the intrinsic kinetics (Chapter 2, Section 2 (A). 2. 4). With increase in temperature from 398 K to 423 K the increase in rate of hydrogenation was lower than the case when the temperature was increased from 373 K to 398 K (Figure 3.10).

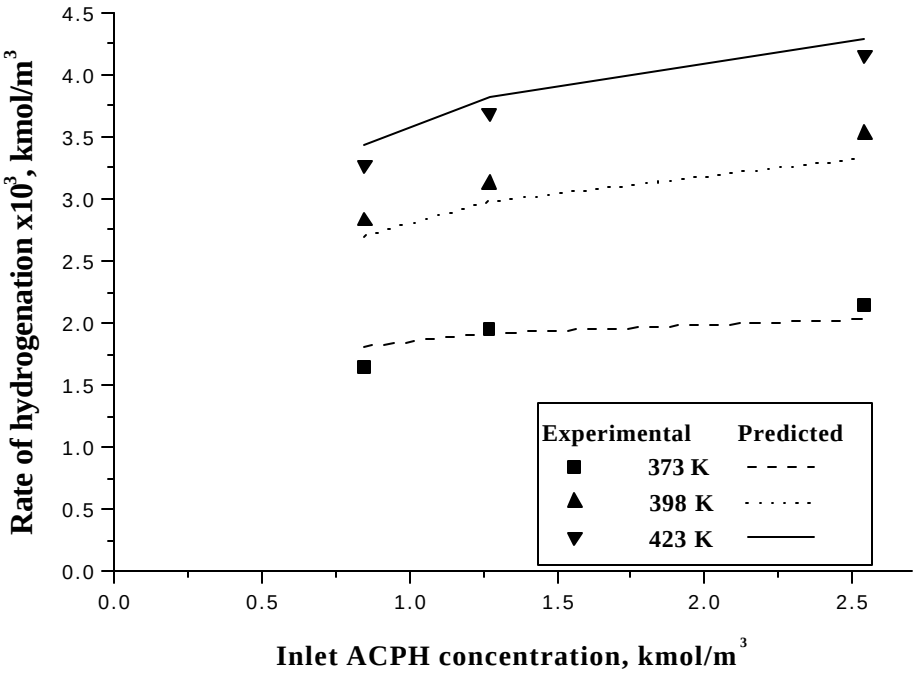

Figure 3.10: Variation of Rate of Hydrogenation with Inlet Substrate Concentration.

Reaction Conditions: U_l = 5.4 x10^{-4} m/s, Gas Flow Rate: 30 Nl/h, Reactor pressure: 52 atm

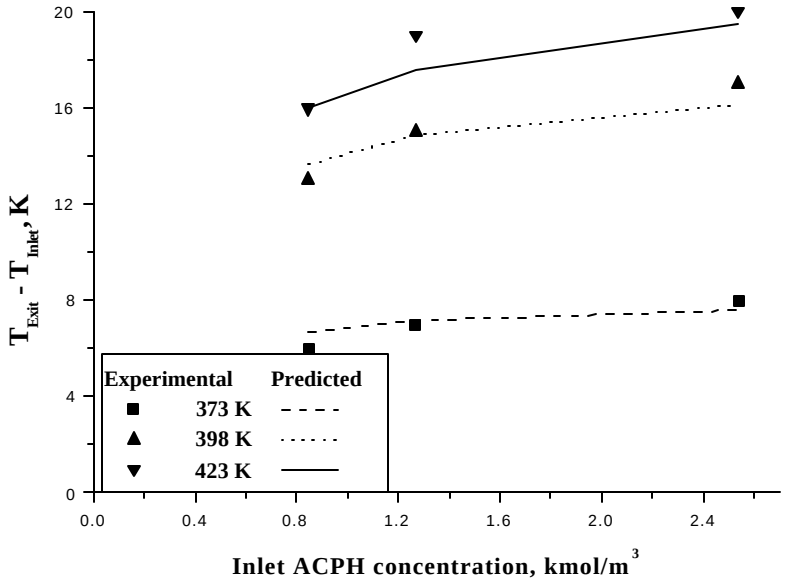

Figure 3.11: Variation Temperature Rise Across the Catalyst Bed with Inlet Substrate Concentration.

Reaction Conditions: $U_l = 5.4 \times 10^{-4}$ m/s, Gas Flow Rate: 30 Nl/h, Reactor Pressure: 52 atm

This observation was a result of relative contribution of chemical reaction and mass transfer rates. Since under the conditions used in this work, both external as well as intraparticle mass transfer limitations are significant (as indicated by liquid velocity and gas velocity effects (Figures 3.5 and 3.15)) one expects a mild temperature dependence as observed. The results shown in Figures 3.10 and 3.11 also indicate, a mild effect of temperature on both rate of hydrogenation as well as temperature rise. With increase in temperature, the solvent evaporation reduced the effective partial pressure of hydrogen and hence the rate enhancement with temperature was less than expected. For example, in the present case for a total reactor pressure of 52 atm, with increase in temperature from 373 to 423 K, the solvent vapor pressure increased from 3.4 atm to 13.61 atm and the corresponding hydrogen partial pressures were 48.6 and 38.9 atm respectively. The trends observed (See Figures 3.10 and 3.11) and the predictions are a consequence of this phenomenon in addition to the usual effect of temperature on model parameters. The rate of hydrogenation was found to increase with increase in hydrogen pressure (Figure 3.12) with almost a linear dependence. The temperature rise observed with increase in pressure

was higher than the corresponding temperature rise due to variation in any other parameter (Figure 3.13).

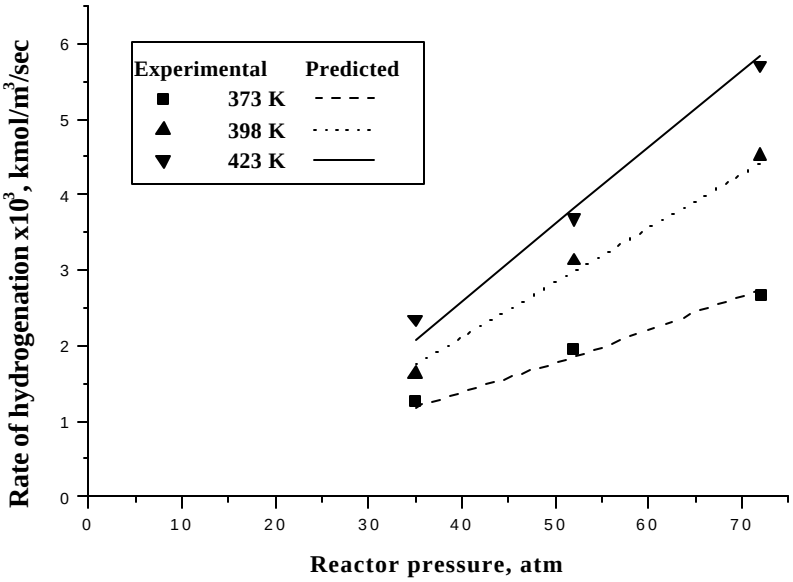

Figure 3.12: Variation of Rate of Hydrogenation with Pressure

Reaction Conditions: U_l = 5.4 x10^{-4} m/s, Gas Flow Rate: 30 Nl/h, Inlet Acetophenone Concentration: 1.27 kmol/m^3

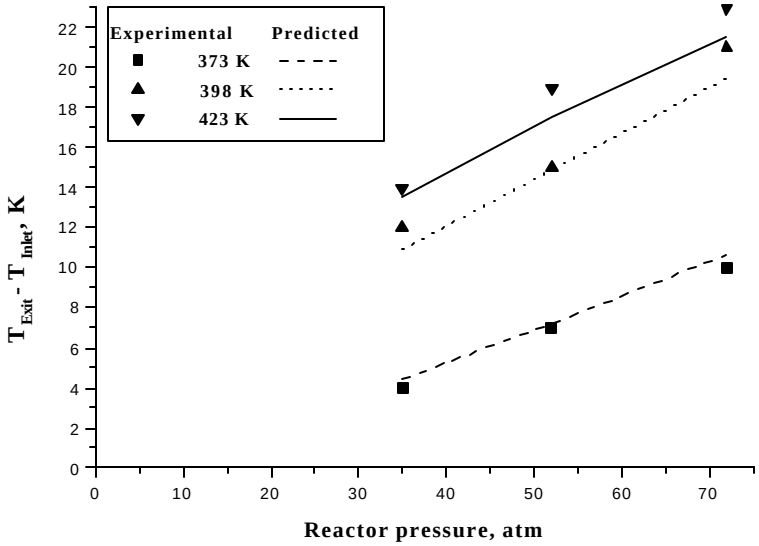

Figure 3.13: Variation of Temperature Rise Across the Catalyst Bed with Pressure

Reaction Conditions: U_l = 5.4 x10^{-4} m/s, Gas Flow Rate: 30 Nl/h, Inlet Acetophenone Concentration: 1.27 kmol/m^3

3.3.4 Effect of Gas Flow Rate

The effect of gas flow rate was investigated by varying the gas velocity from 0.035 m/s to 0.71 m/s at 398 K and at three pressures (52, 35 and 20 atm) and the results are shown in Figures 3.14 and 3.15.

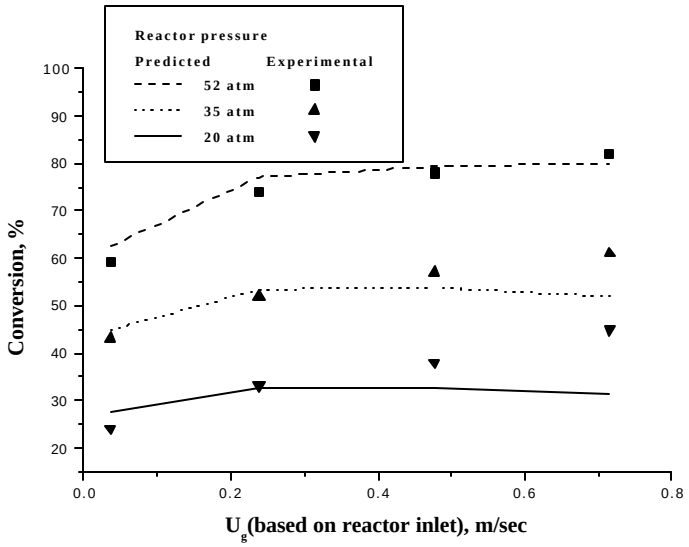

Figure 3.14: Conversion at the Exit vs. Gas Velocity at Different Pressures

Reaction Condition: $U_l = 5.4 \times 10^{-4}$ m/s, Substrate Concentration: 1.27 kmol/m^3, Wall Temperature: 398 K

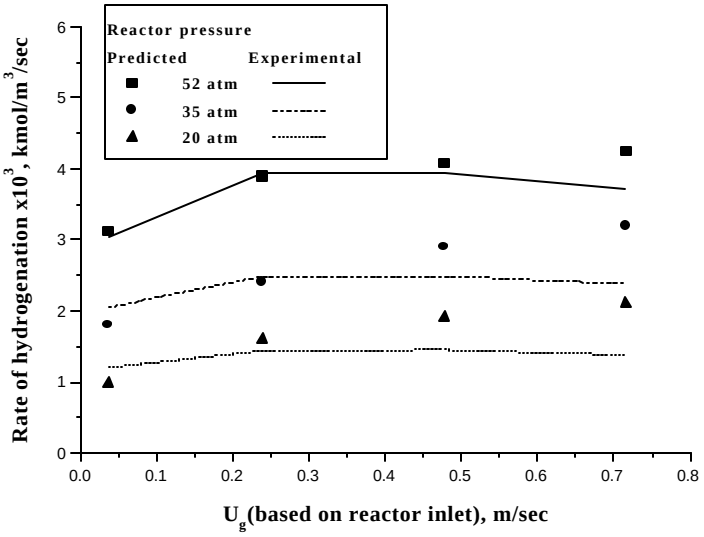

Figure 3.15: Rate of Hydrogenation vs. Gas Velocity at Different Pressures.

Reaction Condition: $U_l = 5.4 \times 10^{-4}$ m/s, Substrate Concentration: 1.27 kmol/m^3, Wall Temperature: 398 K

There was only marginal increase in the conversion as well as rate of hydrogenation with increase in gas velocity. Since the reaction under consideration was limited by gas-liquid mass transfer, one would have expected a stronger effect of gas velocity on the rate of hydrogenation. The variation of gas-liquid mass transfer coefficient ($k_L a_B$) and the wetting efficiency at the exit of the catalyst bed (since both change along the bed length also) with gas velocity calculated theoretically using the correlations suggested by Fukushima and Kusaka[27] and Al-Dahhan and Dudukovic[31] respectively is shown in Figure 3.16. It can be seen that on increasing the gas velocity from 0.035 m/s to 0.23 m/s, value of $k_L a_B$ increases from 1.88 x10^{-2} sec^{-1} to 2.48 x10^{-2} sec^{-1}, but on further increase in the gas velocity, the increase in the value of $k_L a_B$ is not significant. This is because at higher gas velocities (> 0.4 m/s), the liquid velocity decreases considerably inside the reactor due to solvent evaporation and this lowering of liquid velocity nullifies the increase in gas-liquid mass transfer coefficient due to increase in gas velocity. The variation of liquid velocity along the catalyst bed for different gas velocities at 398 K and 52 atm pressure is shown in Figure 3.17. The wetting efficiency calculated theoretically at the exit of the catalyst bed for various gas velocities at 398 K and 52 atm pressure (Figure 3.16) show a marginal decrease, which can result in an increase in the rate of hydrogenation. But at higher gas velocities, the temperature inside the catalyst bed was found to be lower than that for lower gas velocities.

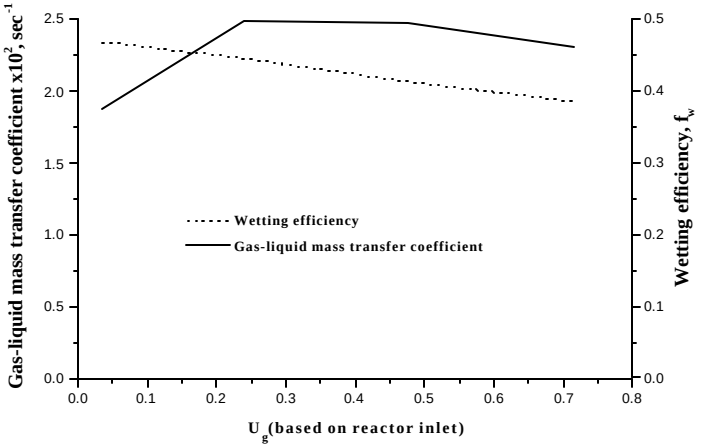

Figure 3.16: Effect of Gas Velocity on $k_L a_B$ (Fukushima and Kusaka[27]) and f_w (Al-Dahhan and Dudukovic[31])

Reaction Conditions: Reactor Pressure: 52 atm, Wall Temperature: 398K, Inlet ACPH Concentration: 1.27 kmol/m^3, U_l: 5.4 x10^{-4} m/s

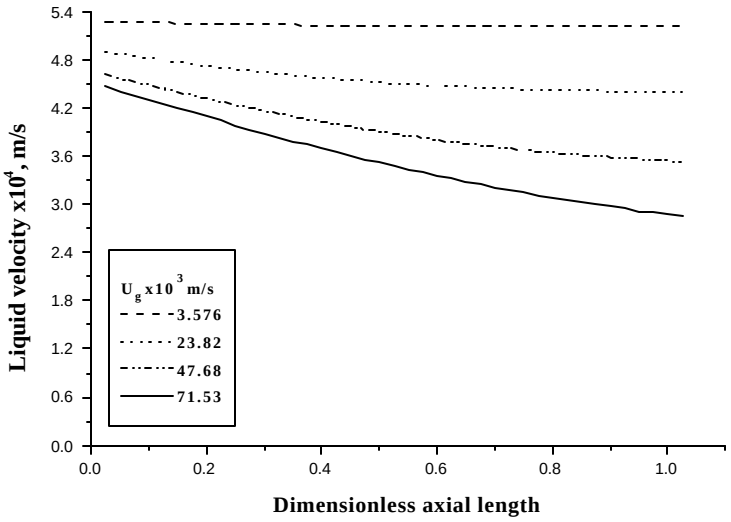

Figure 3.17: Liquid Velocity Distribution Along the Length of the Catalyst Bed for Various Gas Velocities at 52 atm

Reaction Condition: U_l (Inlet of the Reactor) = 5.4 x10^{-4} m/s, Substrate Concentration: 1.27 kmol/m^3, Wall Temperature: 398 K

The temperature distribution inside the catalyst bed for various gas velocities at 398 K and 52 atm pressure is shown in Figure 3.18. In general, when solvent evaporation was significant, it had a direct influence on the gas phase concentration, gas velocity, liquid velocity, wetting efficiency and mass and heat transfer parameters. The opposing effect of these parameters on the rate of hydrogenation explains the mild variation of rates of hydrogenation with gas velocity. The effect of gas velocity on the temperature across the catalyst bed is shown in Figure 3.19. Here also at higher gas velocities, the temperature at the inlet of the catalyst bed was found to be lower than the inlet temperature for lower gas velocities (Figure 3.20). The lower temperature existed at the inlet of the catalyst bed can be attributed to the heat removal by the flowing gas along with the heat removal by the evaporation of the volatile solvent. Here also the model predictions agreed well for these data with appropriate initial conditions. Some theoretical results were also predicted assuming that the inlet catalyst bed temperature was constant (same as the wall temperature) for all gas velocities and the model predictions showed that the temperature rise in the reactor drops after initial rise with increase in gas flow rate (Figure 3.21). The initial increase in temperature rise was in accordance with the increase in global rate of

hydrogenation and at higher gas velocities the temperature rise came down due to higher heat removal by the flowing gas and by solvent evaporation.

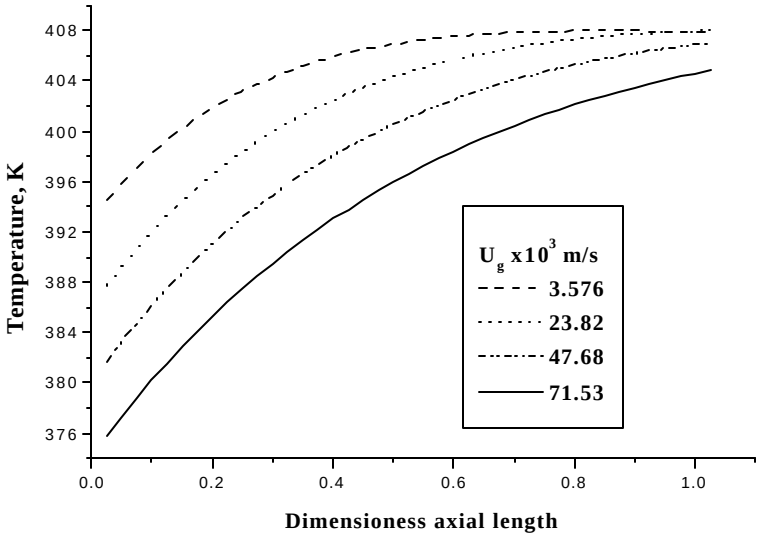

Figure 3.18: Temperature Distribution Along the Length of the Catalyst Bed for Various Gas Velocities at 52 atm

Reaction Condition: U_l (Inlet of the Reactor) = 5.4 x10^{-4} m/s, Substrate Concentration: 1.27 kmol/m^3, Wall Temperature: 398 K

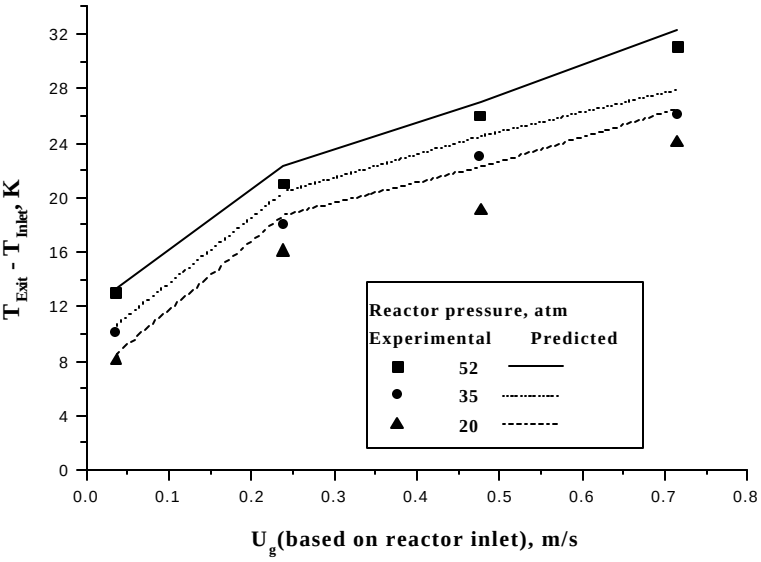

Figure 3.19: Temperature Rise for Various Gas Velocities at Different Pressures

Reaction Condition: U_l = 5.4 x10^{-4} m/s, Inlet ACPH Concentration: 1.27 kmol/m^3, Wall Temperature: 398 K

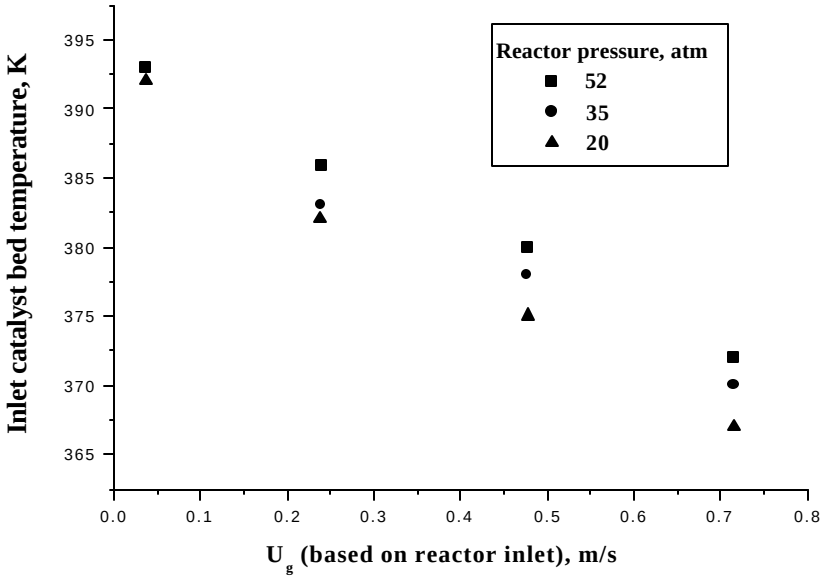

Figure 3.20: Inlet Temperature of the Catalyst Bed for Different Gas Velocities

Reaction conditions: U_l: 5.4 x10^{-4} m/s, Inlet ACPH Concentration: 1.27 kmol/m^3, Wall Temperature: 398 K

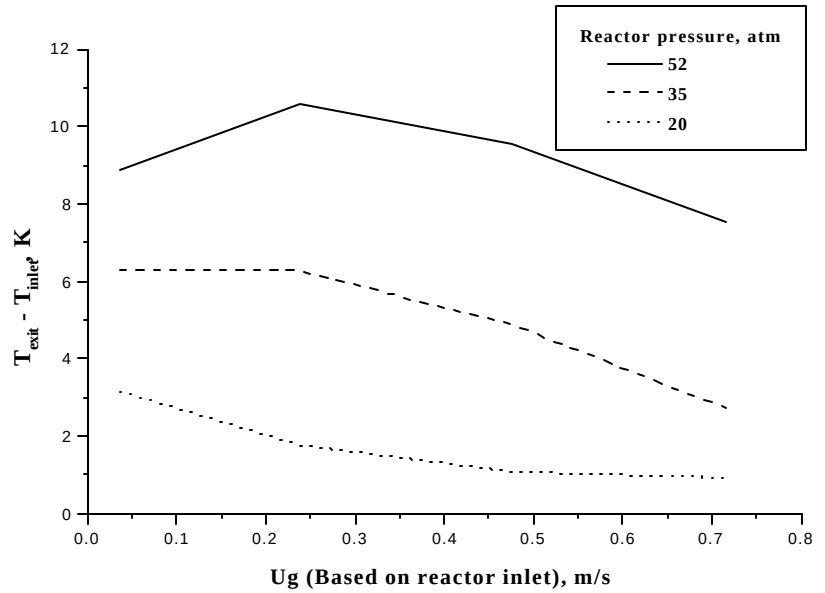

Figure 3.21: Model Prediction of Temperature Rise with Gas Velocity at Constant Inlet Catalyst Bed Temperature

Reaction conditions: Ų: 5.4 x10^{-4} m/s, Inlet ACPH Concentration: 1.27 kmol/m^3, Wall Temperature: 398 K

3.3.5 Effect of Reaction Parameters on Selectivity

The effect of various reaction parameters on the conversion of acetophenone and the product selectivity to 1-phenylethanol and 1-cyclohexylethanol (at 398 K) is shown in Figures 3.22 - 3.25 and are compared with the model predictions. It was found that, under the range of conditions studied the major product was PHET along with considerable amount of CHET. At higher liquid velocities, when the conversions of ACPH was low (~ 30%), PHET selectivity was high (~ 78 - 80%) and at lower liquid velocities (when conversions were high), the selectivity towards CHET increased (~ 9% at a conversion of 30% and 16% at a conversion of 62%). At low inlet concentration of ACPH the amount of CHET observed was comparatively high (for an initial ACPH concentration of 0.85 kmol/m^3 the CHET formed was ~22 % where as for an initial concentration of 1.27 kmol/m^3 it was ~16%). The formation of CHET was higher at higher pressures (26% CHET at a pressure of 72 atm and at a temperature of 398 K and liquid velocity of 5.4 x10^{-4} m/s where as at 35 atm it was only ~10%). With increase in temperature the increase in formation of CHET was marginal (~11 % CHET at 373 K and ~19% at 423 K at a reactor pressure of 52 atm and liquid velocity 5.4 x10^{-4} m/s)

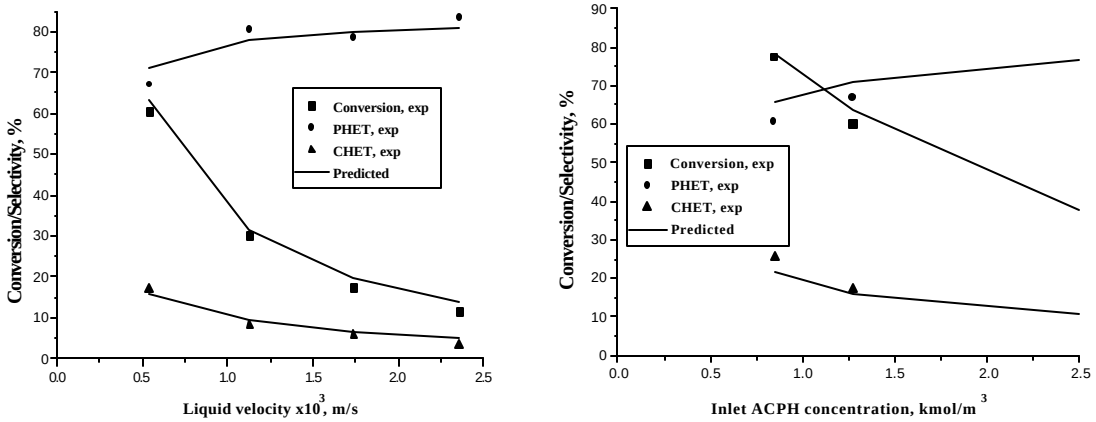

Figures 3.22, 3.23: Effect of Liquid Velocity and ACPH Concentration on Conversion of ACPH and Selectivity to PHET and CHET

Fig. 3.22: Reaction Conditions: Temp.: 398 K, P_{H2}: 52 atm, Substrate Concentration: 1.27 kmol/m^3, Gas Flow Rate: 30 Nl/hr

Fig. 3.23: Reaction Conditions: Temp.: 398 K, P_{H2}: 52 atm, Ų = 5.4 x10^{-4} m/s, Gas Flow Rate: 30 Nl/hr

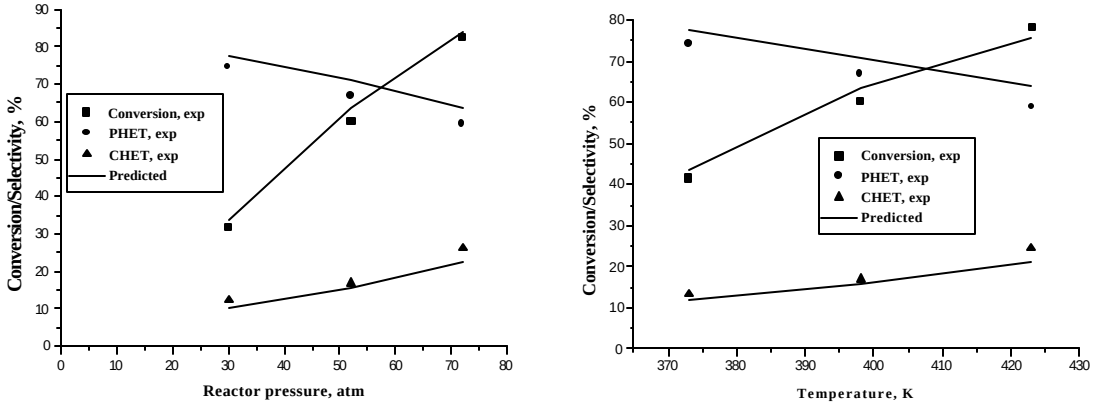

Figures 3.24, 3.25: Effect of Pressure and Temperature on Conversion of ACPH and Selectivity to PHET and CHET.

Fig. 3.24: Reaction Conditions: Temp.: 398 K, U_l = 5.4 x10^{-4} m/s, Substrate Concentration: 1.27 kmol/m^3, Gas Flow Rate: 30 Nl/hr

Fig. 3.25: Reaction Conditions: P_{H2}: 52 atm, Substrate Concentration: 1.27 kmol/m^3, U_l = 5.4 x10^{-4} m/s, Gas Flow Rate: 30 Nl/hr

3.4. Conclusion

Hydrogenation of acetophenone using a supported ruthenium catalyst was studied in a trickle bed reactor. The intrinsic kinetics was studied separately in a semi-batch slurry reactor and a Langmuir-Hinshelwood model considering different adsorption sites for aromatic and non-aromatic functional groups was found to explain the experimentally observed concentration-time profile. Increase in liquid velocity in the trickle bed reactor resulted in lower conversions of acetophenone considerably but had marginal effect on rate of hydrogenation. Of the main factors contributing to the reactor performance, the gas to solid mass transfer and gas to liquid mass transfer were found to be important. Increasing the inlet concentration of acetophenone resulted in marginal increase in rate of hydrogenation. The rate of hydrogenation varied almost linearly with the partial pressure of hydrogen proving the importance of gas phase reactant limitation. Increase in gas velocity was found to increase the conversion and rate of hydrogenation marginally. A plug flow model incorporating the mass transfer effects, partial wetting, non-isothermal effects and solvent evaporation effects was found to explain well the observed reactor

performance. PHET was found to be the major product under the range of conditions studied. CHET formation increased with increase in residence of liquid phase and with increase in reactor pressure.

Notations

a_{sg} dimensionless concentration of hydrogen in catalyst phase exposed to gas

a_{sl} dimensionless concentration of hydrogen in catalyst phase exposed to flowing liquid

a_p external surface area of the pellet, $[6\ (1-\varepsilon_B) / d_p]$, m^{-1}

a_t packing external surface area of the per unit volume of reactor

$[S_{ex}\ (1-\varepsilon_B) / V_B]$, m^{-1}

a_w catalyst area wetted, m^{-1}

B_{li} inlet substrate concentration, $kmol/m^3$

C_{Al} concentration of hydrogen, $kmol/m^3$

C_A^* saturation solubility of H_2, $kmol/m^3$

C_{Asg} concentration of hydrogen on the catalyst surface covered by gas phase, $kmol/m^3$

C_{Asl} concentration of hydrogen on the catalyst surface covered by liquid phase, $kmol/m^3$

C_{il} concentration of i^{th} component in liquid phase, $kmol/m^3$

C_{pg} specific heat capacity of gas, kJ / kg K

C_{pl} specific heat capacity of liquid, kJ / kg K

D_e effective diffusivity of hydrogen, m^2/sec

D_M molecular diffusivity, m^2/sec

d_p catalyst particle diameter, m

d_T reactor diameter, m

f_w externally wetted fraction of catalyst

g gravitational acceleration, kg/m^2

G Gas superficial mass flow rate, $kg\ m^{-2}\ s^{-1}$

Ga'$_L$ dimensionless liquid Galileo number, $\dfrac{d_P^3\,\rho_L^2\,g\,\varepsilon_B^3}{\mu_L^2(1-\varepsilon_B)^3}$

H_e Henry's constant, $kmol/m^3/atm$

$\Delta H_{sol,ev}$ heat removed by solvent evaporation, $kJ/m^3/s$

ΔH_{ev} heat of evaporation of the solvent, kJ/kmol

i_l dimensionless concentration of i^{th} component in liquid phase

K_A adsorption constant of hydrogen, $m^3/kmol$

K_{BX} adsorption constants of ACPH on X type of sites, $m^3/kmol$

K'_{BY} adsorption constants of ACPH on y type of sites, $m^3/kmol$

K_{DX} adsorption constant of CHET on X type of sites, $m^3/kmol$

$k_g a_p$ gas-solid mass transfer coefficient, s^{-1}

k_I clubbed rate constant for corresponding reaction step in simplified reaction scheme

k_i' rate constant for corresponding reaction step in simplified reaction scheme, $(m^3/kg)(m^3/kmol/sec)$

k_{i1} dimensionless rate constants

k_j dimensionless adsorption constants, j = B, C, D

$k_L a_B$ gas-liquid mass transfer coefficient, s^{-1}

$k_s a_p$ liquid-solid mass transfer coefficient, s^{-1}

L liquid superficial mass flow rate, kg m^{-2} s^{-1}

M_{sol} the molar flow of solvent in kmol/s

M_{H2} H_2 molar flow in kmol/s

P_{H_2} hydrogen partial pressure, atm

P_{sol} solvent vapor pressure, atm

P_{tot} total reactor pressure, atm

Pr_l Prandtl number of the liquid ($\mu_l C_{pl} / \lambda_l$)

q_B stoichiometric coefficient, B_{li} / C_A*

R catalyst pellet radius, m

Re'_L dimensionless liquid Reynolds number, $\frac{U_L \rho_L d_P}{\mu_L (1-\varepsilon_B)}$

Re_L liquid Reynold's number, $\frac{L d_P}{\mu_L}$

Re_G gas Reynold's number, $\frac{G d_P}{\mu_G}$

R_{H2} rate of hydrogenation, kmol/m3/sec

r_I rate of corresponding steps as shown in simplified reaction scheme

Sc_l Schmidt number, $\frac{\mu_L}{D_e \rho_l}$

S_p geometric surface area of the particle, m^2

T inlet temperature, K

T_b temperature of the bed, K

T_w temperature of the wall, K

U_g superficial gas velocity, m/s

U_l superficial liquid velocity, m/s

U_w bed to wall heat transfers coefficient, $kJ/m^2/K/sec$

W weight of catalyst, kg/m^3

We_l liquid Weber number, $L^2 d_P/(\sigma_l \rho_l)$

x axial distance of the catalyst bed, m

X_{sol} mole fraction of solvent in the gas phase

X_G modified Lockhart-Martinelli parameter

ϕ_0 defined by eq. 3.15

ϕ theile modulus

ϕ_{sol} number of moles of solvent getting transferred to the gas phase, kmol/m^3/s

f_{tot} total molar flow rate of gas in kmol/m^3/s at any point inside the reactor

τ tortousity factor

β_1 defined by equation

β_2 defined by equation

χ_A defined by eq. 3.19

ε_B bed porosity

θ_b dimensionless temperature of the bed

θ_w dimensionless temperature of the wall

η_c total effectiveness factor of the catalyst

η_{cg} effectiveness factor of the catalyst covered by gas phase

η_{cl} effectiveness factor of the catalyst covered by liquid phase

ρ_g density of gas, kg/m^3

α_{gl} dimensionless g-l mass transfer coefficient

ΔH_i heat of reaction per mole of hydrogen for the step i in the simplified reaction scheme, kJ/mol

ρ_l density of liquid, kg/m^3

ε_l liquid holdup

α_{ls} dimensionless l-s mass transfer coefficient

ρ_p catalyst pellet density, kg/m^3

$\Delta P/Z$ pressure drop, Pa, m^{-1}

α_r dimensionless reaction rate constant

α_{sg} dimensionless g-s mass transfer coefficient

λ_l liquid thermal conductivity, W/mK

References

1. Al-Dahhan M. H., Larachi F., Dudukovic M. P. and Laurent A., High Pressure Trickle-Bed Reactors: A Review, Ind. Eng. Chem. Res., 36, 3292, 1997

2. Al-Dahhan M. H and Dudukovic M. P., Catalyst Bed Dilution for improving catalyst wetting in laboratory trickle bed reactors, AIChE J., 42 (9), 2595, 1996

3. Valerius G., Zhu X., Hofmann H., Arntz D. and Haas T., Modelling of a trickle-bed reactor II. The hydrogenation of 3-hydroxypropanal to 1,3-propanediol, Chem. Eng. Proc., 35, 11, 1996

4. Castellari A. T., Cechini J. O., Gabarian L. J. and Haure P. M., Gas-phase reaction in a trickle-bed reactor operated al low liquid flow rates, AIChE J., 43, 7, P. 1813, 1997

5. Rajashekharam M. V., Jaganathan R. and Chaudhari R. V., A trickle-bed reactor model for hydrogenation of 2,4 dinitrotoluene: experimental verification, Chem. Eng. Sci., 53(4), 787, 1998

6. Khadilkar M. R., Jiang Y., Al-Dahhan M., Dudukovic M. P., Chou S. K., Ahmed G. and Kahney R., Investigations of a complex reaction network: I Experiments in a high-pressure trickle bed reactor, AIChE J., 44 **(**4), 912, 1998

7. Huang T. and Kang B., Naphthalene Hydrogenation over Pt/Al_2O_3 Catalyst in a Trickle Bed Reactor, Ind. Eng. Chem. Res., 34, 2349, 1995

8. Bergault I., Rajashekharam M. V., Chaudhari R. V., Schweich D. and Delmas H., Modelling of comparison of acetophenone hydrogenation in trickle-bed and slurry airlift reactors, Chem. Eng. Sci., 52 (21/22), 4033, 1997

9. Mears D., The role of liquid holdup and effective wetting in the performance of trickle bed reactors, Adv. Chem. Ser. No. 133, North Holland Publishing Co., Amstredam, 1974

10. Henry H. C. and Gilbert J. B., Scale-up of pilot-plant data for catalytic hydroprocessing, Ind. Eng. Chem. Proc. Des. Dev., 12, 328, 1973

11. Ramachandran P. A. and Smith J. M., Mixing cell model for design of trickle bed reactor, Chem. Eng. J., 17, 91, 1979

12. Hinduja M. J., Sundaresan S. and Jackson R., A crossflow model of dispersion in packed bed reactors, AIChE J., 26(2), 274, 1980

13. Ramachandran P. A. and Smith J. M., Effectiveness factors in trickle-bed reactors, AIChE J., 25, 538, 1979

14. Dudukovic M. P., Catalyst effectiveness factor and contacting efficiency in trickle-bed reactors, AIChE J., 23, 940, 1977

15. Mills P. L. and Dudukovic M. P., A dual series solution for the effectiveness factor of partially wetted catalysts in trickle bed reactors, Ind. Eng. Chem. Fundam., 18, 139, 1979

16. Mills P. L. and Dudukovic M. P., Analysis of catalyst effectiveness in trickle-bed reactors processing volatile or nonvolatile reactants, Chem. Eng. Sci., 35, 2267, 1980

17. Herskowitz M., carbonell R. G. and Smith J. M., Effectiveness factors and mass transfer in trickle-bed reactors, AIChE J., 25, 272, 1979

18. Goto S., Lakota A. and Levec J., Effectiveness factors of nth order kinetics in trickle bed reactors, Chem. Eng. Sci., 36, 157, 1981

19. Bischoff K. B., Effectiveness factors for general reaction rate forms. AIChE J., 11, 351, 1965

20. Tan C. S., and Smith J. M., Catalyst particle effectiveness with unsymmetrical boundary conditions, Chem. Eng.Sci., 35, 1601, 1980

21. Beaudry E. G., Dudukovic M. P. and Mills P. L., Trickle-bed reactors: liquid diffusional effects in a gas-limited reaction, AIChE J., 33(9), 1435, 1987

22. Khadilkar M. R., Mills P. L. and Dudukovic M. P., Trickle-bed reactor models for systems with a volatile liquid phase, Chem. Eng. Sci., 54, 2421, 1999

23. Ramachandran P. A. and Chaudhari R. V., Three phase catalytic reactors, Gorden breach science publishers, New York, 1983

24. Schlessinger G. G., Vapor pressure of organic compounds, Handbook of chemistry and Physics, Chemical Rubber Co., (CRC), D155, 1970

25. Perry's Chemical Engineering Hand Book (sixth edition), Robert H. Perry and Don Green, Mcgraw-Hill International editions, Chemical Engineering Series (1984)

26. Wilke C. R. and Chang P., Correlation for diffusion coefficients in dilute solutions, AIChE J., 1, 264, 1955

27. Fukushima S. and Kusaka K., Liquid Phase volumetric and mass transfer coefficient, and boundary of hydrodynamic flow region in packed column with cocurrent downward flow, J. Chem. Eng. Japan, 10 (6), 468, 1977

28. Satterfield C. N., Vab Eek M. W. and Bliss G. S., Liquid-solid mass transfer in packed beds with down flow cocurrent gas-liquid flow, AIChE. J, 24, 709, 1978

29. Larachi F., Laurent A., Midoux N. and Wild G., Experimental Study of a Trickle-Bed Reactor Operating at High Pressure: Two-phase Pressure Drop and Liquid Saturation, Chem. Eng. Sci., 46 (5/6), 1233, 1991

30. Specchia V. and Baldi G., Heat transfer in trickle bed reactors, Chem. Eng. Commun., 3, 483, 1979

31. Al-Dahhan M. H., and Dudukovic M. P., Catalyst wetting Efficiency In trickle-bed Reactors at high pressure, Chem. Eng. Sci., 50 (15), 2377, 1995

32. Charpentier J. C. and Favier M., Some liquid holdup experimental data in trickle bed reactors for foaming and no-foaming hydrocarbons. AIChE J., 21, 1213, 1975

Chapter 4

Hydrogenation of Acetophenone in a Fixed Bed Up-Flow Reactor Using Supported Ruthenium Catalyst

4.0 Introduction

Fixed bed gas-liquid-solid reactors, wherein gaseous and liquid reactants co-currently flow upwards over a catalyst bed find applications in a wide variety of industrial processes. These include hydrodesulfurization of petroleum fractions, hydrocracking, hydrogenation of nitro compounds, amination of alcohols, ethynylation of formaldehyde to butynediol and waste water treatment.[1,2] The conditions around the catalyst particles are more uniformly maintained in the up-flow operation compared to trickle bed. The higher liquid holdup and effective liquid-solid contact results in better heat dissipation in case of exothermic reactions and can be advantageous for reactions where the temperature dependence of selectivity is sensitive. Design aspects of co-current up-flow reactors were reviewed by Hofmann[1] and Shah,[3] while a comparison of correlations for mass transfer and hydrodynamic parameters is given by Ramachandran and Chaudhari.[2] The generally used reactor model is a one-dimensional heterogeneous model taking into consideration the back mixing of gas and liquid phases.

Several reports on reactor performance in up-flow reactors for hydrogenation reactions are published,[4,5,9] and most of these studies were carried out under isothermal conditions. Liquid phase hydrogenation of maleic anhydride was investigated by Herrmann and Emig[5] in a fixed bed up-flow reactor using copper based catalysts. The effect of reaction parameters on the selectivity of γ-butyrolactone was studied. They reported that at higher concentrations of maleic anhydride (0.5 mol/L) and at higher temperature (> 500 K) the selectivity for γ-butyrolactone increased but with increase in pressure, the selectivity for 1,4-butanedoil was found to increase. They proposed a theoretical model based on these results, which was used to predict reactor performance behavior beyond the limits of the apparatus, and the reaction conditions used. van Gelder et al.[6,7] described a reactor model for the hydrogenation of 2,4,6- trinitrotoluene in an up-flow reactor in the presence of an evaporating solvent to absorb the heat of reaction. Details of the investigations on fixed bed up-flow reactor performance studies have been discussed in Chapter 1, Section 1.2.4.2.1.

Comparison of the performance for up-flow and down-flow fixed bed multiphase reactors is of interest to understand clearly the distinguishing features of these two modes. Studies on comparison of up and down-flow modes involving both theoretical

and experimental aspects reported in literature[2,8,9,10,11] are discussed in Chapter 1, Section 1.2.4.3.

In this chapter, an experimental study on the hydrogenation of acetophenone using ruthenium supported on alumina catalyst in a high-pressure fixed bed up-flow reactor is presented. Reactor performance was investigated over a wide range of operating conditions such as liquid velocity, inlet concentration of substrate, reactor pressure, gas velocity and temperature. A theoretical plug flow model has been developed for predicting the steady state reactor performance under non-isothermal conditions, incorporating the mass transfer effects of the gaseous hydrogen and evaporation effects of the volatile solvent. A comparison of the steady state performances of fixed bed up-flow and trickle bed reactors operated under identical reaction conditions was done. In order to explain the concentration and temperature profiles observed in the fixed bed up-flow reactor during the start-up transient period, a dynamic non-isothermal three-phase heterogeneous model taking into consideration the axial mixing of the liquid phase was also developed.

4.1 Experimental

4.1.1 Materials

Acetophenone (Aldrich, USA) and methanol (S.D. Fine. Chem., India) were used as procured. Hydrogen and nitrogen were obtained from M/s Indian Oxygen Ltd., India and 2%Ru/Al_2O_3 pellets were procured from Arrorey Mathey, India and the specifications of the catalyst are same as given in Chapter 3, Section 3.1.1.

4.1.2 Equipment

The experiments were carried out in the reactor setup described in Chapter 3, Section 3.1.2 for trickle bed studies with appropriate modifications for up-flow operation of gas and liquid feeds as shown in Figure 4.1.

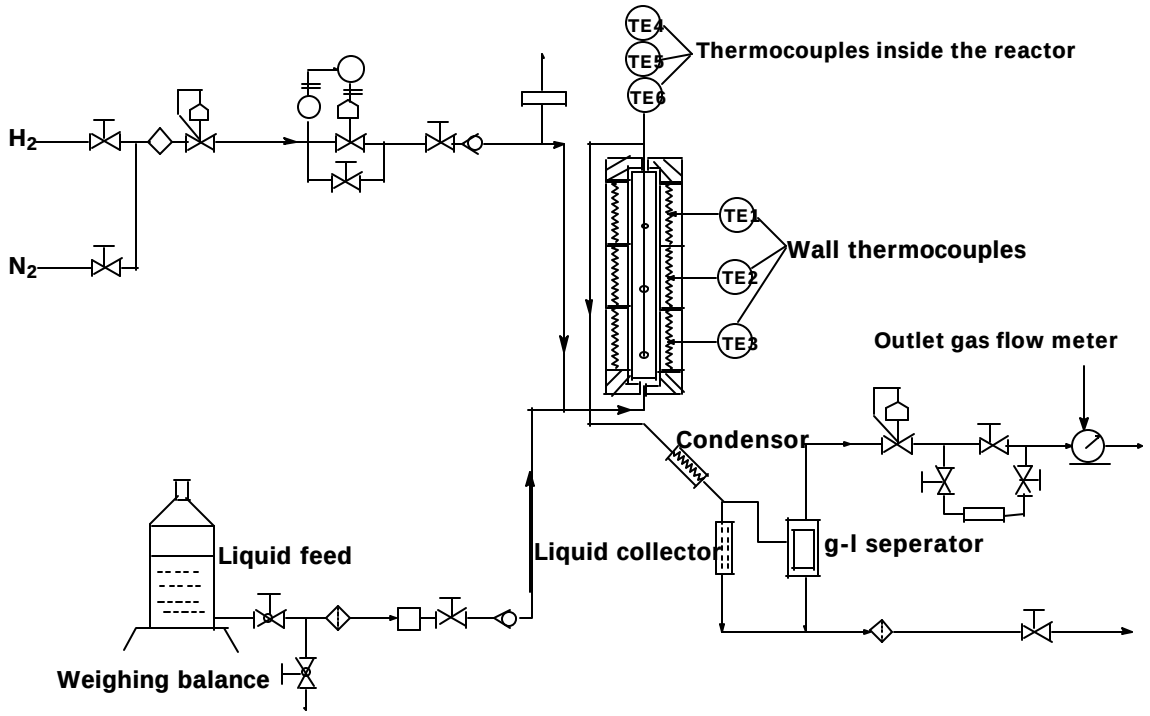

Figure 4.1: Schematic of the Fixed Bed Reactor with Cocurrent Up-flow

4.1.3 Experimental Procedure

The experimental procedure followed for up-flow reactor performance studies were similar to that for trickle bed studies as described in Chapter 3, Section 3.1.3 except that gas and liquid feeds were introduced in a co-current up-flow mode. The range of operating conditions studied is given in Table 4.1.

Table 4.1: Range of Operating Conditions

Inlet concentration of ACPH	0.84 - 2.5 kmol/m^3
Reactor pressure	20 – 72 atm
Liquid velocity	0.54 x 10^{-3} – 2.4 x 10^{-3} m/s
Temperature	373 - 423 K
Gas flow rate	30 – 600 Nl/h

The details of the analysis method used were the same as described in Chapter 2, Section 2 (A). 1.3 as reaction system investigated was the same.

4.2 Model for Up-flow Reactor

The basic differences in the trickle bed and up-flow reactors were that in the latter case, catalyst particles are completely wetted with liquid (wetting efficiency, f_w = 1) and the mass transfer, heat transfer and hydrodynamic parameters would be different. The mass and heat balance equations described in Chapter 3 for the trickle bed reactor was used for up-flow reactor with f_w = 1 and appropriate correlations used for estimating the various mass and heat transfer parameters. The correlations used for evaluation of hydrodynamic and mass and heat transfer parameters for the up-flow mode are presented in Table 4.2. With these correlations, theoretical predictions for up-flow reactor were made following the procedure described in Chapter 3.

4.3 Results and Discussion

Hydrogenation experiments were carried out at different reaction conditions to observe total rate of hydrogenation, conversion of acetophenone, product distribution at exit of the reactor and temperature rise across the catalyst bed. The experiments were carried out for a time duration of 1-3 hours to ensure steady state operation as indicated by constant exit concentrations. For the range in which experimental data were observed, the steady state reactor performance was also predicted using the theoretical model described above.

The total rate of hydrogenation was calculated as:

$$R_A = \frac{U_l}{L}\left(3C_l + D_l + 4E_l + 2F_l\right) \qquad (4.1)$$

Where, U_l is the liquid velocity in m/s, L is the length of the catalyst bed in m, C_l, D_l, E_l *and* F_l are the concentrations of CHMK, PHET, CHET and ETBE respectively in the liquid phase at the exit of the reactor in kmol/m^3.

The conversion of acetophenone was calculated as:

$$X_{ACPH} = (1 - b_l)\, x\, 100 \qquad (4.2)$$

where b_l is the dimensionless concentration of acetophenone at the reactor outlet.

Table 4.2: Correlations for Model Parameters for Fixed Bed Up-flow Reactor

Parameter	Correlation	Reference
Gas-liquid mass transfer coefficient, $k_L a_B$	$k_L a_B = 5.48x10^{-3}\left[U_l \boldsymbol{d}_{gl}\right]^{0.5}$	Reiss [12]
Pressure drop per unit length of reactor, $\mathbf{d_{gl}}$	$\left[\boldsymbol{d}_{gl}\right]^{0.5} = \frac{2 f_{gl} U_g^2 \boldsymbol{r}_g}{d_{pe}}$	Turpin and Huntington [13]
Liquid-solid mass transfer coefficient, k_s	$k_s = \left(0.48 \ln\left(\frac{\mathrm{Re}_G 10^2}{\mathrm{Re}_L}\right) - 0.03\left(\ln\left(\frac{\mathrm{Re}_G 10^2}{\mathrm{Re}_L}\right)\right)^2 - 0.3\right)\frac{D_{12} Sh_0}{d_p}$	Specchia et al.[14]
Molecular diffusivity, D_M	$D_M = \frac{7.4\ x10^{-8} T (xM_W)^{\frac{1}{2}}}{m_L V_M^{0.6}}$	Wilke and Chang [15]
Liquid hold up, ε_l	$\boldsymbol{e}_l = \boldsymbol{e}_B 1.47\ \mathrm{Re}_l^{0.11}\ \mathrm{Re}_G^{-0.19}\left(a_p d_p\right)^{-0.41}$	Stiegel and Shah [16]
Pectlet number for liquid phase, Pe_L	$Pe_L = \boldsymbol{e}_l 0.128\ \mathrm{Re}_l^{0.245}\ \mathrm{Re}_G^{-0.16}\left(a_p d_p\right)^{0.53}$	Stiegel and Shah [16]
Bed to wall heat transfer coefficient	$\frac{U_W d_{ec}}{\boldsymbol{l}_L} = 0.26\ \mathrm{Re}'^{0.43}_l\ \mathrm{Pr}_L^{1/3}$	Sokolov et al.[17]

The selectivity towards a particular product was defined as:

$$\%\ Selectivity = \frac{No.\ of\ moles\ of\ product\ formed}{No.\ of\ moles\ of\ substrate\ converted} \times 100 \qquad (4.3)$$

The temperature rise, ΔT, across the catalyst bed was calculated as:

$$\Delta T = T_{exit} - T_{inlet} \qquad (4.4)$$

4.3.1 Effect of Liquid Velocity

The Effect of liquid velocity on conversion and rate of hydrogenation are shown in Figures 4.2 and 4.3. It was found that the conversion decreases with increasing liquid velocity as expected in accordance with the residence time of the liquid phase. Increasing liquid velocity was found to have almost no effect on rate of hydrogenation. The observed mild dependence of rate on U_l indicates that the external mass transfer (gas-liquid and liquid-solid) resistances may be negligible. To ensure this, the observed rate was compared with the maximum rates of gas-liquid and liquid-solid mass transfer (given as $k_l a_b\ A_{gi}/H_A$ and $k_s a_p\ A_{gi}/H_A$ respectively based on inlet conditions). The ratio of rate of hydrogenation to the maximum rate of gas-liquid mass transfer was found to be in the range of 0.26 – 0.15 for a corresponding liquid velocity from 5.4 $x10^{-4}$m/s to 2.36 $x10^{-3}$ m/s. The corresponding range for the ratio of rate of hydrogenation to maximum liquid-solid mass transfer rates was 0.075 – 0.068, indicating that the effects of both gas-liquid and liquid-solid mass transfer on the reaction rates were low. The temperature rise across the catalyst bed was found to increase with increase in liquid velocity as shown in Figure 4.4. This is because, at higher liquid velocities, the temperature of the inlet of catalyst bed was lower than that at lower liquid velocities. For the experimental set up used, at higher liquid velocities, the temperature of liquid feed at catalyst bed inlet does not attain the set wall temperature. The experimentally observed temperature at the inlet of the catalyst bed for the various liquid velocities studied is shown in Figure 4.5 (these values were used as the inlet catalyst bed temperature for model predictions). This explains the trends observed in Figure 4.4 and the predicted temperature rise was also found to agree well with the experimental values with appropriate initial conditions.

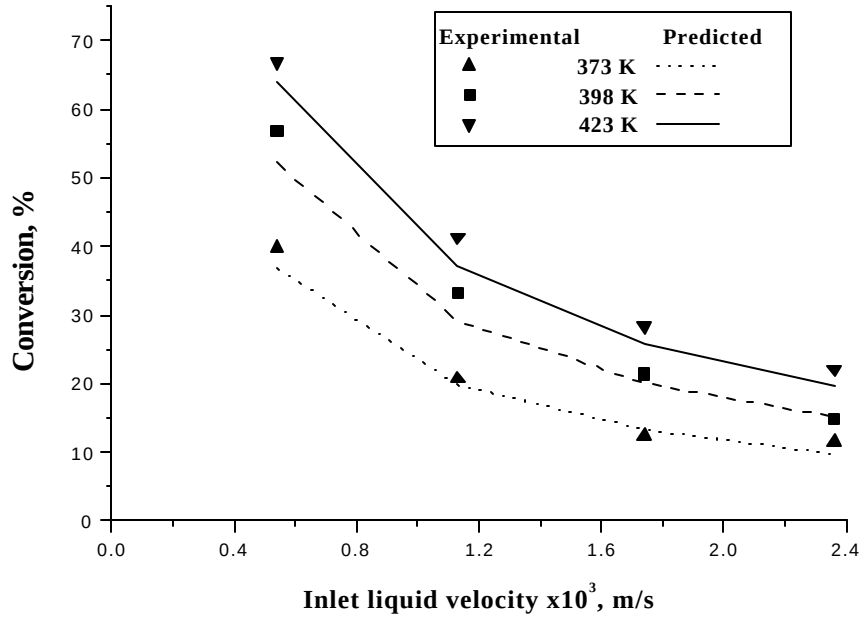

Figure 4.2: Effect of Liquid Velocity on Conversion

Reaction Conditions: Reactor Pressure: 52 atm, Inlet ACPH Concentration: 1.27kmol/m^3, Gas Flow Rate: 30 Nl/h

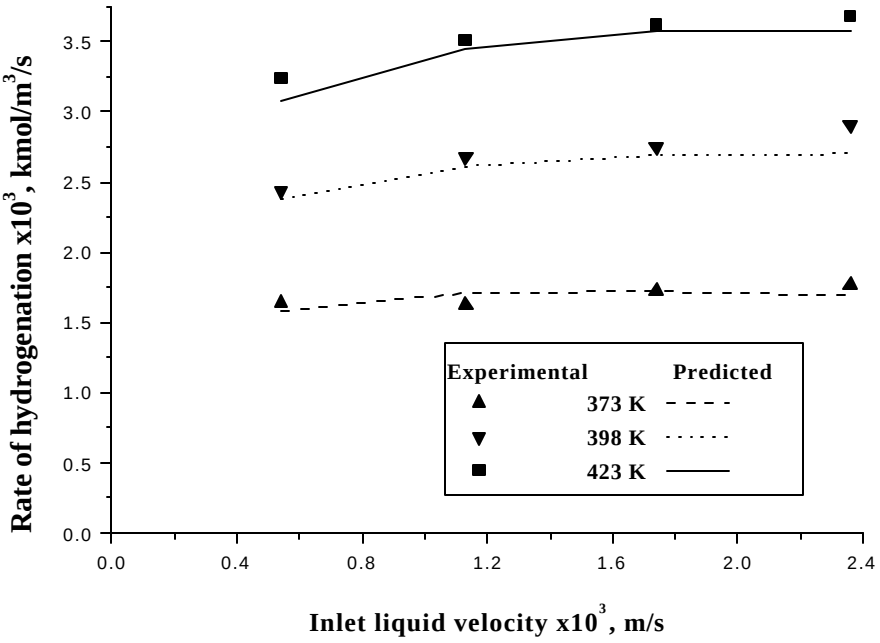

Figure 4.3: Effect of Liquid Velocity on Rate of Hydrogenation

Reaction Conditions: Reactor Pressure: 52 atm, Inlet ACPH Concentration: 1.27 kmol/m^3, Gas Flow Rate: 30 Nl/h

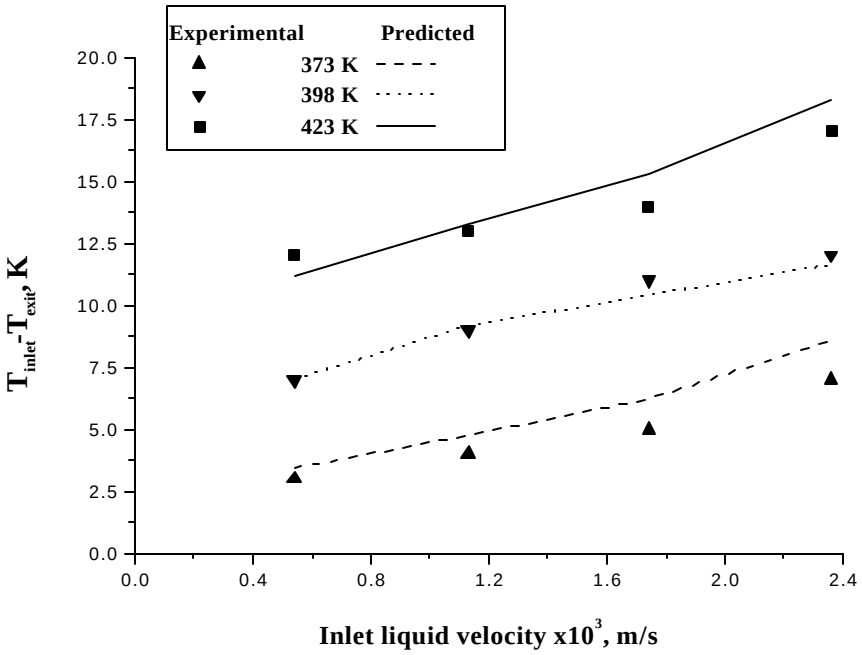

Figure 4.4: Effect of Liquid Velocity on Temperature Rise Across Catalyst Bed

Reaction Conditions: Reactor Pressure: 52 atm, Inlet ACPH Concentration: 1.27kmol/m^3, Gas Flow Rate: 30 Nl/h

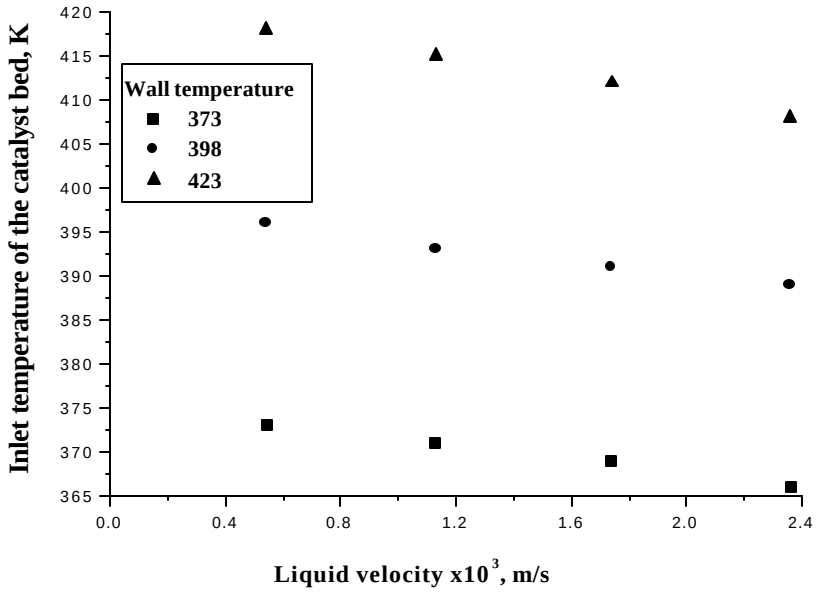

Figure 4.5: Inlet Temperature of the Catalyst Bed for Different Liquid Velocities

Reaction conditions: Reactor Pressure: 52 atm, Inlet ACPH Concentration: 1.27kmol/m^3, Gas Flow Rate: 30 Nl/h

Model predictions assuming inlet catalyst bed temperature same as the wall temperature showed a decrease in the temperature rise with increasing liquid velocity as shown in Figure 4.6. The decrease in temperature rise with liquid velocity at constant inlet bed temperature was due to efficient heat removal by the flowing liquid at higher liquid velocities. At higher liquid velocities, the heat transfer across the reactor wall was also found to be more efficient. The bed to wall heat transfer coefficient was found to increase from 0.113 to 0.1965 kJ/m^2/K/sec when the liquid velocity was increased from 5.4 x10^{-4} m/s to 2.36 x10^{-3} m/s at a wall temperature of 398 K, as calculated by the correlation suggested by Sokolov et al.[17]

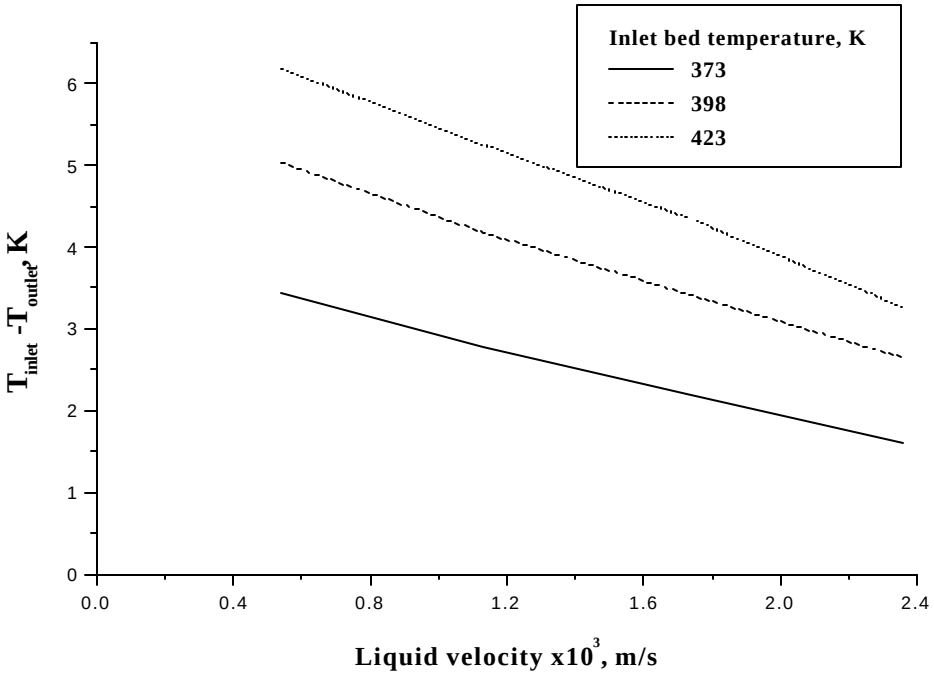

Figure 4.6: Theoretical Predictions of Temperature Rise at Constant Catalyst Bed Inlet Temperature

Reaction Conditions: Reactor Pressure: 52 atm, Inlet ACPH Concentration: 1.27kmol/m^3, Gas Flow Rate: 30 Nl/h

4.3.2 Effect of Inlet substrate concentration and pressure

On increasing the inlet concentration of ACPH from 0.84 – 2.34 kmol/m^3, the conversion decreased where as the rate of hydrogenation showed a marginal increase (Figures 4.7, 4.8). These observations agreed well with the model predictions and the

mild dependence of the rate of hydrogenation on inlet acetophenone concentration was in accordance with the intrinsic kinetics (See Chapter 2, Section: 2 (A). 2. 4.).

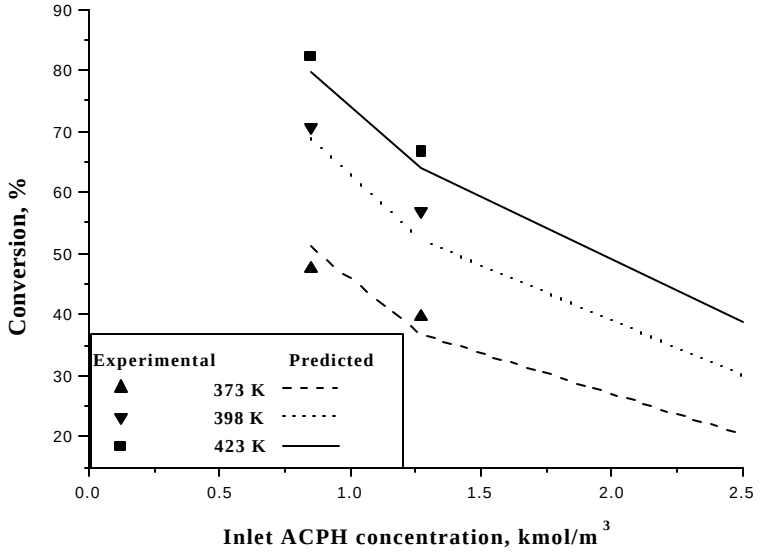

Figure 4.7: Conversions at Varying Inlet Substrate Concentrations

Reaction Conditions: U_l: 5.4 x10^{-4} m/s, Gas Flow Rate: 30 Nl/h, Reactor Pressure: 52 atm

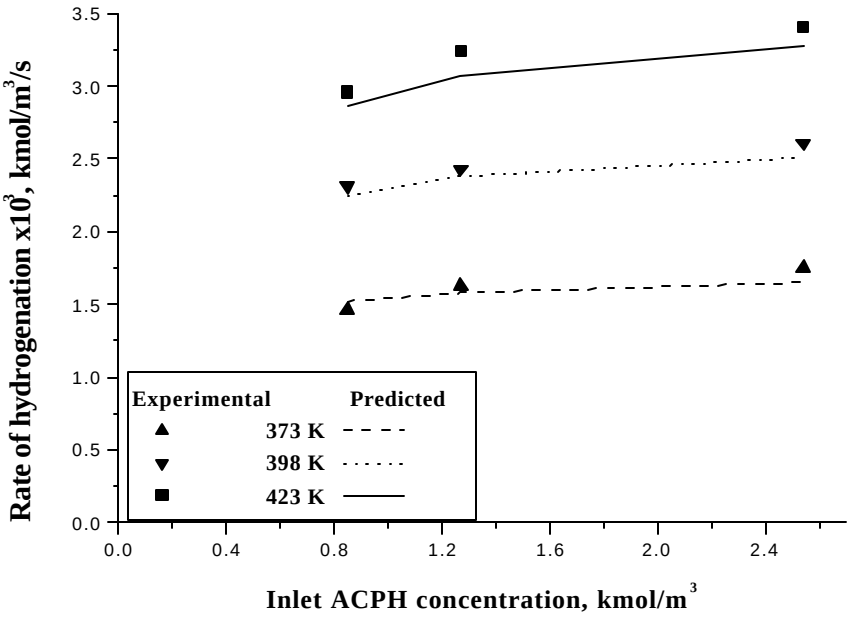

Figure 4.8: Variation of Global Rate of Hydrogenation with Inlet Substrate Concentration

Reaction Conditions: U_l: 5.4 x10^{-4} m/s, Gas Flow Rate: 30 Nl/h, Reactor Pressure: 52 atm

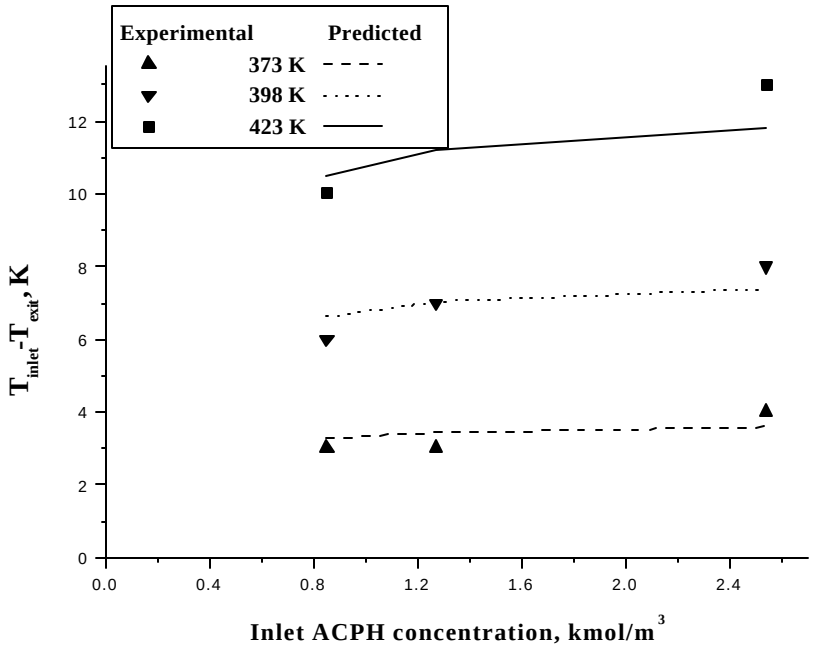

Figure 4.9: Temperature Rise with Varying Inlet ACPH Concentrations

Reaction Conditions: U_l: 5.4 x10^{-4} m/s, Gas Flow Rate: 30 Nl/h, Reactor Pressure: 52 atm

The temperature rise observed for different inlet concentrations of ACPH and at various temperatures is given in Figure 4.9 and it was found that the temperature rise was not significant at high concentration and was in accordance with the marginal increase in rate of hydrogenation. The increase in rate of hydrogenation on increasing the temperature from 398 K to 423 K was lower than the increase in rate on raising the temperature from 373 K to 398 K. The lowering of hydrogen partial pressures at higher temperatures due to the increased contribution of solvent vapor pressure to the total reactor pressure can be the reason for this. For a total reactor pressure of 52 atm, the partial pressures of hydrogen (P_{H2}) at 373, 398 and 423 K were 48.6, 45.20 and 38.39 atm respectively, showing the decreased contribution of P_{H2} at the highest temperature, 423 K.

The conversion as well as rate of hydrogenation was found to increase with increase in hydrogen pressure (Figures 4.10 and 4.11). From the marginal effect of inlet ACPH concentration on rate of hydrogenation and almost a linear dependence on hydrogen partial pressure, it is clear that gaseous hydrogen is the limiting reactant. The

temperature rise across the catalyst bed was found to increase with pressure (Figure 4.12).

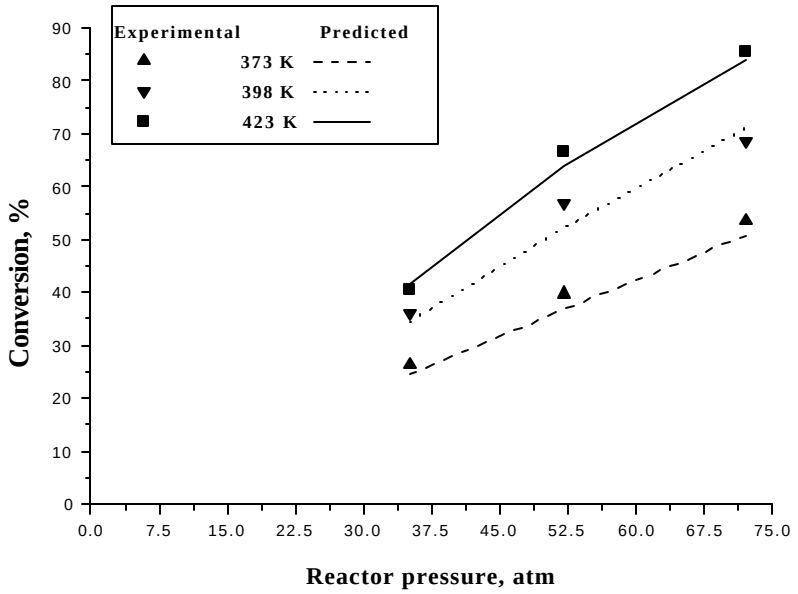

Figure 4.10: Conversion at the Exit with Varying Pressure

Reaction Conditions: Ų: 5.4 x10^{-4} m/s, Gas Flow Rate: 30 Nl/h, Inlet ACPH Concentration: 1.27 kmol/m^3

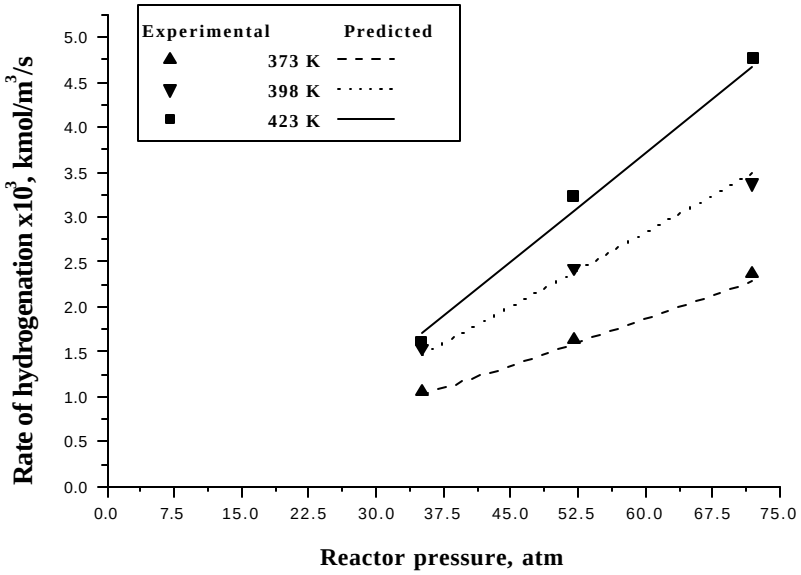

Figure 4.11: Variation of Rate of Hydrogenation with Pressure

Reaction Conditions: Ų: 5.4 x10^{-4} m/s, Gas How Rate: 30 Nl/h, Inlet ACPH Concentration: 1.27 kmol/m^3

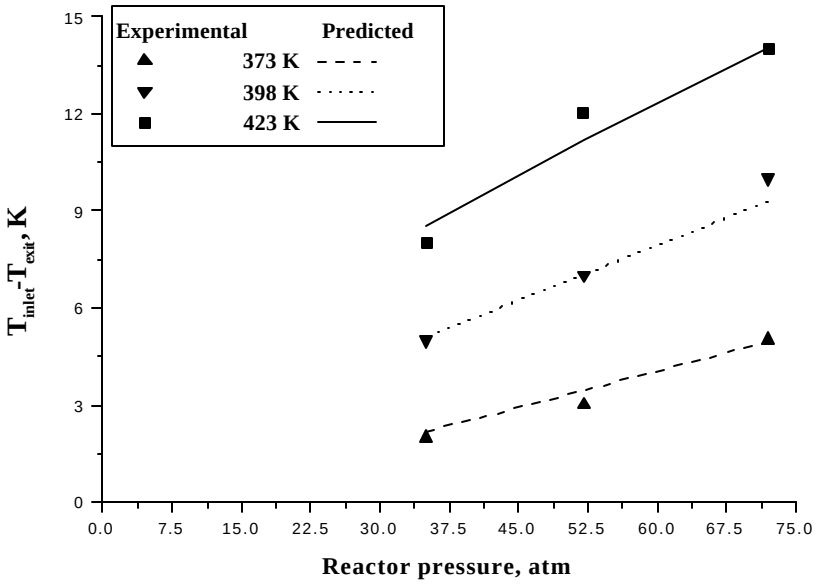

Figure 4.12: Variation in Temperature Rise with Pressure

Reaction Conditions: Ų: 5.4 x10^{-4} m/s, Gas Flow Rate: 30 Nl/h, Inlet ACPH Concentration: 1.27 kmol/m^3

4.3.3 Effect of Gas Flow Rate

In order to study the effect of gas velocity on the reactor performance, the gas flow rate was varied from 30 Nl/h to 600 Nl/h. The conversion as well as rate of hydrogenation was found to increase marginally with increase in gas velocity at 398 K and 52 atm pressure, whereas the gas velocity was found to have almost no effect at lower pressures at 398 K (Figure 4.13 and 4.14). This mild effect of gas velocity on the rates indicates the low influence of the external mass transfer effects on the reactor performance. In the case of up-flow reactor also, the inlet temperature of the catalyst bed was found to be lower than the wall temperature at high gas velocities due to the heat removal by the flowing gas and by solvent evaporation. The temperature distribution inside the catalyst bed, predicted theoretically, at 398 K and 52 atm, for different gas velocities is shown in Figure 4.15. In accordance with the temperature distribution and gas velocities inside the reactor, the liquid velocity will also change along the catalyst bed length. The model prediction on the variation in liquid velocity along the bed length for various gas velocities at 398 K and 52 atm is given in Figure 4.16.

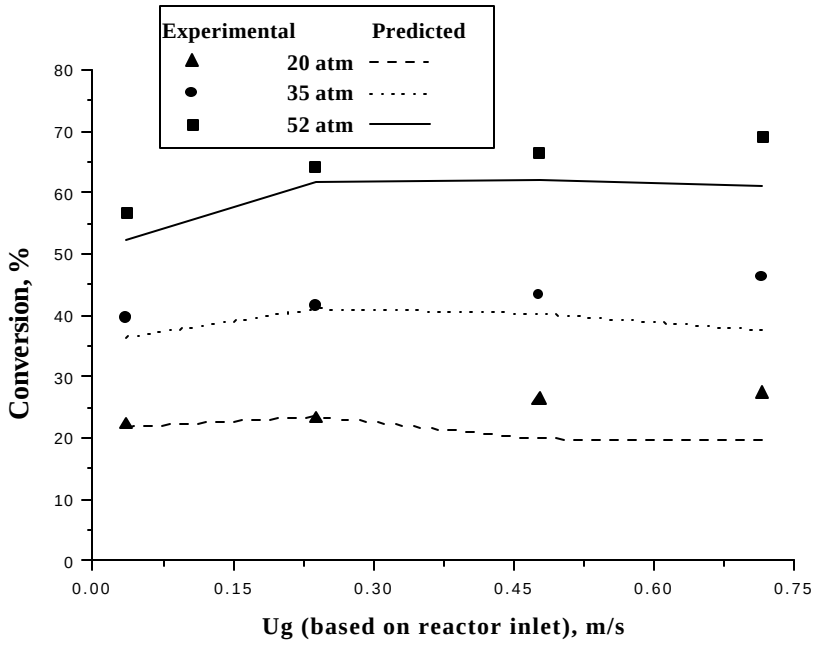

Figure 4.13: Conversion at the Exit vs Gas Velocity at Different Pressures

Reaction Conditions: U_l = 5.4 x10^{-4} m/s, Substrate Concentration: 1.27 kmol/m^3, Wall Temperature: 398 K

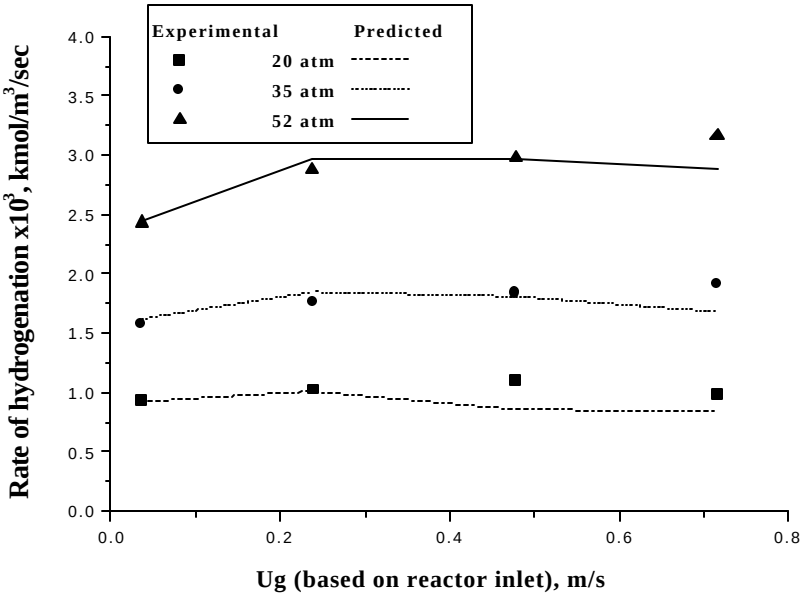

Figure 4.14: Variation of Rate of Hydrogenation with Gas Velocity at Different Pressures

Reaction Conditions: U_l = 5.4 x10^{-4} m/s, Substrate Concentration: 1.27 kmol/m^3, Wall Temperature: 398 K

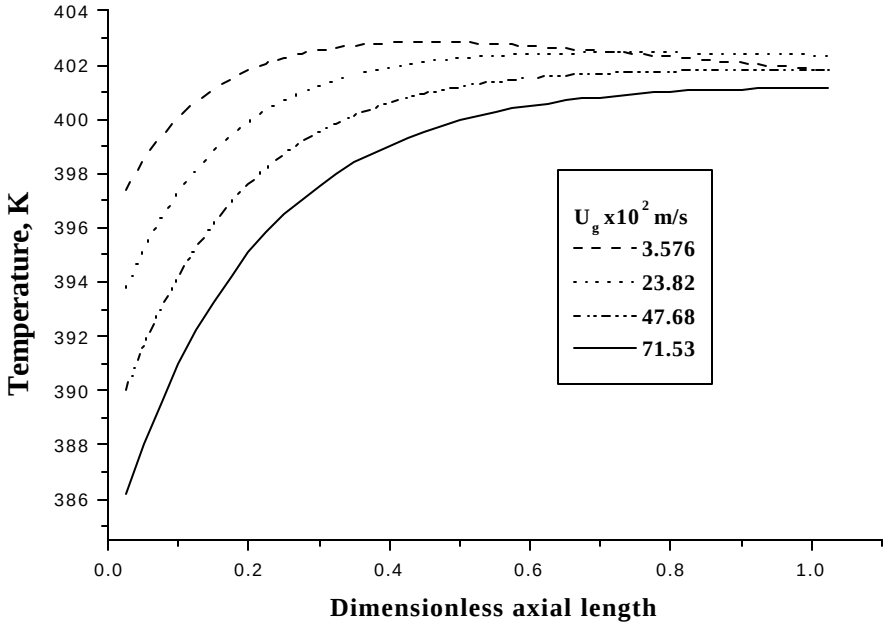

Figure 4. 15: Temperature Distribution Along the Length of the Catalyst Bed for Various Gas Velocities at 52 atm

Reaction conditions: U_l: 5.4 x10^{-4} m/s, Sub. Con.: 1.27 kmol/m^3, Wall temperature: 398 K

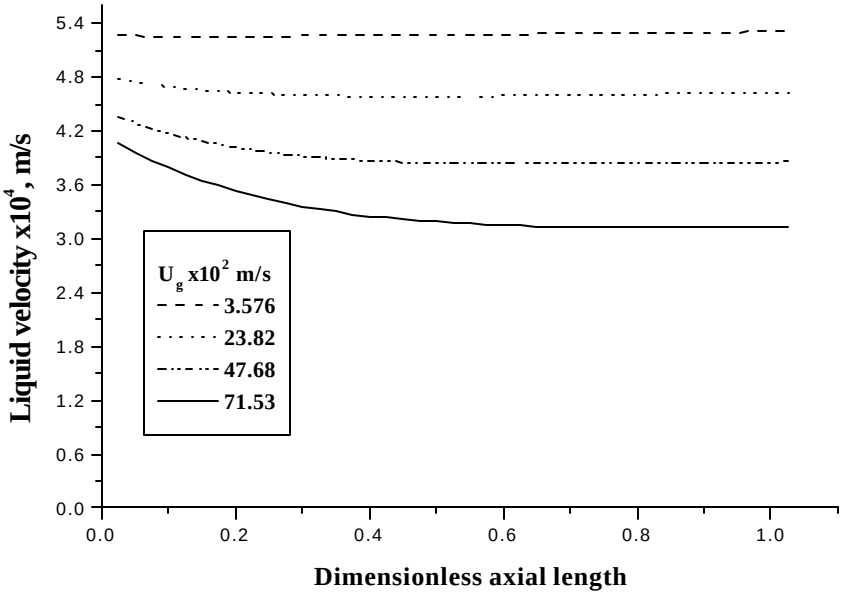

Figure 4.16: Liquid Velocity Distribution Along the Length of the Catalyst Bed for Various Gas Velocities at 52 atm

Reaction Conditions: U_l: 5.4 x10^{-4} m/s, Sub. Con.: 1.27 kmol/m^3, Wall temperature: 398 K

4.3.4 Selectivity Behavior

The effect of various reaction parameters on the conversion of acetophenone and the product selectivity to the two important products 1-phenylethanol and 1-cyclohexylethanol determined are shown in Figures 4.17 to 4.20 along with theoretical predictions, using the model developed for up-flow reactor. It was found that, under the range of conditions studied, the major product found in the up-flow reactor was PHET along with considerable amount of CHET and ETBE. At lower conversions of ACPH (~ 35%), PHET selectivity was high (79 - 82%) and as the residence time of the liquid increased, the selectivity towards CHET increased (~ 8% at a conversion of 25% and 18% at a conversion of 64%) as expected, since it was formed by the hydrogenation of PHET. The formation of CHET was higher at higher pressures (12 and 25% for reactor pressures 35 and 72 atm respectively at 423 K and at a liquid velocity of 5.4 $x10^{-4}$m/s). On increasing the reaction temperature, even though the selectivity to CHET increased, the formation of the side product ETBE was also higher (13 and 25% selectivity to CHET at 373 and 423 K respectively for a reactor pressure of 72 atm and at a liquid velocity of 5.4 $x10^{-4}$m/s and the selectivity to ETBE under similar conditions were 1.4 and 8.2 % respectively).

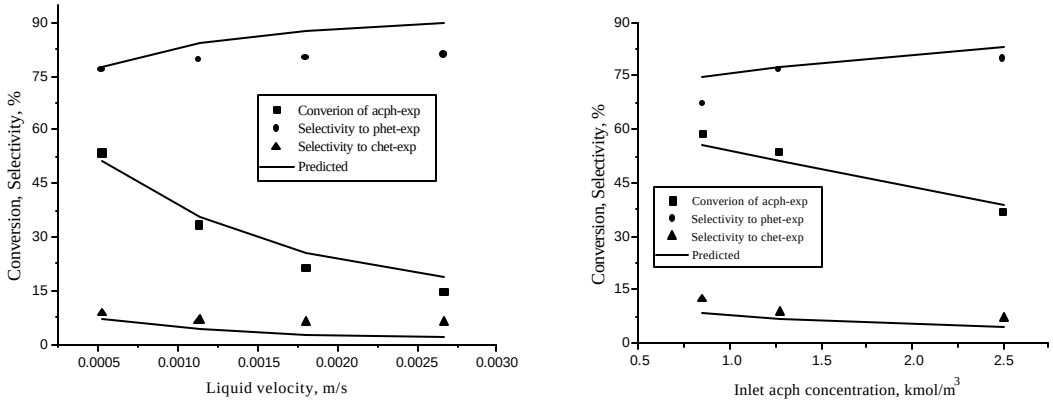

Figures 4.17, 4.18: Effect of Liquid Velocity and ACPH Concentration on Conversion of ACPH and Selectivity to PHET and CHET

Figure 4.17: Reaction conditions: Temperature: 398 K, Reactor Pressure: 52 atm, Inlet ACPH Concentration: 1.27 kmol/m^3, Gas Flow Rate: 30 Nl/hr

Figure 4.18: Reaction conditions: Temperature: 398 K, Reactor Pressure: 52 atm, Ų = 5.4 $x10^{-4}$ m/s, Gas Flow Rate: 30 Nl/hr

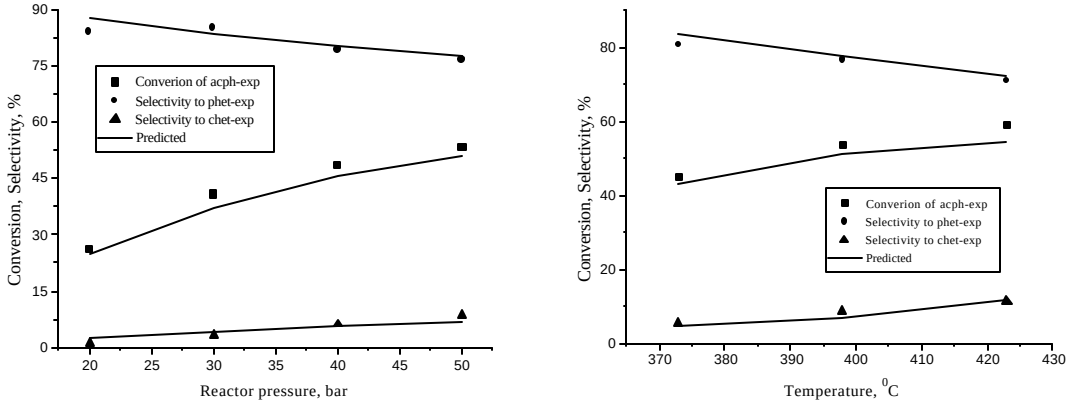

Figures 4.19, 4.20: Effect of Pressure and Temperature on Conversion of ACPH and Selectivity to PHET and CHET

Figure 4.19: Reaction conditions: Temperature: 398 K, U_l = 5.4 x10^{-4} m/s, Inlet ACPH Concentration: 1.27 kmol/m^3, Gas Flow Rate: 30 Nl/hr

Figure 4.20: Reaction conditions: Reactor Pressure: 52 atm, Inlet ACPH Concentration: 1.27 kmol/m^3, U_l = 5.4 x10^{-4} m/s, Gas Flow Rate: 30 Nl/hr

On comparison of these results with TBR performance, it was found that under similar reaction conditions, even though conversion of acetophenone was less in up-flow reactor, the selectivity towards PHET was higher and selectivity to CHET was lower in the up-flow reactor (~70 and 76% selectivity to PHET in TBR and up-flow respectively at 398 K, 52 atm reactor pressure and liquid velocity, 5.4 x10^{-4}m/s and the corresponding selectivity to CHET under similar conditions in the up-flow and down-flow mode were 13 and 16% respectively). This is expected, as the rate of hydrogenation is high in the case of TBR reactor due to external catalyst partial wetting.

4.3.5 Comparison of Down-flow and Up-flow Performance

For comparing the performance of up-flow and down-flow mode of operations, data at one temperature (398 K) was considered. On increasing the liquid velocity from 5.4 x10^{-4}m/s to 2.36 x10^{-3}m/s, it was found that the rate of hydrogenation increased marginally (from 2.4 x10^{-3} to 2.8 x10^{-3}kmol/m^3/sec) for the up-flow mode whereas for down-flow it decreased marginally (3.1 x10^{-3} to 2.7 x10^{-3}m/s) (Figure 4.21). In the up-flow mode, catalyst particles are completely covered by liquid, whereas in the trickle bed, a significant partial wetting exists in the range of U_l studied. The higher rate for the

trickle bed at low liquid velocity (5.4 $x10^{-4}$m/s) is due to the direct mass transfer of gas phase reactant to the partially wetted catalyst surface eliminating gas-liquid and liquid-solid mass transfer resistances. Since the rate of gas-particle mass transfer is high, a higher rate is expected in TBR at low liquid velocities. At higher liquid velocities, the rates in both up-flow and down-flow mode of operations become almost similar. At higher liquid velocities the gas-liquid and liquid-solid mass transfer in up-flow reactor is more efficient than in down-flow reactor and hence the contribution by this increased gas-liquid mass transfer in up-flow mode can make up for the increased rate in trickle bed due to partial wetting.

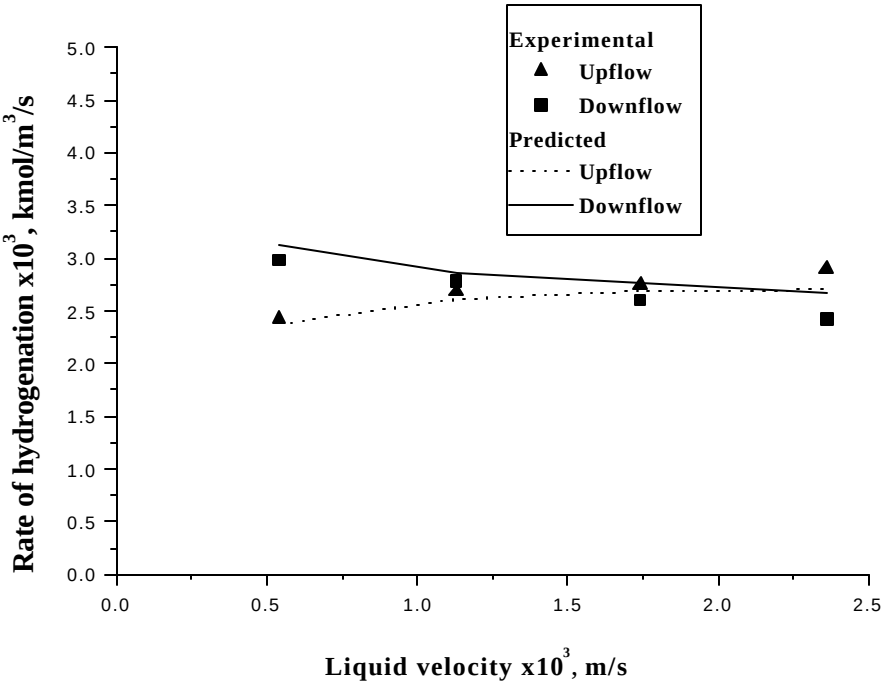

Figure 4.21: Effect of Liquid Velocity on Up-flow and TBR Performance

Reaction conditions; Reactor Pressure: 52 atm, Wall Temperature: 398 K, Gas Flow Rate: 30 Nl/h, Inlet ACPH Concentration: 1.27kmol/m^3

The effect of pressure and inlet substrate concentration on rate of hydrogenation in up-flow and down-flow operations is shown in Figures 4.22 and 4.23. For these studies, the liquid velocity used was in the lower range (5.4 $x10^{-4}$ m/s) and hence TBR

outperformed the up-flow reactor due to higher contribution by direct gas-solid mass transfer for partially wetted catalysts.

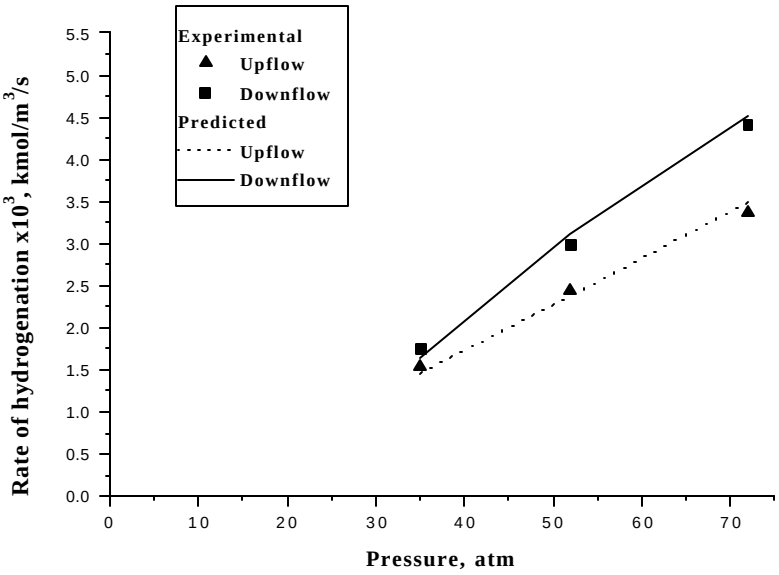

Figure 4.22: Effect of Inlet ACPH Concentration on Up-flow and TBR Performance

Reaction conditions: Uₗ: 5.4 x10^{-4} m/s, Inlet ACPH Concentration: 1.27kmol/m^3, Wall Temperature: 398 K, Gas Flow Rate: 30 Nl/h

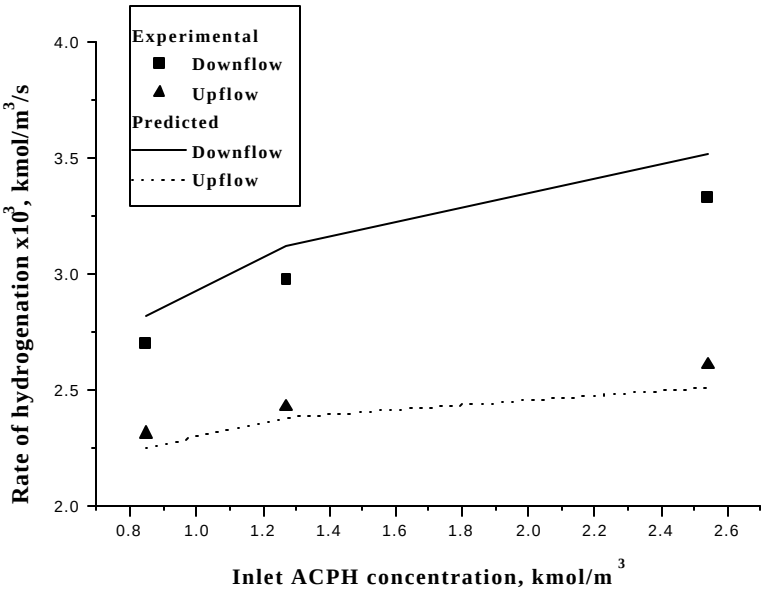

Figure 4.23: Effect of Pressure on Up-flow and TBR Performance

Reaction conditions: Uₗ : 5.4 x10^{-4} m/s, Gas Flow Rate: 30 Nl/h, Wall Temperature: 398 K, Reactor Pressure: 52 atm

The higher rate in TBR was also due to the higher temperature rise observed in TBR compared to the up-flow reactor under similar reaction conditions. For example, the temperature rise across the catalyst bed in a TBR for the reaction conditions: wall temperature; 398 K, inlet ACPH concentration; 1.27 kmol/m^3, pressure; 52 atm and liquid velocity; 5.4 x10^{-4}m/s was ~15 K whereas the corresponding temperature rise in an up-flow reactor under identical condition was ~7 K. The low temperature rise in an up-flow reactor can be attributed to the better heat dissipation due to higher liquid holdup.

In order to compare the effect of gas velocity on the reactor performance of both up-flow and down-flow mode of operation, the change in rate of hydrogenation on increasing the gas velocity from 35.4 x10^{-3} to 71.53 x10^{-2} m/s (calculated based on reactor inlet conditions) was considered and is shown in Figure 4.24. It can be seen that the rates are higher in a trickle bed reactor, than in an up-flow reactor under identical reaction conditions. In TBR, as the gas velocity was increased, more solvent got vaporized and the liquid velocity came down leading to more catalyst getting exposed to the gas phase and hence enhanced rate.

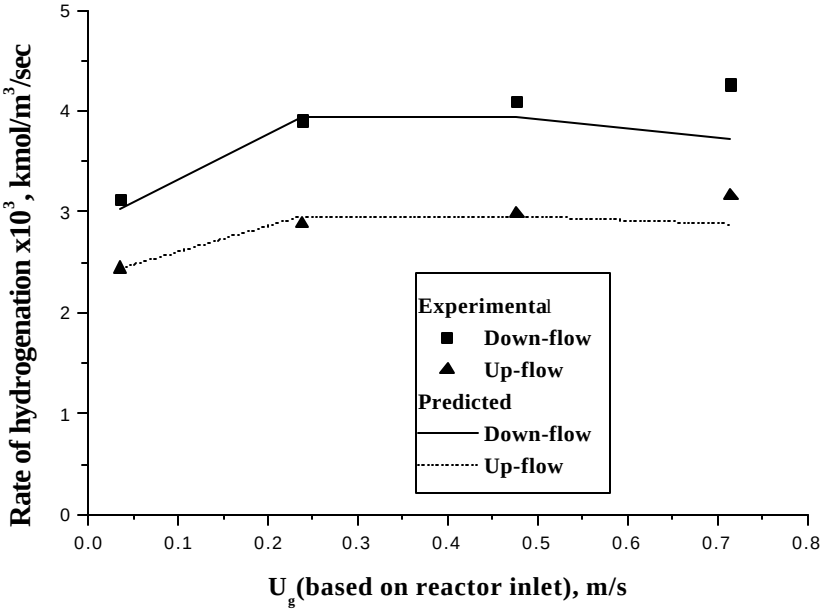

Figure 4.24: Effect of Gas Velocity on Rate of Hydrogenation in Up-flow and Down-Flow Mode of Operations

Reaction Conditions: U_l (inlet of the reactor): 5.4 x10^{-4} m/s, Inlet ACPH Concentration: 1.27 kmol/m^3, Wall Temperature: 398 K, Reactor Pressure: 52 atm

As shown in the earlier sections, temperature rise observed in an up-flow reactor was considerably lower than the corresponding temperature rise in a TBR. The higher temperature rise observed in a TBR can be due to the inefficient heat transfer across the reactor wall due to liquid flow maldistribution. In an up-flow reactor due to the higher liquid holdup, the heat transfer properties are more efficient and results in a better dissipation of heat than in a TBR (the bed to wall heat transfer coefficient in a TBR for reaction conditions: wall temperature; 398 K, inlet ACPH concentration; 1.27 kmol/m^3, pressure; 52 atm and liquid velocity; 5.4 x10^{-4} m/s was 0.07 kJ/m^2/K/sec and the corresponding value for the up-flow reactor under identical reaction conditions was 0.12 kJ/m^2/K/sec). It can be concluded that in reactions were temperature plays a major role in the selectivity distribution of the desired products and also in cases where there is a chance of catalyst deactivation due to temperature rise, an up-flow reactor can be preferred over a TBR due to its efficient heat removal properties.

4.3.6 Dynamic Behavior of Up-flow Reactor

In order to understand the dynamic behavior of the reactor in the startup period, concentration and temperature profiles with time, before reaching steady state, was investigated. Since the reactor was having provision for sampling only at the exit, samples were taken at the exit every 2 minutes till reaching steady state and analyzed. In order to explain the observed concentration and temperature profiles, a dynamic non-isothermal three-phase heterogeneous model taking into consideration the axial mixing of the liquid phase was developed. In an up flow reactor, since the catalysts are completely wetted, for a more accurate prediction of the dynamic behavior of the reactor, an apparent kinetics was made use of. The apparent kinetics of the reaction under conditions of complete catalyst wetting was studied in a basket type of reactor in absence of external mass transfer resistances (gas-liquid and liquid-solid mass transfer resistances). The apparent kinetics trends observed were similar to that observed for the intrinsic kinetic studies and hence the same model was used. The optimized rate constants represent the product of intrinsic kinetic rate constants and the catalyst effectiveness factor; η_c. The values of the rate parameters were obtained by optimization at three temperatures (373 K, 398 K and 423 K) and from its temperature dependency, the activation energies for the

rate constants and heat of adsorption for the corresponding adsorption constants were determined and are given in Table 3.

Table 4.3: Rate Parameters and it's Temperature Dependency

Rate constants at 398K	Activation energy, kJ/mol	Adsorption constants at 398 K	Heat of adsorption, kJ/mol
$k'_1 = 4.67 \times 10^{-6}$	24.9	$K_{BX} = 12.27$	-2.9
$k'_2 = 1.62 \times 10^{-5}$	19.10	$K'_{BY} = 4.24$	-1.5
$k'_3 = 11.83 \times 10^{-5}$	24.16	$K_{DX} = 1.49$	-3.6
$k'_4 = 1.59 \times 10^{-5}$	27.03	$K'_{DY} = 0.86$	-2.8

4.3.6.1 Reactor Model

4.3.6.1.1 Model Assumptions

1. Solvent vaporization effects were assumed to be negligible
2. The concentration variation of hydrogen in the gas phase along the length of catalyst bed was negligible [2]
3. At the catalyst bed inlet, the substrate solution was assumed to be saturated with hydrogen.
4. The radial gradients for concentration as well as temperature were assumed to be negligible.
5. The solid-liquid mass transfer resistance of liquid phase reactants and products were neglected
6. The heat transfer resistance between the gas, liquid and catalyst phases was assumed to be negligible and was assumed to exist at the same temperature.
7. The specific heat capacity of liquid phase components was assumed to be constant through out the length of the catalyst bed.

4.3.6.1.2 Mass Balance

Hydrogen in liquid phase

$$\varepsilon_l \frac{\partial C_{H,l}}{\partial t} = \varepsilon_l D_{el} \frac{\partial^2 C_{H,l}}{\partial x^2} - U_l \frac{\partial C_{H,l}}{\partial x} + k_L a_B (C_H^* - C_{H,l}) - k_s a_p (C_{H,l} - C_{H,s}) \qquad (4.5)$$

and $k_s a_p (C_{H,l} - C_{H,s}) = w R_H$ (4.6)

For liquid phase components

$$\varepsilon_l \frac{\partial C_{I,l}}{\partial t} = \varepsilon_l D_{el} \frac{\partial^2 C_{I,l}}{\partial x^2} - U_l \frac{\partial C_{I,l}}{\partial x} + w R_i \quad (4.7)$$

The mass balance in the dimensionless form for hydrogen can be written as

$$\frac{\partial C_{h,l}}{\partial t} = \frac{U_l}{\varepsilon_l L}\left[\frac{\varepsilon_l}{Pe_l}\frac{\partial^2 C_{h,l}}{\partial z^2} - \frac{\partial C_{h,l}}{\partial z} + \frac{k_L a_B L}{U_l}(1 - C_{h,l}) - \frac{k_s a_p L}{U_l}(C_{h,l} - C_{h,s})\right] \quad (4.8)$$

Where $z = \frac{x}{L}$ and $C_{h,l} = \frac{C_{h,l}}{C_H^*}$

For liquid phase components

$$\frac{\partial C_{i,l}}{\partial t} = \frac{U_l}{\varepsilon_l L}\left[\frac{\varepsilon_l}{Pe_l}\frac{\partial^2 C_{i,l}}{\partial z^2} - \frac{\partial C_{h,l}}{\partial z} + \frac{L w R_i'}{U_l}\right] \quad (4.9)$$

Where $C_{i,l} = \frac{C_{I,l}}{B_{l,i}}$ and R_i' is the dimensionless rate of formation of component i.

Boundary conditions

For both hydrogen and liquid phase components

At z=0, $\left(\frac{\partial C_i}{\partial z}\right) = \varepsilon_l P_{el} (C_{i,l} - C_{i,inlet})$ (4.10)

At z=1, $\left(\frac{\partial C_i}{\partial z}\right) = 0$ (4.11)

4.3.6.1.3 Heat Balance

For liquid phase

$$\varepsilon_l \rho_l C_{P,l} \frac{\partial T_l}{\partial x} = \lambda_l \frac{\partial^2 T_l}{\partial x^2} - U_l \rho_l C_{P,l} \frac{\partial T_l}{\partial x} - \sum \Delta H_i R_i - \frac{hA}{V_R}(T_l - T_W) \quad (4.12)$$

This can be written in the dimensionless form as,

$$\frac{\partial \Theta_l}{\partial t} = \frac{U_L}{\varepsilon_l L}\left[\frac{\lambda_l}{U_l \rho_l C_{P,l} L}\frac{\partial^2 \Theta_l}{\partial z^2} - \frac{\partial \Theta_l}{\partial z} - \frac{L}{U_l \rho_l C_{P,l} T_I}\sum \Delta H_i R_i' - \frac{U_w A L}{U_l \rho_l C_{P,l} V_R}(\Theta_l - 1)\right] \quad (4.13)$$

Boundary conditions

At z =0, $\frac{\partial \Theta_l}{\partial z} = \frac{U_l \rho_l C_{Pl} L}{\lambda_L}(1 - \Theta_l)$ (4.14)

At z=1, $\frac{\partial \Theta_l}{\partial z} = 0$ (4.15)

The set of partial differential equations were converted to ordinary differential equations by discretization of spatial derivatives using finite difference and solved using LSODE.[18]
The correlations used for determining various reaction parameters are same as in Table 2.

The un-steady state performance of the reactor for the present system was studied for few experiments. The distribution of ACPH, PHET and temperature along the length of the bed under transient conditions is shown in the Figures 4.25 to 4.27. It was found that the steady state was reached in 7-8 minutes. At the initial condition, it was assumed that the reactor was saturated with the substrate before the starting of the reaction. Since the concentration as well as temperature gradients were not steep at any point inside the reactor the number of grid points N = 10 was found to explain the observed concentration as well as temperature profile. The variation of concentration of various liquid phase components at the outlet with varying reaction time is shown in the Figure 4.28 and was found to agree well with the model predictions.

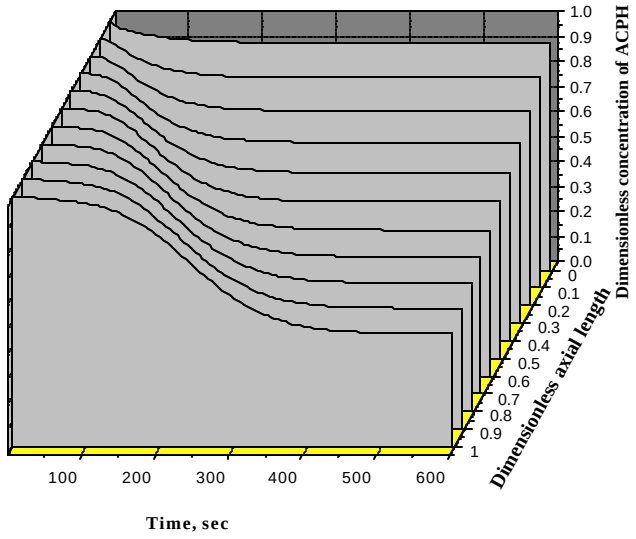

Figure 4.25: Distribution of ACPH Along the Length of the Bed Under Initial Transient Conditions

Reaction conditions, Ų: 5.4 x10^{-4} m/s, Reactor Pressure: 52 atm, Temp: 398 K, Gas How Rate: 30 Nl/h

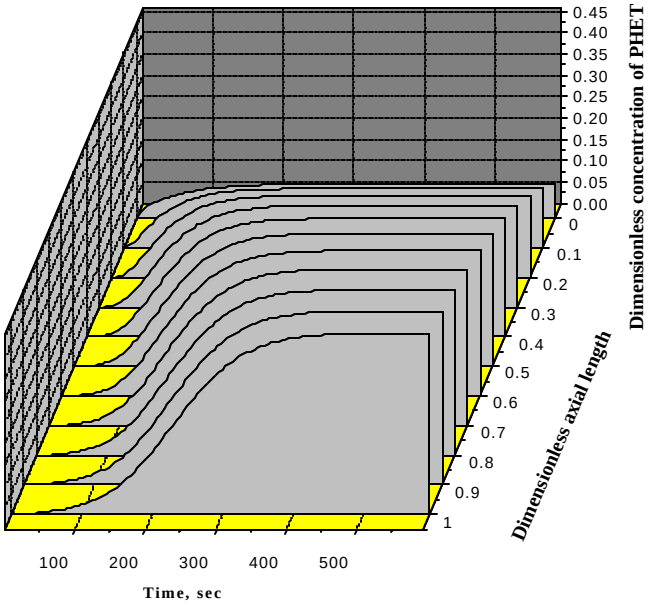

Figure 4.26: Distribution of PHET Along the Length of the Bed in Initial Period

Reaction conditions, Ų: 5.4 x10^{-4} m/s, Reactor Pressure: 52 atm, Temp: 398 K, Gas How Rate: 30 Nl/h

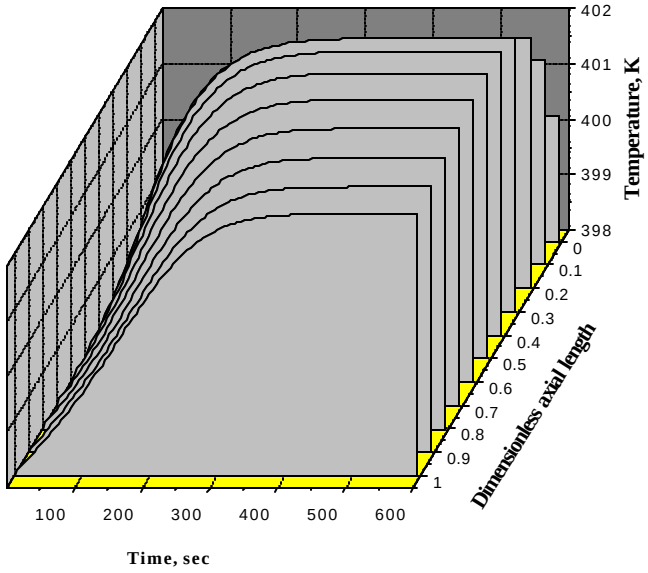

Figure 4.27: Distribution of Temperature Along the Length of the Bed Under Initial Transient Conditions

Reaction conditions, Ų: 5.4 x10^{-4} m/s, Reactor Pressure: 52 atm, Temp: 398 K, Gas How Rate: 30 Nl/h

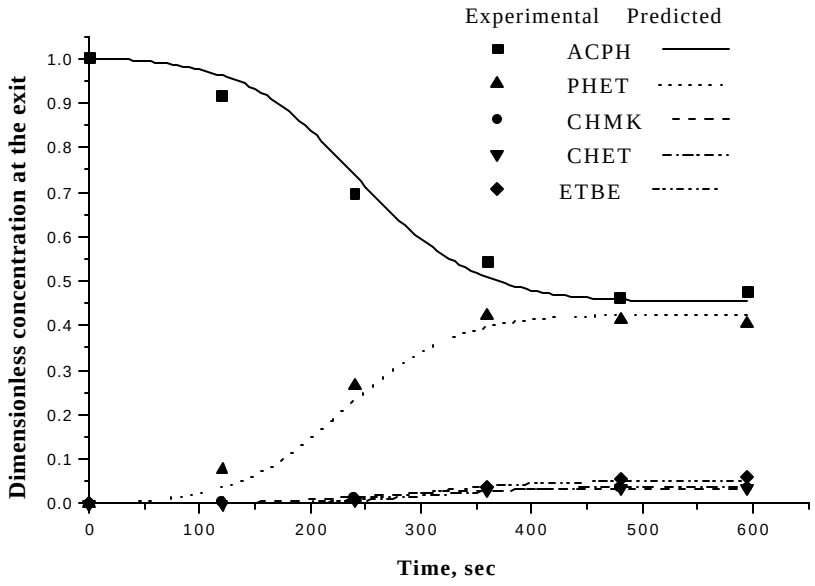

Figure 4.28: Distribution of Various Liquid Phase Components at the Exit of the Reactor

Reaction conditions, Ų: 5.4 x10^{-4} m/s, Reactor Pressure: 52 atm, Temp: 398 K, Gas How Rate: 30 Nl/h

4.4 Conclusion

Hydrogenation of acetophenone using 2%Ru/Al_2O_3 catalyst was investigated in a fixed bed reactor with cocurrent up-flow. It was observed that gas velocity, liquid velocity and inlet concentration of ACPH had only a mild influence on the reaction rates, while with respect to hydrogen partial pressure and temperature the rates increased significantly. In order to explain these results theoretical models for steady state conditions as well as dynamic analysis were developed. The model predictions agreed well for almost all the experimental data indicating that detailed theoretical models can be reliably used for predicting the reactor performance. The literature correlations were found to be satisfactory. The temperature rise observed was not very large, but within the range of model predictions. Finally the experimental data from the up-flow reactor were compared with the corresponding results in a trickle bed reactor and observed that under conditions of low liquid velocity TBR outperformed up-flow reactor, where as at higher liquid velocities the rates were almost similar in both cases.

Notations

B_{li} inlet substrate concentration, kmol/m^3

C_H^* saturation solubility of H_2, kmol/m^3

$C_{H,l}$ concentration of hydrogen in the liquid phase, kmol/ m^3

$C_{H,s}$ concentration of hydrogen on the catalyst surface, kmol/m^3

$C_{h,l}$ dimensionless concentration of hydrogen in the liquid phase, kmol/ m^3

$C_{h,s}$ dimensionless concentration of hydrogen on the catalyst surface, kmol/m^3

$C_{I,l}$ concentration of i^{th} component in liquid phase, kmol/m^3

$C_{i,l}$ dimensionless concentration of i^{th} component in liquid phase, kmol/m^3

C_{pg} specific heat capacity of gas, kJ / kg K

C_{pl} specific heat capacity of liquid, kJ / kg K

D_e effective diffusivity of hydrogen, m^2/sec

D_{el} axial dispersion coefficient of liquid phase, m^2s^{-1}

d_p catalyst particle diameter, m

H_e Henry's constant, kmol/m^3/atm

K_{BX} adsorption constants of ACPH on X type of sites, m^3/kmol

K'_{BY} adsorption constants of ACPH on Y type of sites, m^3/kmol

K_{DX} adsorption constant of PHET on X type of sites, m^3/kmol

K'_{DY} adsorption constant of PHET on Y type of sites, m^3/kmol

k_i' rate constant for corresponding reaction step in simplified reaction scheme, $(m^3/kg)(m^3/kmol/sec)$

$k_L a_B$ gas-liquid mass transfer coefficient, s^{-1}

$k_s a_p$ liquid-solid mass transfer coefficient, s^{-1}

L Catalyst bed length

Pe_L Peclet number, $\frac{L U_l}{D_{el}}$

P_{H_2} hydrogen partial pressure, atm

q_B stoichiometric coefficient, B_{li} / C_A^*

R catalyst pellet radius, m

Re'_L dimensionless liquid Reynolds number, $\frac{U_L \rho_L d_P}{\mu_L (1-\varepsilon_B)}$

Re_L liquid Reynold's number, $\frac{L d_P}{\mu_L}$

R_{H2} rate of hydrogenation, kmol/m3/sec

R_I rate of corresponding steps as shown in simplified reaction scheme

Sc_l Schmidt number, $\frac{\mu_L}{D_e \rho_l}$

T_l temperature of liquid phase, K

T_w temperature of the wall, K

U_g superficial gas velocity, m/s

U_l superficial liquid velocity, m/s

U_w bed to wall heat transfer coefficient, $kJ/m^2/K/sec$

W weight of catalyst, kg/m^3

x axial distance of the catalyst bed, m

z dimensionless axial distance

ε_B bed porosity

θ dimensionless temperature

ρ_g density of gas, kg/m^3

ΔH_i heat of reaction per mole of hydrogen for the step i in the simplified reaction scheme, kJ/mol

ρ_l density of liquid, kg/m^3

ε_l liquid holdup

ρ_p catalyst pellet density, kg/m^3

$\Delta P/Z$ pressure drop, Pa, m^{-1}

μ viscosity of liquid, Pa s

References

1. Hofmann H. P., Multi phase catalytic packed-bed reactors, Catal. Rev.-Sci. Eng., 17(1), 71-117, 1978

2. Ramachandran P. A., and Chaudhari R. V., 'Three phase catalytic reactors', Gorden breach science publishers, New York, (1983)

3. Shah Y.T., Gas-Liquid-Solid reactor design, McGraw-Hill, New York (1979)

4. Mochizuki S. and Matsui T., Selective hydrogenation and mass transfer in a fixed bed catalytic reactor with gas-liquid concurrent upflow, AIChE J., 22 (5), 904, 1976

5. Herrmann U. and Emig G., Liquid phase hydrogenation of maleic anhydride to 1-4, butanediol in a packed bubble column reactor, Ind. Eng. Chem. Res., 37, 759 1998

6. Van Gelder K. B., Damhof J. K., Krouenga P. J. and Westertrep K. R., Three phase packed bed reactor with an evaporating solvent I: Experimental: The hydrogenation of 2,4,6 - trinitrotoluene in methanol , Chem. Eng. Sci., 45, 3159, 1990

7. Van Gelder, K. B., Borman P. C., Weenink R. E. and Westertrep K. R., Three phase packed bed reactor with an evaporating solvent II: Modelling the reactor, Chem. Eng. Sci., 45, 3171, 1990

8. Wind et al. Upflow versus downflow testing of hydrotreating catalysts. Applied Catalysis. 43, 239, 1988

9. Goto S. and Mabuchi K., Oxidation of ethanol in gas-liquid cocurrent up-flow and downflow reactors, Can. J. Chem. Eng., 62, 865, 1984

10. Mills P. L., Beaudry E. G. and Dudukovic M. P., Comparison and prediction of reactor performance for packed beds with two-phase flow : downflow, upflow and countercurrent flow, I. Chem. Eng. Symp. Ser., 87, 527, 1984

11. Leung P., Zorrillla C., Recasens F. and Smith J.M., Hydration of isobutene in liquid-full and trickle bed reactors, AIChE J., 32 (11), 1839, 1986

12. Reiss L. P., Cocurrent Gas-Liquid contacting in packed columns, Ind. Eng. Chem. Proc. Des. Dev., 6, 486, 1967

13. Turpin J. L., Huntington R. L., Prediction of pressure drop for two-phase, two-component concurrent flow in packed beds, AIChE J., 13, 1196, 1967

14. Specchia V., Baldi G. and Gianetto A., Solid-Liquid mass transfer in cocurrent two-phase flow packed beds, Ind. Eng. Chem. Proc. Des. Dev., 17, 362, 1978

15. Wilke C. R. and Chang P., Correlation of diffusion co-efficients in dilute solutions, AIChE J., 1, 264, 1955

16. Stiegel G. J., and Shah Y. T., Backmixing and liquid holdup in a gas-liquid cocurrent upflow packed bubble column, Ind. Eng. Chem. Proc. Des. Dev., 16, 37, 1977

17. Sokolov V. N., Yablokova M. A. and Krylov V. N., Heat transfer to the wall in a gas-liquid reactor with stationary granular bed, J. Appl. Chem. USSR (Zh. Khim.), 56, 554, 1983

18. Hindmarsh A., ODEPACK, a systematized collection of collection of ODE solvers. In scientific Computing edited by Stepleman J.S. et al., IMACS North-Holland, Amstredam, 1983

Chapter – 5

Hydrogenation of Acetophenone Using Supported Ruthenium Catalysts: Activity-Selectivity Studies

5.0 Introduction

As seen in Chapter 1, Section 1.1, most of the works on acetophenone hydrogenation are patented and detailed investigations on various aspects that influence the reaction rates and selectivity of this industrially important reaction system are scarce. Even though many catalysts exist for the selective hydrogenation of ACPH to PHET, the literature on selective synthesis of 1-cyclohexylethanol reveals that the catalysts mainly used are rhodium-based catalysts. The potential of ruthenium as an alternative catalyst has not been exploited despite the fact that ruthenium is much cheaper than other transition metal catalysts like rhodium, palladium and platinum. In this chapter, a detailed investigation on the hydrogenation of acetophenone using supported Ru catalysts has been reported. The influence of various parameters like solvents, catalyst activation temperature, metal loading, supports and method of catalyst preparation on activity and selectivity are investigated. Also, the effect of various promoters on the activity and selectivity has been studied. Screening of various supported transition metal catalysts was also done. Conditions were optimized to get selective formation of PHET and CHET with high reaction rates. The various supported Ru catalysts were characterized using surface characterization techniques like BET surface area measurements, XRD, XPS and TEM.

5.1 Experimental

The hydrogenation experiments were carried out in semi-batch slurry reactor, the details of which along with experimental procedure and the analytical details are given in Chapter-2, Section 2 (A). 1.3.

5.1.1 Preparation of Supported Ruthenium Catalysts: Precipitation Method

Required amount of support was charged along with distilled water and the slurry was stirred for 2 hrs in a round bottom flask fitted with a half moon stirrer, condenser and an addition funnel in a water bath maintained at ~ 368 K. Required amount of ruthenium trichloride dissolved in distilled water was added drop wise. After stirring for three hours, aqueous ammonia solution was added drop wise to the stirring solution until the solution became strongly alkaline (PH = ~10) to precipitate $RuCl_3$ as ruthenium hydroxide. The

solution was then allowed to stir for 3-4 hrs. The contents were then filtered, washed using hot distilled water and dried in an oven at 393 K for 8 hrs and then activated at 573 K for 7 hrs under hydrogen flow. After activation, the catalyst was brought to room temperature, flushed with nitrogen and used for reaction.

5.1.2 Preparation of Supported Ruthenium Catalyst by Impregnation Method

Known amount of support was dispersed in a solvent used for impregnation and the suspension was stirred for 3 hrs. Required amount of ruthenium trichloride dissolved in the same solvent was added drop wise to the suspension using an addition funnel. After addition was complete, the solution was stirred for 4 hrs more and then the solvent was evaporated in a rotavapor with a high rotation speed. The catalyst precursor thus impregnated on the support was dried in an oven at 393 K for 7 hrs and then activated at 573 K for 7 hrs under hydrogen flow. After activation, the catalyst was brought to room temperature and flushed with nitrogen and used for reaction. The solvents used for impregnation were water and ethanol.

5.1.3 Preparation of Palladium Supported on Carbon Catalyst

For the preparation of 3% Pd/C, a solution of palladium (II) chloride in HCl (1 N) was obtained by warming for 2 hrs. This solution was added drop-wise to a stirred hot (353K) suspension of activated charcoal in water and stirred for 5-6 hrs until the supernatant solution became colorless. Formaldehyde was then added, followed by 30% NaOH solution sufficient to make the suspension strongly alkaline and kept under stirring for 2-3 hrs. The catalyst was then filtered, washed with distilled water (until the pH became neutral) and dried under vacuum at 333 K.

5.1.4 Preparation of Ni Supported on Carbon Catalyst

A slurry of activated carbon in water was stirred for 2 hrs in a round bottom flask fitted with half moon stirrer, condenser and an addition funnel in a water bath maintained at ~ 368 K. To this, aqueous solution of $Ni(NO_3)_2.6H_2O$ was added drop wise. After stirring for 5 hrs, 10% ammonium carbonate solution was added drop wise and the addition continued till a pH value of 10 was attained and the stirring was continued for 2

hrs. The slurry was filtered to obtain a black cake and the colorless filtrate confirmed the complete precipitation of Ni as Ni carbonate. The cake was dried overnight at 393 K and calcined in activation furnace at 673 K under N_2 flow for 10 hrs. The calcined catalyst was then reduced under H_2 flow at 773 K for 10 hrs. The catalyst was passivated under N_2 flow for 2 hrs before using for hydrogenation.

3%Rh/C used in this study was procured from Degussa, Germany.

5.1.5 X-Ray Photoelectron Spectroscopy

The X-Ray Photoelectron Spectroscopy (XPS) measurements were carried out on a VG MicroTech ESCA 3000 instrument using un-monochromatized Mg K_α radiation (photon energy = 1253.6 eV) at a pass energy of 50 eV and electron takeoff angle (angle between electron emission direction and surface plane) of 60^o. The overall resolution was ~ 1 eV for the XPS measurements. The sample was placed in a container and mounted on the sample probe. The sample was subjected to evacuation at 10^{-8} torr during data collection. C_{1S} spectra was used as a reference with a binding energy value of 284.6 eV and the spectra of different samples were corrected for surface charging.

5.1.6 X-Ray Diffraction

The XRD analysis of the catalyst samples were carried out on Philips model No. 1730 using Ni filtered Cu Kα radiation and a proportional counter detector at a scan rate of 4^0/min. The samples were placed in geometrically equal holders having the same weight and were uniformly prepared.

5.1.7 Transmission Electron Microscopy

The TEM measurements were carried out on a Jeol Model 1200EX instrument operated at an accelerating voltage of 120 kV. The catalyst powder was dispersed in isopropyl alcohol and the suspension was deposited on a copper grid.

5.2 Results and Discussion

Studies were carried out to investigate the effect of different parameters that affect the rate of hydrogenation and selectivity distribution of products in the hydrogenation of acetophenone. The activity of a particular catalyst was evaluated in terms of turn over frequency, defined as:

$$TOF = \frac{No.\ of\ moles\ of\ H_2\ consumed}{No.\ of\ moles\ of\ catalyst \times time\ in\ hours}, hr^{-1}$$

The conversion of the substrate was calculated as:

$$\%\ Conversion = \frac{Initial\ concentration\ of\ substrate - Final\ concentration\ of\ substrate}{Initial\ concentration\ of\ substrate} \times 100$$

The selectivity towards a particular product was defined as:

$$\%\ Selectivity = \frac{No.\ of\ moles\ of\ product\ formed}{No.\ of\ moles\ of\ substrate\ converted} \times 100$$

5.2.1 Catalyst Characterization

5.2.1.1 XPS Measurements

XPS spectra of the 2%Ru/Al_2O_3 catalyst activated at 373 K and 573 K and the non-activated catalysts were recorded and the peaks observed at different binding energies were used to interpret the nature of the catalysts and other species present on the catalyst surface. The various peaks observed in different ranges and the corresponding binding energy values are given in Figures 5.1 – 5.5. The binding energy (B.E) peaks present at ~74 eV correspond to Al in Al_2O_3 (Figure 5.1). For the catalysts activated at higher temperature, there was a slight shift in the maxima towards the higher B.E. This can be attributed to the loss of water of hydration present as $Al_2O_3.nH_2O$ to Al_2O_3. As shown in Figure 5.2, the binding energy values ~200 eV show the presence of residual chlorine present and the peaks correspond to Cl 2p. The increase in intensity of the chloride peaks at higher temperature can be due to the segregation of chloride ions on the

surface at higher temperatures. The residual chlorine remaining on the catalyst surface is in the unreacted form.

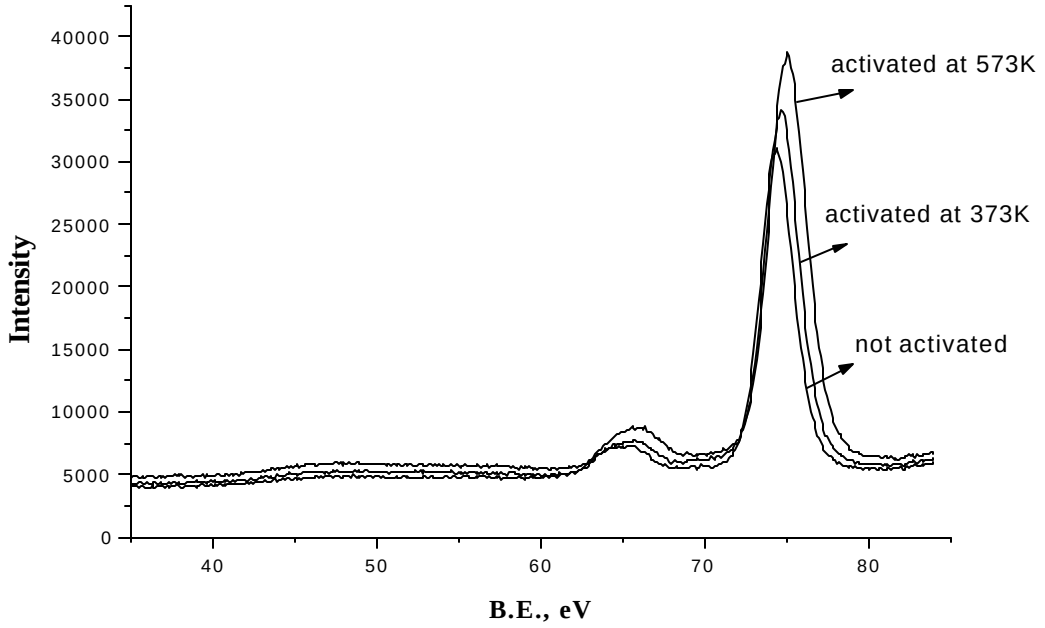

Figure 5.1: XPS Peaks Corresponding to Al in Al_2O_3

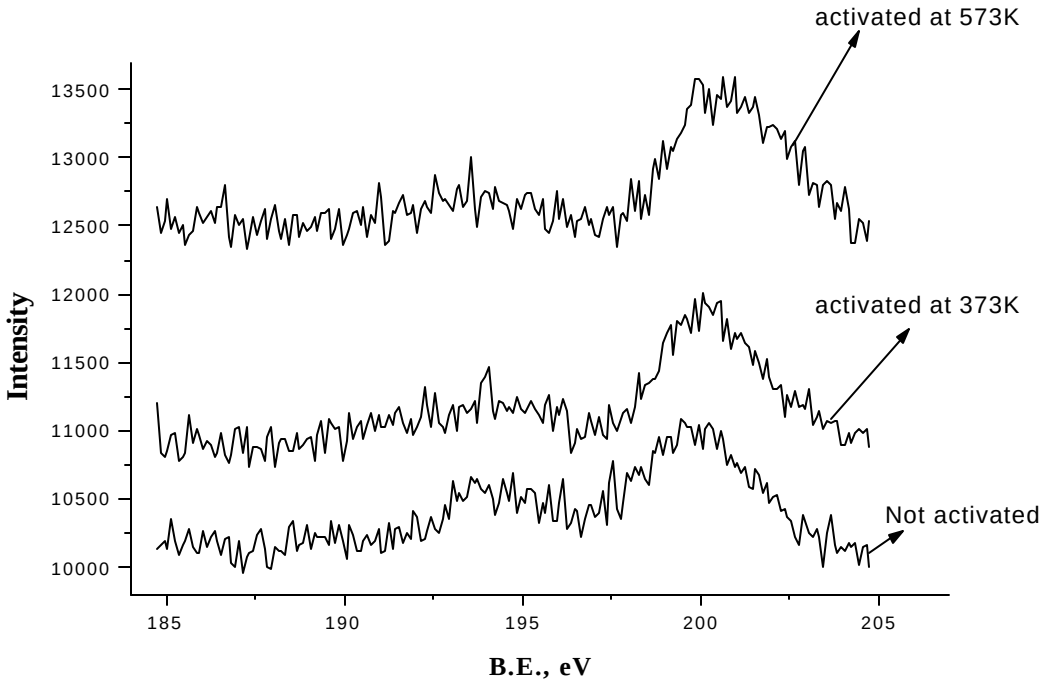

Figure 5.2: XPS Peaks Corresponding to Chlorine Present on the Catalyst Surface

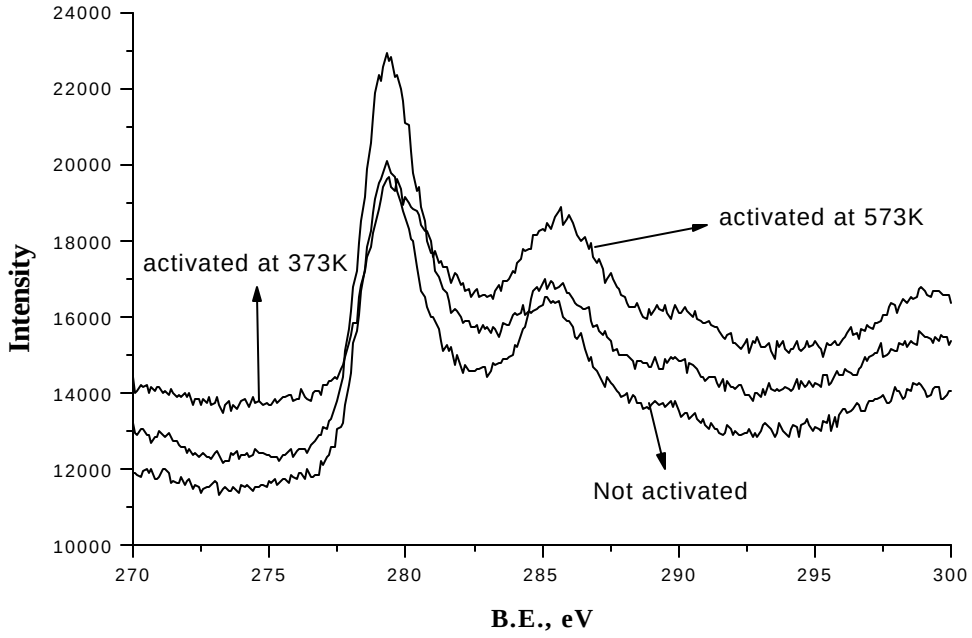

Figure 5.3: XPS Peaks Corresponding to Ru $3d_{3/2 - 5/2}$ and C 1s

The XPS peak corresponding to Ru $3d_{5/2}$ binding energy come in the region 279-282 eV (Figure 5.3) and the value of 279.2 eV can be assigned to Ru^0, 279.8 eV to Ru in RuO_2 and 281.8 eV corresponds to Ru in RuO_3.[1] It was concluded that the amount of RuO_3 was very less in all the three catalysts. The amount of RuO_2 present in the non-activated catalyst was found to be very high. For catalysts activated under hydrogen atmosphere at higher temperatures, a peak at 279.2 was observed which was more pronounced for the catalyst activated at 573 K. Tsisun et al.[2] have found that treatment of supported ruthenium catalyst at 573 K under hydrogen atmosphere will result in 70% Ru reduction. The Ru $3d_{3/2}$ component is hidden by C 1s peak from the hydrocarbon contaminant in the spectrometer. Another characteristic ruthenium peak corresponding to Ru $3p_{3/2}$ comes in the region of 462-465 eV (Figure 5.4). The binding energy values of Ru $3p_{3/2}$ was found to be 465.3, 464.6 and 463 eV corresponding to the catalyst which was non-activated, activated at 373 K and that activated at 573 K, respectively showing a change in the oxidation state. This was in accordance with trend observed by Tsisun et al.[2]

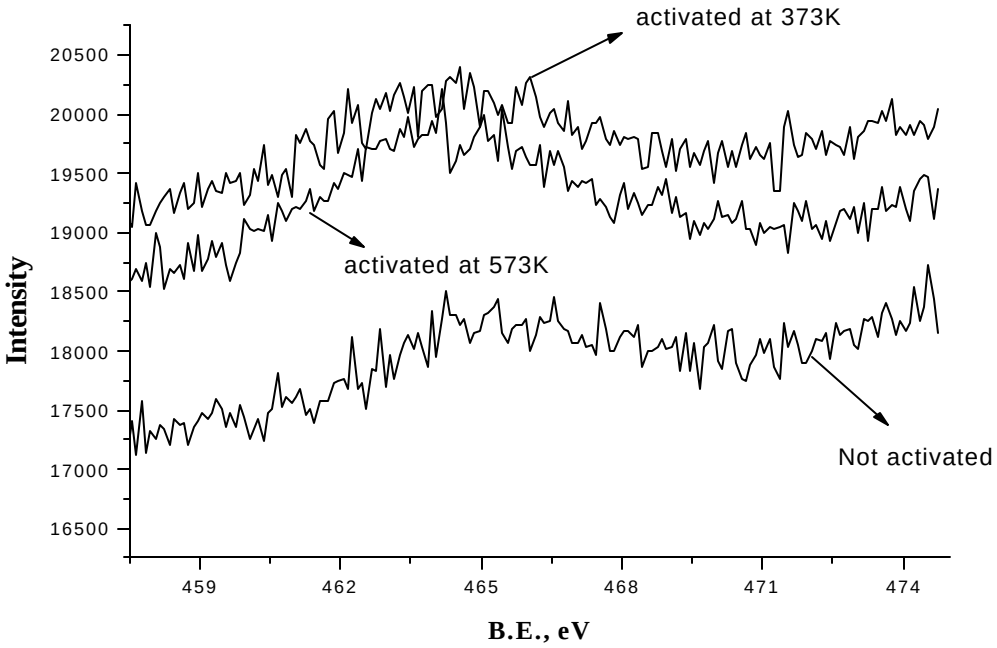

Figure 5.4: XPS Peaks for Ru $3P_{3/2}$

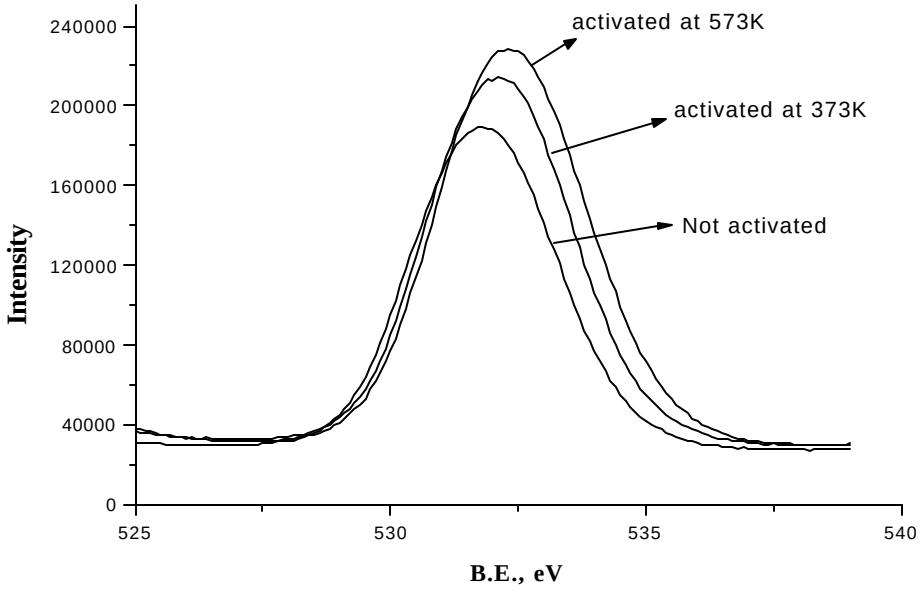

Figure 5.5: XPS Peaks for Oxygen Present in Al_2O_3

The peak observed at ~532.0 eV in the spectrum (Figure 5.5) corresponds to the oxygen present in the support, Al_2O_3, for non-activated catalyst and a slight increment in binding energies with increase in activation temperatures can be attributed to the loss of hydroxyl groups at high temperatures. In conclusion, in all the samples, Al_2O_3 remains as the same with no change in the structure. Only Ru is undergoing a change in oxidation states with increase in temperature.

The XPS spectra of catalysts prepared by impregnation technique followed by activation at 573 K under hydrogen atmosphere (Figure 5.6) showed similar XPS spectra of characteristics Ru peaks in the range of 263 –266 eV.

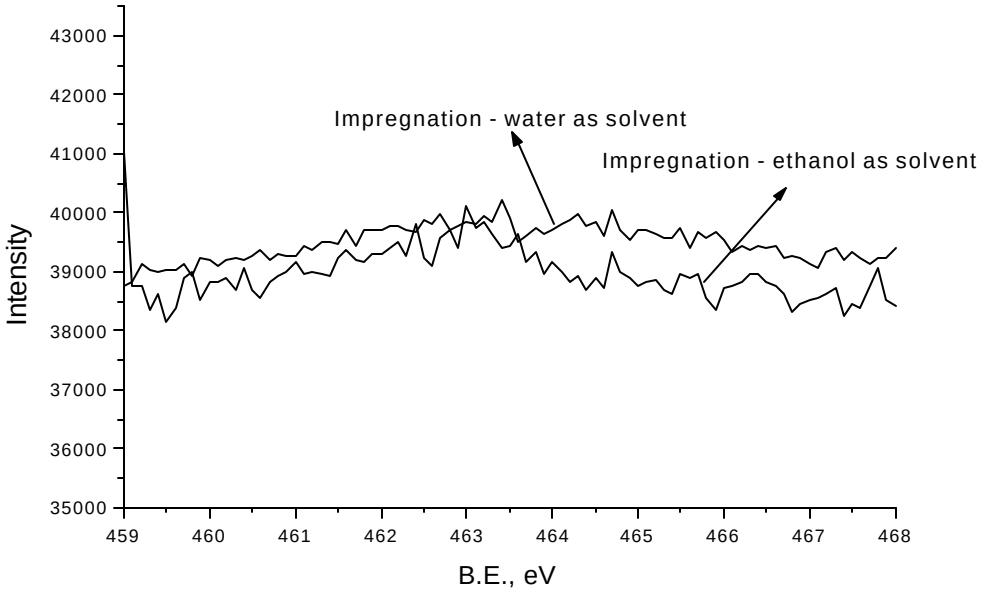

Figure 5.6: XPS of Ru Catalysts Prepared by Impregnation Method Using Ethanol and Water as the Impregnation Solvents

5.2.1.2 XRD measurements

The XRD spectra of γ-alumina, 2%Ru/Al_2O_3 and 5% Ru/Al_2O_3 are shown in Figures 5.7, 5.8 and 5.9. The spectra of γ-alumina and 2%Ru/Al_2O_3 were identical indicating that the peaks corresponding to Ru are not detected at 2% metal loading. Even at a slower scanning rate of 0.2^0/min, Ru peaks were not detected for 2% Ru loading. The spectra of 5% Ru/Al_2O_3 showed the characteristic Ru peaks indicating that the XRD patterns are detectable only at higher metal loadings.

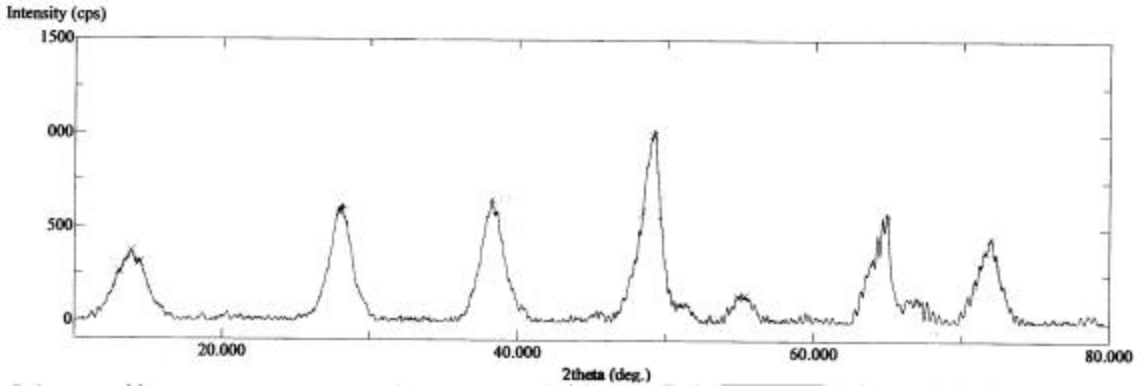

Figure 5.7: The XRD Spectra of g-alumina

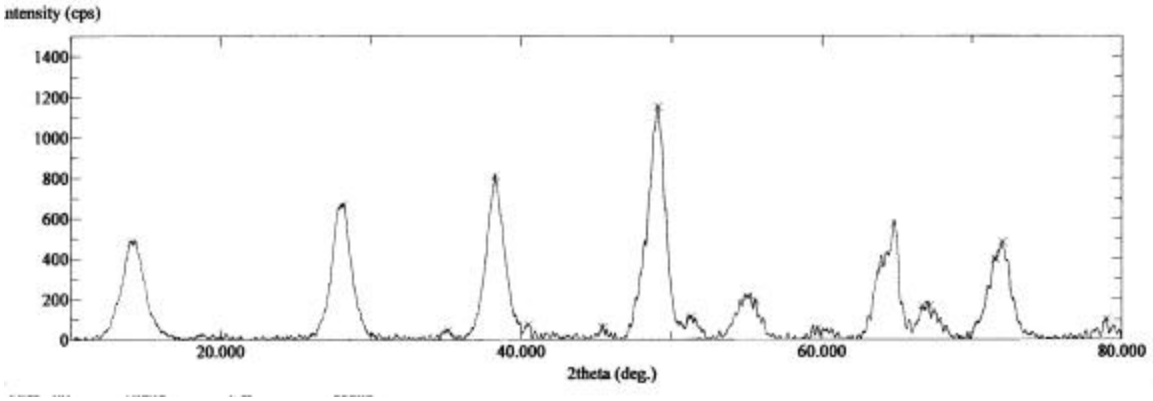

Figure 5.8: The XRD Spectra of 2%Ru/Al_2O_3

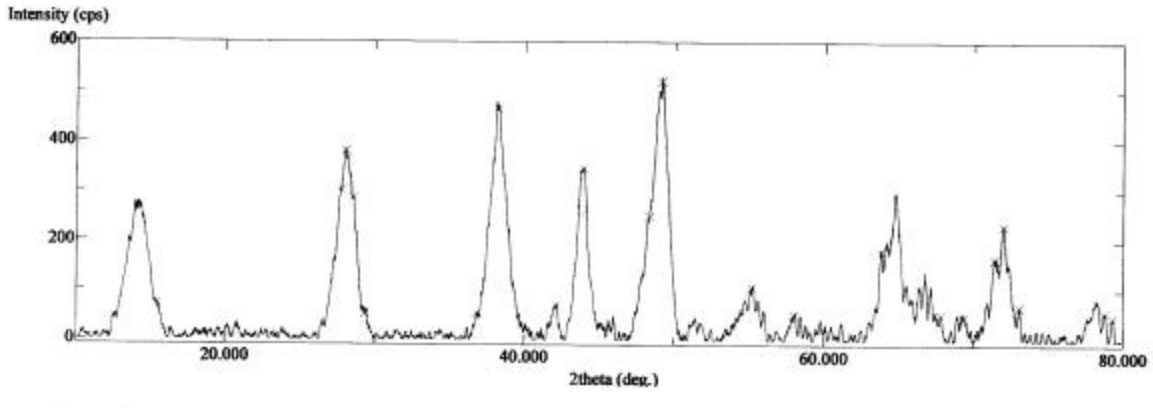

Figure 5.9: The XRD Spectra of 5%Ru/Al_2O_3

The characteristic Ru peaks were observed at 2θ values of 43.89^0 (100% Intensity) and 42.19^0 (32% intensity) corresponding to Ru 101 and 002 planes. Alumina peaks overlapped the peak at a 2θ value of 38.38^0 corresponding to Ru 101 plane. The absence of peaks corresponding to RuO_2 species confirmed that most of the Ru species existed in Ru^0 state.

5.2.1.3 Transmission Electron Micrographs

The TEM micrograph for the 2%Ru/Al_2O_3 catalyst prepared by precipitation technique is shown in Figure 5.10. Metal clusters on the support were not in uniform size and some of the agglomerates were of bigger size in the range of ~30 nm, where as smaller metal clusters of ~10-12 nm were also present. The TEM micrographs of the 2%Ru/Al_2O_3 catalyst prepared using ethanol as the impregnation solvent were more uniform in size and bigger clusters were not found. The sizes of the clusters observed varied from 9 – 16 nm as shown in Figure 5.11.

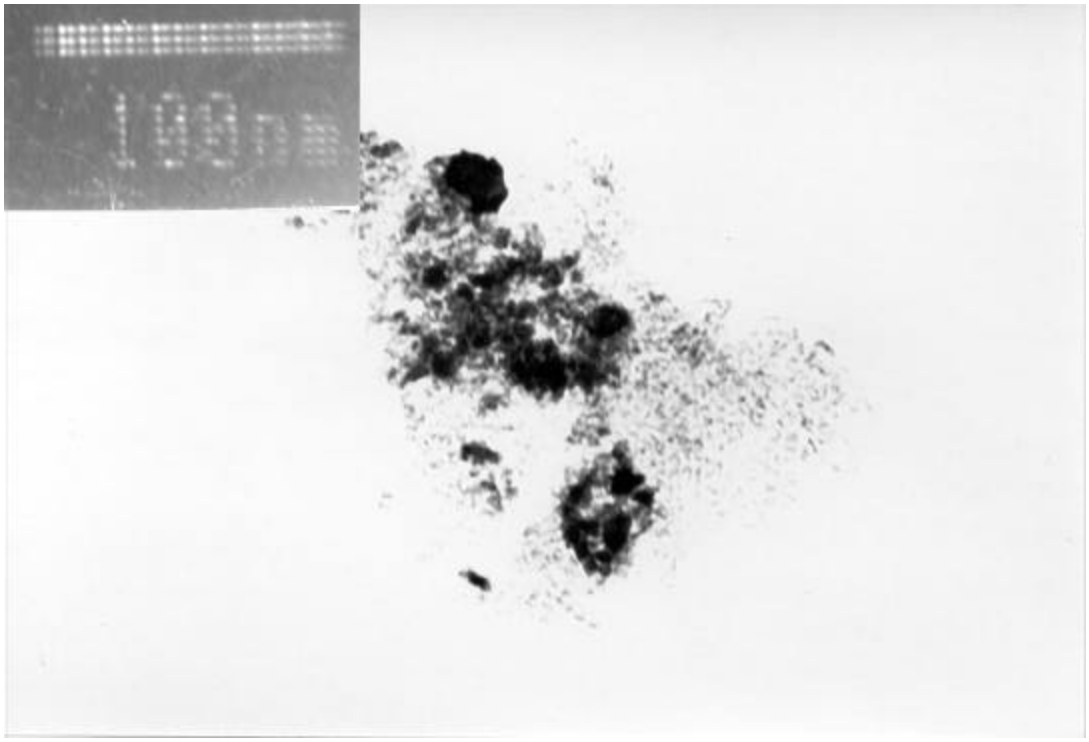

Figure 5. 10: TEM Photographs of 2%Ru/Al_2O_3 Catalyst Prepared by Precipitation Technique

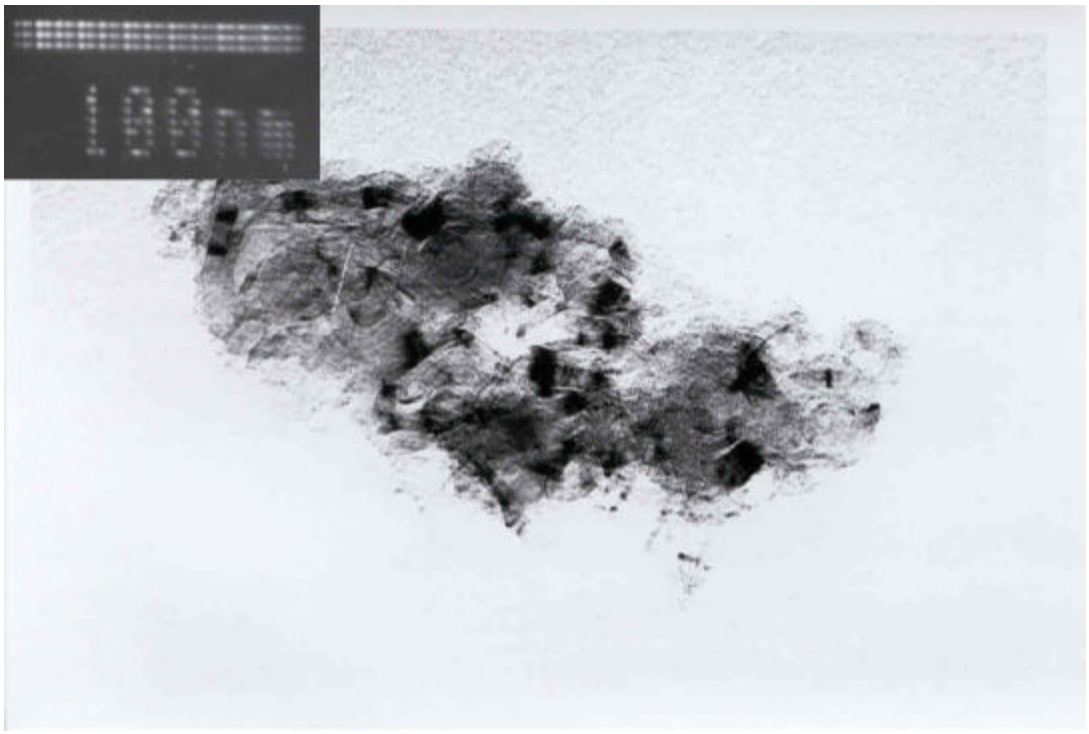

Figure 5. 11: TEM Photographs of 2%Ru/Al_2O_3 Catalyst Prepared by Impregnation Technique

5.2.2 Solvent Effects

In order to study the influence of solvents on the reaction rates and selectivity distribution, various polar alcoholic and non-polar hydrocarbon solvents were screened. In polar solvents, C_1-C_6 alcohols were screened and the reaction rates calculated in terms of TOF are given in Figure 5.12. It was observed that ethanol, isopropanol and 1-heptanol gave the highest rates of hydrogenation. The conversion and selectivity distribution when different alcohols were used as solvents is given in Table 5.1. It was observed that with methanol as the solvent the formation of CHMK was low (~15%), whereas it was one of the major products with higher alcohols (~36% with iso-propanol) as solvents. Since almost all the studies reported in earlier chapters were done with methanol as the solvent, PHET was considered as the major intermediate for the formation of CHET from ACPH and this is true as the percentage of PHET formed was very high in methanol (~58% at 40% conversion), whereas that of CHMK was low (~15%).

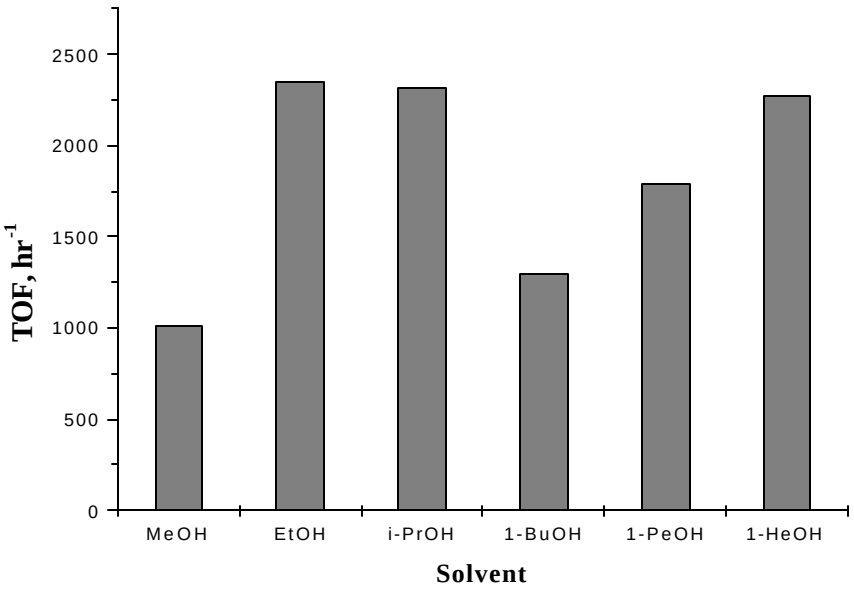

Figure 5.12: Effect of Alcoholic Solvents on TOF Based on Consumption of Hydrogen

Reaction Conditions: Catalyst: 2%Ru/Al_2O_3 (prepared by precipitation method), ACPH Concentration: 0.841 kmol/m^3, Temp: 398 K, P_{H2}: 47.6 atm, Cat. Wt.: 3 kg/m^3, Reaction Time: 2 hrs

Table 5.1: Conversion and Selectivity with Various Alcoholic Solvents

Solvent	Conversion, %	Selectivity, %			
		CHMK	PHET	CHET	ETBE
MeOH	70.65	15.30	42.97	15.14	26.58
EtOH	99.55	28.69	5.91	55.66	9.74
i-PrOH	98.31	35.83	6.46	51.99	5.72
1-BuOH	70.53	30.59	34.45	31.46	3.50
1-PeOH	85.85	33.83	16.20	38.37	11.60
1-HepOH	98.56	36.27	11.01	50.57	2.25

Reaction Conditions: Catalyst: 2%Ru/Al_2O_3 (Prepared by Precipitation Method), ACPH Concentration: 0.841 kmol/m^3, Temp: 398 K, P_{H2}: 47.6 atm, Cat. Wt.: 3 kg/m^3, Reaction Time: 2 hrs

Since the formation of CHMK was high (28-36%) when higher alcohols were used as solvents, it was concluded that the alkyl group of the solvents played an important role in determining the reaction intermediates for the formation of CHET from ACPH. The concentration-time profiles when methanol, ethanol and iso-propanol were used as solvents are given in Figures 5.13 – 5.15. With ethanol and iso-propanol as the solvents, the CHMK formation was much higher than that with methanol. In order to compare and understand the main intermediates contributing to the formation of CHET from ACPH, when different alcohols were used as solvents, the selectivity towards the formation of PHET and CHMK at 40% conversion of acetophenone was considered and plotted along with the dielectric constant corresponding to each alcohol (Figure 5.16). With methanol as the solvent, the selectivity towards CHMK was only 17% and with ethanol it was 27%. For higher alcohols it was observed that both PHET and CHMK were contributing almost equally for the formation of CHET (35-40% of both PHET and CHMK).

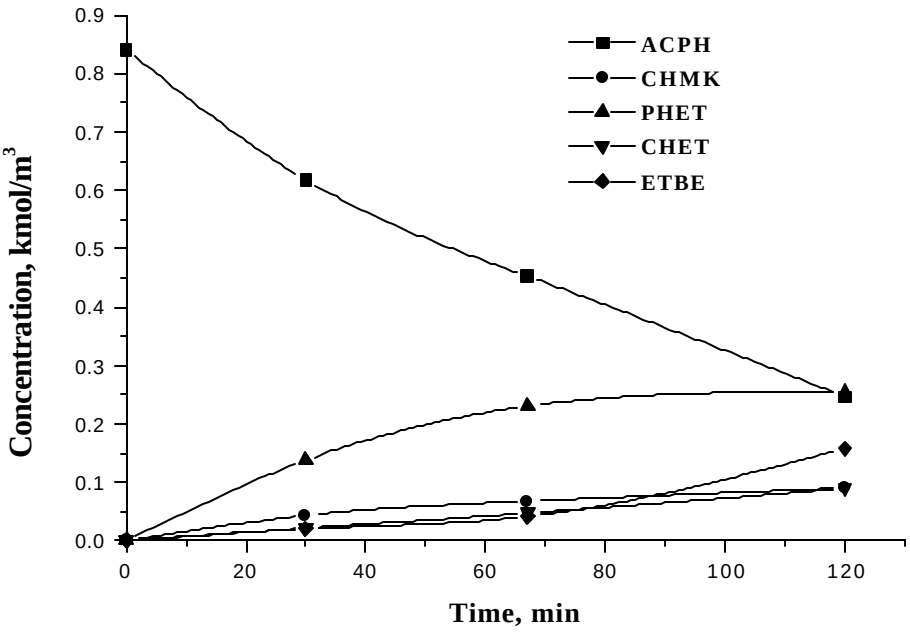

Figure 5.13: Concentration – Time Profile with Methanol as Solvent

Reaction Conditions: Catalyst: 2%Ru/Al_2O_3 (Prepared by Precipitation Method), ACPH Concentration: 0.841 kmol/m^3, Temp: 398 K, P_{H2}: 47.6 atm, Cat. Wt.: 3 kg/m^3, Reaction Time: 2 hrs

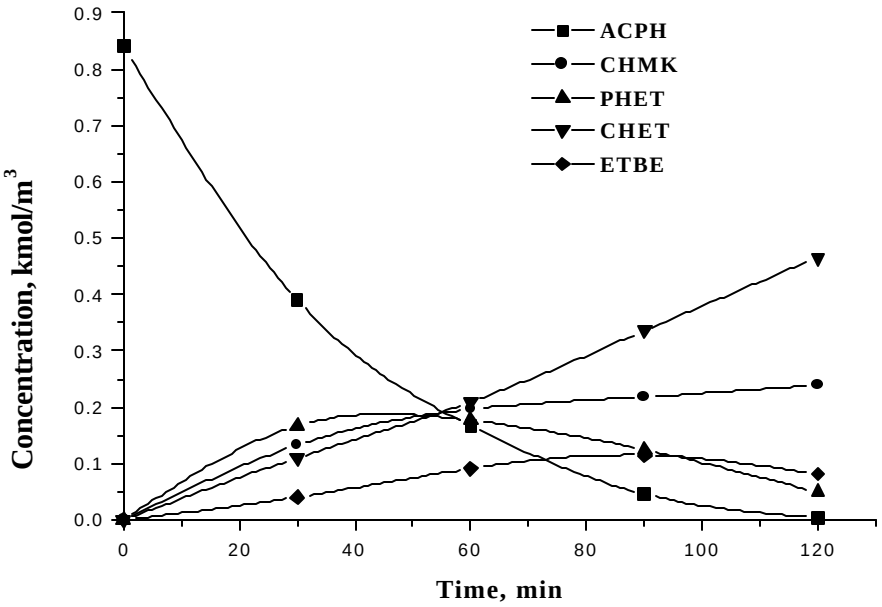

Figure 5.14: Concentration – Time Profile with Ethanol as Solvent

Reaction Conditions: Catalyst: 2%Ru/Al_2O_3 (Prepared by Precipitation Method), ACPH Concentration: 0.841 kmol/m^3, Temp: 398 K, P_{H2}: 47.6 atm, Cat. Wt.: 3 kg/m^3, Reaction Time: 2 hrs

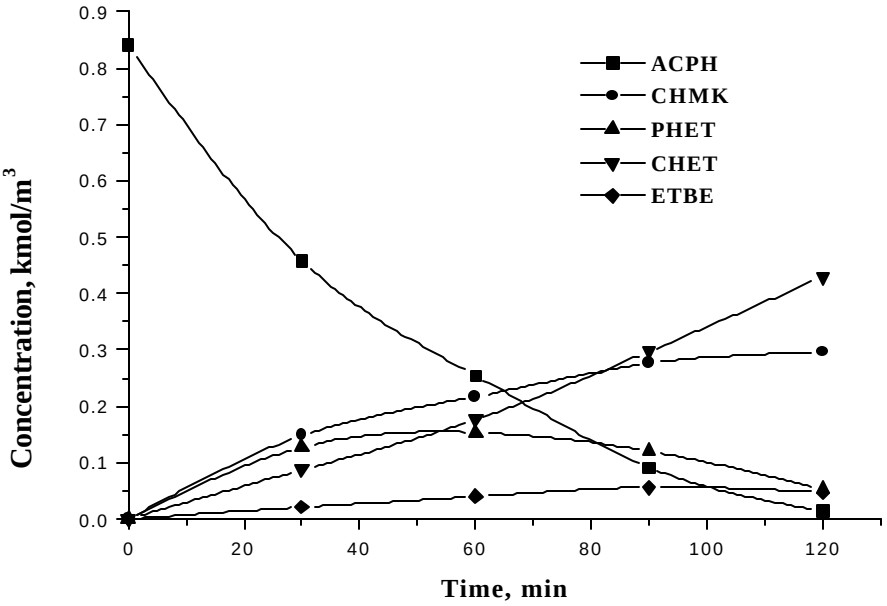

Figure 5.15: Concentration – Time Profile with i-Propanol as Solvent

Reaction Conditions: Catalyst: 2%Ru/Al_2O_3 (Prepared by Precipitation Method), ACPH Concentration: 0.841 kmol/m^3, Temp: 398 K, P_{H2}: 47.6 atm, Cat. Wt.: 3 kg/m^3, Reaction Time: 2 hrs

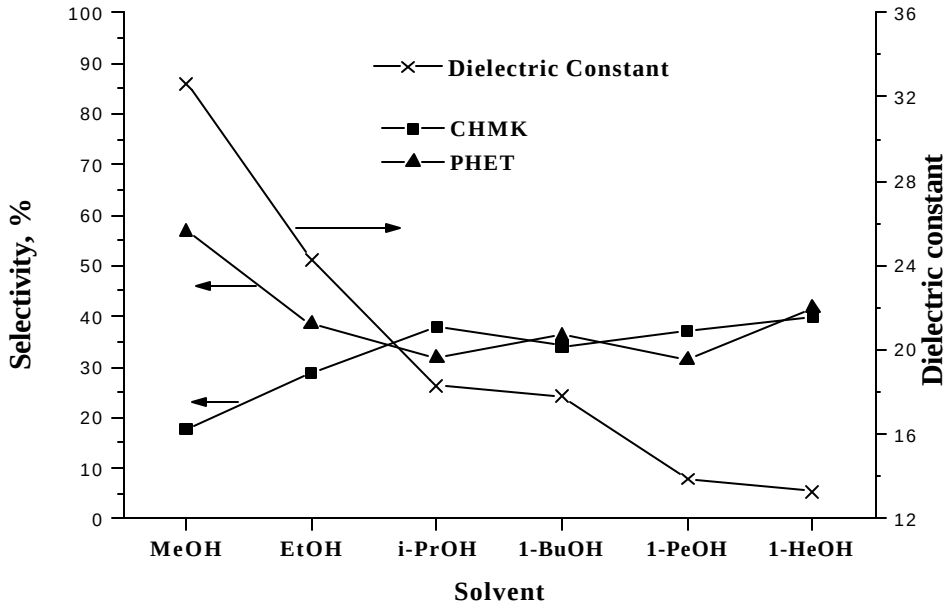

Figure 5.16: Selectivity to CHMK and PHET at 40% Conversion when Different Alcoholic Solvents were Used

Reaction Conditions: Catalyst: 2%Ru/Al_2O_3 (Prepared by Precipitation Method), ACPH Concentration: 0.841 kmol/m^3, Temp: 398 K, P_{H2}: 47.6 atm, Cat. Wt.: 3 kg/m^3

With lower alcohols, the higher selectivity to PHET can be explained on the basis of inhibition of ring hydrogenation by polar solvent molecules and has a correlation with dielectric constant of the solvent.[3] The polar solvent molecules surrounding the catalyst particles inhibit the less polar aromatic ring from getting adsorbed on the catalyst surface, whereas the adsorption of polar ketone moiety is favored. From the values of dielectric constant for alcoholic solvents given in Figure 5.16, it is seen that for higher alcohols, the dielectric constant values are low and hence higher formation of CHMK. Another important conclusion made was that the formation of the side product ethyl benzene was higher (~26% at 71% conversion) when methanol was used as the solvent (See Table 5.1). With ethanol even though the formation of ethyl benzene was considerable, while with higher alcoholic solvents its formation was comparatively low (5-10%). This is expected, as with higher alcohols, the formation of PHET is lower and hence ETBE formation was also low.

When non-polar hydrocarbons were used as the solvents, the reaction rates were higher compared to that of methanol and were in the range of rates observed with ethanol and isopropanol as solvents as shown in Figure 5.17.

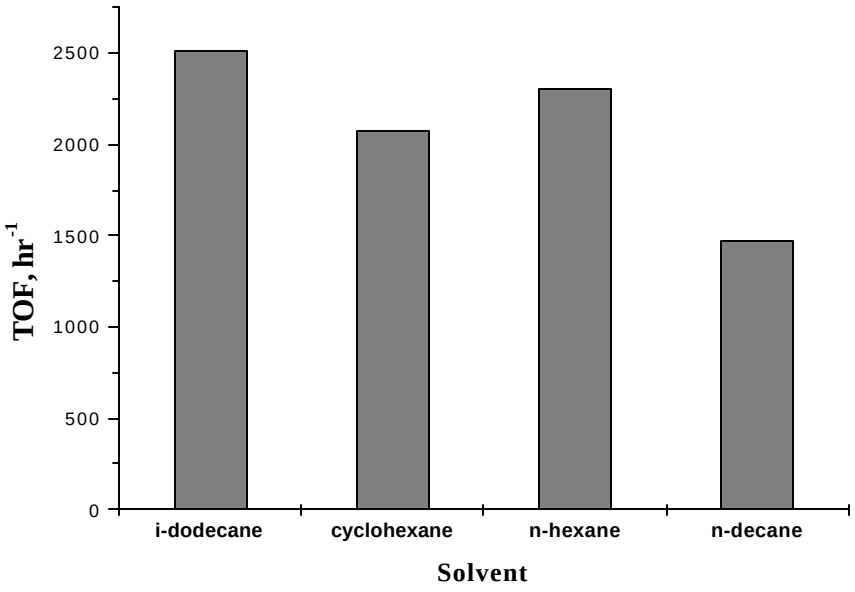

Figure 5.17: Effect of Non-Polar Solvents on Reaction Rate

Reaction Conditions: Catalyst: 2%Ru/Al_2O_3 (Prepared by Precipitation Method), ACPH Concentration: 0.841 kmol/m^3, Temp: 398 K, P_{H2}: 47.6 atm, Cat. Wt.: 3 kg/m^3, Reaction Time: 2 hrs

The rate behavior observed with hydrocarbon solvents was in accordance with hydrogen solubility in these solvents. These solvents were also found to be excellent for the selective hydrogenation of acetophenone to 1-cyclohexylethanol (Table 5.2). With these solvents, the amount of PHET formed (2-16%) during the reaction course was very low in comparison with CHMK (~60%) formation. Another noticeable feature when non-polar hydrocarbons were used as the solvents was the low formation of the side product ethyl benzene (2-4%). Since ETBE is formed from PHET by dehydration (to give styrene) followed by subsequent hydrogenation of the styrene the low formation of PHET during the reaction course lead to the low formation of ETBE. Thus, a non-polar hydrocarbon solvent can be used for the selective formation of 1-cyclohexylethanol from acetophenone with high reaction rates.

Table 5.2: Conversion and Selectivity with Various Non-Polar Solvents

Solvent	Conversion, %	Selectivity, %			
		CHMK	PHET	CHET	ETBE
i-dodecane	100	33.36	2.31	61.22	2.09
cyclohexane	90.97	57.67	5.12	34.43	2.78
n-hexane	97.66	57.35	2.03	38.28	2.33
n-decane	70.95	49.93	16.34	29.67	4.06

Reaction Conditions: ACPH Concentration: 0.841 kmol/m^3, Temp: 398 K, P_{H2}: 47.6 atm, Cat. Wt.: 3 kg/m^3, Reaction Time: 2 hrs

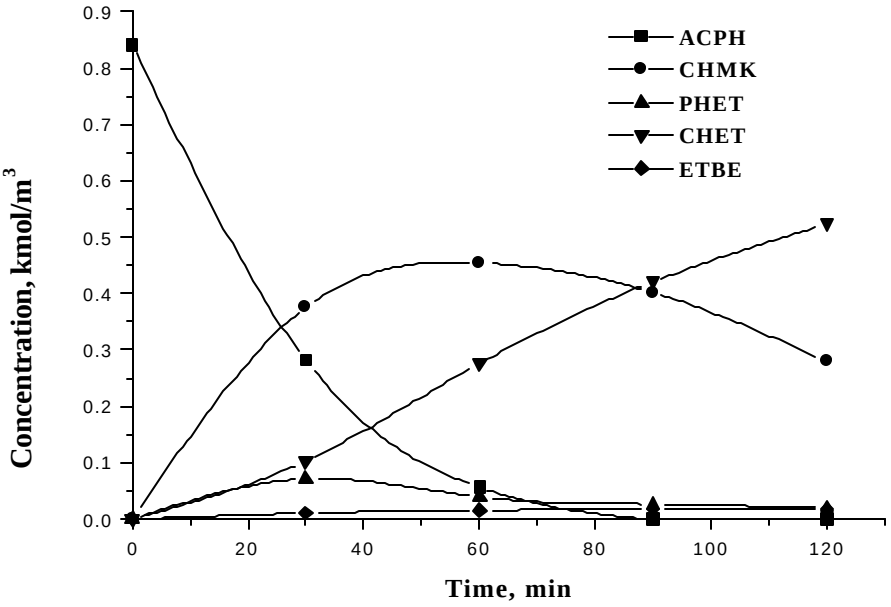

Figure 5.18: Concentration – Time Profile With i-Dodecane as Solvent

Reaction Conditions: Catalyst: 2%Ru/Al_2O_3 (Prepared by Precipitation Method), ACPH Concentration: 0.841 kmol/m^3, Temp: 398 K, P_{H2}: 47.6 atm, Cat. Wt.: 3 kg/m^3, Reaction Time: 2 hrs

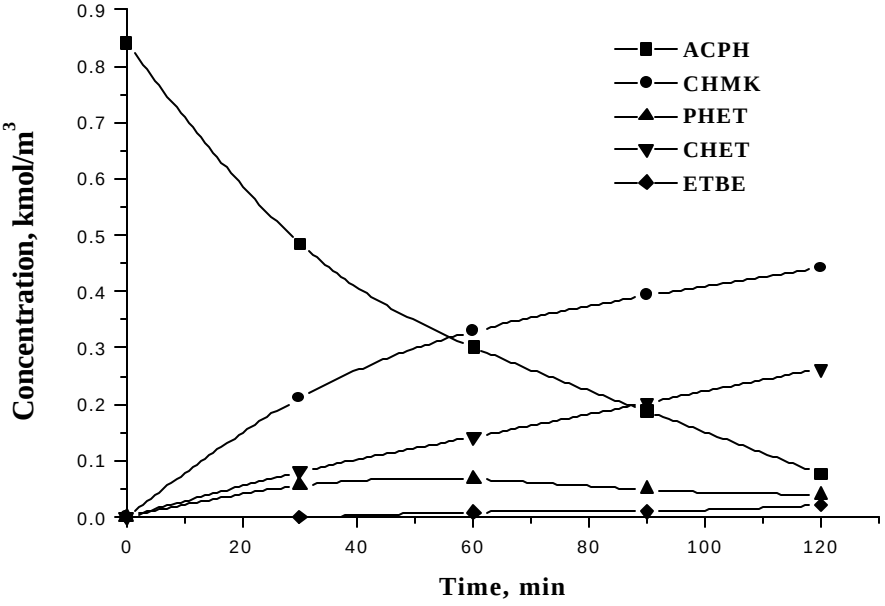

Figure 5.19: Concentration – Time Profile with Cyclohexane as Solvent

Reaction Conditions: Catalyst: 2%Ru/Al_2O_3 (Prepared by Precipitation Method), ACPH Concentration: 0.841 kmol/m^3, Temp: 398 K, P_{H2}: 47.6 atm, Cat. Wt.: 3 kg/m^3, Reaction Time: 2 hrs

In order to understand the main reaction scheme operating for the formation of CHET, with non-polar hydrocarbons as the solvent, the concentration-time profiles obtained with iso-dodecane and cyclohexane as the solvents were considered (Figures 5.18 and 5.19). With non-polar hydrocarbon solvents, the reaction pathway for CHET formation shifted entirely from PHET (when methanol was used) as the intermediate to CHMK. In order to explain the shift in the reaction scheme (the reaction scheme is shown in Chapter 2, Figure 2.3), the value of the dielectric constants of all the hydrocarbon solvents used were compared and all the values were found to be very low (~2.0) and thus as explained in the previous section, the non-polar solvents facilitate the adsorption of the less polar aromatic ring of ACPH on the catalyst surface resulting in ring hydrogenation.

In order to get a clearer picture of the shift in reaction path way when methanol, a higher alcohol and a non-polar hydrocarbon were used as the solvents, the selectivity towards the formation of two intermediates PHET and CHMK were considered at 40% conversions for reactions carried out with these solvents under identical reaction conditions (Figure 5.20).

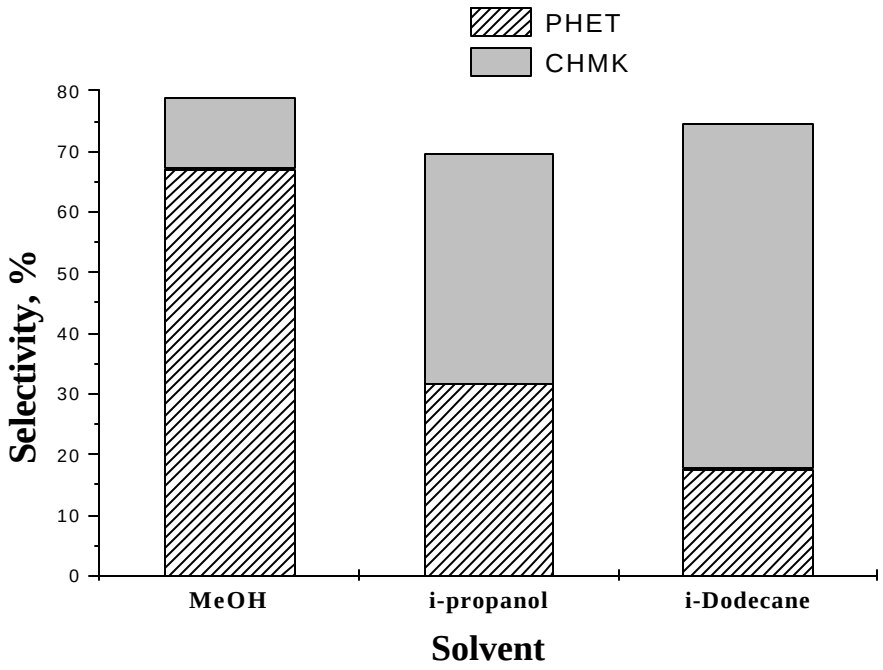

Figure 5.20: Selectivity to CHMK and PHET at 40% Conversion when Methanol, i-Propanol and i-Dodecane were Used as Solvents

Reaction Conditions: Catalyst: 2%Ru/Al_2O_3 (Prepared by Precipitation Method), ACPH Concentration: 0.841 kmol/m^3, Temp: 398 K, P_{H2}: 47.6 atm, Cat. Wt.: 3 kg/m^3

It was observed that the main intermediate for the formation of CHET shifted from PHET to CHMK by the change in solvents from methanol to i-dodecane. The dielectric constant corresponding to these three solvents were in the decreasing order of 32.63, 18.30 and 2.014, thus clearly explaining the shift in the reaction scheme from PHET to CHMK.

Since selective formation of CHET was one of our main aims, reactions were carried out with non-polar hydrocarbon solvents with higher catalyst loading and the reactions were taken to completion. It was found that CHET was formed selectively with 100% conversion of acetophenone (Table 5.3). In conclusion, for the selective formation of CHET, non-polar solvents like cyclohexane should be preferred to a polar solvent like methanol and reaction parameters should be adjusted so that higher reaction rates are obtained.

Table 5.3: Selective Hydrogenation of ACPH to CHET

Solvent	Reaction Time, min	Conversion, %	CHET, %	TOF. H_2 (hr^{-1})
n-hexane	40	100	99.55	3685
Cyclohexane	35	100	98.07	4332

Reaction Conditions: Catalyst: 2%Ru/Al_2O_3 (Prepared by Precipitation Method), ACPH concentration: 1.27 kmol/m^3, Temp: 398 K, P_{H2} : 47.6 atm, Cat. Wt. : 10 kg/m^3

5.2.3 Hydrogenation of Acetophenone in a Four Phase System

Investigations were further extended to a four-phase system for the selective synthesis of CHET from acetophenone. Water was selected as the second liquid phase as acetophenone and 1-cyclohexyl ethanol are not soluble in water. The main advantage of this particular system is that the 2%Ru/Al_2O_3 catalyst remains in the aqueous phase and the liquid reactant and products remain in the organic phase. The aqueous phase containing catalyst can be efficiently recycled and thus catalyst filtration can be avoided. Experiments were carried out in a batch slurry reactor using such a four-phase system. After the first experiment, the reaction contents were brought to room temperature, the gas was released and the aqueous and the organic layers were separated using a separation funnel. The aqueous dense layer remained as the bottom layer along with the catalyst particles. The higher affinity of the inorganic metal supported catalyst to water can be due to higher polarity of water. Thus, for recycle studies, the aqueous phase containing catalyst was recovered by phase separation and was again charged into the reactor with fresh acetophenone and the reaction was continued. It was found that even after four recycles, there was no loss in the catalyst activity (Figure 5.21). The conversion of ACPH and selectivity of various components obtained in these experiments are given in Table 5.4. It was observed, with water as a second liquid phase, selective formation of CHET was possible without compromising the reaction rates. The small amount of CHMK remaining in the reaction mixture would also have been converted to CHET, if reaction would have been continued for more time. This system can be of great advantage, if operated in a continuous stirred tank reactor, since the product formed

CHET, remains as the top layer and can be withdrawn easily, whereas, catalyst with the aqueous solution remains as the lower layer.

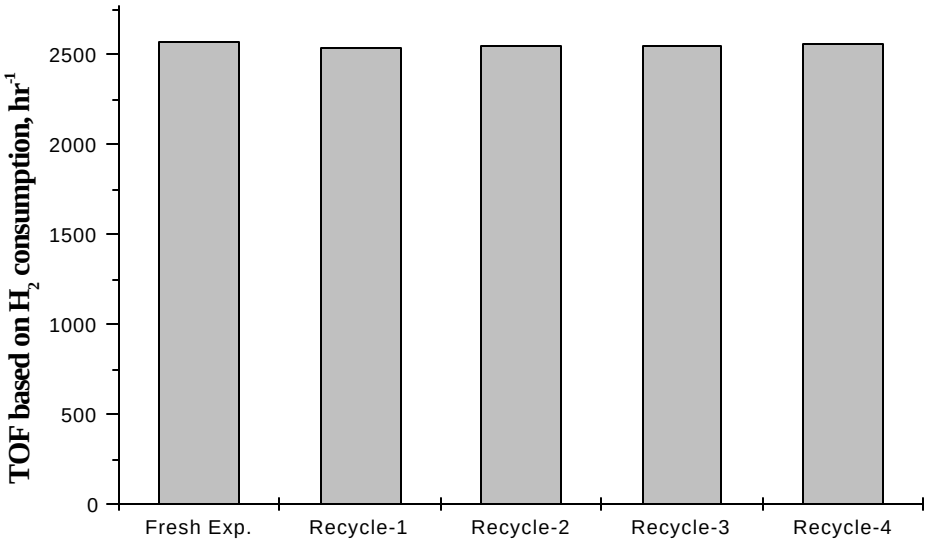

Figure 5.21: Catalyst Activity in Terms of TOF for Fresh and Recycle Experiments for the Four-Phase System

Table 5.4: Conversion and Selectivity Distribution for Fresh and Recycle Experiments

Experiment	Conversion, %	Selectivity, %			
		CHMK	PHET	CHET	ETBE
Fresh	100	0	0	100	0
Recycle 1	98.77	2.35	0	97.64	0
Recycle 2	100	3.13	0	98.77	0
Recycle 3	100	2.43	0	97.57	0
Recycle 4	100	2.12	0	97.88	0

Reaction Conditions: Catalyst: 2%Ru/Al_2O_3 (Prepared by Precipitation Method), ACPH Concentration: 1.27 kmol/m^3, Temp: 398 K, P_{H2}: 47.6 atm, Cat. Wt.: 10 kg/m^3, Reaction Time: 1 hr

5.2.4 Effect of Activation Temperature of Catalyst

In order to study the effect of the catalyst reduction temperature under hydrogen atmosphere, the catalyst (2%Ru/Al_2O_3) was reduced under hydrogen atmosphere at different temperatures ranging from 373 K to 673 K. There was not much change in the formation of the side product ethyl benzene with catalysts activated at different temperatures as shown in Table 5.5.

Table 5.5: Effect of Activation Temperature of Catalyst

Catalyst activation	Conversion, %	Selectivity, %				TOF, hr^{-1}
		CHMK	PHET	CHET	ETBE	
No activation	52.75	13.98	56.57	9.74	19.69	660
100^0C	62.41	15.19	49.33	14.93	20.55	865
200^0C	93.73	17.18	22.06	31.36	29.39	1693
300^0C	70.65	15.30	42.97	15.14	26.58	1014
400^0C	73.59	16.97	39.64	19.36	29.04	1126

Reaction Conditions: Catalyst: 2%Ru/Al_2O_3 (Prepared by Precipitation Method), ACPH Concentration: 0.841 kmol/m^3, Solvent: Methanol, Temp: 398 K, P_{H2}: 47.6 atm, Cat. Wt.: 3 kg/m^3

The XPS analysis of the samples (Section 5.2.1.1) showed that there was a change in the oxidation states of Ru when activated at higher temperatures. The binding energy values of the Ru $3P_{3/2}$ was found to be 465.32, 464.62 and 463 eV corresponding to non-activated, catalyst activated at 373 K and that activated at 573 K showing a change in the oxidation state. Since the reaction takes place even with the non-activated catalysts, it can be concluded that not only Ru^0 but also Ru existing as oxides also catalyses the reaction. The maximum rate was observed with the catalyst activated at 473 K.

5.2.5 Effect of Supports

Since support can play an important role in many hydrogenation reactions catalyzed by supported metal catalysts, ruthenium catalysts on various supports such as Al_2O_3, TiO_2, activated carbon and NaY were prepared by precipitation technique. All the catalysts were activated at 573 K for 7hrs and the results are presented in Table 5.6. It was observed that the observed rates were maximum with NaY as the support followed by activated carbon (Table 5.6). With NaY and carbon as supports, considerable amount of ethyl cyclohexane formation (5-10%) was observed due to the hydrogenation of ethyl benzene.

Table 5.6: Effect of Various Supports

Support	Conversion, %	Selectivity, %				TOF, hr^{-1}
		CHMK	PHET	CHET	ETBE	
Alumina	70.65	15.30	42.97	15.14	26.58	1014
TiO_2	49.89	11.40	47.91	15.02	25.66	683
C**	92.22	8.75	40.04	12.74	33.46	1268
NaY*	100	4.44	0	77.76	7.71	2760

Reaction Conditions: ACPH Concentration: 0.841 kmol/m^3, Solvent: Methanol, Temp: 398 K, P_{H2}: 47.6 atm, Cat. Wt.: 3 kg/m^3

** Ethyl Cyclohexane formed with a selectivity of 5.03 %

*Ethyl Cyclohexane formed with a selectivity of 10.08 %

It is well known that titania supported ruthenium catalysts show enhanced selectivity towards the carbonyl group with respect to the hydrogenation of aromatic ring, due to the metal support interaction.[4] Strong metal support interactions are usually observed with titania supported catalysts activated at high temperatures like 773 K. For the catalysts activated at lower temperatures, the metal support interaction will be less effective compared to that activated at higher temperatures. In the present case since the catalyst

was activated at a lower temperature (573 K) the effect of metal support interaction was not very predominant. The percentage of PHET formed with TiO_2, as support was not very high compared with other supports as shown in Table 5.6. Among the various supported catalysts used in the present work, the surface area of the 2%Ru/Al_2O_3 catalyst was found to be very high. The observed trends in the reaction rates can be explained on the basis of the surface area distribution of the various supported catalysts given in Table 5.7.

Table 5.7: Surface Area of Various Supported Ruthenium Catalysts

Support used	Surface area, m^2/gm
Al_2O_3	160.8
TiO_2	13.1
C	274.6
NaY	396.4

5.2.6 Effect of Metal Loading

To study the effect of metal loading on the reaction rates and selectivity, catalysts were prepared with 2, 3 and 5% ruthenium on alumina by precipitation technique, as the support. The maximum catalyst activity was observed with 2% Ru loading and beyond which, the TOF was found to decrease (Table 5.8). By increasing the metal loading it is not necessary that all the metal will be utilized for reaction. The dispersion of the metal plays a major role in determining the catalyst activity. With higher metal loading, the formation of side product ethyl benzene was found to be less as shown in Table 5.8.

Table 5.8: Rate and Selectivity Distribution for Various Metal Loadings

% of Ru	Conversion, %	Selectivity, %				TOF, hr^{-1}
		CHMK	PHET	CHET	ETBE	
2%Ru	70.65	15.30	42.97	15.14	26.58	1014
3%Ru*	99.3	17.24	2.89	53.05	8.17	800
5%Ru	97.51	23.92	43.05	23.10	9.92	635

Reaction Conditions: Catalyst Support: Al_2O_3, ACPH Concentration: 0.841 kmol/m^3, Solvent: Methanol, Temp: 398 K, P_{H2}: 47.6 atm, Cat. Wt.: 3 kg/m^3

* Ethyl Cyclohexane was observed with a selectivity of 17.13 %

5.2.7 Effect of Catalyst Preparation Method

Apart from the catalysts prepared by precipitation technique, catalysts were also prepared by impregnation method as described in the experimental section. Water and ethanol were used as the solvents for preparing catalysts by impregnation method. The aim for preparing catalysts with ethanol and with water was to check whether the impregnation solvent medium plays any role in determining the catalyst properties. The XPS pattern of both the catalysts prepared by impregnation techniques were found to be similar. Kluson et al.[5] made a similar observation for ruthenium catalyst prepared from the same solvents. The activity and selectivity behavior observed for the catalysts prepared by impregnation technique along with that of the catalysts prepared by precipitation technique are shown in Table 5.9. The higher activity observed for the catalysts prepared by the impregnation technique may be due to a better dispersion of the catalyst particles as shown in the TEM Figures 5.7 and 5.8. In case of impregnation method, the catalysts prepared using ethanol as the impregnating solvent showed higher activity compared to that with the catalysts prepared by water as the impregnating solvent.

Table 5.9: Rate and Selectivity Distribution for Catalysts Prepared by Precipitation and Impregnation Techniques

Method of Prep.	Conv., %	Selectivity, %				TOF, hr^{-1}
		CHMK	PHET	CHET	ETBE	
Precipitation	70.65	15.30	42.97	15.14	26.58	1014
Impregnation (Solvent: water)	84.19	11.14	52.29	15.33	18.23	1110
Impregnation (Solvent: ethanol)	96.10	10.10	56.54	15.14	17.61	1254

Reaction Conditions: Catalyst: 2%Ru/Al_2O_3, ACPH Concentration: 0.841 $kmol/m^3$, Solvent: Methanol, Temp: 398 K, P_{H2}: 47.6 atm, Cat. Wt.: 3 kg/m^3

The higher rates observed for the catalysts prepared with ethanol as the impregnating solvent than water as the impregnating solvent can be explained on the basis of the coordinating ability of the impregnation solvent. Ethanol has weaker complexing ability than water and accordingly the activity of the alcohol prepared ruthenium catalysts were higher due to the inclusion of the impregnating solvent in the catalyst after the activation.[5] A similar result was obtained for the hydrogenation of benzene to cyclohexene using supported ruthenium catalysts.[5] Another important point to be noted from the selectivity point of view is that the selectivity for PHET in reactions carried out with the catalysts prepared by impregnation technique was comparatively higher than that with the catalysts prepared by precipitation technique. The amount of CHET formed was less in the case of these catalysts, where as the formation of the side product ethyl benzene was almost similar in all the cases.

5.2.8 Effect of Promoters

The effect of promoters on ruthenium-catalyzed hydrogenation of acetophenone was studied to understand its effect on the selectivity distribution and rates as given in Table 5.10.

Table 5.10: Effect of Promoters

S. No.	Promoter	Conversion %	Selectivity, %				TOF, hr^{-1}
			CHMK	PHET	CHET	ETBE	
1	0.5 ml, 1 N NaOH	2.71	0	100	0	0	25
2	1.2 ml, 0.02 N NaOH	85.69	27.03	58.28	12.67	2.00	606
3	0.5 ml Et_3N	41.98	11.42	81.74	6.4	0.43	423
4	1.2 ml, 0.02 N NaOH + 0.5 ml Et_3N	66.48	12.48	79.65	7.51	0.36	696
5	1.5 ml ammonia	26.22	7.01	88.84	4.14	0.0	234
6	0.1gm $ZnCl_2$	0	0	0	0	0	0
7	30 mg $ZnCl_2$	7.98	14.69	65.97	8.87	10.46	113

Reaction Conditions: Catalyst: 2%Ru/Al_2O_3 (Prepared by Precipitation Method), ACPH Concentration: 0.841 kmol/m^3, Solvent: Methanol, Temp: 398 K, P_{H2}: 47.6 atm, Cat. Wt.: 3 kg/m^3

The addition of NaOH (1.2 ml, 0.02 N) was found to drastically reduce the formation of the side product, ethyl benzene (Table 5.10, S. No. 2). The presence of NaOH in methanol would have generated sodium methoxide making the reaction medium alkaline. The basic nature of the medium can arrest other side reactions, which involve hydrogenolysis and dehydration of the secondary alcohol derivative, and the arrest of these reactions by NaOH may be the probable reason for high selectivity towards PHET.[6] Addition of organic promoter base like triethyl amine with a lone pair of electrons on the nitrogen atom was also found to reduce the formation of ethyl benzene (Table 5.10, S. No. 3). The basic triethyl amine may be blocking the sites responsible for dehydration of the alcohol. But addition of these modifiers in higher concentrations was found to reduce

the reaction rates considerably, which can be an indirect evidence for the fact that these modifiers are blocking the active sites of the catalyst (Table 5.10, S. No. 1 & 5). Addition of alkaline ammonia solution (contains ~25% NH_3) was also found to reduce the formation of ethyl benzene (Table 5.10, S. No. 5). But none of these modifiers were found to block the active sites responsible for the aromatic ring hydrogenation alone. The addition of inorganic metal salts like $ZnCl_2$ was found to have almost no effect on selectivity and higher concentration of $ZnCl_2$ found to stop the reaction (Table 5.10, S. No. 6).

5.2.9 Screening of Other Supported Metal Catalysts

Other supported metal catalysts were also screened with the view of selecting suitable catalysts for the synthesis of PHET and CHET. The screened catalysts include Ni, Pd and Rh along with ruthenium. Carbon was chosen as the support in order to avoid any interaction of support in the reaction.

Table 5.11: Screening of Supported Transition Metal Catalysts with Solvent Methanol

Catalyst	Conversion, %	Selectivity, %				TOF, hr^{-1}
		CHMK	PHET	CHET	ETBE	
3%Ru/C	96.56	8.75	36.04	29.74	25.46	1460
3%Ni/C*	19.13	0	88.28	0	1.2	72
3%Pd/C**	100	0	71.19	0	18.58	920
3%Rh/C***	100	1.44	67.62	1.54	27.41	863

Reaction Conditions: ACPH Concentration: 0.841 kmol/m^3, Solvent: Methanol, Temp: 398 K, P_{H2}: 47.6 atm, Cat. Wt.: 3 kg/m^3

*1-phenethylmethylether formation with selectivity of 10.52%

** 1-phenethylmethylether formation with selectivity of 10.22%

*** 1-phenethylmethylether formation with selectivity of 2.52%

Studies were carried out with both methanol and cyclohexane as solvents since it is known that the solvent influences the reaction schemes considerably in many cases. The results of the catalyst screening carried out with methanol as a solvent are given in Table 5.11. Pd and Ni supported catalysts were found to give a better selectivity towards PHET in comparison with Rh and Ru supported catalysts. Even though Rh is known to give ring-hydrogenated products, only small amount of ring-hydrogenated products were observed with methanol as the solvent. In the case of Ni supported catalysts, the reaction was found to be very slow, but selectivity towards PHET was high. With supported Ni and Pd catalysts considerable amount of 1-phenethylmethylether was formed. It is known that in presence of Ni and Pd catalysts PHET form ether by the interaction with methanol.[6] The acidic protonic sites present on the catalyst surface are responsible for the formation of 1-phenethylmethylether formation.[6]

Screening of above mentioned catalysts were also done with cyclohexane as the solvent to avoid any type of solvent interaction in the reaction and the results are given in Table 5.12.

Table 5.12: Screening of Supported Transition Metal Catalysts with Cyclohexane as Solvent

Catalyst	Conversion, %	Selectivity, %				TOF, hr^{-1}
		CHMK	PHET	CHET	ETBE	
3%Ru/C*	98.49	46.73	1.74	48.68	1.36	1867
3%Ni/C	3.78	0	100	0	0.0	10.37
3%Pd/C	87.76	0	85.81	0	14.19	663
3%Rh/C**	78.67	6.38	71.47	8.64	10.45	812

Reaction Conditions: ACPH Concentration: 0.841 kmol/m^3, Solvent: Methanol, Temp: 398 K, P_{H2}: 47.6 atm, Cat. Wt.: 3 kg/m^3

* Ethyl Cyclohexane was observed with a selectivity of 1.47 %

**Ethyl Cyclohexane was observed with a selectivity of 3.96 %

With Cyclohexane as the solvent, the reaction rate for Ni catalyst was found to be very low. In all the cases, the formation of ethyl benzene was found to be less than methanol as the solvent indicating that methanol plays a role in the formation of ethyl benzene. Even though the selectivity for PHET with Ni and Pd catalysts was high with cyclohexane as solvent, the reaction rates were found to be lower than that observed for methanol as the solvent.

5.3 Conclusions

Supported ruthenium catalysts prepared by precipitation technique and impregnation technique showed the presence of some extent of ruthenium oxide even after activation at 573 K. With methanol as solvent, CHET formation took place mainly through PHET as the intermediate for supported ruthenium catalysts. With higher alcohols, CHET formation through CHMK and PHET as the intermediates in almost equal amounts was observed and with non-polar hydrocarbon solvents, reaction proceeded mainly through CHMK as the intermediate. With non-polar hydrocarbon solvents, 99% selectivity towards CHET was obtained where as with alcoholic solvents considerable amount of the side product, ethyl benzene, formation was observed. Studies with water as the immiscible phase with acetophenone was found to give high rates and high selectivity (> 98%) towards CHET. The catalysts were found to remain in the aqueous phase, which was recycled successfully four times, and in all the recycles the rates were found to be similar and the selectivity towards CHET was maintained. Ruthenium supported on NaY was found to give the maximum reaction rates owing to its high surface area. Catalysts prepared by impregnation technique were found to give a better activity than the catalysts prepared by precipitation technique and ethanol as the impregnation solvent was found to be better rates than water as the impregnation solvent. Addition of basic promoters like NaOH and triethylamine was found to suppress the formation of the side product, ethyl benzene, with ruthenium as catalyst and methanol as the solvent. Screening of other supported metal catalysts showed that Ni and Pd catalysts gave better selectivity towards PHET.

References

1. Nagai M., Koizumi K. and Omi S., NH_3-TDP and XPS studies of Ru/Al_2O_3 catalyst and HDS activity, Catalysis Today, 35, 393, 1997

2. Tsisun E.L., Nefedov B.K., Shpiro E.S., Antoshin G.V. and Minachev Kh. M., XPS studies of Ru in γ-Al_2O_3 supported catalysts

3. Masson J., Cividino P., Bonnier J.M., and Fouilloux P., Selective hydrogenation of acetophenone on unpromoted Raney Ni: Influence of reaction conditions, Heterogeneous Catalysis and Fine Chemicals II, Stud. Surf. Sci. Catal., 245, 1991

4. Kluson P. and Cerveny L., Selective hydrogenation over ruthenium catalysts, Applied catalysis A: General, 128, 13, 1995

5. Kluson P., Cerveny L., and Had J., Preparation and properties of ruthenium supported catalysts, Cat. Lett., 23, 299, 1994

6. Rajashekharam M.V., Thesis submitted to the university of Pune, India (1997)

List of Publications Based on Present Work

1. Supported Ni and Ru catalysts for hydrogenation of p-Isobutyl acetophenone: a catalyst comparison study
   S.P. Mathew. M.V. Rajashekharam and R.V. Chaudhari
   Studies in Surface Science and catalysis, 113 (1998), P. 349

2. Hydrogenation of p-isobutyl acetophenone using a Ru/Al_2O_3 catalyst: Reaction kinetics and modeling of a semi batch slurry reactor
   S.P. Mathew, M.V. Rajashekharam and R.V. Chaudhari
   Catalysis Today 49 (1999), P. 49

3. Hydrogenation of Acetophenone Using Supported Ruthenium Catalysts: Kinetics, Intraparticle Diffusional and Non-isothermal effects
   S.P. Mathew, P.R. Gunjal and R.V. Chaudhari, ready for communication

4. Hydrogenation of Acetophenone Using Ru/Al_2O_3 Catalyst in a Trickle Bed Reactor
   S.P. Mathew, P.L. Mills and R.V. Chaudhari, ready for communication

5. Hydrogenation of Acetophenone in a Packed Bubble Column Reactor: Reactor Performance and Comparison with Downflow Operation
   S.P. Mathew and R.V. Chaudhari., ready for communication

6. Solvent effects in hydrogenation of aromatic ketons with ruthenium supported catalysts
   S.P. Mathew and R.V. Chaudhari, ready for communication

Papers / Posters presented Based on Present Work

1. Supported Ni and Ru catalysts for hydrogenation of p-Isobutyl acetophenone: a catalyst comparison study

   S.P. Mathew, M.V. Rajashekharam and R.V. Chaudhari (Presented at National symposium on catalysis, Dehradun, India, 1998

2. Hydrogenation of p-isobutyl acetophenone using a Ru/Al_2O_3 catalyst : Reaction kinetics and modeling of a semi batch slurry reactor

   S.P. Mathew, M.V. Rajashekharam and R.V. Chaudhari (Presented at IPCAT-1, Cape Town, South Africa, 1999)

3. Hydrogenation of Acetophenone Using Ru/Al_2O_3 Catalyst in a Trickle Bed Reactor, **S.P. Mathew,** P. Gunjal, R.V. Chaudhari and P.L. Mills, (Presented at AIChE Annual Meeting at USA during October 31–November 5, 1999).

4. Selective Hydrogenation of Acetophenone to 1-Phenylethanol and 1-Cyclohexylethanol Using Supported Metal Catalysts, **S.P. Mathew** and R.V. Chaudhari, (Presented at IPCAT-2, Pune, India, 2001)